THE UNIVERSITY
of EDINBURGH

A Rapid Three-dimensional Photonic Scanning System for Body Volume Measurement and Body Shape Visualization

Chuang-Yuan Chiu

Doctor of Philosophy

The University of Edinburgh

2015

Abstract

Traditional three-dimensional (3D) photonic scanning (3DPS) can be used to obtain body volume data and to enable visualization of 3D body shape in one rapid scan, which is helpful for determining people's obesity level, health risk and sport performance as well as motivating individuals to reduce weight efficiently. Nevertheless, traditional 3DPS is restricted to expensive and fixed hardware and specific software that requires specialist interpretation in laboratory settings, which reduces possible applications. Therefore, the purpose of this research was to develop a fast, inexpensive, portable and automatic 3DPS system to measure body volume data and to display body shape in 3D. To ensure that the system could be used for monitoring changes over time, the accuracy and reliability of the estimated body volumes were also established.

Four studies and one technical description were conducted to achieve the purpose of this research. In the first three studies, a new technique, DScan, was developed that could generate individual 3D human models and calculate body volume. In Study 1, the reliability of the body dimension features obtained by four extraction methods was compared to find an appropriate method to improve the quality of extracted body dimension features. In Study 2, two different parameter groups were compared to enable subsequent selection of appropriate parameters to generate realistic 3D human models. A procedure and a program were presented which can set the parameters to match the extracted features and generate individual 3D human models effectively. In Study 3, Blender scripts and shell scripts were used to develop a customized program which can obtain body volume data from generated 3D human models. In Study 4, the

accuracy and the reliability of the body volume data acquired from DScan were examined by comparing with the traditional 3DPS and the geometric modelling technique, elliptical zone (E-Zone). In the technical description, a Body Shape Monitoring System (BSMS) which can help non-expert users complete the DScan procedure and visualize body shape changes was introduced. The processing speed, cost and portability of the introduced BSMS were also shown in the technical description.

The accuracy of the BSMS for whole-body volume indicated by an inter-method relative technical error of measurement was within 5% of that obtained from the traditional 3DPS. The repeated reliability expressed as an intra-method relative technical error of measurement was under 3% for whole-body volume. The accuracy and the reliability of the BSMS for segmental volumes (upper torso, lower torso, upper arm, lower arm, thigh and shank) indicated by inter-method and intra-method relative technical error of measurements were less than 10% and 5% respectively. These were similar to those obtained by the E-Zone.

The BSMS reduces the requirement of hardware, software and expert knowledge as well as the processing time compared to other techniques of quantifying whole-body volume and segmental volumes. The GUI of the BSMS enables it to be used without specific training in computer programing or machine operation. The system is highly portable, and its components are inexpensive (under £700). Each analysis can be completed in three minutes without requiring subjective interpretations. The results showed that the system has the potential to be applied in the domains of health and medicine, the fashion industry, ergonomics, and sports science. Further studies should

be conducted to develop a complete system which is consequently suitable for home use.

Declaration

I hereby declare that the work contained in this thesis, submitted in partial fulfilment of the award of PhD at the University of Edinburgh, is my own, and was completed without collaboration or assistance from others, expect as stated in acknowledgements. Some figures available publically on the World Wide Web have been used in the thesis to illustrate methods and commercial products used in the research. The work has not been submitted for any other degree or professional qualification.

Signed:

Chuang-Yuan Chiu

Acknowledgements

I would like to express my acknowledgements to the people who made the contribution to this thesis.

I would like to thank my supervisors Prof Ross Sanders and Dr Samantha Fawkner for their guidance, mentoring and continued support throughout my thesis.

I would like to thank Dr David Pease for letting me access the 3D scanner and conduct my research in Australian Institute of Sport. I also appreciate his help for complete part of mesh editing tasks.

I would like to thank all the participants, the operators of the 3D scanner and the recorders for anthropometric tests. Because of your help, the data collection process went smoothly and efficiently.

I would like to thank Dr Simon Coleman for the advice and comments during my writing.

I would like to thank my colleagues and the staffs in CARE and ISPEHS and friends at the University of Sydney for helping me absorb the knowledge in Sports Sciences.

Finally, I would like to thank my lovely families for giving me the warmest and strongest support when I came across difficulties.

Contents

List of Figures

List of Tables

List of Algorithms

List of Equations

Glossary

3D point cloud	A set of 3D points which are described by 3D coordinates (X, Y, and Z).
Anatomical landmark	The location on the human body which is defined by the specific site on the skeleton.
Adipose tissue	The adipose tissue is loose connective tissue in an animal body which is composed of adipocytes.
Animation rigging	The 'skeleton' of the 3D models which are used for changing the shape of 3D models in different poses.
Body Volume Index	A method that uses regional body volume to quantify human body shape.
Blender	A software for computer graphics which can be used for editing 3D meshes or generating 3D animation.
BSMS	BSMS is the abbreviation of body shape monitoring system which can help users complete the 3D scanning procedure and visualise the body shape change.
BVH	A motion capture format which records the joint angles in different time.

Calibration	A process to understand the scales of image captured by a camera to improve the measurement accuracy.
Computer aided design software	The software which can help the user complete design tasks such as 3D mesh editing, 3D mesh analysis with a computer system.
Corresponding points	If there are two vertices on two different mesh and these two vertices describe the same position on the real object, each vertex is the corresponding point of another vertex.
Deformation	A 3D mesh or an image changes its geometric shape.
Fat-free mass	The mass of body fat tissue
Fat mass	The mass of tissue which is not fat-free mass (e.g. bone, muscle)
Free-form deformation	A type of deformation technique used in computer graphics for changing the shape of 3D meshes.
Graphic user interface	One kind of computer interface which allows users to operate the system or software with graphic tools such as icons.
Mesh	A mesh is composed by faces, edges and vertices for illustrating specific shapes of objects in 3D.

MySQL	A software for database management which can help users store data, search the stored data, etc.
Noise	Part of captured data which might generate some error during the analysis.
Non-rigid body	A type of body which is not solid, and its geometry can be deformed by applying external force.
Non-rigid registration	A computer vision technique to find the corresponding points from two images or two meshes of one object that in two different poses.
Registration	A computer vision technique to find the corresponding points from two images or two meshes.
Registered mesh	If the vertex number, vertex order, edge number and edge order of a mesh is the same as the template mesh, the mesh is a registered mesh.
Silhouette image	An image which used single colour to represent the background and another colour to illustrate the foreground.
Somatotype	A categorisation method for illustrating human body shape.

Smoothing	A process that makes the surface of the 3D mesh become smooth.
Template	A base mesh or image which can be deformed by altering its parameters and align to the target source (other mesh or image).
Tetrahedron volume techniques	The techniques that separate the triangular meshes into a set of tetrahedrons and calculates the volume by computing and accumulating the volume of each tetrahedron.
Tissue	Tissue is a biological term which refers to a group of similar cells with a specific function.

List of Abbreviations

2D = two-dimension or two-dimensional

3D = three-dimension or three-dimensional

3DPS = 3D photonic scanning

ρ = whole-body density

a = the angle between the horizontal and the limb (shank, thigh, upper arm or lower arm)

App = applications

BIA = bioelectrical impedance

BVH = Biovision Hierarchy format

BVI = body volume index

BSMS = Body Shape Monitoring System

c = body dimension candidate

CAD = computer aided design

CT = computed tomography

D_{water} = the density of water in underwater weighing test

d = the human model deformation function for template model matching

DXA = dual X-ray absorptiometry

E-Zone = elliptical zone method

$f = (f_1, \cdots, f_n)$ = extracted features for template model matching

$\bar{F}_i$ = the mean of features in two feature sets (f1 and f2) for the i^{th} participant's body dimension

f1 and f2 = two sets of body dimension features extracted from manual input and depth images

FFD = free-form deformation

g = the acceleration due to gravity

GUI = graphic user interface(s)

ICC = intraclass correlation coefficient

Inter absolute TEM = inter-method absolute technical error of measurements

Inter relative TEM = inter-method relative technical error of measurements

Intra absolute TEM = intra-method absolute technical error of measurements

Intra relative TEM = intra-method relative technical error of measurements

IR = infrared ray

ISAA = International Standards for Anthropometric Assessment

ISAK = International Society for the Advancement of Kinanthropometry

ISO = International Organization for Standardization

IVNA = in vivo neutron activation

LP = local parameters

Lv1, Lv2, Lv3, Lv4 = four specific levels used for the definition of four torso breadth

M = composition function for template model matching

$m = (m_1, \dots, m_n)$ = measurements for template model matching

$\bar{M}_i$ = the mean of the corresponding measurements in m11 and m21 or m12 and m22 for the i^{th} participant's body dimensions

m11, m21, m12, m22 = four sets of measurement obtained from the deformed 3D human model

$Mass$ = total body mass

MH = MakeHuman

MHX = MakeHuman eXchange file format

M_{i1} and M_{i2} = the first and second measurements separately obtained by a method for the i^{th} participant

$\bar{M}_{i1}$ and $\bar{M}_{i2}$ = the mean of repeated measurements separately obtained by a testing method and a reference method for the i^{th} participant

MP = macro parametersMRI = magnetic resonance imaging

OP1 and OP2 = two operator who processed the data in this research

$p = (p_1, \dots, p_n)$ = parameters for template model matching

$\hat{p} = (\widehat{p_1}, \dots, \widehat{p_n})$ = the best match parameters for template model matching

$(pc_1, pc_2, \cdots, pc_{30})$ = 'pre-candidate' of each body dimension extracted from depth images

PG1 = the first parameter group adjusted from those proposed by Pirker et al. (2009)

PG2 = the second parameter group adjusted from those proposed by (Van Deun et al., 2011)

r = residual volume

S = a body shape for template model matching

$\hat{S}$ = the individual human model for template model matching

SCAPE = shape completion and animation of people

SDK = software development kit

TEM = technical error of measurements

TenBo = tensor-based human body model

TB1, TB2, TB3, TB4 = four torso breadth features extracted from depth images

TBK = total body potassium

TBW = total body water

TEM = technical error of measurements

N = representative of the number of participants in this research

V = whole-body volume

v = a participant's whole-body volume obtained from underwater weighing test

w_{air} = a participant's weight measured in air, as used in an underwater weighing test

WHR = waist-to-hip ratio

w_{water} = a participant's hydrostatic weight in underwater weighing test

Chapter 1 Introduction

1.1 Background

A range of body measurements have been introduced for a variety of reasons, including determining or estimating people's obesity level, health risk and sport performance. These body measurements can be roughly categorized into three types; body size and shape, segmental volume, and body composition.

Body size and shape, includes somatotype, segmental lengths and breadths and girths. Particular body shapes are related to obesity-related diseases and sport performance. For example, waist girth can be used to estimate fat distribution (Ketel et al., 2007) and has been used as a tool to determine obesity levels (Consultation, 2008). Price et al. (2006) found that people aged 75 years or above with low waist-to-hip ratio (WHR) have lower mortality than the ones with high WHR and Carter and Heath (1990) indicated that different associations exist between disease and somatotype components. With respect to sport performance, Ackland (2006) reviewed a large body of literature that demonstrates that elite athletes usually have anthropometric characteristics that are significantly different from the normal population.

Segmental volumes provide additional useful information to understand people's physiques and some advanced references for estimating fat distribution (Daniell et al., 2014; Wells, 2012). Abdominal volume index (Guerrero-Romero & Rodríguez-Morán, 2003) and body volume index (Muralidhara, 2015) are useful to determine obesity level since they indicate indirectly the amount of abdominal fat. Lee et al. (2015) also showed that the segmental volume ratio between thigh and torso and thigh to abdomen-hip were highly related to the visceral adipose tissue deposition. In addition,

volumetric ratio of the trunk and legs (Wilson, Kanaya, et al., 2013) is an effective body measurement to predict the health risk of diabetes and mortality. With respect to performance sport, Schranz et al. (2010) used 3D photonic scanning technology (3DPS) to extract segmental volume data and used these as the parameters to distinguish performance rowers from the normal population. Moreover, Schranz et al. (2012) showed that the anthropometric characteristics including segmental volumes provide more information pertinent to sport performance than the characteristics excluding segmental volumes. Estimated segmental volumes can also be used in biomechanics analysis (Deffeyes & Sanders, 2005; Wicke et al., 2009).

The assessment of body composition determines proportions of protein, fat, water and mineral components in the body. It is most commonly reported as the ratio of fat mass and fat-free mass and has been widely used for obesity diagnosis (Okorodudu et al., 2010; World Health Organization, 1995). Some diseases might cause abnormal body composition such as Cushing's syndrome (Rebuffé-Scrive et al., 1988; Wajchenberg et al., 1995). Furthermore, body composition is also associated with sport performance. From a biomechanical aspect, a higher body fat mass leads to increased demand for energy consumption and has a negative influence on performance (Ackland et al., 2012; Duthie et al., 2003). Body composition can be used to distinguish between athletes at different performance levels and has been suggested to be useful for monitoring training effects (Milsom et al., 2015).

These body measurements can provide information to help people assess obesity level, health risk, fitness, condition and sport performance. Therefore, monitoring allows the effect of sport and exercise training or nutrition interventions to be determined. For

example, Keating et al. (2014) measured the whole and segmental body composition data before and after 12 weeks of exercise intervention and compared the effect of different training approaches. Danielsen et al. (2013) introduced a lifestyle program including a large amount of physical activity to participants and observed its influence on changes in body composition and Evans et al. (2012) accessed the effect of different diets on body composition changes.

It is therefore clear that accurate and reliable tools are needed to obtain these body measurements and various methods have been developed. Segmental length, breadth and girths can be determined by manual anthropometric measurement (Stewart et al., 2011) or estimated from 2D images (Lin & Wang, 2012; Meunier & Yin, 2000) or 3D models (Weiss et al., 2011). Heath-Carter somatotype (Carter & Heath, 1990), the most common somatotype approach, is defined by manual anthropometry or 2D images. Olds et al. (2013) indicated that 3DPS could determine individual somatotype and therefore avoid traditional anthropometry and 2D image methods.

Segmental volume can be measured by different approaches. The abdominal volume index (Guerrero-Romero & Rodríguez-Morán, 2003) and segmental volume ratio (Wilson, Kanaya, et al., 2013) are acquired by manual anthropometric measurement and dual X-ray absorptiometry (DXA) scan respectively. However, other medical scanners including magnetic resonance imaging (MRI) and computed tomography (CT) or some 3DPS techniques (Collins, 2006; Lee et al., 2015) can be applied to understand the volume of body segments.

Several analysis methods have been developed for understanding human body composition including laboratory methods (Rolland, 2012) and portable methods

(Mulholland & Rolland, 2012). According to reviews (Mulholland & Rolland, 2012; Rolland, 2012), the methods include cadaver analysis, underwater weighing, air displacement plethysmography, isotope dilution methods, medical imaging methods, DXA, 3DPS, surface anthropometry, near infrared interactance, bioelectrical impedance, and ultrasound.

Among these analysis methods, 3DPS is a newer, emerging technology. It can acquire all three kinds of measurement, body size and shape, segmental volume and body composition, in one rapid scan (Muralidhara, 2015; Treleaven & Wells, 2007; Wang et al., 2006). Three-dimensional surface scanners with corresponding software can measure anthropometric variables (segmental length, height, breadth and girth) and body volume (whole-body volume and segmental volumes) so it can be applied to determine body composition, body size and shape, and segmental volumes. Treleaven and Wells (2007), Schranz et al. (2010) and Schranz et al. (2012) indicated that 3DPS is a useful technology for healthcare and sport performance determination since the anthropometric characteristics measured by 3DPS can enable prediction of obesity level, health risk and sport performance and the measurement process is fast and with less limitations (e.g. radiation) than using medical scanners. The other advantage of 3D scanning is that the body shape change can be visualised. This information of body measurements and the visualization of body shapes can motivate people to reduce weight (Boelaert et al., 2008) since people are interested in the appearance of their bodies (Treleaven & Wells, 2007).

The 3DPS technology which used the fixed scanners has been compared with water displacement methods establishing its good accuracy and reliability for the acquisition

of individual body volume data (Collins, 2006; Wang et al., 2006). The fast 3D scanning process is beneficial for data collection in large cohort studies (Stewart, 2010). Nevertheless, traditional 3DPS is restricted to expensive and non-portable hardware and specific software that requires specialist interpretation in laboratory settings. Because of the limitations, this technology can only be applied to specific participants.

An automatic, portable inexpensive 3DPS system could be of benefit to researchers, nutritionists, fitness coaches, and health-conscious individuals. Researchers could travel to several places and complete the measurement tests with the portable system. Such a system would enable research to be conducted in field studies with large cohorts of participants inexpensively. Nutritionists and fitness coaches could easily have their own system and bring the simple equipment system to different places. These specialists could then serve more clients without any requirement for post-processing (e.g. manual operation for hole-filling and segmentation) and monitor the changes in their body measurement. It is then helpful to provide effective suggestions relating to diet and exercise by referring clients to the scanning results conducted with the system. Individuals could also use such technologies to obtain their body measurement by themselves. This can avoid traveling to specific laboratories to meet specialists and using expensive facilities.

Several portable and cost effective 3DPS approaches have been developed (Daanen & Ter Haar, 2013). However, most of the approaches were concentrated on anthropometric measures such as waist girth and arm span length (Tong et al., 2012; Weiss et al., 2011; Xu et al., 2013). The accuracy and reliability of body volume data

including whole-body volume and segmental volume are unknown. A few studies, such as the method presented by Pirker et al. (2009), evaluated the accuracy of body volume data but the methods involve manual digitizing and the reliability is unknown. The unknown reliability means that these methods cannot be used for monitoring. The elliptical zone method, E-Zone (Deffeyes & Sanders, 2005; Sanders et al., 2015), is the only method whose reliability of the acquisition of body volume data has been examined. However, the data for the accuracy of body volumes acquired from E-Zone is not complete (Wicke & Lopers, 2003). The accuracy of body volume data for trunk and upper limbs is lacking, which are important measures for determining people's obesity level, health risk, fitness, condition and sport performance. There is currently no 3DPS system which is fast, inexpensive, portable, and automatic and for which the accuracy and reliability for body volume acquisition is known.

1.2 Purpose

The purpose of this research was therefore to develop a fast, portable, inexpensive and automatic system to build individual 3D human models for acquiring multiple body measurements and visualizing body shape variation[1]. To ensure that the system can be used for measurements and monitoring, the accuracy and reliability of the estimated body volumes needed to be established. In particular, the system was required to be sufficiently accurate and reliable to detect small changes in body shape and volume with confidence. Thus, accuracy and reliability tests for whole-body volume and segmental volumes were conducted in this research. Because the system was designed to measure only the whole-body volume for estimating body composition level,

[1] The definition of visualizing body shape is that the shape of the whole-body can be shown in the same posture and compared with other scanning results.

accuracy and reliability tests focused on quantifying whole-body volume rather than body composition per se.

To ensure that the system could be used extensively to address prevalent public health issues, particular features and criteria were identified. It needed to be almost as simple as using weighing scales but with the benefit of having much more useful and meaningful information regarding how the changes have occurred. Specific considerations included processing speed, portability, cost and the requirement of expert knowledge.

Nevertheless, this research concentrated on providing a proof of the developed concept system which could acquire useful information (body measurements) for researchers and showing a first step towards developing a system for end-users in the home. Thus, this research should not imply that the developed concept system is close to completion and consequently suitable for home use. Therefore, the test participants were limited to males since the cloth for females (e.g. bra) might have generated high errors for body volume measurement when using 3DPS and lead to errors in analyses. The user centred design of the system was not in the scope of this research. The criteria relating to accuracy, reliability, speed, portability, cost and automation are outlined below.

1.2.1 Accuracy

In this research, the inter-method relative technical error of measurements (inter relative TEM) were used to quantify the accuracy of body volume data obtained from the developing methods. The inter relative TEM calculated the ratio of inter-method absolute technical error of measurements (inter absolute TEM) and the variable average value, as defined in Equation (1) and Equation (2) (Perini et al., 2005).

$$\text{Inter absolute TEM} = \sqrt{\frac{\sum_{i=1}^{N}(\bar{M}_{i1} - \bar{M}_{i2})^2}{2 * N}} \quad (1)$$

$$\text{Inter relative TEM} = \frac{\text{Inter absolute TEM}}{\frac{\sum_{i=1}^{N}(\bar{M}_{i1} + \bar{M}_{i2})}{2 * N}} * 100\% \quad (2)$$

where N is representative of the number of participants, $\bar{M}_{i1}$ and $\bar{M}_{i2}$ denote the mean of repeated measurements separately obtained by a testing method and the reference method for the i^{th} participant.

This research aims to provide the accurate estimation of whole-body volume within 5% TEM and the accurate approximation of large segmental volumes (apart from head, neck, hand, foot segments) within 10% TEM. The criterion value refers to the accuracy of other simplified 3D scanning methods (Pirker et al., 2009; Wicke & Lopers, 2003). Wicke and Lopers (2003) showed the error for whole-body volume acquired from E-Zone was less than 5%. Combining the results of both studies (Pirker et al., 2009; Wicke & Lopers, 2003), the error for segmental volume acquired from the simplified 3D scanning method is between 0.1% and 24.3 %. Therefore, the approximate mean value, 10%, was chosen as the criterion value for segmental volume in this research.

1.2.2 Reliability

In this research, the intra-method relative technical error of measurements (intra relative TEM) were used to quantify the reliability of body volume data obtained from the developing methods. The intra relative TEM calculated the ratio of intra-method absolute technical error of measurements (intra absolute TEM) and the variable average value, is defined as in Equation (3) and Equation (4) (Perini et al., 2005).

$$\text{Intra absolute TEM} = \sqrt{\frac{\sum_{i=1}^{N}(M_{i1} - M_{i2})^2}{2 * N}} \quad (3)$$

$$\text{Intra relative TEM} = \frac{\text{Intra absolute TEM}}{\frac{\sum_{i=1}^{N}(M_{i1} + M_{i2})}{2 * N}} * 100\% \quad (4)$$

where N is representative of the number of participants, M_{i1} and M_{i2} denote the measurements obtained in first and second trials separately for the i^{th} participant.

The research aims to provide a reliable method for monitoring the change of body volume data. Ideally, the reliability of the developing method would be similar to the reliability of the 3D photonic scanning method. Referring to the previous study (Collins, 2006), the research aims to provide a reliable estimation of body volume data within 5% TEM. In addition to the result presented by Collins (2006), Sanders et al. (2015) mentioned that the value, 5%, has been used as a useful criterion for reporting overall reliability in accordance with convention.

1.2.3 Speed

The whole process of body volume measurement for the developing method should take less than 10 minutes. The criteria of the processing speed in this research, 10 minutes, referred to the post-process time of E-Zone (Wicke & Lopers, 2003). Therefore, the developing method should not contain any time-consuming post processes such as the manual digitizing for edge detection in E-Zone (Deffeyes & Sanders, 2005) and the 3D scanning mesh editing (Ma et al., 2011).

1.2.4 Automation[2]

To ensure that the system could be used by non-expert users, the process of human model building should not require complex manual measurement and precise palpation for anatomical landmarks. For the same reason, the system was developed without reliance on invasive methods or medical scanning techniques such as DXA, CT or MRI since this kind of machinery usually needs to be operated by specialists with licenses. Furthermore, the human post-processes such as digitizing (Deffeyes & Sanders, 2005), 3D mesh editing (Ma et al., 2011) or parameter altering (Lin & Wang, 2012) need to be avoided.

To enable all individuals to make use of the hardware and software, an automatic system for monitoring body shapes was required. Consequently, the system needed to contain graphic user interfaces enabling use without any programming skills. After placing the capturing system and connecting to the operation laptop, users just need to enter their basic information (gender, age, height, and mass; all of which are easy to measure or determined) into a graphic user interface and press the 'start button'. Then all the processes of image capturing, model generation and body volume calculation can be completed automatically. Furthermore, a database system was required to assess longitudinal changes.

[2] 'Automation' in this research was defined as: the whole measurement process for body volume data acquisition can be completed automatically without palpation, technical expertise in programming, software and hardware operation. The whole process excludes setting up the hardware and entering basic information (gender, age, height, and mass; all of which are easy to measure or be determined).

1.2.5 Portability

To ensure portability, the equipment comprising the system, including an operation laptop and an image capturing system, needed to be less than 7 kilograms and small in size (for example, could be 'carry-on baggage' in airline travel). The lightweight and small size ensures the system can meet the allowance of carry-on baggage for most airlines. In addition, the system must be useable in most indoor environments such as living rooms at homes.

1.2.6 Cost

The cost of hardware of the system, including an operation computer and a camera device, should be under £1,000 to ensure affordability for a normal family or a practitioner. The price criterion, £1,000, referred to the cost of equipment in previous studies (Cui et al., 2013; Wang et al., 2012; Weiss et al., 2011; Xu et al., 2013). This price criterion is much lower than other commercial body scanning systems which usually cost from US$10,000 ($TC^2$ KX-16, Cary, NC, USA; around £6,600; currency rate: 24.Nov.2015) to US$240,000 (Cyberware, Monterey CA, USA; around £158,600; currency rate: 24.Nov.2015) (Daanen & Ter Haar, 2013). The cost of a commercial body scanning system may not include the price of the associated software for acquiring anthropometric measurements and body volume data.

1.3 Structure of the Thesis

The remainder of this thesis is structured as follows. Chapter 2 is a concise review of literature related to this research. From Chapter 3 to Chapter 7, four studies and one technical description are illustrated to achieve the research purposes. Figure 1 shows the main contribution of each study and the technical description (please see 2.4 for

further details). Chapter 1 provides a general discussion. The conclusion and the plans for future research are presented in Chapter 1.

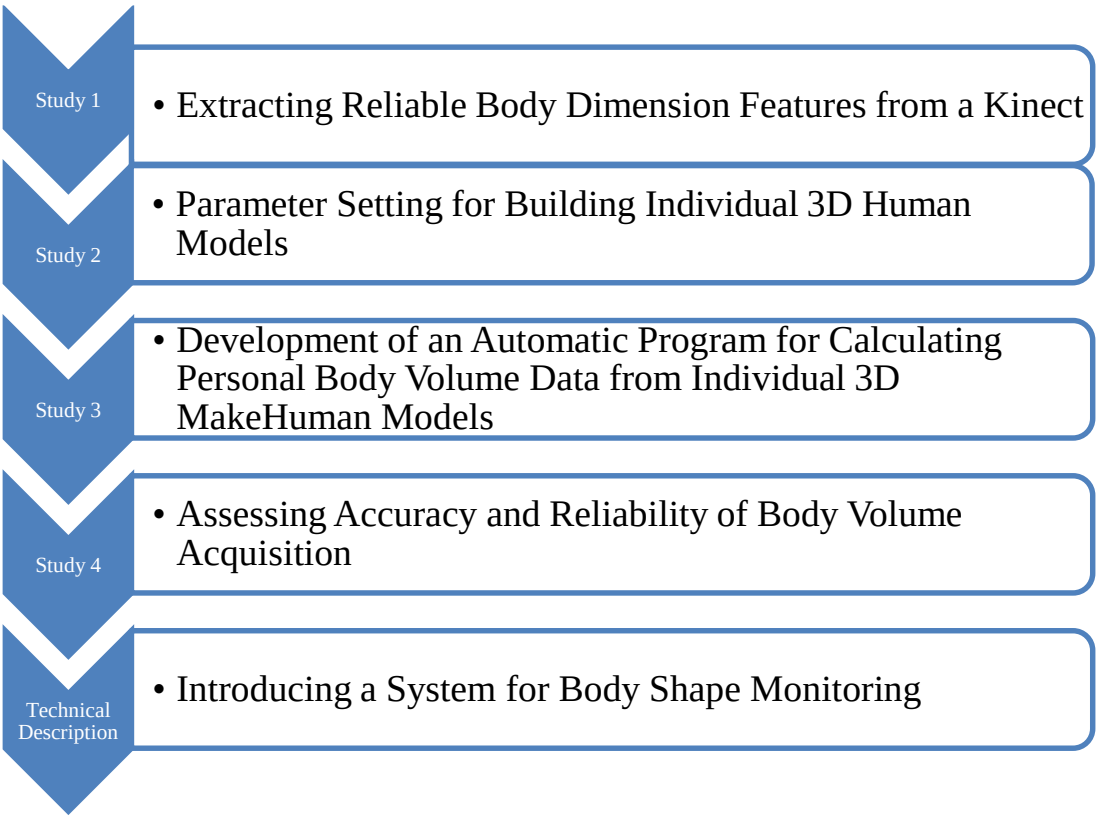

Figure 1 The main contribution for the four studies and one technical description of this research

Chapter 2 Literature Review

In this research, a new 3DPS system is proposed to enable monitoring of body volumes and body shape changes. The whole-body volume can subsequently be used for estimating body composition. Thus, traditional analysis methods of segmental volume and body composition (whole-body volume) is reviewed concisely. Following this, a review of 3D human modelling techniques is presented. In the first Section (2.1), different analysis methods of segmental volumes and body composition are described. The advantages and disadvantages of these methods are also discussed to examine whether there is any current method which can achieve the purpose of this thesis in terms of accuracy, reliability, processing speed, automation, portability and cost. In the second Section (2.2), the methods of generating individual 3D human models are reviewed. The limitations and benefit of each approach are illustrated. The following Section (2.3) established the need for a body shape visualization and monitoring system. The conclusion and implications are illustrated in the final Section (2.4).

2.1 Traditional Analysis Methods for Acquiring Segmental Volumes and Body Composition

In this research, the developed system is to be used for monitoring the changes of body volume and shape. Therefore, the review focuses on the methods which can be used for living participants and cadaver analyses (Braune & Fischer, 1889; Clauser et al., 1969; Dempster, 1955) are excluded. Several methods have been developed for segmental volumes and body composition analysis of living people. In the following sections, water displacement, underwater weighing, medical imaging methods, DXA, 3D photonic scanning, surface anthropometry, air displacement plethysmography, isotope dilution, near infrared interactance, bioelectrical impedance methods and

ultrasound are described and key limitations with reference to assessment of body volume articulated. Of these, underwater weighing, air displacement plethysmography, isotope dilution methods and near infrared interactance and ultrasound can be used only for body composition analysis whereas the other methods can be applied to both segmental volume acquisition and body composition analysis. A critique of estimating body composition from whole-body volume is presented in the Section 2.1.11.

2.1.1 Water Displacement and Underwater Weighing

The water displacement method applies Archimedes' principle to calculate segmental volumes and whole-body volume. The whole-body volume in conjunction with body mass can be used to estimate the body composition by referring to the known densities of body tissues (Brožek et al., 1963; Siri, 1956). Participants are requested to submerge their body or segments under the water level and the whole-body and segmental volumes are measured by observing the displacement of water. Dempster (1955) measured the additional amount of water displaced while immersing segments to determine segmental volumes. Katch et al. (1974) measured the volume of the overflow of water to obtain segmental and whole-body volume.

Underwater weighing (hydrostatic weighing) measures whole-body volume when a participant is fully immersed. Collins (2006) used this technique to assess the body weight difference in air and whilst submerged to determine the whole-body volume. The following equations are used to estimate body volume, where the volume of the participant is v, weight is w_{air} and his or her hydrostatic weight is w_{water}.

By Archimedes' principle,

$$\text{Weight of displaced fluid (kgw)} = (w_{air} - w_{water}) = B \quad (5)$$

where B is the buoyancy force acting on the participant.

Since the participant is insoluble in water, the volume of displaced fluid is equal to the volume of the participant (v). Thus,

$$\text{Weight of displaced fluid (kgw)} = v \times D_{water} \times g \quad (6)$$

where D_{water} is the density of water and g is the acceleration due to gravity.

The participant's whole-body volume can be calculated by Equation (7).

$$v\ (litre) = \frac{w_{air} - w_{water}}{D_{water} \times g} \quad (7)$$

These techniques are reproducible and relatively inexpensive so some sports studies have used this method to obtain body composition or segmental volume. Camic et al. (2014) used the underwater weighing method to determine the body composition to investigate the influence of polyethylene glycosylated creatine supplementation. Dempster (1955) used water displacement to calculate segmental volume and estimated body segment parameters. Underwater weighing and water displacement can obtain body volume data directly and accurately. The precision error of underwater weighing for whole-body volume and water displacement for segmental volume acquisition has been demonstrated to be lower than 1% (Collins, 2006).

The equipment for measuring body volume data by this technique is non-portable. A large tank is required to let the participant immerse completely for conducting underwater weighing (Rolland, 2012) or measuring the volume of the overflow of

water (Katch et al., 1974). Numbers of specific tanks for different segments are needed to measure the segmental volumes by water displacement method (Drillis et al., 1964). This facility requirement makes it difficult for the general public to conduct these tests at home to measure and monitor their body volume data.

Acquiring both whole-body volume and segmental volume from these techniques requires conducting different tests separately, which causes the processing time for complete body volume data to be considerably longer than other techniques. The tests also need an operator for measurement which decreases the automation. Furthermore, the body shape variation cannot be visualized.

2.1.2 Air Displacement Plethysmography

A method of measuring whole-body volume based on application of Archimedes' Principle has been developed resulting in a commercial product 'Bod Pod' (COSMED, Roma, Italy). A participant enters a special cabin with sensors which can detect changes in air pressure from which a measure of air displacement is derived. Associated software can determine the whole-body volume. Fields et al. (2000) showed the volume obtained from Bod Pod compares very favourably to the volume acquired from hydrostatic weighing. The review conducted by Rolland (2012) indicated that the accuracy and the reliability error of this technique (5%; 4.5%) was slightly poorer than those of underwater weighing (3-4%; 2%). However, the tool has been used for longitudinal studies. Ford et al. (2012) used this technique to measure the body composition variation after a 15-week accumulated brisk walking programme and found the programme can reduce around 2% body fat (about 0.5 kg).

Although Bod Pod is quick and reliable (Rolland, 2012), an operator is needed to complete the tests since the participant cannot operate the system in the cabin of Bod Pod. Furthermore, this technique can obtain only whole-body volume and needs expensive and non-portable equipment which limits the extent of its use (Wang et al., 2006).

2.1.3 Isotope Dilution Methods

Isotope dilution methods estimate the body composition by measuring the mass of total body water (TBW) and is based on the assumption that around 73% of the fat free mass is due to TBW (Kulwich et al., 1958). Participants first receive a dose of isotope intravenously or orally. Then, participants' body fluid is collected as a sample within a short time. The amount of total body water is measured by tracking the ratio of isotope in the sample. The body composition can be determined from the amount of total body water.

The relationship between TBW and body composition is a rough approximation which is affected by age (Fomon et al., 1982) and disease (Kotler et al., 1999). The hydration of the fat-free mass for different individuals could be varied from 65% to 81% (Lohman et al., 2000). Therefore, the accuracy and reliability of this technique that uses constant hydration coefficients are questionable. Furthermore, there are a couple of limitations to this technique which increases the difficulty of applying it to body composition monitoring. For example, these methods need to be conducted in specific laboratories because of the radioactivity of the isotope. Some oral or intravenous isotopes may contain some health risks so technical expertise is required and this analysis method cannot be conducted frequently. A couple of hours are required to

ensure the administered isotope spreads evenly throughout the water compartments of participants' bodies. The Isotope dilution method can only estimate the body composition but not body volume data and body shape visualization.

2.1.4 Medical Imaging Methods

Medical scanners such as total body potassium (TBK), in vivo neutron activation (IVNA), MRI and CT can also measure body composition (Rolland, 2012). TBK and IVNA use gamma rays to quantify the amount of specific elements (^{40}K or H, C, N, O, Na, Ca, P and Cl). Because of the consistent proportion of the element to whole-body volume, the body composition can be determined. However, there is an assumption that proportionality is constant, whereas proportions vary among individuals and contribute to errors in body composition estimates.

CT and MRI scanning with their associated software can build individual 3D human models by detecting the variation of projected X-ray or the change of magnetic fields (Ackland et al., 2012). The 3D human model can be used for calculating whole-body density to determine the body composition. The scanning data can also be applied to acquire segmental volumes. Computer aided design (CAD) software can segment the 3D human model by referring to the skeletal positions. Then segmental volumes can be obtained from the segmented 3D human model. Both CT and MRI scanning have been regarded as reference methods since they are the most accurate method for living participants (Ackland et al., 2012).

The major difficulty of applying the medical imaging methods to body shape monitoring is that they are expensive and accompanied by health risks to the

participants. Medical scanners are highly priced and need certificated operators to manage the scanning. The testing process including the post-analysis is time-consuming. Furthermore, associated software is required for obtaining the body composition or body volume data. These non-risk free methods are therefore hard to apply for monitoring purposes.

2.1.5 Dual X-ray Absorptiometry (DXA)

DXA scanning can be used to determine segmental volumes and body composition. It projects gamma emissions in different energies to detect the mass of different tissues including muscle, fat and bone in an orthogonal scan. Thus, body composition can be acquired from DXA scanning tests (Ackland et al., 2012; Rolland, 2012). The segmental body volume can be estimated by assumed the densities of different tissues after selecting the regions of interest manually (Wilson, Fan, et al., 2013).

Wang et al. (1996) and Kim et al. (2002) compared the body composition acquired from DXA with the results obtained from CT and MRI respectively. Both studies showed that DXA can estimate body composition accurately. Lohman et al. (2000) reviewed the previous studies and concluded that the error of DXA for body composition determination was within 1 to 3%. The reliability error of DXA for body composition measurement was under 2% in previous studies (Bailey et al., 2001; Trutschnigg et al., 2008). However, the analysis of segmental body composition which can be used for estimating segmental volume needs manual digitizing and the within assessor and between assessors error could approach 4% and 6% respectively (Burkhart et al., 2009).

Because of the good accuracy and reliability for body composition analysis, DXA has been widely used in sports sciences. For instance, Garthe et al. (2012) used DXA to monitor body composition variation while applying different weight-gain approaches. Sutton et al. (2009) used DXA to measure and compare the body composition of soccer players in different positions, international status and ethnicity.

However, some limitations exist which means DXA is unsuitable for monitoring the variation of body composition. For instance, specific software, and expensive, non-portable hardware and operational knowledge are required. The anatomical landmark detection from the DXA images also requires specific training. Because of the radiation issues, operators must be certificated and users cannot use DXA for frequent monitoring of body shape (Ackland et al., 2012). Although the scanning process is fast, the post process for obtaining segmental volume requires manual digitizing which increases the whole analysis time.

2.1.6 3D Photonic Scanning (3DPS)

Three dimensional photonic scanning (3DPS), also called 3D scanning technology or 3D surface scanning, is currently the only non-invasive technique which can be used for acquiring all of segmental volumes, body composition and body shape variations longitudinally.

2.1.6.1 Traditional 3D Photonic Scanning

Traditional 3D scanners such as VITUS XXL (Human Solutions GmbH, Kaiserslautern, Germany) usually use a set of scanning heads including single laser

projectors with multiple cameras (Daanen & van de Water, 1998). During the process, the machine moves the scanning heads vertically. The laser projectors project laser stripes on the scanning objects (the human body) and the multiple cameras capture the images to record the deformation of projected stripes. The VITUS XXL includes 4 scanning heads and can capture the 120cm×120cm×210cm scanning volume (Daanen & Ter Haar, 2013). The 3D information (3D point cloud) can be computed by referring the projected laser position shown in the images captured by different cameras. The corresponding software then can build an individual 3D human model comprising a mesh of triangles from the 3D point cloud.

The markers can be placed on the anatomical landmarks prior to the scanning processes. The 3D human model can be edited by CAD software by referring to the marker positions to obtain the segmental 3D human model, and the segmental volumes can be calculated from the triangular meshes. Three dimensional human models can be applied to determine the whole-body volume and segmental volumes. Then body composition can be calculated from the whole-body volume in conjunction with body mass (Brožek et al., 1963; Siri, 1956).

Previous studies demonstrated that the intra-assessor and inter-assessor reliability of the traditional 3DPS for obtaining body volume data is good, even though the analysis involves some manual post-processing (intra-assessor error < 2% (Collins, 2006); inter-assessor error<1% (Ma et al., 2011)). The error values were lower than the values for DXA methods. Wang et al. (2006) also compared the traditional 3DPS with the underwater weighing techniques and found that 3DPS usually over-estimated the total body fat with the non-significant difference around 1%. Moreover, the segmental

volume data can also be obtained accurately with small error (<3.2% (Collins, 2006)). Collins (2006) showed similar test results, indicating that accurate body volume data (error for both whole-body volume and segmental volume less than 2%) can be obtained by the traditional 3DPS techniques with a specific type of scanner which needs manual post-process.

The traditional 3DPS has been widely used in sports science research. For instance, Schranz et al. (2010) used the traditional 3DPS to measure segmental volume data and investigate the volume difference between rowers and a sample from the normal population. Olds et al. (2013) used this technique to obtain the parameters included in surface anthropometry (breadths, girths and lengths) and segmental volume for somatotype determination.

Given that this technique is non-invasive and without radiation risks, it can be used frequently to visualize body shape variation by overlapping scans in different trials. However, to date, one of the main drawbacks is that use of these methods is limited by expensive hardware and software. The hardware and software needs trained people to operate which decreases the automation of this technique. Furthermore, the manual post-processing such as mesh reconstruction is usually time-consuming and needs technical expertise (Ma et al., 2011).

2.1.6.2 Elliptical Zone Method (E-Zone)

E-Zone (Deffeyes & Sanders, 2005) is a 3D photonic scanning method which can obtain whole-body volume and segmental volumes with inexpensive and portable equipment. E-Zone applies the theory proposed by Jensen (1978), whereby the

segmental shape can be approximated by a series of elliptical cylinders. The front and side view images of a participant are captured by two calibrated cameras as shown in Figure 2. The body outline and segmental endpoints are identified by manual digitizing. After the digitizing process, each body segment can be approximated by a series of elliptical cylinders for the calculation of whole-body volume and segmental volume as shown in Figure 3.

E-Zone has been used for obtaining body segment parameters in several studies (McCabe et al., 2011; McCabe & Sanders, 2012; Oliveira et al., 2015). Compared with traditional 3DPS, the equipment of E-Zone provides an inexpensive and portable solution. Although E-Zone analysis requires a time-consuming manual digitizing process, the intra-assessor and inter-assessor reliability for the acquisition of body volume data remains good (within 5% error for main body segments) (Sanders et al., 2015). Abe et al. (2010) used 3D photonic scanning to compare with E-Zone but only elaborate the error range for accuracy (<30%). To date, there are no data that indicate the accuracy for segmental volumes obtained from E-Zone.

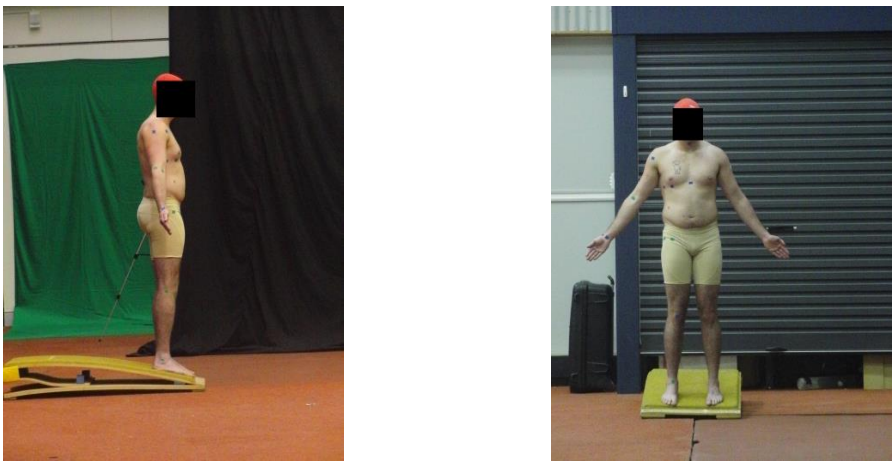

Figure 2 Front view and side view images captured for E-Zone.

Apart from E-Zone, some geometric modelling techniques also use different geometry to approximate body segments and estimate the body volume data. For instance, Yeadon (1990) and Wicke et al. (2009) used a stadium model and an adapted elliptical model separately to approximate the torso segments. Wicke and Dumas (2014) used the adjusted elliptical model to estimate the trunk volume. However, all of those methods rely on manual digitizing and the inter-assessor reliability has not been established.

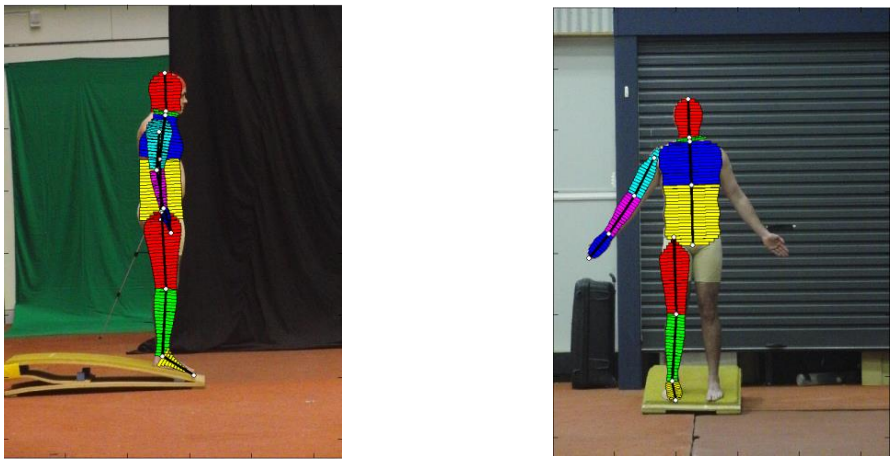

Figure 3 Each body segment can be approximated by a series of elliptical cylinders.

2.1.7 Surface Anthropometry

Manual anthropometry is a portable method for obtaining segmental body volume and body composition. Multiple measurements can be used to estimate segmental volumes from the mathematical formulas (Clauser et al., 1969; Guerrero-Romero & Rodríguez-Morán, 2003; Hanavan Jr, 1964; Katch et al., 1974; Katch & Katch, 1974). A sum of skinfold measures can be used to estimate the body fat underlying the skin which can then be extrapolated to estimate the percentage of body fat (Yuhasz, 1974). However, the body shape variation cannot be visualized by this method.

True skinfolds can only be measured manually. However, surface measurements including length, width and girth can be measured directly or estimated from images or 3D human models. The images include 2D, depth and medical scanning captured by normal cameras, depth cameras (Xtion Pro Live and Microsoft Kinect) and CT, DXA, or MRI scanners. The methods of estimating from medical scanning results and 3D human models are not discussed in this section since they can be used to acquire segmental volumes and whole-body volume directly (Figure 4).

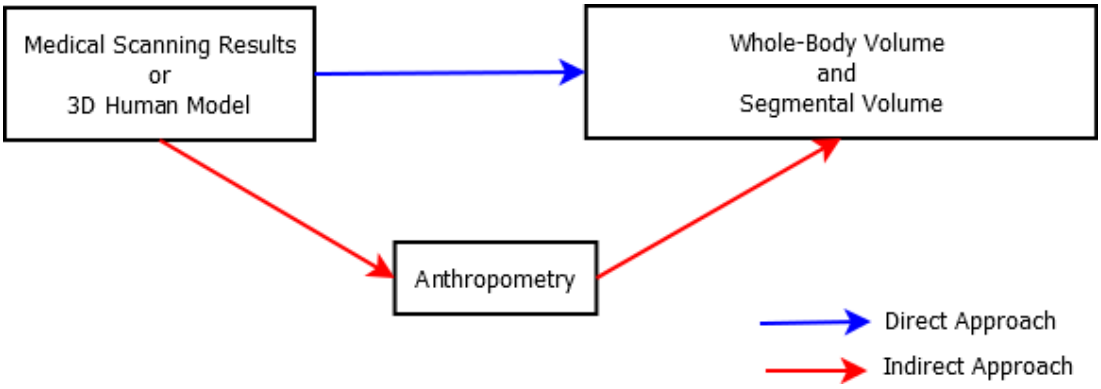

Figure 4 Two approaches to measure the whole-body volume and segmental volumes from medical scanning or 3D human models

The following sections illustrate manual measurement and estimating methods.

2.1.7.1 Manual Measurement

Manual measurement is the most direct technique for acquiring anthropometric data. A trained anthropometrist can measure the anthropometric values accurately and consistently. Manual measurement has been applied widely in ergonomics, sports science, and health monitoring (Norton & Olds, 1996). To reduce errors in measurement, standardized measurement protocols including the equipment,

methodologies, and participants' poses have been designed. Different fields use various measurement protocols. ISO standards such as ISO 7250-1:2008 has been used in engineering applications and International Standards for Anthropometric Assessment (ISAA standard and ISAK measurement protocol (Stewart et al., 2011)) have been popular in the area of sports and health.

The accuracy of this technique for obtaining body composition is dependent upon the participant group and the mathematical models. The standard error of the estimate of generalised equations can be as high as 5% (Durnin & Womersley, 1974). The error of whole-body volume acquisition is 3.3% and the error range of segmental volume is roughly between 5% and 10% (Katch et al., 1974).

Manual anthropometry is a portable, reliable method. However, the time-consuming measurement process, the requirement to have expensive, specific equipment and technical expertise for high-precision measurement is one of the main limitations for body shape monitoring.

2.1.7.2 Estimating from Two-dimensional Images

Anthropometric data can be obtained from 2D images of a participant using anatomical landmarks and measuring the distance on the images with reference to a scale obtained through calibration. Meunier and Yin (2000) and Lin and Wang (2012) captured participants' images from front and side views by calibrated cameras. Then, the anatomical landmarks were detected automatically by observing the changes of body contours. After detecting the anatomical landmarks from the captured images, the individual anthropometric data were obtained. Segment lengths and breadth were

determined as the distance between two landmark points. The circumference was estimated by applying geometric assumptions. The geometric assumption such as elliptical approximation used breadth and depth as the axis of ellipses to estimate the girth measurements which is similar to the concept in previous literature (Jensen, 1978).

However, estimating anthropometric data from 2D images requires silhouette images to detect anatomical landmarks accurately. The challenges of obtaining silhouette images are discussed in Section 2.2.1.1.1. Some body landmarks such as the elbow are not easy to identify from the silhouettes. The anthropometric data may be manually digitised from normal images captured in an ordinary environment (Barron & Kakadiaris, 2000). However, manual digitizing introduces some human error and the breadth might be affected by the poor quality of silhouettes images.

'Image registration' is a computer vision technique to find the corresponding points from two images. The corresponding points in the standard images with known positions of joints can be found in silhouette images. Thus, using this technique, the anatomical landmarks can be found automatically (Chen & Cipolla, 2011). However, one of the main difficulties is that it usually relies on a complex mathematical calculation, which might be time-consuming.

Another challenge is edge detection in the side view images. Participants' arms and body are overlapped in the side view images and the edge of the arms cannot be identified easily from the 2D images and the girths of arms cannot be calculated from the elliptical assumption alone. Therefore, additional assumptions are required. For example, the arm depth may be assumed to be the same as the breadth and the arm

girth, that is, it is approximated as a circle. Alternatively, participants can move their arms and change the overlapping area of their arms and shoulders to obtain the boundaries of their arm separately (Stancic et al., 2009). The complete edge of the arm can be obtained by combining the separated boundaries obtained while moving the arm into different orientations. However, one of the principle limitations is that this technique requires additional time for image processing because it is based on video capturing instead of obtaining a few key frames.

Overall, there is no method which can estimate the anthropometric data from 2D images both quickly and automatically. The limitations in speed or automation increase the difficulties of acquiring body composition and segmental volume from 2D images.

2.1.7.3 Estimating from Depth Images

Depth cameras such as 'Microsoft Kinect' (Microsoft, Redmond, Washington, the U.S.) and 'Asus Xtion Pro Live' (Asus, Taipei, Taiwan) with their corresponding software can detect the joints and segment edges of participants in an image, so they can avoid some difficulties while estimating anthropometric data from 2D images. Samejima et al. (2012) used a Microsoft Kinect to capture depth images and applied Kinect SDK to identify joint positions and edges of human bodies to obtain the anthropometric data. Even though the depth camera reduced the limitation in terms of speed, automation, portability and cost, one of the main limitations was that the poor resolution and noisy nature reduced the accuracy and reliability (depth cameras are discussed in more detail in Section 2.2.1.1.5). To date, there is no study that has used the anthropometric data obtained from depth images to estimate the body composition

and segmental volume. The accuracy and reliability for estimating body composition and segmental volume from depth images is therefore unknown.

2.1.8 Near Infrared Interactance

Near infrared interactance distinguishes between pure fat and pure water based on the absorption of light at 930 nm and 970 nm respectively (Conway et al., 1984). This enables the body composition to be predicted mathematically. Advantages of the system include portable and inexpensive equipment. These methods can complete body composition analysis directly and rapidly with low error for repeated measurement, under 5% (Jensky-Squires et al., 2008; Schreiner et al., 1995).

However, one of the main limitations is that the accuracy of near infrared interactance for a particular group, such as morbidly obese participants, might need further improvement (Mulholland & Rolland, 2012). Compared with the body composition measured by DXA, the error of this technique for different age groups (18-80) is usually higher than 10% (Jensky-Squires et al., 2008).

The specific equipment might also require technical expertise to operate. In addition, it cannot obtain segmental volumes and visualize body shape variation. In other words, only body composition data can be obtained from the near infrared interactance analysis.

2.1.9 Bioelectrical Impedance

Bioelectrical impedance (BIA) is a portable method of determining the total body water and fat free mass based on the different electrical reactance and resistance of fat and water (Kyle et al., 2004). In the BIA test, a small current is introduced through

two electrodes placed on a participant and the electrical impedance can be measured. The body composition data can then be estimated from the electrical impedance. BIA facilities such as some InBody analysers (InBodt Co., Ltd., Seoul, Korea) can measure the segmental fat percentage and segmental mass which can be used for calculating segmental volume data with reference to the densities of different tissues. With its assumptions, BIA can measure the body composition and body volume data rapidly and automatically. The facilities for BIA are much more portable and cost-effective than the scanners of MRI, CT, DXA and the traditional 3DPS.

Because of its high performance in speed, automation, portability and cost, BIA has been used widely. For example, Elferink-Gemser et al. (2012) used the BIA method to investigate the body composition change from the season 2000/2001 to 2009/2010 for around 500 football players in different age groups (from U13 to U19). Konarski et al. (2012) applied this technique and found that the body composition changed significantly during a training and competition macrocycle.

Nevertheless, one of the main limitations of BIA tests is that the results are affected by factors such as exercise and food consumption which alter body fluid (Mulholland & Rolland, 2012). Jensky-Squires et al. (2008) compared the body composition obtained from DXA with different types of BIA systems (In Body 320 and Omron) for participants in different age groups. Although the reliability of BIA is good (the error between 0.6% and 3.0%), the accuracy of BIA compared with DXA was poor, with the error approximately from 3% to 15%. Furthermore, to date, there are no data which have demonstrated the accuracy for segmental volume acquired from BIA and body shape variation cannot be visualized by this method.

2.1.10 Ultrasound

Ultrasound is a portable technique for body composition analysis. It can detect the tissue thickness by measuring the reflection of projected waves (Fanelli & Kuczmarski, 1984; Stouffer, 1968). When the projected ultrasound meets the boundary between two different body tissues such as skin and fat, or fat and muscle, one part of the projected ultrasound is reflected and the other part can pass through the boundaries. Regional tissue thickness can be measured via the measurement of images which depict boundaries where the acoustic properties change.

The instruments that use these techniques are light weight (Mulholland & Rolland, 2012) and some types of ultrasound facilities can predict body composition with acceptable accuracy and reliability (Abe et al., 1994; Fanelli & Kuczmarski, 1984; Takai et al., 2013). Bodymetrix (IntelaMetrix, Inc., Livermore, California, the U.S.) provides an automatic measurement method which can avoid manual digitizing on the ultrasound plots for determining the thickness of different tissue. Sundgot-Borgen and Garthe (2011) suggested that this technique could be used for monitoring the change of body composition variation when athletes attempt to reduce weight. Nevertheless, one of the primary limitations of this technique is the requirement of technical expertise and hardware cost (Mulholland & Rolland, 2012). Moreover, ultrasound methods cannot be used for the acquisition of segmental volumes and visualizing body shape.

2.1.11 The Relationship between Body Composition and Whole-Body Volume

Due to the various densities of muscle, fat and bone, body composition can be calculated from the whole-body volume in conjunction with body mass (Brožek et al., 1963; Siri, 1956). Equation (8) and Equation (9) shows the formula developed by Brožek et al. (1963) and Siri (1956) respectively.

$$\text{Body Fat percentage (Brožek et al., 1963)} = \left(\frac{4.57}{\rho} - 4.142\right) \times 100\% \quad (8)$$

$$\text{Body Fat percentage (Siri, 1956)} = \left(\frac{4.95}{\rho} - 4.50\right) \times 100\% \quad (9)$$

where ρ stands for the whole-body density which is calculated by Equation (10).

$$\rho = \frac{Mass}{(V - r)} \quad (10)$$

where the $Mass$ is the total body mass, V represents the whole-body volume and r stands for the residual volume of air in the lungs and enteric gas within the body.

Two main limitations need to be considered while calculating body composition from whole-body volume. First, it is assumed that the density of body tissues (fat, bone, muscle) and the proportion of bone and muscle are constant between individuals. However, the density of body tissues and the proportion of bone and muscle varies according to different factors including gender, age, disease, etc (Ellis, 2000; Rolland,

2012). These assumptions can lead to errors of 3-4% while using volumes obtained from underwater weighing to estimate body composition (Ellis, 2000).

Second, the residual volume (r) needs to be measured by an extra process for calculating accurate body volume, or estimated. In other words, the whole-body volume does not include air in the body.

Although these limitations are important considerations when developing a tool to assess body composition, the focus of the current work is to develop a tool that can assess body volume with accuracy and reliability. Exploring the shortcomings of converting body volume to body composition per se are beyond the scope of this thesis.

2.1.12 Summary

Table 1 provides an overview of the methods introduced in this section. It can be seen that there is currently no method which can fulfil all the criteria for this research, that is, a fast, automatic, portable, inexpensive system which can measure the body composition (or whole-body volume) and segmental volume with certain accuracy and reliability.

Several methods have been developed for body composition analysis of living humans. Due to the various densities of muscle, fat and bone, water displacement, underwater weighing, air displacement plethysmography and 3D photonic scanning can calculate the body volume and estimate the body composition. Isotope dilution methods apply the assumption that the administered isotope is spread evenly within participants' bodies to determine the body composition. Medical imaging methods, DXA, near infrared interactance, ultrasound and BIA apply doses (such as projecting X-ray and

ultrasound) and observe the different reaction of body tissues (e.g. reflect or absorb the projections) to determine the amount of body tissues. Anthropometric techniques measure the body surface shape and skinfolds to estimate body composition by using mathematical models.

Water displacement, medical imaging methods (CT and MRI), DXA, 3D photonic scanning, surface anthropometry and BIA can be used for segmental volume estimation. Water displacement applies Archimedes' principle to measure the segmental volumes directly. CT, MRI and traditional 3D photonic scanning calculate segmental volumes by using CAD software to edit generated 3D human model. E-Zone uses geometric assumption to estimate segmental volumes. DXA and BIA estimate the segmental volume data with the reference to the volume of different tissues. The segmental volumes also can be estimated from the anthropometric data mathematically.

Even though many methods can obtain both body composition and segmental volumes, only the traditional 3D photonic scanning can deliver the segmental volume and body composition (whole-body volume) with good accuracy and reliability as well as visualize body shape variation without health risk. Applying the 3D photonic scanning techniques for understanding individual body shape and body measurements can complete all measures in one rapid scan which avoids conducting several different time-consuming tests.

Table 1 Comparison for the measurement techniques of body composition and body volume[3].

Techniques	Accuracy	Reliability	Speed	Automation	Portability	Cost	Abilities
Water Displacement Underwater Weighing	Good (body composition and body volume)	Good (body composition and body volume)	Low	Low	Low	Low	Body composition and body volume
Air Displacement Plethysmography	Good	Good	High	Low	Low	High	Body composition and body volume
Isotope Dilution Methods	Poor	Poor	Low	Low	Low	High	Body composition only
Medical Imaging Methods (MRI and CT)	Good (body composition)	Unknown	Low	Low	Low	High	Body composition and body volume
DXA	Good (body composition)	Good (body composition) Poor (body volume)	Low	Low	Low	High	Body composition and body volume[4]
Traditional 3DPS	Good (body composition and body volume)	Good (body composition and body volume)	Low	Low	Low	High	Enable to visualize body shape change
E-Zone	Unknown	Good (body volume)	Low	Low	High	Low	Body composition and body volume
Surface Anthropometry	Good (body composition and body volume)	Good	Low	Low	High	Low[5]	Body composition and body volume[6]
Near Infrared Interactance	Poor	Good	High	Low	High	Low	Body composition only
Bioelectrical Impedance	Poor (body composition) Unknown (body volume)	Poor (body composition) Unknown (body volume)	High	High	High	Low	Body composition and body volume
Ultrasound	Good	Good	High	Low	High	High	Body composition only

[3] The definition of good in accuracy, reliability, high in speed, automation, portability and low in cost means the technique can achieve the corresponding purpose of this research (see section 1.2). For example, the good accuracy means that the error of body composition or whole-body volume estimation is less than 5%. By contrast, the definition of poor in accuracy, reliability, low in speed, automation, portability and high in cost means the technique cannot achieve the corresponding purpose of this research (see section 1.2).

[4] DXA estimates body volume instead of direct measurement.

[5] Expensive, specific equipment and accredited anthropometrists are required for high-precision measurement.

[6] Bioelectrical Impedance estimates body volume instead of direct measurement.

2.2 Methods of Generating Individual Three-dimensional Human Models

In the last two decades, many techniques for 3D scanning technologies have been developed and applied in various disciplines (D'Apuzzo, 2009; Daanen & Ter Haar, 2013). They use different approaches to extract features of the body. The features can be 3D point clouds, 2D silhouettes, or body dimensions to generate individual 3D human models as shown in Figure 5. Active scanning systems use laser or high strength light to project specific patterns (stripes or regular dots) on the participants and extract the features from the deformation of projected pictures. By contrast, passive methods extract the features from 2D images without any projection. Manual anthropometric measurement is a traditional feature extraction approach without any need for image capturing. The features are extracted from representative body dimensions. More details about feature extraction are introduced in Section 2.2.1.

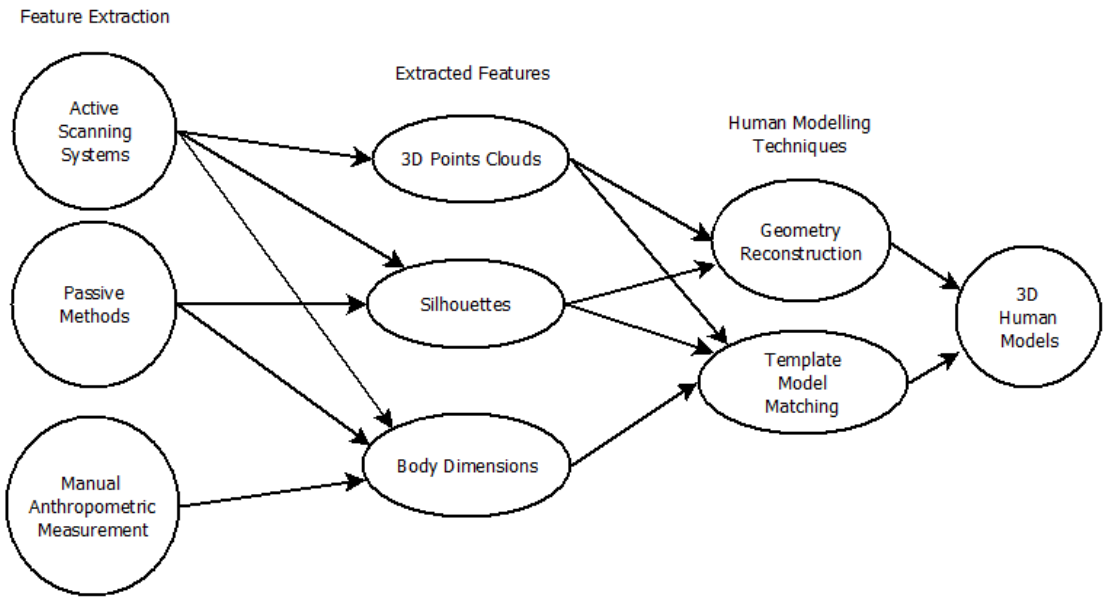

Figure 5 3D scanning technologies

After feature extraction, 3D point clouds, silhouette images or body dimensions can be obtained. The 3D human model can be built from the features by human modelling techniques, geometric reconstruction (only for point cloud and silhouette features) or template model matching (for all three kinds of features, 3D point clouds, silhouettes, and body dimensions). For geometric reconstruction, techniques are applied to combine the information of the 3D point clouds or the silhouettes from different capturing directions (described in Section 2.2.2.1).

Template model matching is another kind of human modelling technique. The shape of a template 3D human model can be deformed to fit the extracted features. For example, a virtual parametric human model is deformed by altering the parameters so the shape of the model can fit the point clouds, as in Figure 6. The deformed human model represents the participant's individual human model. More details about template model matching are described in Section 2.2.2.2.

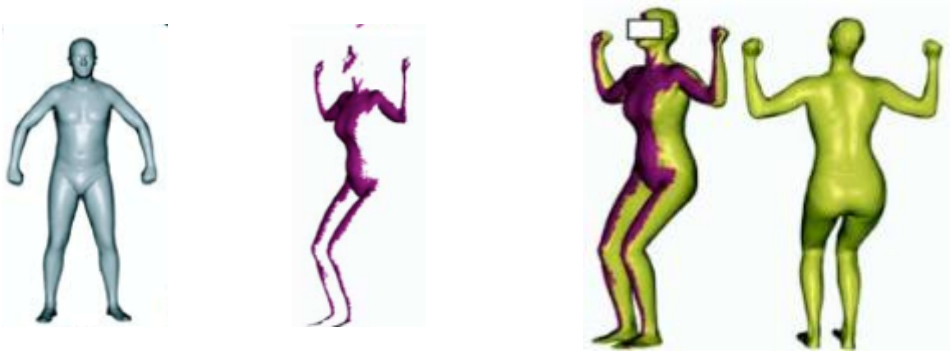

A B C

Figure 6 An example of deformable model matching. (A) A template model which is a parametric model; (B) Extracted features, point clouds; (C) Altering the parameters so the template model (yellow) can fit the features (purple) and obtaining the shape (two views).[7]

[7] The figure is adapted from http://robotics.stanford.edu/~drago/Papers/shapecomp.pdf

2.2.1 Feature Extraction

Three feature extraction approaches including passive methods, active scanning systems and manual anthropometric measurement are described here in Section 2.2.1. Passive methods can extract silhouette and body dimension features. Active scanning can extract three kinds of feature, 3D point clouds, silhouette images, and body dimensions. Manual anthropometric measurements can obtain only body dimension features (Figure 7).

2.2.1.1 Passive Methods

The passive methods are the techniques for feature extraction without any external projection. The features include silhouette images (Section 2.2.1.1.1) and body dimensions (Section 2.2.1.1.2).

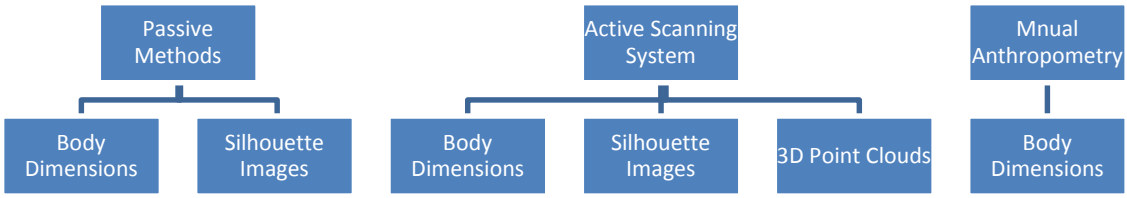

Figure 7 The relationship between feature extraction approaches and the extracted feature types.

2.2.1.1.1 Silhouette Extraction from Passive Methods

Two image processing techniques, ‘image subtraction’ and ‘chroma-key’, are used widely to obtain silhouette images. The following sections illustrate the detail of these techniques.

Image Subtraction

While applying the image subtraction technique, one image without the participant and another with the participant are captured from a fixed camera. The only difference between these two pictures is the participant (foreground) so the same part (background) can be easily subtracted.

Limitations of Image Subtraction

Unchecked light sources and noisy environments creating shadows or moving background objects affect the accuracy of the silhouette. Thus, these methods are usually implemented in indoor environments with stable light sources, single colour backgrounds, and static cameras to extract the silhouette easily.

Chroma-key

Another silhouette extraction technique from 2D images, 'chroma-key', uses 'chroma screens', single colour cloths, to simplify the background. It increases contrast between participants (foreground) and background in colour or hue so the silhouette can be acquired as shown in Figure 8.

Limitations of Chroma-key

Some limitations of the 'chroma-key' techniques continue to exist. First, users of the method need big screens, usually larger than 3×4 metres and time is required to prepare for data capture. If users need to obtain silhouettes from different directions simultaneously, the screens need to be placed around the participants and thus the

whole background system tends to be non-portable. Second, if participants' clothing contains certain colours which are similar to the 'chroma-key screen', the silhouettes extracted are likely to contain errors.

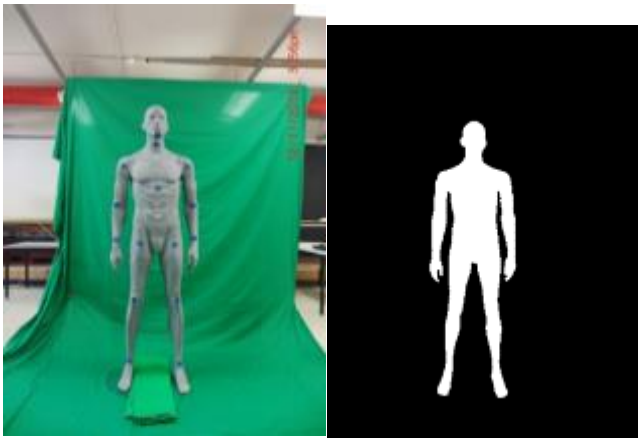

Figure 8 An example of silhouette extraction using the 'chroma-key' technique.

2.2.1.1.2 Body Dimension from Passive Methods

Body dimension features can be extracted also from 2D images. However, silhouette extraction is a necessary initial process for the feature extraction of body shape measurements. For example, Lin and Wang (2012) estimated breadth and depth measurements from silhouette images. Although some active edge detection techniques such as 'canny edge' (Bao et al., 2005) and 'snake' (Kass et al., 1988) have been applied, the testing environment was constrained to laboratories with controlled lighting conditions and simple background.

Anatomical landmark detection is another challenge when extracting body dimensions from normal colour images. Manual digitizing has been the most straight forward method but the reliability and accuracy depend on the user's specific knowledge of

anatomy. Digitizing work increases the post-processing time, especially for large numbers of body dimension extractions. Some automatic digitizing methods have been developed. However, most of them rely on accurate silhouette extraction or need complicated computation (described in Section 2.1.7.2). Although the processing speed of computers has increased, the data processing demands are very high and repeated calculations are required to optimise the results.

2.2.1.1.3 Commercial Active Scanning Systems

Traditional Laser Scanners

Commercial active scanning systems such as traditional 3D laser scanners or structured light systems use projectors and receivers to avoid complicated silhouette extraction tasks associated with 2D images. 3D laser scanners such as VITUS XXL (Human Solutions GmbH, Kaiserslautern, Germany), a typical active scanning approach (Weiss et al., 2011), projects a laser stripe on the participant and uses a camera to record the pattern. Then, 3D point clouds, the points with 3D coordinates, can be collected according to the deformation of the laser stripe.

Traditional Structured Light Systems

Use of structured light systems such as Body Volume Index Scanners (BVI scanners,Birmingham, UK) is the other standard approach for obtaining personal models (Weiss et al., 2011). Similar to laser scanners, the systems project still light patterns onto the human body and acquire the images from cameras. After that, the

systems can also obtain 3D point clouds mathematically from the deformation of the light stripes.

Limitations of Traditional Laser Scanners and Structured Light Systems

Three dimensional laser scanners or structured light systems are usually costly (Tong et al., 2012) and non-portable even though they can generate accurate 3D information rapidly. Hence, users usually need to go to specific locations for scanning. It is not convenient for users to monitor their body shape frequently. Besides, specific software is usually needed to operate traditional 3D laser scanners and structured light systems.

Portable 3D Scanning System

Traditional laser scanners and structured light systems were non-portable which restricts their applications. Hence, some companies provided portable 3D scanning solution for extracting features in order to obtain 3D human models. For instance, Artec Eva, Artec Spider (Palo Alto, CA, USA), HDI Advance (LMI Technology, Delta, BC, Canada), Creaform HandySCAN System (Ametek, Berwyn, PA, USA) used similar principles to the traditional 3D laser scanners and structured light systems to obtain 3D point clouds locally. During the process, an operator usually needs to move the handy scanning head (the scanning system) to capture local 3D point clouds for the scanning objects (the human body) from different directions.

Another portable 3D Scanning System such as Leica ScanStation10 (St. Gallen, Switzerland) used a time-of-flight camera to obtain the 3D information in order to build 3D human models. The time-of-flight camera projects light onto the scanning

object (the 3D human body) and measures the reflection time of the projected light in order to determine the distance between the camera and the scanning object and build the 3D point clouds of the scanning object.

Limitations of Portable 3D Scanning System

Although researchers can conduct tests in different places with a portable 3D scanning system, the cost of portable 3D scanning systems is still high. For instance, the Artec Eva costs €13,700 (around £9,600; currency rate: 24.Nov.2015) which is not including the cost of corresponding software and controlled laptop. Furthermore, an extra person is required to operate a portable 3D scanning system to capture data around the scanning person. This reduces the automation of this solution. The scanning methods conducted by different people might affect the generation of the 3D human models. To date, no regulations or studies indicate how to obtain the 3D model with high accuracy and reliability from a portable 3D scanning system.

2.2.1.1.4 Medical Scanner

Medical imaging systems such as MRI (Pearsall et al., 1994) are active scanning systems. The scanners contain sensors that can observe the variation of projected frequency signal or magnetic fields. In addition to surface point clouds or silhouettes, medical imaging systems reveal the interior structure since the frequency signal passes through the body. In other words, the extracted features provide additional information for 3D human modelling.

Nevertheless, they have similar limitations compared to the surface scanners such as laser scanners and structured light scanners. They are all highly expensive and non-portable. Also, some medical scanners have risks for health and so cannot be used regularly to monitor body shape variations. Besides, the medical scanners usually need certificated licenses to operate and individuals cannot complete the scanning process by themselves.

2.2.1.1.5 Depth Cameras

Recently, 'depth cameras' such as 'Microsoft Kinect' and 'Asus Xtion Pro Live' have been developed. These offer an economical method of building 3D human models (Tong et al., 2012). Each depth camera contains three lenses as shown in Figure 9. The middle lens is a colour sensor which can capture images with red, green and blue components as a normal webcam. The left one is an infrared ray (IR) projector and the right one is an IR sensor. The IR projector can emit a 'speckle pattern' on objects. The IR sensor can capture the deformation of the pattern. The Primesense chip which is also built into the depth camera can calculate the distance between the object and the depth camera by referring to the deformation of the pattern (Garcia & Zalevsky, 2008). This is useful in order to extract features.

Figure 9 A depth camera, Microsoft Kinect[8].

[8] The figure is adapted from https://en.wikipedia.org/wiki/Kinect#/media/File:Xbox-360-Kinect-Standalone.png

The following sections describe the detail about generating 3D point clouds, extracting silhouettes and obtaining body dimensions using depth cameras.

Generating Depth Maps and 3D Point Clouds with a Depth Camera

The associated software, OpenNI (OpenNI, 2012) or Kinect SDK (Microsoft, 2015b), can generate the depth maps (depth images) as shown in Figure 10. The darkness depends on the distance of the depth camera from objects. In addition, the focal length of the IR sensor is fixed and the value of depth (z coordinate) is known so the x and y coordinates can be calculated. Thus, both OpenNI and Kinect SDK can convert depth images to three dimensional (3D) point clouds as shown in Figure 11.

Figure 10 A depth image captured from a depth camera.

Silhouette Extraction with a Depth Camera

Silhouette extractions can be more easily completed from depth images than normal colour images since it can avoid some noise in 2D images such as shadow. For instance, NiTE (OpenNI, 2012), Kinect SDK (Microsoft, 2015b) and Point Cloud Library (Rusu & Cousins, 2011) can complete silhouette extraction as shown in Figure 12. The generation of depth images can avoid some adverse effects of different light directions and illumination since it relies on IR projection and sensing. However, the result might be affected by the sunlight because the sun also emits infrared rays (IR). Thus, data collection needs to be conducted in indoor environments to avoid direct sunlight on depth cameras or participants.

Figure 11 3D Point Cloud can be converted from depth images captured by a depth camera (one 3D point cloud views from two directions).

Obtaining Body Dimensions with a Depth Camera

Both silhouettes and 3D point clouds can be obtained from depth images. In other words, more information can be captured easily from depth images than 2D images. Thus, the skeleton joints can be detected automatically and avoid complex

mathematical computation. The associated software of the depth camera such as Microsoft Kinect SDK and NiTE can detect the joints of the body without any manual digitizing. The joint information can be used for obtaining anthropometric data which can represent body dimension features (Samejima et al., 2012).

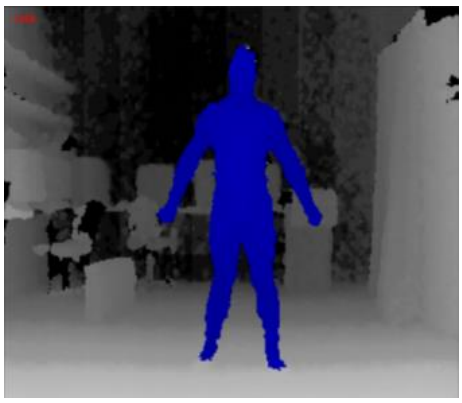

Figure 12 An extracted silhouette from a depth image

Point Cloud Library and Viim SDK (http://www.covii.pt/viim/) are other software options which have similar functions for detecting skeleton joints. The hardware requirement of Point Cloud Library is higher than other software since it uses a graphic card for calculation and Viim SDK requires a licensing fee that prevents free access.

Advantage of Depth Cameras for Feature Extraction

The invention of depth cameras reduces the barriers of delivering active scanning. The depth cameras with their associated software and programmes can provide a fast, portable, inexpensive and automatic method for feature extraction.

‘Microsoft Kinect’ with its SDK is under £150 and the requirement of computer operation is comparatively lower than other active scanning methods. The commercial 3D body scanners are usually controlled by high speed computers with graphic cards.

The cost of hardware for the depth camera application is lower than other active scanning methods including non-portable and portable solutions. Users can also use a laptop to connect a depth camera and complete feature extraction so it is much more portable than other traditional laser scanners and structure light systems. Although some commercial companies also provide transportable solutions for the traditional laser scanners such as Cartesia Portable 3D Body Scanner (Spacevision Inc., Tokyo, Japan) and Body-ScanFit system (Cad Modelling Ergonomics, Firenze Italy), their equipment is usually over thirty kilograms.

The inexpensive and portable depth camera with its associated software and programme can extract 3D point clouds, silhouette and body dimensions in one rapid scan. Furthermore, no extra manual digitizing work is needed for the detection of body edges or anatomical joints. Applying a depth camera to extract three kinds of features is time-efficient because it is fully-automatic without post-processing works.

While applying a depth camera for feature extractions no markers are needed for identifying the body joints. Thus, no expert knowledge of palpation is needed for detection of anatomical landmarks. Because of the fully-automatic feature extraction process, users do not need to learn complicated software and hardware operations. Using the depth cameras for feature extraction is an automatic method to obtain 3D point clouds, silhouette images and body dimensions.

2.2.1.2 Manual Anthropometric Measurements

Manual anthropometric measurement is a feature extraction technique without image capturing. The body dimensions obtained can be used for estimating individual body shapes. Manual anthropometry is the traditional method to obtain body dimensions. Callipers, anthropometric tapes and segmometers are used for measuring surface anthropometric data including girths, lengths and breadths which can represent body dimension features. However, expert knowledge is needed for detecting anatomical landmarks. The specific knowledge is also essential to operate the equipment properly and correctly. Besides, the equipment sometimes is not cost-effective even though it is very portable. For example, the Rosscraft Centurion Kit (Rosscraft Innovations Inc., Vancouver, Canada) costs more than US$1200 (around £770, currency rate: 04.Aug.2015). Lastly, measuring one's own body dimension features is very difficult.

2.2.2 Human Modelling

Human modelling approaches can be applied to obtain 3D human models after obtaining the features (3D point clouds, silhouette images or body dimensions). Geometric reconstruction and template matching are two main human modelling approaches. Geometric reconstruction can combine the features of 3D point clouds and silhouette images and generate 3D human models. Template matching can generate individual 3D human models by deforming the template model to fit the extracted features. The following illustrates the detail of the two different approaches.

2.2.2.1 Geometric Reconstruction

Geometric reconstruction is a traditional method to combine the features (silhouettes or 3D point clouds) captured from different directions. 'Visual hull' is a traditional geometric reconstruction to combine silhouette images and build individual 3D human models (described in Section 2.2.2.1.1). However, traditional visual hull contains many restrictions so some improvements have been introduced (Section 2.2.2.1.2). In addition to combining silhouette features, the 3D point clouds also can be reconstructed geometrically to build individual 3D human models (Section 2.2.2.1.3).

2.2.2.1.1 Visual Hull

Geometric reconstruction techniques can be used in conjunction with the silhouette features to build individual human models. The '4D View Solutions' system (Grenoble, France) applies geometric reconstruction techniques to process extracted silhouette features and build individual 3D human models. After obtaining silhouettes from the images captured from different directions simultaneously, each silhouette can project a 'visual cone' as shown Figure 13. The intersection of the visual cones forms a visual hull, the individual 3D human model, as shown in Figure 14. The whole process of the 4D View Solution is shown in Figure 15.

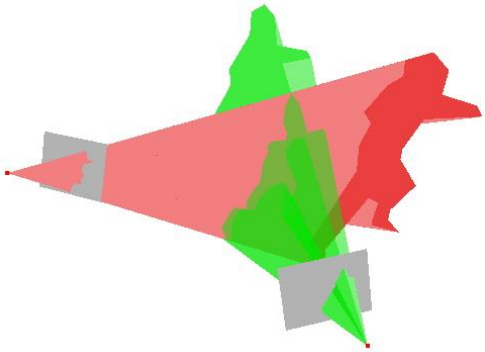

Figure 13 Each silhouette can project a visual cone.[9]

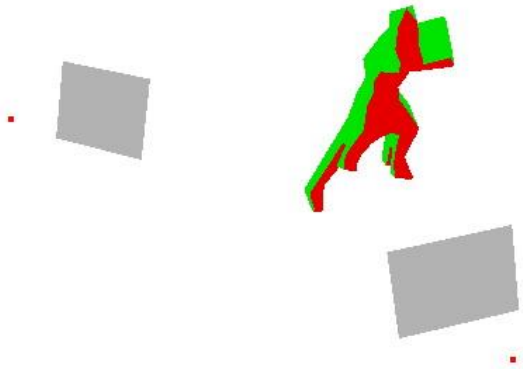

Figure 14 The intersection of visual cones forms a visual hull.[10]

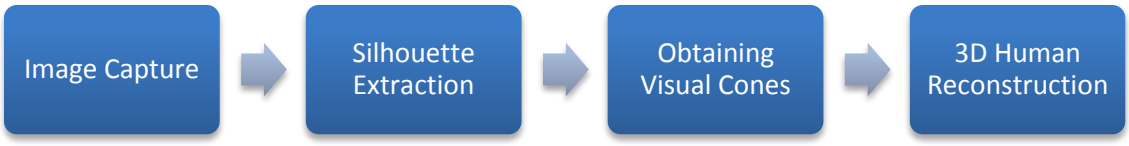

Figure 15 The Process of the 4D View Solution

[9] The figure is from http://en.wikipedia.org/wiki/File:SilhouetteCones.jpg.
[10] The figure is from http://en.wikipedia.org/wiki/File:VisualHull.jpg.

2.2.2.1.2 Limitations of Traditional Visual Hull

Visual hull approaches usually involve some inconvenience and additional processes such as synchronizing the capturing system, correction of lens distortion, camera calibration, post-processing and silhouette extraction. The following sections illustrate the detail of the limitations except the ones of silhouette extraction (described in Section 2.2.1.1). The adopted method of processing unsynchronized and uncalibrated data is introduced and the main reason that it cannot be the human modelling method for this research is explained.

Synchronizing the Capturing System

Humans have non-rigid bodies, which means it is nearly impossible to obtain exactly the same silhouette at different times of sampling. To avoid occlusion problems and to produce a detailed visual hull, capturing images from different directions with multiple synchronized cameras are necessary (Sinha & Pollefeys, 2004). The synchronized cameras can also ensure that most detail can be retained while applying visual hull techniques to reconstruct the shapes. However, multiple cameras increase the cost for obtaining 3D human models which makes the method cannot meet the requirement in terms of cost.

Correction of Lens Distortion and Camera Calibration

Because each camera introduces errors that differ according to the distortion characteristics of the lenses, a straight line can appear as a curved line in the images captured by various cameras. Therefore, distortion correction is usually essential for

obtaining accurate visual hulls. Matusik et al. (2000) used the Sony DFW500 FireWire video cameras which corrects for the lens distortion to capture images for visual hull reconstruction. Nevertheless, these corrections involve extra work and increase the testing time which makes the method cannot meet the requirement in terms of low processing time.

Camera calibration due to the difference of cameras is essential for this kind of technique to project visual cones in the same relative size (Ladikos et al., 2008). For example, different cameras have various focal lengths so the scale of silhouettes should be known from calibration to obtain correct intersections of visual cones. Matusik et al. (2000) and Ladikos et al. (2008) used multiple calibrated cameras for image capturing of visual hull tests. Similar to the correction of distortion, the camera calibrations involve extra work and increase the testing time which means that this method cannot meet the criteria in terms of low processing time.

Processing with Unsynchronized and Uncalibrated Data

Recently, some techniques have been developed to overcome the limitations of visual hull approaches. For instance, Sinha and Pollefeys (2004) used matching techniques to build visual hulls from unsynchronized and uncalibrated video. The Random Sample Consensus based algorithm (Bolles & Fischler, 1981) was used to find the correspondence points in each frame and compare the position of these points. In this way, the position of each camera can be known and the videos can also be synchronized automatically. After that, the visual hull can be used to build the shape of the participant. Nevertheless, the models generated by this method have not been

used for obtaining anthropometric data and body volume data so the accuracy and reliability are still unknown.

2.2.2.1.3 Building Human Model from 3D Point Clouds

The features of 3D point clouds can be reconstructed to generate individual human models. Different reconstruction techniques have been used according to the feature extraction methods. The human model can be built from commercial solutions, multiple depth cameras, a single moving depth camera or a single fixed depth camera. These four main categories are discussed below.

Commercial Solutions

Commercial solutions such as traditional laser body scanners, structure light scanner and portable 3D scanning systems (see Section 2.2.1.1.3) use registration techniques or calculate from camera positions to determine the corresponding points of point clouds captured from different directions. Then, the point clouds can be aligned to form 3D human models. Although the processing time of this reconstruction is fast, the commercial solutions are expensive, and the output models contain some occlusion problems, and post-processing is needed to fill the 'holes' in the models.

Building the Human Model with Multiple Depth Cameras

Extracting 3D point cloud features from multiple directions with a turntable to rotate participants while capturing by a small number of fixed depth cameras can solve occlusion problems inexpensively. Tong et al. (2012) captured the depth images with

three depth cameras from multiple directions while a participant stood on a turntable. Then, non-rigid registration techniques were applied so the 3D point clouds could be combined even though the human had small movements while scanning. The output models become complete without 'holes'. Although the occlusion problems can be solved inexpensively and without post processing, the need to have several synchronized depth cameras makes it complicated for home application (Wang, Choi, & Medioni, 2012). Thus, this system is unsuitable for general use where people usually need to build the model with simple equipment rather than multiple cameras.

Building the Human Model with a Single Moving Depth Camera

The Skanect system (ManCTL, France) simplifies the requirement of capturing devices. It uses a moving depth camera to capture the 3D point clouds from different angles. Then the registration techniques are applied to align the captured 3D point clouds and generate individual 3D human models. The scanning process needs an operator to move the capturing device manually. The scanning method involves long scanning time and the accuracy might be affected by the participant moving and not holding their breath during the process.

Building the Human Model with a Single Fixed Depth Camera

Multiple depth cameras (Tong et al., 2012), or the moving depth camera have been used to overcome the difficulties associated with poor resolution of a single depth camera. A single depth camera can generate only rough 3D point clouds with a lot of noise. It also increases the difficulty of aligning the 3D point clouds captured from different directions since the matching points are hard to find. To overcome this

problem, geometric assumptions can be applied. Wang et al. (2012) used cylindrical models to approximate individual 3D human models so that smooth models could be obtained by using one fixed depth camera. Another solution, 'super resolution', is a technique to improve the resolution of images. The depth images after super resolution can generate precise 3D point clouds which is helpful for reducing noise and aligning the 3D point clouds captured from different directions. Cui et al. (2013) applied this technique to enhance the resolution of capturing depth images and building the individual human models by using single depth cameras. However, the segment endpoints of the human model built with a single fixed Kinect might need manual digitizing, which increases the requirement of processing time and technical expertise.

2.2.2.2 Template Model Matching

Geometric reconstruction needs the features, silhouettes or 3D point clouds extracted from different directions to reconstruct 3D human models. Template model matching can build 3D human models with sparse 3D point clouds (Pirker et al., 2009), single silhouette images (Peng et al., 2009) and few body dimensions (Wuhrer & Shu, 2013). In other words, template model matching can accept incomplete feature information.

The advantage of using models built by template matching is that it is much easier to determine the body segment endpoints on the individual human model transformed from the template than from geometric reconstruction. No other post-processing is required to determine body segment endpoints. This can save time for measuring the anthropometric data and calculating body volume data. Furthermore, it can easily inject animation skeletons (animation rigging) into the generated models referring to the vertex location of joints. The human models can be adjusted in the same posture

which benefits mapping of results and observing body shape variations. For instance, Barmpoutis (2012) generated 3D models by the template matching techniques and mapping two scanning results to demonstrate body shape variation.

The following sections refer to the methods adopted in previous research (Peng et al., 2009; Pirker et al., 2009; Wuhrer & Shu, 2013) to illustrate the concept of template model matching techniques.

A template human model can be deformed into a different body shape (S) by indicating parameters ($p = (p_1, \dots, p_n)$) as shown in Equation (11).

$$\mathrm{S} = d(p) = d(p_1, \dots, p_n) \tag{11}$$

where d is the model deformation function. New human models with various body shapes (S) can be generated. From the generated human models, the features (3D point clouds, silhouettes images and body dimensions) can be extracted. The features extracted from deformable models are called 'measurements' ($m = (m_1, \dots, m_n)$) in the following sections to distinguish the features obtained from real humans.

If M is the function for extracting measurements from a deformable model, the relationship between parameters ($p = (p_1, \dots, p_n)$) and the measurements ($m = (m_1, \dots, m_n)$) can be represented by the composition function M(d) as Equation (12).

$$(m_1, \dots, m_n) = m = \mathrm{M}(S) = M[d(p)] = M[d(p_1, \dots, p_n)] \tag{12}$$

The parameters ($p = (p_1, \dots, p_n)$) are altered so the measurements of the deformed template human model can match the extracted features ($f = (f_1, \cdots, f_n)$) obtained from a real human as shown in Equation (13).

$$(\widehat{p_1}, \dots, \widehat{p_n}) = \hat{p} = \underset{p}{\operatorname{argmin}}(\|f - m\|) \\ = \underset{p}{\operatorname{argmin}}\{\|f - M[d(p)]\|\} \tag{13}$$

where $\hat{p} = (\widehat{p_1}, \dots, \widehat{p_n})$ are the 'best match' parameters which can minimise the errors between the measurements and the features.

After obtaining the best match parameters ($\hat{p} = (\widehat{p_1}, \dots, \widehat{p_n})$), the individual human model ($\hat{S}$) can be determined by Equation (14).

$$\hat{\mathrm{S}} = d(\hat{p}) = d(\widehat{p_1}, \dots, \widehat{p_n}) \tag{14}$$

The deformation of template human models can be categorised into 'statistical modelling' and 'computer graphic transformation'. The statistical modelling is the deformation function built from a body scanning data set (described in Section 2.2.2.2.1). The computer graphic transformation uses geometric techniques to deform 3D human models without any need of a data set for building the deformation function (described in Section 2.2.2.2.2).

2.2.2.2.1 Statistical Modelling

The statistical modelling applied machine learning techniques to build the deformation functions from training data sets. Hence, the deformation function established by statistical modelling generates 3D human models by referring the analysis results of training data sets. For instance, Anguelov et al. (2005) used a commercial whole-body scanner to build posture and body shape data sets (training data sets) as shown in Figure 16. Then, machine learning techniques were used to obtain an average 3D

human model (template model) and established the pose and shape deformation functions from the data sets (Figure 17). The deformation function illustrated how the geometry of average 3D human model changed in different poses or body shape. The average 3D human model and the deformation function is called the SCAPE (Shape Completion and Animation of People) model. The SCAPE model can deform and match the incomplete scanning data to generate a complete 3D human body shape (Figure 18).

Matching the Sparse 3D Point Clouds

Weiss et al. (2011) and Xu et al. (2013) used a SCAPE model to match the 3D point clouds captured by a depth camera (Kinect). The template model matching approach can overcome the poor resolution of the captured depth images (3D point clouds) and build smooth individual 3D human models. Yinpeng et al. (2013) used similar methods to build a tensor-based human body model (TenBo) from a scanning data set. The deformation can generate more accurate body shapes in different poses and also be applied to match the data captured from a depth camera.

Figure 16 The posture data set was built in the study (Anguelov, et al., 2005).[11]

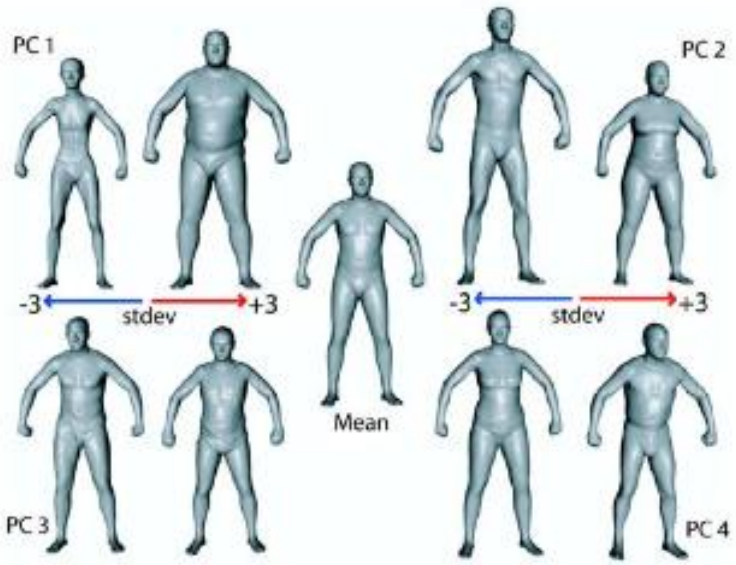

Figure 17 The SCAPE model in the study (Anguelov, et al., 2005).[12]

[11] The figureFigure 16 is from https://graphics.soe.ucsc.edu/private/data/SCAPE/.
[12] The figure is from http://robotics.stanford.edu/~drago/Papers/shapecomp.pdf.

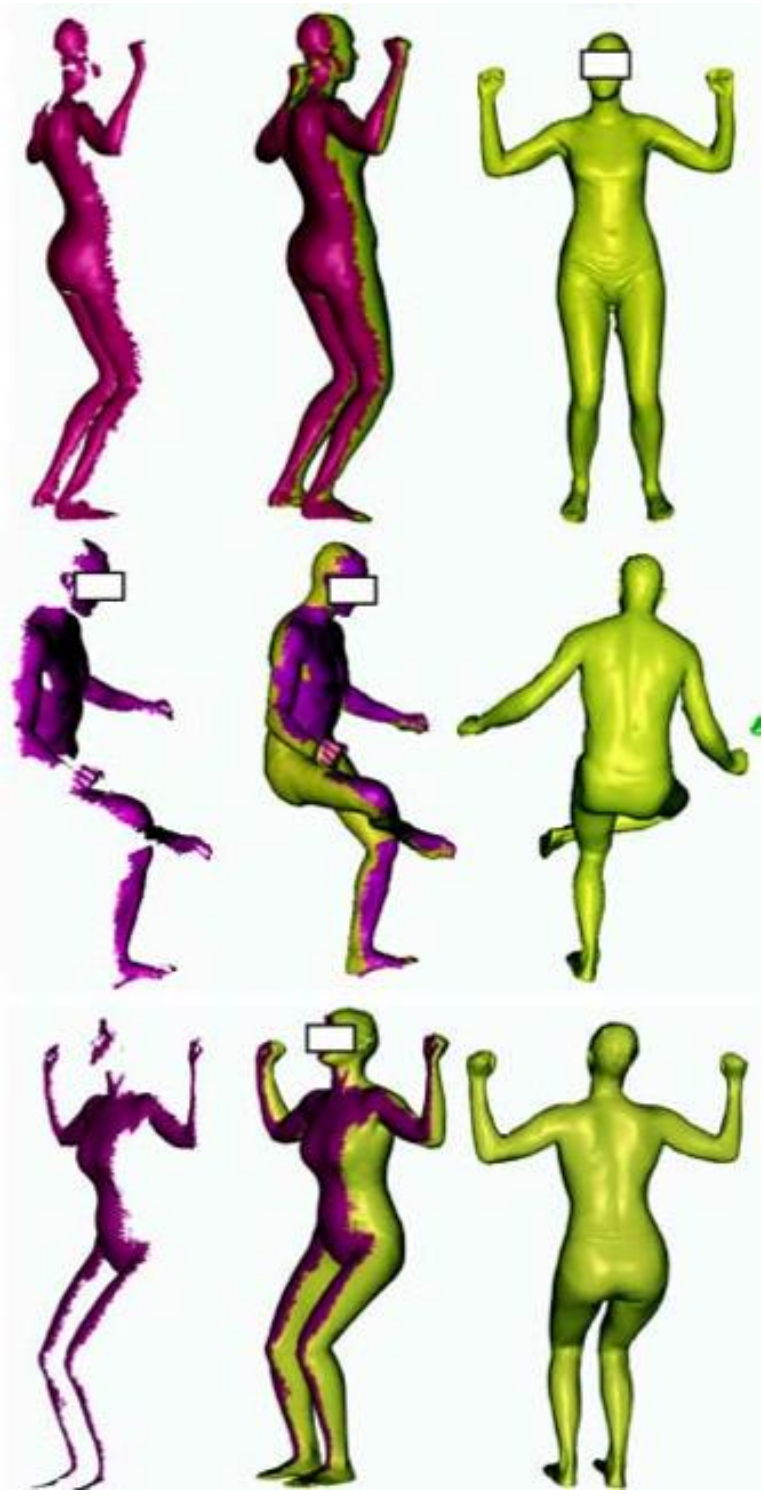

Figure 18 Using the SCAPE model to match the incomplete scanning data to generate a complete 3D human body shape. [13]

[13] The figure is adapted from http://robotics.stanford.edu/~drago/Papers/shapecomp.pdf.

Matching Silhouette Features

In addition to sparse 3D point clouds, template model matching can be applied for silhouette features. Peng et al. (2009) employed Anguelov et al.'s (2005) techniques to reduce the number of cameras so that individual 3D models can be built from single images. The silhouettes were extracted from single images by GrabCut (Rother et al., 2004). GrabCut is an interactive segmentation technique in which users choose the foreground and background parts approximately and the algorithm can segment the foreground automatically. After repeated selection and segmentation, the foreground can be separated completely. Participants' poses were estimated by using clicked points on the human images. After collecting the information, deformable 3D human models were applied to match the pose and silhouette.

Matching Body Dimension Features

Apart from using template models matching the features of sparse 3D point clouds and silhouettes, template models also can be used to match the body dimension features for generating individual 3D human models. Wuhrer & Shu (2011) applied data mining techniques, a procedure of analysing information from statistical aspects, to build a deformable template model. The template model can deform into different shapes to match the personal body dimension features. The individual 3D human models can be built after the matching process.

Limitations of Statistical Modelling

Using statistical modelling, the deformation function built from the data set can enable simulation of different body shapes. The accuracy of the deformed models might rely on very large data sets in various body shapes. In other words, the deformation function built with an athlete's body shape data set might not generate accurate 3D human models for obese groups. Also, the accuracy and reliability of whole-body volume and segmental volume acquisition from the models built by statistical modelling is unknown. Previous research (Weiss et al., 2011; Xu et al., 2013) is focussed on the accuracy of estimating surface anthropometric measurements (segment length and girth) from the deformed template models instead of acquiring body volume. The error of the arm length, chest girth, neck to hip distance, hip girth and thigh girth was between 1.3 to 3.5 cm. However, no relative error data have been elaborated so the accuracy of these techniques cannot be determined.

2.2.2.2.2 Computer Graphic Transformation

Computer graphic transformation is another deformation approach. The template model was established by artists or built from a training data set. The deformation functions were the mathematical transformations used in computer graphics such as free-form deformation (FFD). Thus, the deformation functions built by the techniques of computer graphic transformations do not need a training data set. For example, Lin and Wang (2012) applied the FFD to transform the shape of the template model. The deformed template can match the side and front silhouette images and the individual 3D human model can be built.

MakeHuman (MH) is open source software. The template model of MakeHuman was established by artists and the deformation function of poses and shapes was applied the mathematical transformations used in computer graphics (Bastioni et al., 2008). Using this software can build 3D human models by indicating the values of MH parameters and using computer graphic transformation to deform a base mesh. The values of MH parameters are between 0 and 1 or -1 and 1. Each MH model is deformed from a base mesh (the template mesh) which contains 14596 vertices and 27640 faces by altering parameters such as age, gender, ethnic factors, girths and segmental length, as illustrated by Bastioni et al. (2008). For example, age and ethnic parameters can change the base mesh shape and generate different MH models as shown in Figure 19.

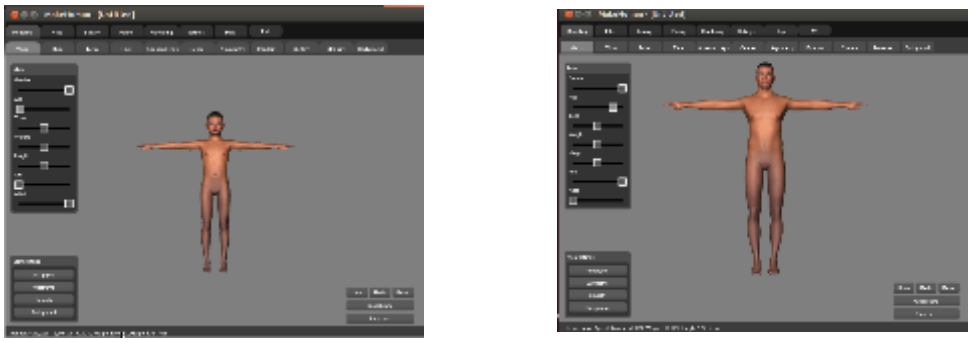

A B

Figure 19 Altering 'age' and 'ethnics' parameters to obtain an Asian child MH model (A) and an African adult model (B)

The MH model has also been used for matching the features (3D point clouds) obtained from multiple cameras (Pirker et al., 2009). This method used the MH model to complement the capturing results so that the lying participants' 3D models could be built. For this method, complex equipment was used to obtain quality 3D point clouds and manual digitizing was needed for indicating the joint positions.

2.2.3 Summary

Passive methods, active scanning systems, and manual anthropometric measurements are three kinds of feature extraction for building individual 3D human models. Many simplified techniques have been developed for passive methods to increase the processing speed and simplify the camera setup (synchronizing and calibration). Extracting silhouettes must be conducted in laboratories where the lighting can be controlled. Although chroma-key techniques can reduce the environment limitation, extra equipment, the chroma-key screen, is necessary and portability is limited.

Manual anthropometric measurements can be used to obtain the features of body dimensions, with portable equipment and within a large range of environmental conditions. However, expert knowledge is needed for determining the location of anatomical landmarks. It is nearly impossible for users to extract their own features by measuring themselves.

Traditional active scanning systems require highly expensive machinery (commercial or medical scanners) and corresponding software but the development of depth cameras seems to have reduced the cost limitation. The inexpensive depth cameras with their corresponding software can obtain 3D point clouds and silhouette features similar to those acquired from commercial scanners. Furthermore, using the £150 portable equipment, Microsoft Kinect or Asus Xtion Pro Live with corresponding software can help users extract features without expert knowledge. In other words, the development of depth cameras provides a fast, inexpensive and portable method of feature extraction.

After feature extraction, human modelling techniques, geometric reconstruction, or template matching, can be employed to obtain individual 3D human models. For geometric reconstruction, the model can reflect the detail. Nevertheless, post processing is needed for the detection of anatomical landmarks (segment endpoints) which are used for measuring segmental volume data. The 3D human models generated by geometric reconstruction methods need manual interpretation for identifying segment endpoints which increases the processing time and the need of expert knowledge.

Conversely, the anatomical body landmarks can be easily identified from the 3D human model generated by template model matching approaches since all vertices are registered. Figure 20 illustrates the concept of registered vertices. After the template mesh (Figure 20 - A) deforms to a new mesh as shown in Figure 20 - B, all the vertices are registered. It means that the order of vertex indexes (i.e. vertex order; 1 – 2 – 4 – 3) and the vertex numbers (4 vertices) of the deformed mesh should be the same as the ones of the original template mesh. If the vertex order (1 – 2 – 3 – 4) or the vertex number (6 vertices) is different from the original template mesh as shown in Figure 20 – C and Figure 20 – D respectively, the vertices are non-registered. For the human model with registered vertices, users only need to identify the vertex indices and the anatomical landmarks can be easily identified. For example, the vertex index of the right wrist is always the same in every MH model. The post-processing can be automatic so the human models are generated quickly and easily. Comparing two deformations of template human models, statistical modelling and computer graphic transformation, the former might need large data sets to simulate accurate individual models for a specific group. To our knowledge, there is currently no available data set

for obese populations. Using computer graphic transformation techniques can reduce the time and cost of the data collection process since there is no need to build a training data set.

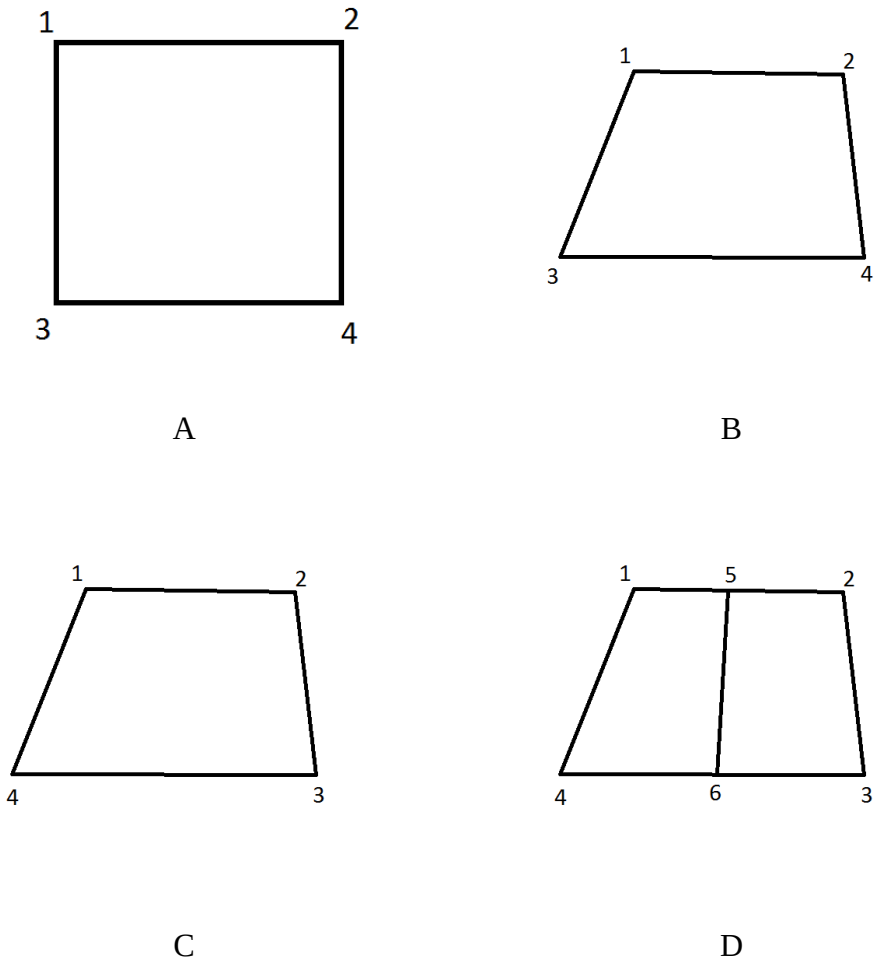

Figure 20 Illustration of registered and non-registered vertices. (A) Template mesh (B) The deformed template mesh with registered vertices (C) a mesh with non-registered vertices (vertex order is different from the template mesh) (D) a mesh with non-registered vertices (vertex number is different from the template mesh)

2.3 The Need for a Body Shape Visualization and Monitoring System

Currently, people care about their health. Numerous body mass monitoring software products and computer programs such as applications (Apps) have been developed. For example, users can record their body mass, exercise and diet in 'Diet Diary' (http://www.medhelp.org/chrome/diet_diary) and changes in body mass can be shown in the quantitative output. Users can also understand and monitor their nutrition status by using this kind of software.

Wearable sensors are used in some sport products such as Nike+ (Nike, Portland, Oregon, the U.S.) to track and record individuals' motion including running distance and speed. People's exercise record can be shown in the graph by the corresponding software or Apps. Users can monitor their progress by observing the record.

Some software can simulate body shape change such as BMI visualizer (http://www.bmivisualizer.com/) but they do not truly reflect the individual variation. Body shape changes can be visualized by some software with commercial 3D photonic scanners such as the body volume index (BVI) scanner which maps two scanning results into one image. Nevertheless, the software is only compatible with specific commercial scanners which are affordable for a limited number of organisations.

Therefore, developing a new body shape monitoring system for a simple scanning system is essential since current systems are not suitable. A new body shape monitoring system is required to provide the information of personal body measurements and allow visualization of body shape.

2.4 Conclusion and Implications

The purpose of this research was to develop a fast, portable, inexpensive and automatic system to build individual 3D human models for acquiring multiple body measurements and visualizing body shape variation. According to the review in Section 2.1, 3DPS is the only method that enables accurate and reliable body volume data to be obtained and body shape to be visualized from a single rapid scan without health risks. However, traditional 3DPSs are non-portable and expensive. The statement of the problem is as follows: Obtaining body volume data from the 3D human model acquired from 3DPS needs technical expertise and time-consuming post processing. Thus, traditional 3DPS techniques need to be adapted to develop a new method for achieving the purpose of this research.

According to the review in Section 2.2, feature extraction and human modelling are two crucial steps for generating individual 3D human models. Microsoft Kinect with its SDK can simplify feature extraction works (Section 2.2.1). Although this technique can provide a fast, inexpensive and portable method for feature extraction, the noise of Microsoft Kinect and different scanning poses affect the quality of extracted features. Therefore, the aim of the first study of this research (Study 1) was to develop approaches for improving the quality of extracted features in order to generate realistic 3D human models for obtaining accurate and reliable body volume data.

To simplify the post-processing work required in quantifying body volume data from 3D human models, this research applied the computer graphic transformation functions in MH to deform the template MH model and generate realistic individual 3D human models. However, the knowledge required to set MH parameters to deform

the template model to match the features extracted from depth images was lacking. Thus, the aim of the second study (Study 2) was to develop an effective procedure and a program for setting parameters to generate individual 3D human models.

By using the program developed in Study 2, individual 3D human models can be generated by in MakeHuman eXchange file format (MHX) easily. However, there is no program which can calculate the whole and segmental volumes from the MHX files directly. To solve this problem, the aim of the third study (Study 3) was to develop a customized program which can obtain body volume data after inputting the MH model (MHX file). The program was required to enable fast and fully automatic output of whole-body and segmental volumes by avoiding manual software operation (e.g. manual digitizing).

The accuracy and reliability of the body volume data acquired from the proposed method in Study 1, Study 2 and Study 3 should be quantified to ensure that it can be used for measurement and monitoring purposes. Thus, the aim of the fourth study (Study 4) was to establish the accuracy and reliability of the developed method.

To enable general users to monitor and visualise body volume and body shape longitudinally an automatic monitoring system was required. Therefore, the aim of the technical description was introduce an automatic monitoring system to help people without technical expertise to measure and monitor their body shape change easily. The processing speed, cost and portability of the system were also examined in this technical description.

Figure 21 shows the four studies and one technical description of this research.

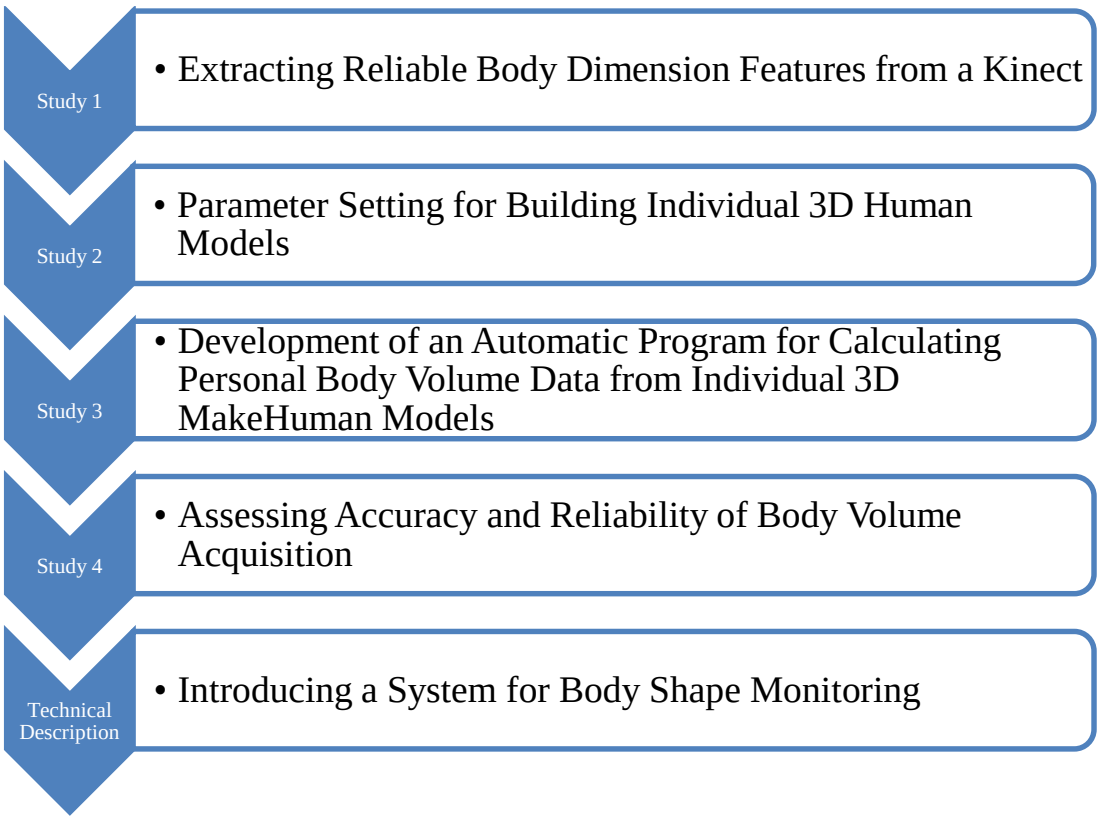

Figure 21 Four main Studies and one technical description of this research

Chapter 3 Study 1. Extracting Reliable Body Dimension Features from a Kinect System

3.1 Introduction

The purpose of this research was to develop an accurate, reliable, fast, automatic, portable, and inexpensive system to build 3D human models for acquiring personal body volume data. Referring to the illustration in Section 2.2, feature extraction is a crucial step to collect information for generating individual 3D human models. For instance, Weiss et al. (2011) extracted the features of 3D point clouds and silhouettes with a Kinect system. Section 2.2.1.1.5 indicated that, using a Kinect system including a depth camera and its corresponding software, the depth images and skeleton joint coordinates can be obtained without manual digitizing or anatomical landmarks. This means that features can be extracted with a portable and cost-effective device automatically (Tong et al., 2012; Wang et al., 2012; Weiss et al., 2011; Xu et al., 2013). For example, Weiss et al. (2011) used a Kinect system to complete the process of silhouette extraction, 3D point cloud acquisition and anatomical landmark detection automatically. Using a Kinect system to extract features is therefore an attractive choice of technique for the purposes of this thesis.

However, the previous studies (Tong et al., 2012; Wang et al., 2012; Weiss et al., 2011; Xu et al., 2013) used geometric reconstruction (see Section 2.2.2.1) and statistical modelling (see Section 2.2.2.2.1) to generate individual 3D human models. There are some limitations of these approaches with respect to this research (see the discussion in Section 2.2). By contrast, computer graphic transformation techniques for human modelling enable to reduce the time and cost for the data collection process (see

Section 2.2.2.2.2 and Section 2.2.3). The features used in previous studies might not be suitable for the computer graphic transformation techniques of this research. Furthermore, no studies have been conducted to investigate which features are most appropriate and how they could be obtained from a Kinect system to generate individual human models for body volume calculation. The following sections discuss 1) what types of features should be selected, 2) how the features can be identified and 3) how to extract features with a Kinect system.

3.1.1 Feature Type Selection

Body dimensions, silhouettes and 3D point clouds are the three types of features which can be extracted from a Kinect system and can be used to generate individual 3D human models (Chen et al., 2011; Peng et al., 2009; Weiss et al., 2011). While conducting template model matching with the 3D point clouds and silhouettes, the pose parameters and shape parameters need to be altered to match the extracted features.

For example, Weiss et al. (2011) altered pose parameters and shape parameters to change the pose and shape of the template model in order to fit point cloud features. By contrast, using body dimension features in template model matching can avoid the process of altering pose parameters and only the shape parameters need to be altered. For instance, Chen et al. (2011) built individual 3D human models by altering the shape parameters only (instead of altering both pose and shape parameters) to deform the template model for matching the body dimension features extracted from 2D images.

Previous research (Peng et al., 2009; Weiss et al., 2011) assumed a human body is assembled by several segments and the segments connect by joints. Three pose parameters are required for each joint to represent the rotation in x, y, z directions for each segmental mesh. Figure 22 demonstrates the rotations of hand segments in three directions. Numerous pose parameters need to be set to illustrate the postures of the template models precisely while conducting template model matching with 3D point clouds or silhouettes. For instance, the method presented by Weiss et al. (2011) altered 192 postures and 60 shape parameters of the template model to fit point cloud features. Setting parameters to deform the template model to match the features is an optimization problem. Increasing the number of parameters makes the problem more complex and a more time-consuming procedure to solve. The process of the method present by Weiss et al. (2011) took approximately 65 minutes to generate an individual 3D human model.

By contrast, using body dimension features in template model matching can avoid the process of setting the pose parameters. This provides an opportunity to generate individual 3D human models rapidly and is therefore an obvious choice when the end goal is a fast method for acquiring individual body volume data.

Previously, some researchers have shown that the body dimension features can be used for 3D human modelling. Van Deun et al. (2011) generated individual 3D human models with body dimension features from manual measurement. Chen et al. (2011) and Lin and Wang (2012) extracted body dimension features from 2D images and built individual 3D human models. However, as neither of these studies used a Kinect system to extract body dimension features, the techniques need manual digitizing or a

special environment to capture images. To date, no study has demonstrated the ability to use a Kinect system to extract body dimension features in order to generate individual human models and calculate body volume data.

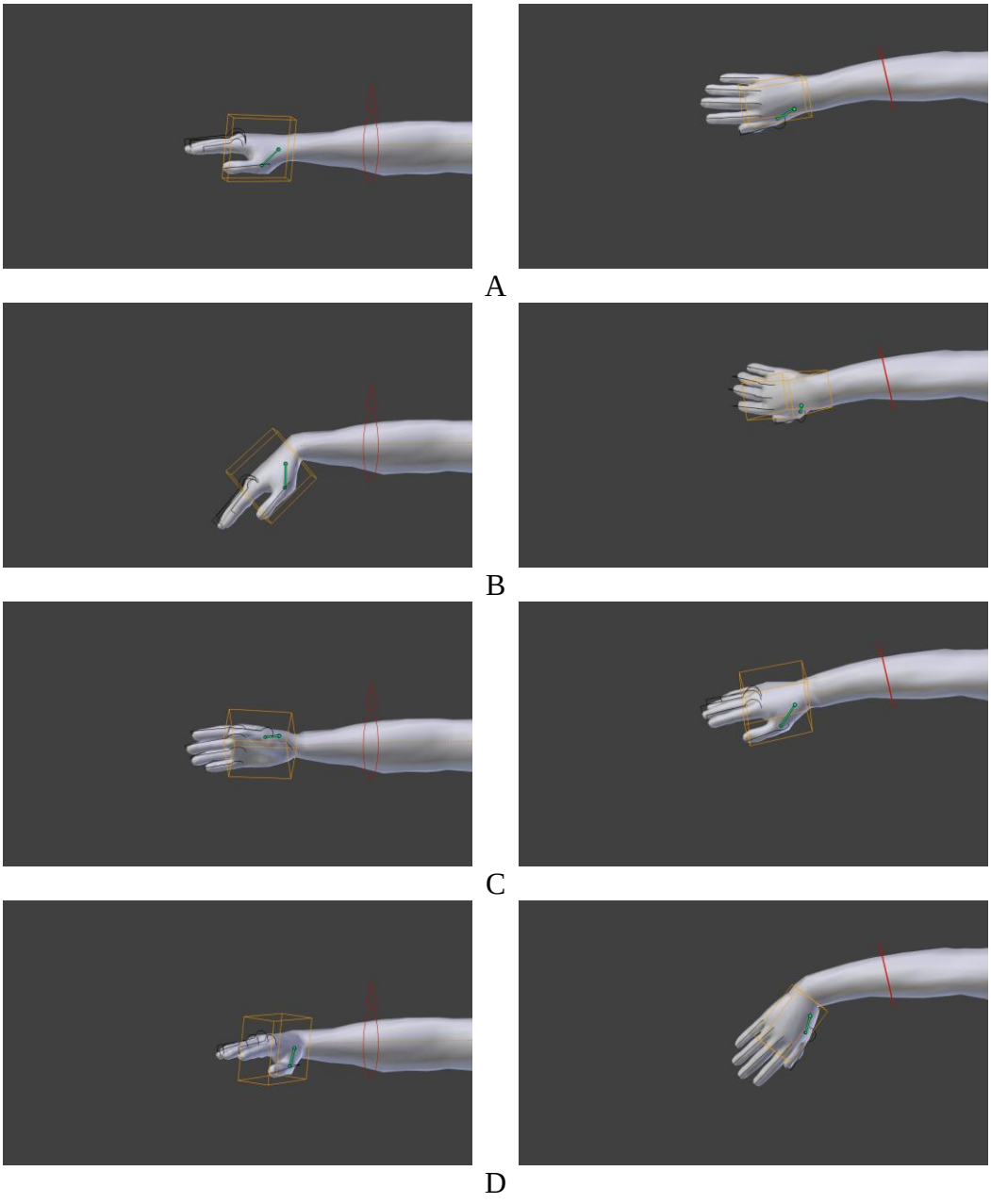

Figure 22 Demonstrating the rotations of hand segments in three directions. (A) Original pose without any rotation (B)The hand segment rotated 45 degrees along the x axis (C) The hand segment rotated 60 degrees along the y axis (D) The hand segment rotated 45 degrees along the z axis

Whilst using a Kinect system to extract body dimension features provides an opportunity to deliver a fast, automatic, portable, and inexpensive process for generating individual human models and calculate body volume data, the answers to two problems are still unknown and have not been investigated in previous studies. The problems are 1) identifying which body dimensions are suitable to be the features used for generating individual 3D human models and 2) determining how to extract these features appropriately with a Kinect system to obtain accurate and reliable body volume data.

3.1.2 Identifying Suitable Body Features to Be Extracted

The shapes of the generated body models are determined by the extracted body dimension features (Chen et al., 2011; Lin & Wang, 2012). Hence, the accuracy and reliability of body dimension features extracted with a Kinect system affect the accuracy and reliability of 3D human model generation and might also influence the body volume acquisition. Thus, the most important criterion for selection of body dimensions to be used as features is the accuracy and reliability with which they can be measured.

The body dimensions include anthropometric and Kinect-based types. The anthropometric type defines the body dimensions with the information of anatomical landmarks. For instance, the upper arm length is the distance between acromiale and radiale. Anatomical landmarks and anthropometric body dimensions can be measured manually with specific protocols such as those adopted by ISAK (Stewart et al., 2011). The anatomical landmarks can be identified also from the depth images captured by a Kinect system to be used for estimating the anthropometric body dimensions

(Samejima et al., 2012). Then the anthropometric body dimensions can be regarded as the representative features for human modelling (Wuhrer & Shu, 2013). Nevertheless, some miscalculation exists in the identification of anatomical landmarks, and the estimation error of the anthropometric body dimensions has been shown to be usually larger than 5% (Samejima et al., 2012). This would lead to poor accuracy while acquiring body volume data since the volume is the product of the linear measurements, and the error would accumulate during the calculation.

Kinect-based body dimensions define the measurements with the information of the Kinect skeleton joints (the Kinect skeleton joints are different from the anatomical landmarks). For example, the distance between two Kinect skeleton joints, 'right hip' and 'right knee', can represent the body dimension 'upper leg length'. Kinect-based body dimensions can be extracted with a Kinect system directly without estimation since the whole process avoids identifying the anatomical landmarks. Theoretically, the accuracy of the Kinect-based body dimension is higher than the anthropometric ones because there is no estimation needed when identifying the Kinect skeleton joints. Previous studies (Samejima et al., 2012; Velardo et al., 2012) have shown that using the Kinect-based body dimension features can provide a more accurate body mass estimation (within 4% error) than the approach applying anthropometric body dimension features (larger than 10% error).

However, Microsoft has not disclosed the relationship between the Kinect skeleton joints (detected by Kinect) and the anatomical landmarks (can be identified by manual palpation). Thus, it is impossible to determine the accuracy of the Kinect skeleton joint detection by comparing with other methods. Therefore, Kinect-based body dimensions

were extracted as the features used for generating 3D human models and it was assumed that the accuracy of these body dimension features extracted from a Kinect system was high enough for estimating body volume. Other research has also relied on the assumption to use a Kinect system for extracting body dimension features and measure body mass accurately.(Velardo & Dugelay, 2012; Velardo et al., 2012).

By contrast, the reliability of body dimension data can be determined easily by repeated measurement. The reliability of the body dimension features extracted with a Kinect system might be affected by the noise of the depth cameras and the scanning pose. The depth cameras do contain some noise (Nguyen, Izadi et al. 2012) as the IR sensor occasionally cannot detect the projection properly and it creates errors in the depth values (z coordinate) as well as miscalculations in other directions (x and y coordinates). As shown in Figure 23, some pixels in the image are black but they are not close to the depth camera.

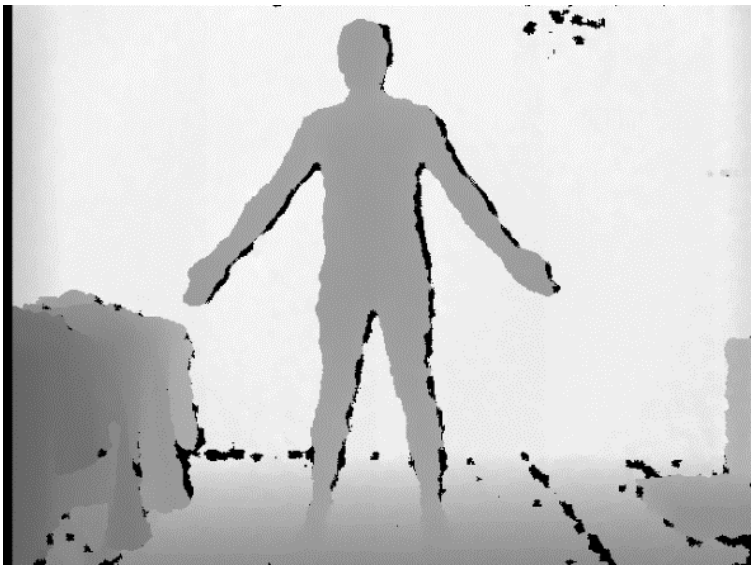

Figure 23 Some pixels in the image are black even though they were not close to the depth camera.

Besides the camera's natural noise, the detection reliability of skeletal joints and body boundaries varies in different scanning poses. The skeleton joint and body boundaries are the most important information in body dimension extraction (Chen et al., 2011; Lin & Wang, 2012) and therefore, the scanning poses might also affect the reliability of extracted candidates. To date, no study has examined the reliability of body dimension assessments using the Kinect system.

3.1.3 How to Extract Features with a Kinect System

Using the appropriate method to extract accurate and reliable body dimension features is helpful to improve the accuracy and reliability of the body volume data acquired from generated individual 3D human models. Because the accuracy of body dimensions extracted with a Kinect system cannot be evaluated, this study aimed to examine the reliable body dimension features and their extraction methods.

To date, there has been a paucity of studies conducted to investigate which body dimensions are most reliable and how to extract those features with a Kinect system. Reliability is affected by two main sources of variability - the noise of cameras, and the poses of the participants adopted for scanning. Theoretically, reliable body dimension features can be obtained by the extraction method which can avoid these two sources of variability while extracting body dimensions. Thus, the first aim of this study was to find an ideal extraction method which minimizes these two sources of variability. Although the ideal extraction method in this study can improve the reliability of extracted body dimensions, the reliability of a small number of body dimensions might still be poor and cause large errors when calculating body volumes.

Therefore, the second aim was to investigate which body dimensions extracted by the determined feature extraction method were highly reliable and could be then used as the features in 3D model generation in the following studies.

Four different extraction protocols were followed, and reliability of body dimensions were compared. Reliable body dimensions with their extraction protocols were subsequently selected for individual human model generation in the subsequent studies.

3.2 Method

3.2.1 Overview

Twenty-two candidates of body dimensions (stature, mass, age, gender, neck height, upper arm length, lower arm length, upper leg height, lower leg length, neck to waist length, waist to hip length, shoulder distance, neck breadth, upper arm breadth, lower arm breadth, torso breadths in four different levels, thigh breadth, calf breadth and ankle breadth) were chosen for feature selections by referring to the MakeHuman 'macro' and 'measure' parameters. These 22 candidates are the potential body dimension features used in this study. If the reliability of the candidate is good enough (less than 5% TEM), the candidate can be a feature used for generating 3D human models. The selection criteria, 5% TEM, is referred to in previous studies (Collins, 2006; Sanders et al., 2015) and the criteria of reliability defined in the research aim (see Section 1.2.2). The 5% error margin is frequently adopted as a useful criterion for repeated measurement Sanders et al. (2015).

Among these candidates, stature and mass were determined by ISAK measurement (Stewart et al., 2011) while age and gender relied on human input. The other candidates were extracted by the depth images captured by a Kinect system.

3.2.2 Participants

Participants were recruited through e-mail or bulletin advertising. All male participants who could attend the test sessions between 18.Mar.2014 and 4.Apr.2014 were invited. This research concentrated on male participants since the cloth for females (e.g. bra) might generate high errors for body volume measurement using 3DPS and lead to errors in analyses. In total, 17 male participants signed an informed consent form (see Appendix A and Appendix A) and completed all the tests. Ethics approval was given by Moray House School of Education Research Ethics Committee at the University of Edinburgh. The masses of the participants ranged from 64.5kg to 97.1kg while the statures ranged from 162.8cm to 189.5cm. Table 2 describes the participants' ages, anthropometric data and their somatotypes. Figure 24 is the somatotype plot and Figure 25 shows the somatotype categories for the participants. Each participant's anthropometric data were measured manually following the ISAK protocol (Stewart et al., 2011) by an accredited anthropometrist. The intra relative TEM for the manual anthropometric measurements used for somatotype detection is shown in Table 3. The intra relative TEM, which calculated the ratio of intra absolute TEM and variable average value, is defined as in the following equations (Equation (15) and Equation (16)) (Perini et al., 2005).

$$\text{Intra absolute TEM} = \sqrt{\frac{\sum_{i=1}^{N}(M_{i1} - M_{i2})^2}{2 * N}} \tag{15}$$

$$\text{Intra relative TEM} = \frac{\text{Intra absolute TEM}}{\frac{\sum_{i=1}^{N}(M_{i1} + M_{i2})}{2 * N}} * 100\% \tag{16}$$

where N is representative of the number of participants, M_{i1} and M_{i2} denote the first and second measurements separately obtained for the i^{th} participant. A lower relative TEM value indicates better reliability. The relative TEM for intra-reliability were calculated with Microsoft Excel (Microsoft®).

The information shown in Table 2, Figure 24 and Figure 25 was obtained by the associated software, Somatotype (http://goulding.ws/somatotype/).

Table 2 The participants' age, anthropometric data and their somatotypes in this research. The definition of SAD is "the three-dimensional distance from a profile to the mean of all profiles" and the definition of HWR is "calculated as stature in cm divided by mass in kg raised to the power 1/3" referring from the somatotype report (http://goulding.ws/somatotype/).

Variable	Median	Mean	SD	Range
Endomorphy	2.9	3.2	1.1	1.4 – 5.0
Mesomorphy	4.6	5.1	1.5	3.2 - 7.9
Ectomorphy	2.1	2.2	1.1	0.5 - 4.6
SAD	1.9	1.9	0.9	0.4 – 3.5
HWR	42.0	42.0	1.7	39.1 - 45.3
Age (year)	31.6	30.2	6.0	20.7 - 41.1
Stature (cm)	184.4	181.5	7.6	162.8 – 189.5
Mass (kg)	82	81.3	9.3	64.5 – 97.1
Triceps SF (mm)	7.9	9.2	3.6	5.0 – 15.9
Subscapular SF (mm)	12.7	13.2	3.9	6.7 – 18.9
Supraspinale SF (mm)	11.7	11.4	4.5	4.5 – 20.0
Calf SF (mm)	7.7	8.2	3.3	4.0 – 15.4
Arm Girth (cm)	34.5	34.4	3.2	28.1 – 39.5
Calf Girth (cm)	37.1	38.0	3.0	33.7 – 43.3
Humerus Breadth (cm)	7.1	7.1	0.5	6.5 – 8.4
Femur Breadth (cm)	9.7	9.9	0.6	9.1 – 11.3

Table 3 The intra relative TEM (%TEM) for the anthropometric measurements used for somatotype detection

Measurement	Intra Relative TEM	Measurement	Intra Relative TEM
Statures in cm	>0.1	Calf SF in mm	1.9
Mass in kg	0.2	Arm Girth in mm	0.3
Triceps SF in mm	2.0	Calf Girth in cm	0.3
Subscapular SF in mm	2.0	Humerus Breadth in cm	0.4
Supraspinale SF in mm	2.1	Femur Breadth in cm	0.5

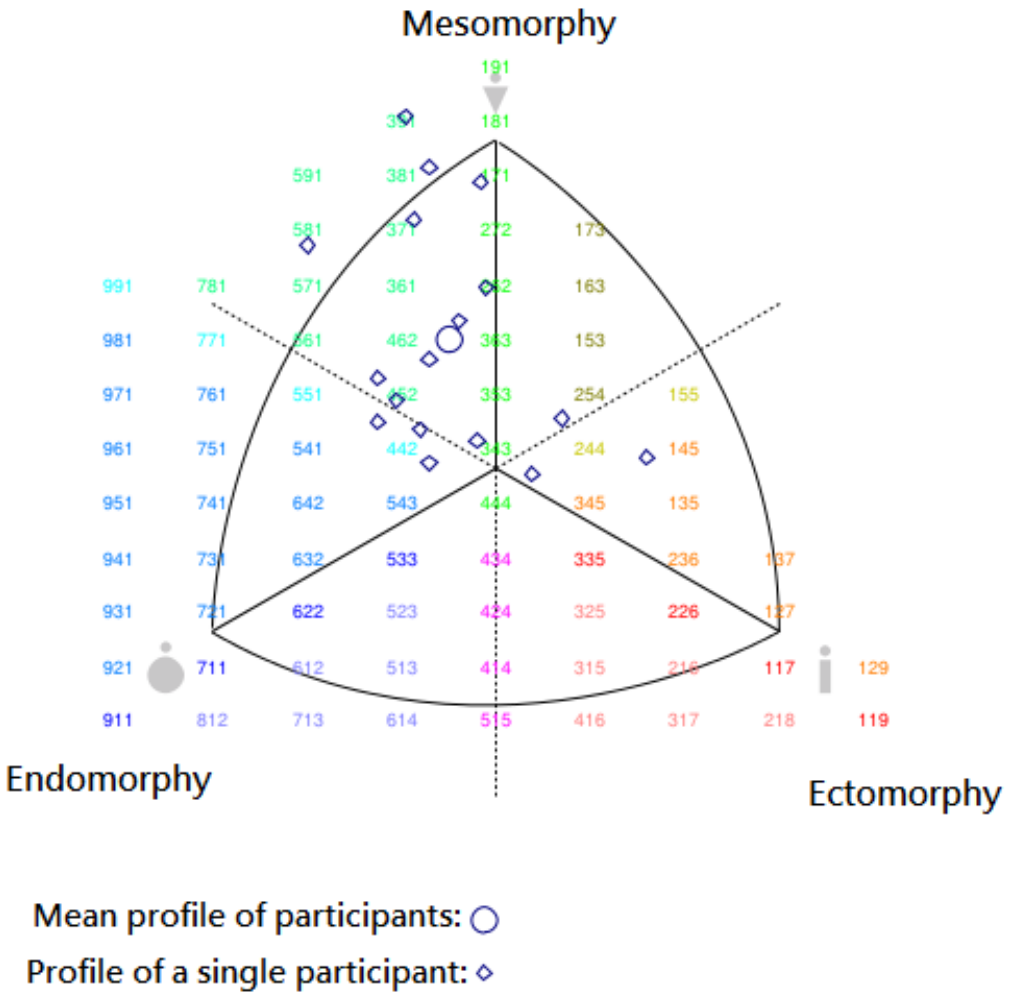

Figure 24 Somatotype plot of participants.

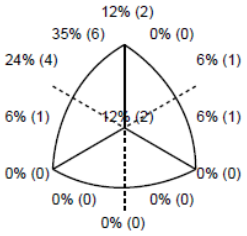

Total number of profiles in document: 17

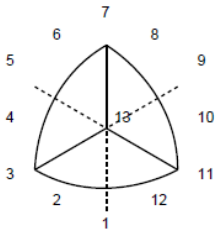

Category Chart Key

1) endomorph-ectomorph
2) ectomorphic endomorph
3) balanced endomorph
4) mesomorphic endomorph
5) mesomorph-endomorph
6) endomorphic mesomorph
7) balanced mesomorph
8) ectomorphic mesomorph
9) mesomorph-ectomorph
10) mesomorphic ectomorph
11) balanced ectomorph
12) endomorphic ectomorph
13) central

Figure 25 Somatotype categories of the participants.

Participants were requested to wear close fitting suits such as triathlon pants and a polyester swimming cap during the tests as shown in Figure 26.

Figure 26 An example of the clothing worn by the participants.

3.2.3 Data Collection

The depth camera (Microsoft Kinect) was positioned approximately 0.9 metres above floor level and 2 to 3 metres in front of the participant so that the whole-body image could be captured as shown in Figure 27. The distance, depending on the height of the participants, ensured that the images of the whole-body were captured and the accuracy and precision of the 3D point clouds were maximised for feature extraction. In this research, all depth images were collected with good lighting conditions and avoided natural or halogen light, as per the instruction of Microsoft (Microsoft, 2015c).

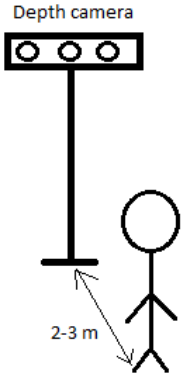

Figure 27 Arrangement while depth image capturing

Participants were requested to stand with two poses (PSI pose and natural pose as shown in Figure 28) during the repeated depth image capturing. The 'PSI pose' is the calibration pose defined by the Kinect chip producer, Primesense (PrimeSensor, 2012). The 'natural pose' was adapted from previous research (Deffeyes & Sanders, 2005; Samejima et al., 2012). Images of participants were captured twice in each pose, and each capture collected 30 depth images. To avoid a breathing artefact, participants were asked to breathe out the air in their lungs to end-tidal level before the

commencement of depth image capturing and hold their breath until the test process finished (approximately 10 seconds).

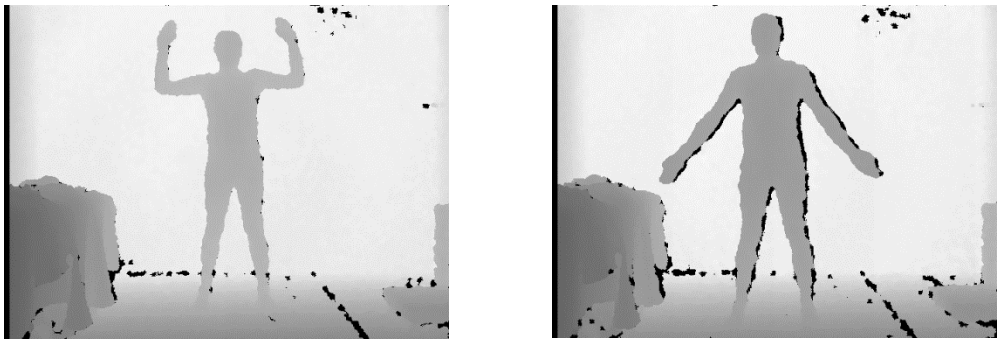

PSI pose Natural pose

Figure 28 The PSI pose and the natural pose.

3.2.4 Experiment Design

Four different extraction protocols were conducted in this study. The first was to extract candidates from single depth images with the PSI pose (candidate extraction 1). Secondly candidates were extracted from single depth images with the natural pose (candidate extraction 2). The third protocol was to extract candidates from multiple depth images with the PSI pose (candidate extraction 3). The final method was to extract candidates from multiple depth images with the natural pose (candidate extraction 4). The reason for using multiple depth images is for applying the customized filter (see Section 3.2.5) to reduce the noise effect.

The collected data (four sets of 30 depth images in two scanning poses) were separated into eight datasets for the four different extraction protocols as shown in Figure 29. The eight datasets include four single image datasets and four multiple image datasets in the PSI and the natural poses. The multiple image dataset acquired all captured images (30 depth images for each participant for one trial) from the collected data

while the single image dataset only obtained the first captured images (one depth image for each participant for one trial) from the collected data. After extraction, the reliability of the candidates extracted by different protocols was compared in order to select the most reliable candidates as features and to determine their extraction procedure.

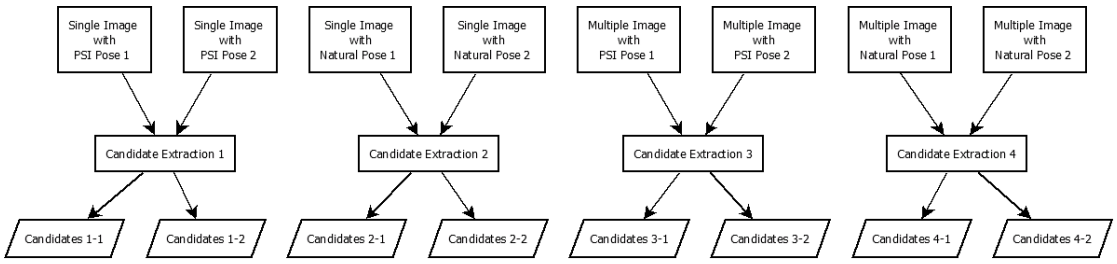

Figure 29 Eight datasets for the four different extraction protocols.

3.2.5 Candidate Extraction

3.2.5.1 Candidate Extractions for the Single Image Dataset

For the single image dataset, the candidate value of each body dimension was extracted from the depth images directly. The extraction of each candidate is illustrated as follows.

Neck height was the distance between two skeletal joints ‘head’ and ‘neck’ as shown in Figure 30. Both skeletal joints were defined by Kinect SDK.

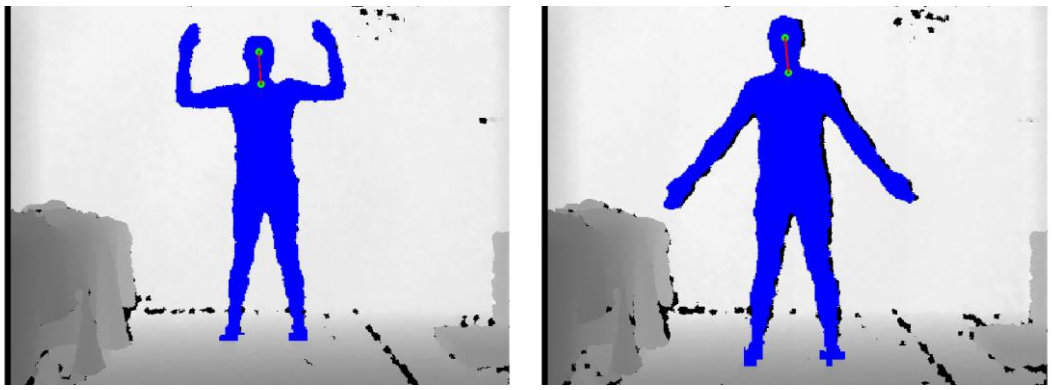

Figure 30 Neck height was the distance between two horizontal planes which determined by two skeletal joints 'head' and 'neck'.

Upper arm length was the distance between 'right shoulder' and 'right elbow' as shown in Figure 31. (The limb skeletal joints are on the left side in the following figures since the depth camera captured the opposite mirror depth image.) 'Right shoulder' and 'right elbow' were both skeletal joints defined by Kinect SDK.

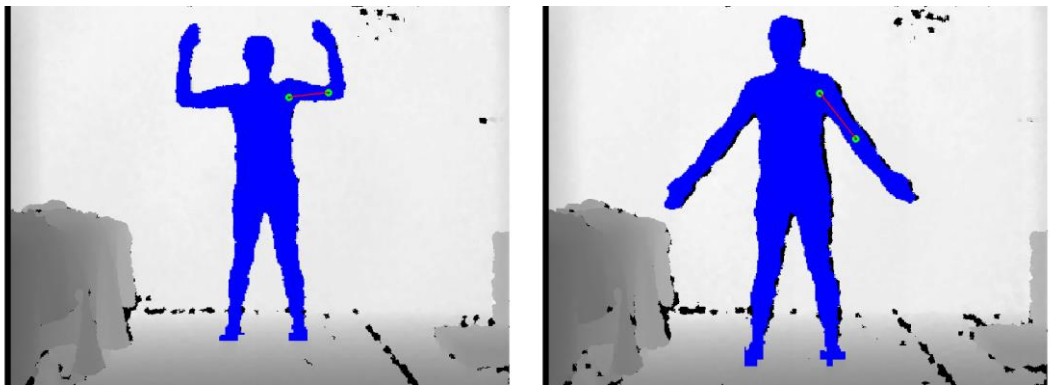

Figure 31 Upper arm length was the distance between 'right shoulder' and 'right elbow'.

Lower arm length was the distance between 'right elbow' and 'right wrist' as shown in Figure 32. The position 'right elbow' and 'right wrist' was determined by using Kinect SDK.

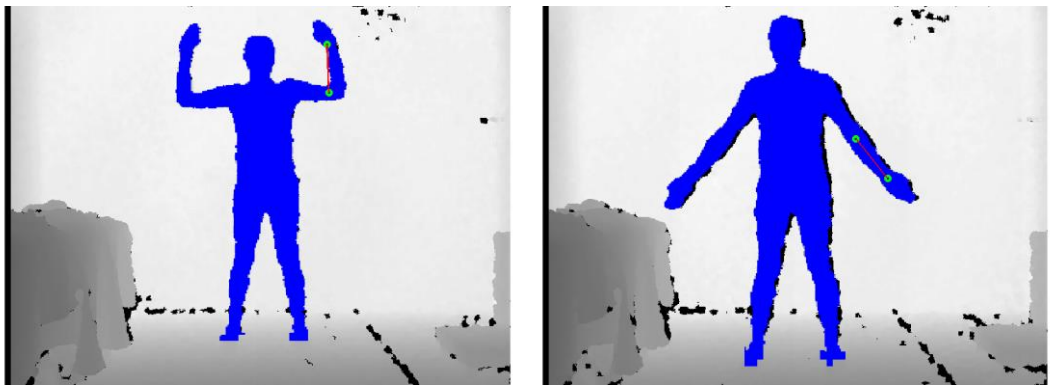

Figure 32 Lower arm length was the distance between ‘right elbow’ and ‘right wrist’.

The definition of upper leg height was the distance between ‘right hip’ and ‘right knee’ as shown in Figure 33. The skeletal joints, ‘right hip’ and ‘right knee’, were both detected by the software, Kinect SDK.

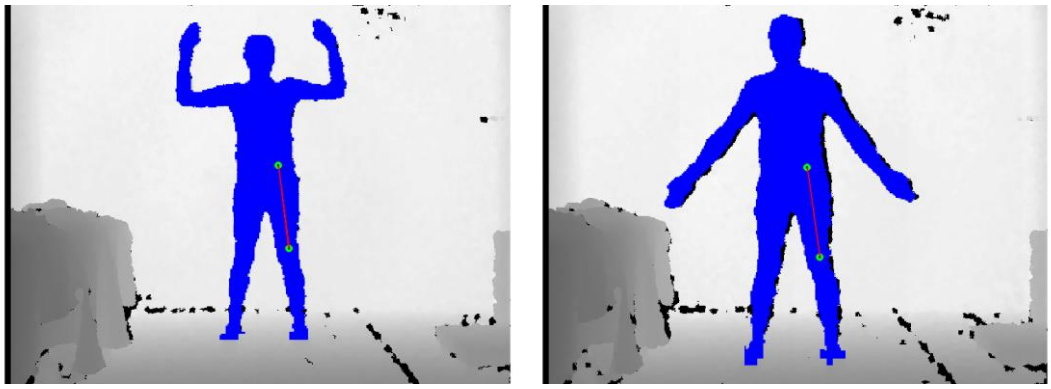

Figure 33 The definition of upper leg height was the distance between ‘right hip’ and ‘right knee’.

Lower leg height was defined as the distance between ‘right knee’ and ‘right ankle’ as shown in Figure 34. ‘Right knee’ and ‘right ankle’ were detected by Kinect SDK.

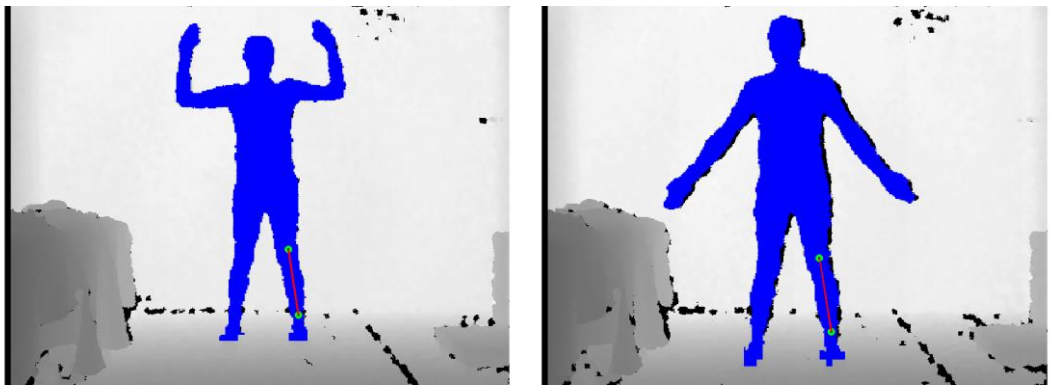

Figure 34 The definition of lower leg height was the distance between 'right knee' and 'right ankle'.

Neck to waist length was defined as the distance between skeletal joints, 'mid spine' and 'neck' as shown in Figure 35. Both skeletal joints were defined by Kinect SDK.

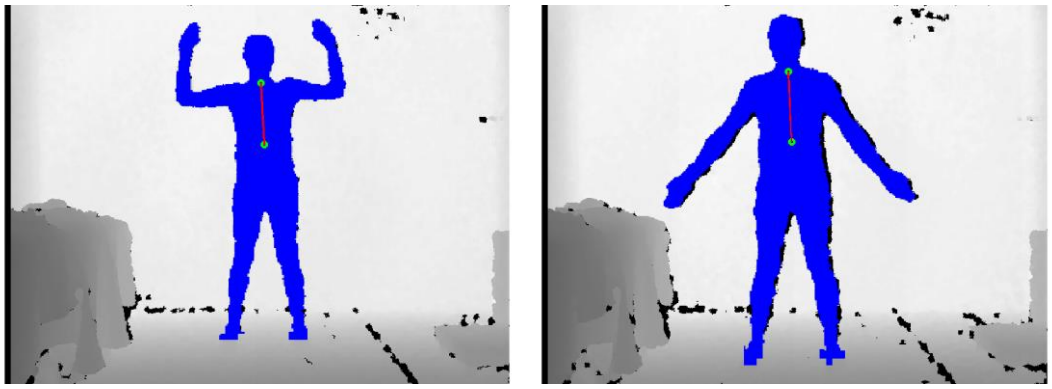

Figure 35 Neck to waist length was defined as the distance between skeletal joints, 'mid spine' and 'neck'.

Waist to hip length was the perpendicular distance from the skeletal joints 'mid spine' to the horizontal middle level between 'right hip' and 'left hip' as shown in Figure 36. 'Mid spine', 'right hip' and 'left hip' were the skeletal joints defined by Kinect SDK.

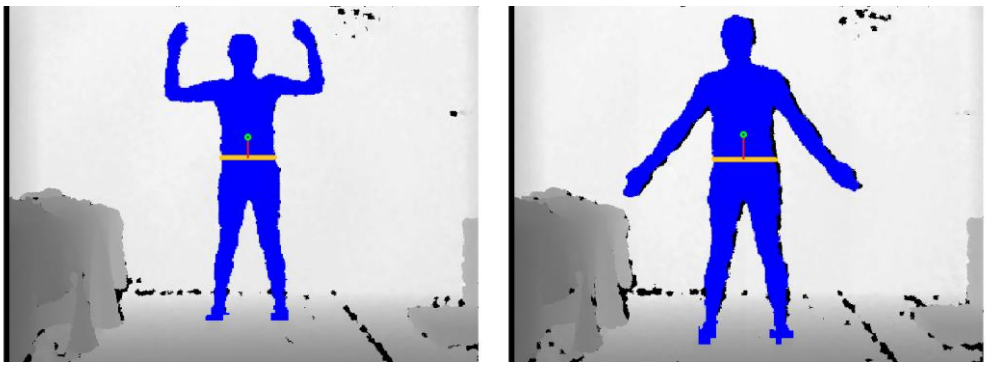

Figure 36 Waist to hip length was the perpendicular distance from the skeletal joints 'mid spine' to the horizontal middle level between 'right hip' and 'left hip'.

Shoulder distance was defined as the distance between two shoulder skeletal joints, 'right shoulder' and 'left shoulder', as shown in Figure 37. 'Right shoulder' and 'left shoulder' were both found by Kinect SDK.

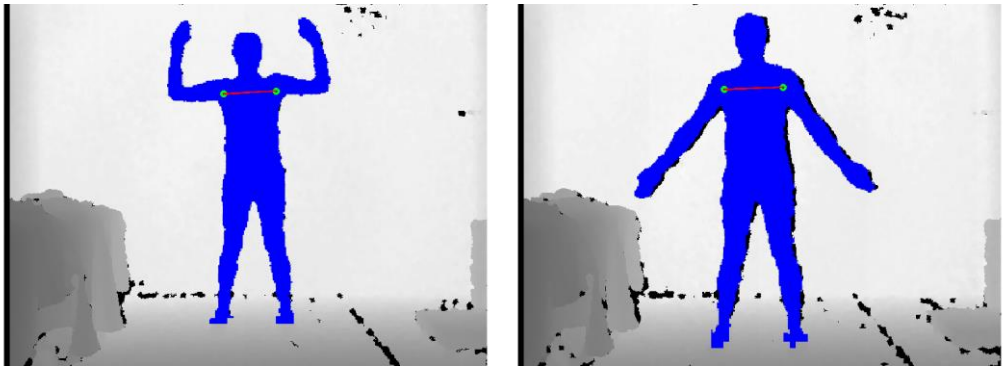

Figure 37 Shoulder distance was defined as the distance between 'right shoulder' and 'left shoulder'.

Neck breadth was defined as the distance across the narrowest horizontal level on the neck segment as shown in Figure 38. The two endpoints of neck segment were defined as 'head' and 'neck' ('head' and 'neck' were the skeletal joints defined by Kinect SDK).

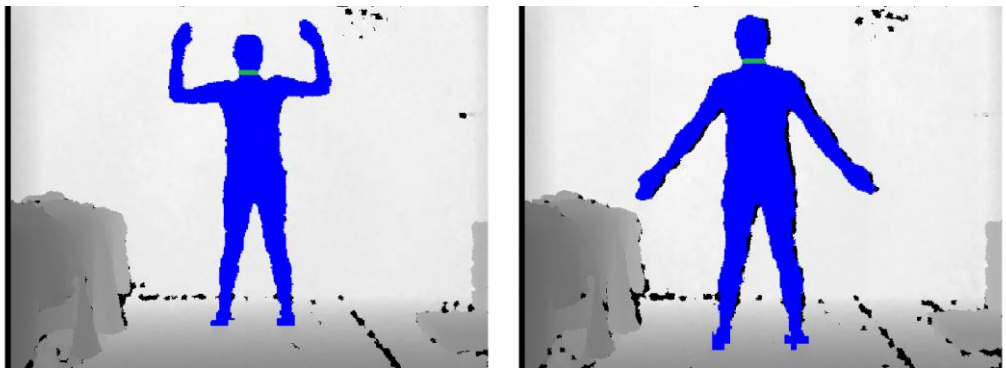

Figure 38 Neck breadth was defined as the narrowest horizontal level on the neck segment.

Upper arm breadth was defined as the width on the defined level on the upper arm as shown in Figure 39. The distance from the defined level to the ‘right shoulder’ was the same as the ones from the defined level to the ‘right elbow’ (‘right shoulder’ and ‘right elbow’ were the skeletal joints defined by Kinect SDK).

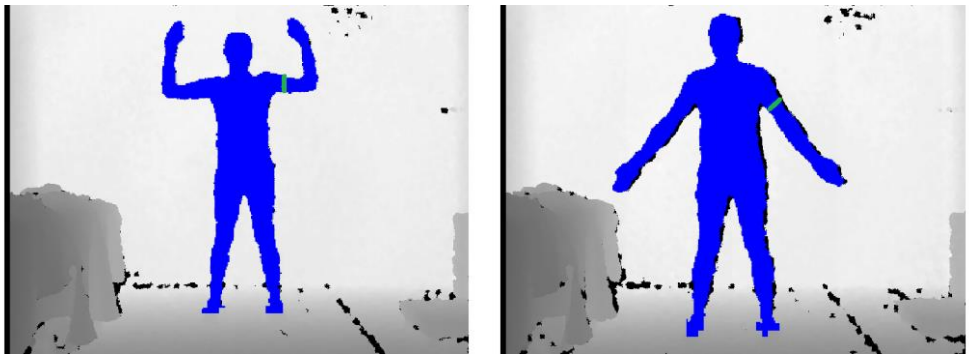

Figure 39 Upper arm breadth was defined as the width on the defined level on the upper arm.

It was difficult for the participants to keep their upper arms exactly horizontal to the floor during the capturing with the PSI pose. Also the upper arm must not be perpendicular to the floor during the capturing with natural pose. Hence, perpendicular to the width of the vertical or horizontal level between ‘right shoulder’ and the ‘right

elbow' was used to estimate the upper arm breadth. The width of the horizontal or vertical middle level between right shoulder and right elbow was calculated first. The distance from the horizontal or vertical middle level to the 'right shoulder' was the same as the distance from the defined level to the 'right elbow'. Then, the upper arm breadth was approximated by calculating the product of the width and the sine value ($\sin a$) as shown in Figure 40. The sine value was determined from the coordinates of 'right shoulder' and the 'right elbow' in the two-dimensional image.

Lower arm breadth was defined as the width on the defined level on the lower arm as shown in Figure 41. The distance from the defined level to the 'right elbow' was the same as the ones from the defined level to the 'right wrist' ('right elbow' and 'right wrist' were the skeletal joints defined by Kinect SDK).

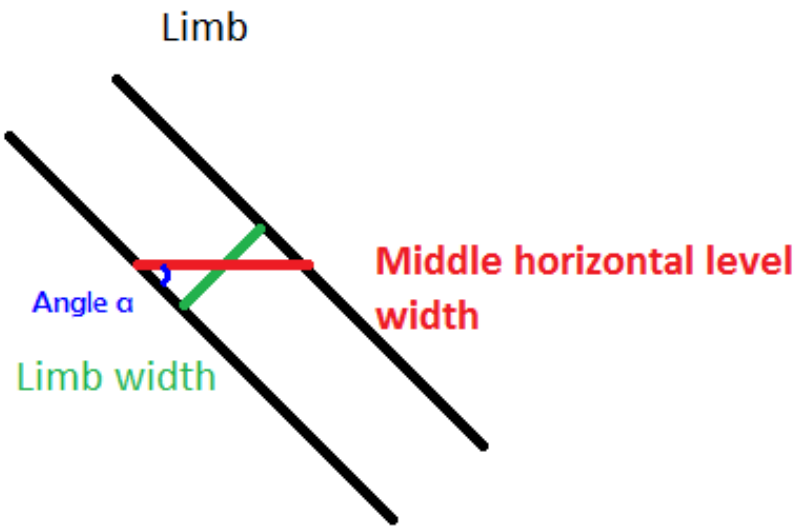

Figure 40 The upper arm breadth (green line) for the natural pose was approximated by calculating the product of the width of middle horizontal level (red line) and the sine value ($\sin a$).

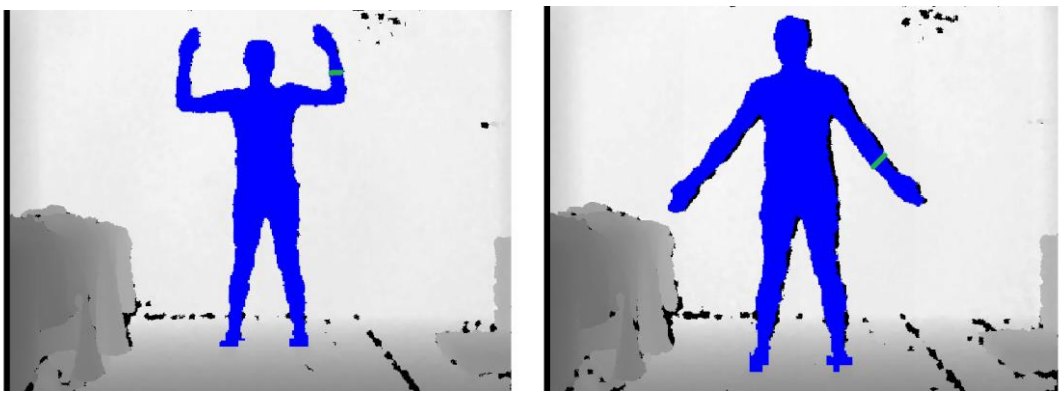

Figure 41 Lower arm breadth was defined as the width on the defined level on the lower arm.

The same issue arose with the lower arm breadth as in the upper arm, so a method of correction similar to that used for the upper arm was performed to calculate lower arm breadth.

The torso breadths (TB1, TB2, TB3 and TB4) were defined as the width at four specific levels (Lv1, Lv2, Lv3 and Lv4) as shown in Figure 42. Lv1 was defined as the middle level between the horizontals of ‘spinespace’ and ‘neck’. ‘Spinespace’ and ‘neck’ are two Kinect SDK defined skeletal joints. Lv2 was the middle level between Lv1 and the horizontal of ‘spinespace’. Lv3 was the horizontal of ‘spinespace’ while Lv4 was defined as the middle level between the horizontals of ‘right hip’ and ‘left hip’, ‘right hip’ and ‘left hip’ were both skeletal joints defined by Kinect SDK.

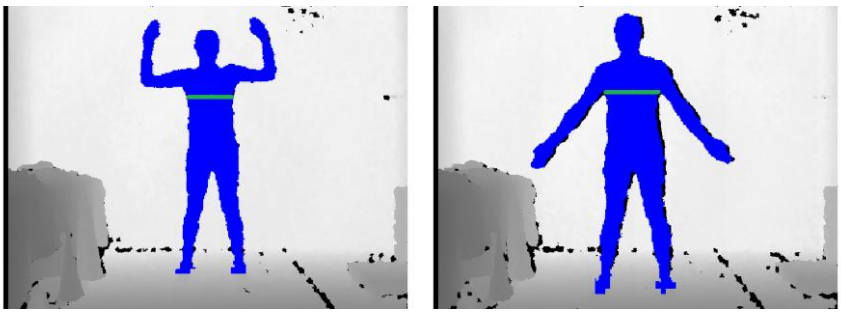

TB1

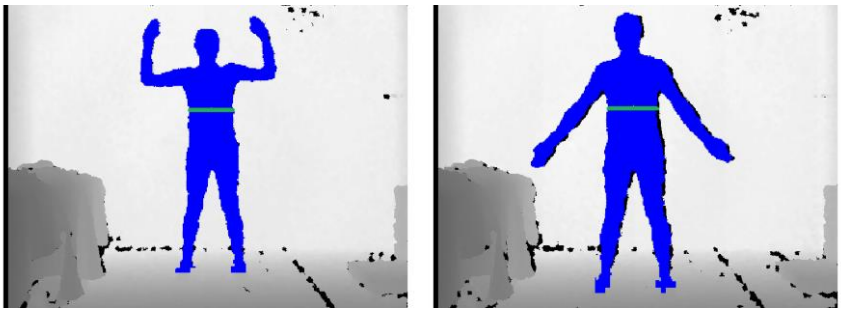

TB2

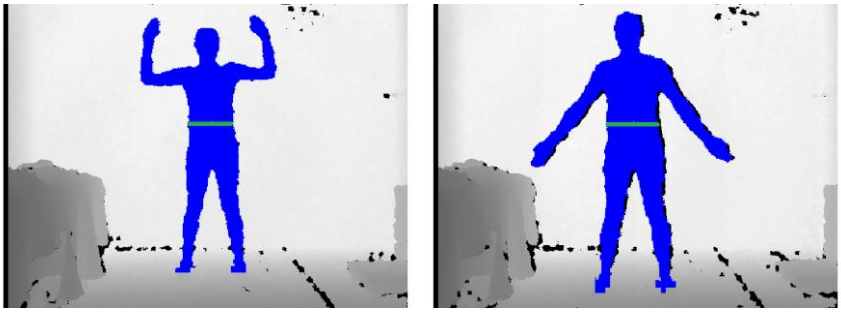

TB3

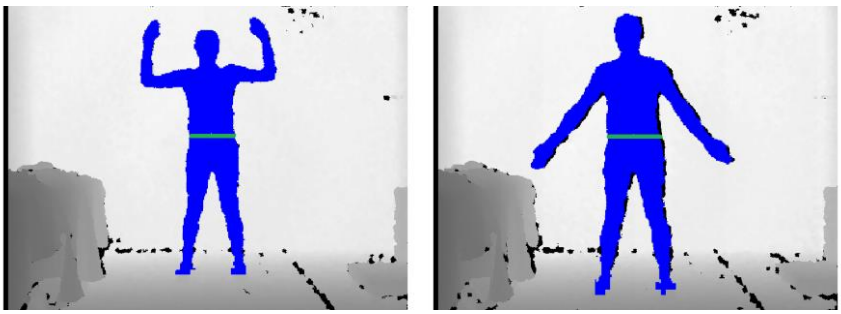

TB4

Figure 42 Torso breadths were defined as the width of the trunk at the specific levels.

Thigh breadth was defined as the width on the defined level on the upper leg as shown in Figure 43. The distance from the defined level to the ‘right hip’ was the same as the ones from the defined level to the ‘right knee’ (‘right hip’ and ‘right knee’ were the

skeletal joints defined by Kinect SDK). The defined level of the upper leg was the perpendicular vertical line of the line from right hip to right knee. Again, it was difficult for the participants to keep their upper leg exactly perpendicular to the floor so the width of the horizontal level between ‘right hip’ and the ‘right knee’ was used to estimate the thigh breadth. The width of the middle horizontal level between right hip and right knee was calculated first. The distance from the horizontal level to the ‘right hip’ was the same as the distance from the defined level to the ‘right knee’ Then, the thigh breadth was approximated by calculating the product of the width and the sine value, similar to the technique for the upper arm breadth.

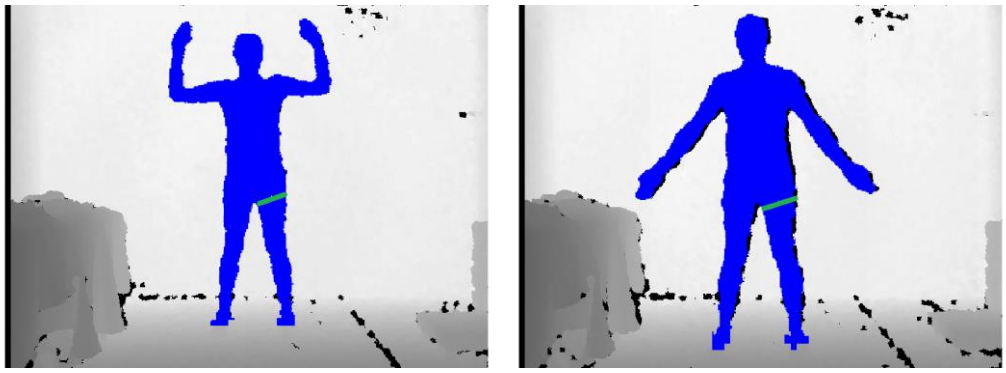

Figure 43 Thigh breadth was defined as the width the defined level on the upper leg.

Calf breadth was defined as the distance across the widest horizontal level on the lower leg as shown in Figure 44. The particular level was parallel to the perpendicular bisector of the line from ‘right ankle’ to ‘right knee’. ‘Right ankle’ and ‘right knee’ were the skeletal joints defined by Kinect SDK. The same issue arose with the calf breadth as in the thigh so a similar method of correction as used for the thigh was performed to calculate calf breadth.

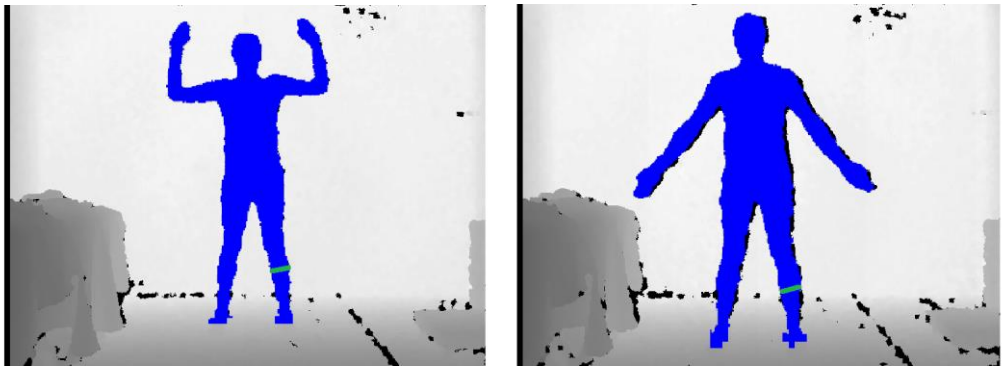

Figure 44 Calf breadth was defined as the width on the middle level of the lower leg.

Ankle breadth was defined as the distance across the narrowest horizontal level on the ankle part as shown in Figure 45. The particular level was parallel to the perpendicular bisector of the line from ‘right ankle’ to ‘right knee’. ‘Right ankle’ and ‘right knee’ were the skeletal joints defined by Kinect SDK. Ankle breadth was corrected using a method similar to that implemented for thigh and calf breadth.

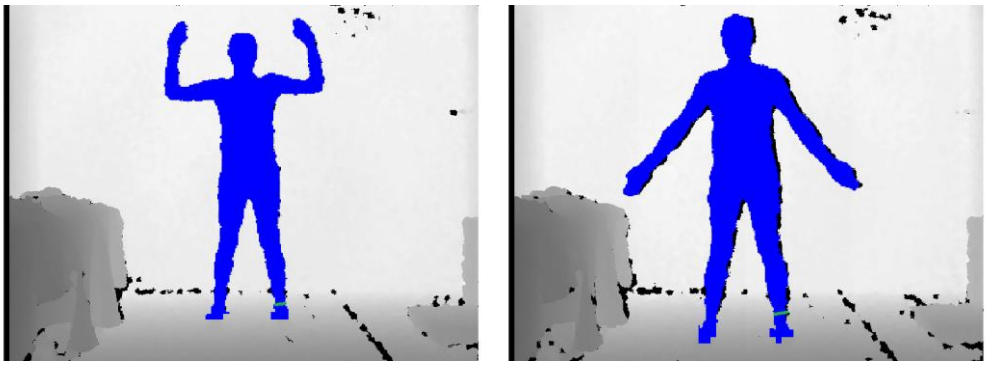

Figure 45 Ankle breadth was defined as the distance across the narrowest horizontal level on the ankle part.

3.2.5.2 Candidate Extraction for the Multiple Image Dataset

For the multiple image dataset, the same methods for candidate extractions using for the single image dataset (3.2.5.1) were applied to extract 'pre-candidate' values of each body dimension from 30 depth frames. For instance, 30 pre-candidate values of shoulder distance were extracted from 30 depth frames by measuring the distance between 'right shoulder' and 'left shoulder' in each frame. Then, the 'pre-candidates' of each body dimension were sorted in order ($pc_1, pc_2, \cdots, pc_{30}$). The mean of the middle ten 'pre-candidate' of each body dimension was defined as the candidate (c) as shown in Equation (17) and Equation (18).

$$pc_1 < pc_2 < \cdots < pc_{30} \tag{17}$$

$$\mathrm{c} = \frac{\sum_{i=11}^{20} pc_i}{10} \tag{18}$$

The reason for taking the average was that we assumed all middle 10 pre-candidates as valid measurements. Therefore, we wanted to consider the effect of all of 10 pre-candidate, instead of using only one single value (e.g. medium), to represent the candidate value.

3.2.6 Statistical Analysis

Two candidate values of body dimension (M_{i1}, M_{i2}) were acquired for each (ith) participant's body dimension in repeated extraction. The intra relative TEM was used to determine the reliability of candidate measurements acquired from different

extraction methods as shown in Equation (15) and Equation (16). The relative TEM for repeated reliability was calculated by Microsoft Excel (Microsoft®).

3.3 Results

Table 4 shows the reliability of candidates of different body dimensions acquired from four extraction methods. Comparing the minimum intra relative TEM of Candidate Extraction 1 and 2 and the one of Candidate Extraction 3 and 4, the reliability of most candidates extracted from multiple depth images is better than the candidates extracted from single images. The reliability of upper arm length (2.6%) and shoulder distance (1.0%) extracted from single images is slightly better than the reliability of the upper arm length (2.6%) and shoulder distance (1.1%) extracted from multiple images.

There are some very high values of intra relative TEM (poor reliability) for the body dimension features extracted from single images (lower arm breadth and TB1 in the single/natural group; TB2, calf and ankle in the single/PSI group). The noise of the depth camera might have caused miscalculation of the boundary coordinates and generated these high values. For instance, a Kinect system can detect the correct depth between the camera and the participant (two to three metres) without the noise effect. With the noise effect, the camera determined the depth between the camera and the participant to be zero metres. Consequently, the range of the body dimension feature can be from zero to three metres which is around 300% (for trunk segment breadths; about 0.5-0.8 metre) to 1000% TEM (for limb segment breadths; about 0.1-0.3 metre)) and cause the high values in single image groups.

Table 4 Reliability (%TEM) of candidates of different body dimensions acquired from four extraction methods (A lower intra relative TEM value indicates better reliability; the lowest intra relative TEM values are in red).

	Candidate Extraction 1 (single/PSI)	Candidate Extraction 2 (single/ natural)	Candidate Extraction 3 (multiple/PSI)	Candidate Extraction 4 (multiple/ natural)
Neck Height	4.7	1.5	3.79	1.5
Upper Arm Length	7.3	2.6	6.45	2.6
Lower Arm Length	7.7	3.3	8.63	3.2
Neck to Waist Length	1.4	1.5	0.9	1.5
Waist to Hip Length	0.7	1.0	0.6	1.0
Shoulder Distance	1.0	1.4	1.1	1.3
Upper Leg Height	1.5	1.6	1.3	1.5
Lower Leg Height	2.3	2.1	1.9	2.1
Neck Breadth	9.8	7.3	4.8	4.1
Upper Arm Breadth	18.8	7.5	12.1	7.2
Lower Arm Breadth	12.2	219.7	10.7	5.9
TB1	7.1	52.7	2.1	11.5
TB2	100.3	25.1	1.7	24.8
TB3	2.5	7.2	1.9	7.0
TB4	2.2	2.7	1.8	1.8
Thigh Breadth	3.7	3.6	1.5	3.1
Calf Breadth	46.0	4.78	22.8	3.4
Ankle Breadth	56.7	10.9	16.4	7.1

The reliability of candidates differed by the scanning pose, shown by comparing the minimum intra relative TEM of Candidate Extraction 1 and 3 and the one of Candidate Extraction 2 and 4. The candidates of neck height, upper arm length, lower arm length, neck breadth, upper arm breadth, lower arm breadth, calf breadth and ankle breadth can be extracted with better reliability by capturing with the natural pose than with the PSI pose. By contrast, extracting the other candidates with the PSI pose can give better reliability than obtaining them with natural pose capturing.

The results demonstrate that multiple image and different poses can improve the reliability of extracted candidates. However, the reliability of upper arm breadth and lower arm breadth extracted from four different methods are still poorer than the other candidates (intra relative TEM > 5%).

3.4 Discussion

The aim of this study was to 1) find an appropriate feature extraction method for increasing the reliability of the extracted body dimensions and 2) investigate which body dimensions extracted by the determined feature extraction method were highly reliable and could be then used as the features in 3D model generation in the following studies. This study used four feature extraction methods to examine whether the noise of the depth cameras and the scanning pose affect the body dimension extraction. This study also provided the reliability data to investigate the body dimensions which are most highly repeatable and can subsequently be used as the features in 3D model generation.

The noise problems of a Kinect system have been found previously (Khoshelham, 2011; Nguyen et al., 2012; Tong et al., 2012) but there is no previous research that examines whether the reliability of body dimensions extracted with a Kinect system are affected by the noise of the camera. This study compared the reliability of body dimensions extracted from single images and multiple images. The results showed that capture of multiple images increased the reliability of candidate extraction, especially for the candidates of body breadth measurements, indicating that the noise of depth cameras affects the candidate extraction. The possible reason that the reliability of breadth candidates is poor in the single image extraction is because noise affects the detection of body boundaries more than the detection of joints (which are towards centres of the segments). Overall, using multiple images to extract features can reduce the negative effects of noise.

Although upper arm length and shoulder distance could be extracted from single images with higher reliability than extraction from multiple images, the difference was very small and the reliability of multiple extraction was less than 3%. Therefore, all features were extracted from multiple images for the following processes of human model generation in this research.

A number of studies have been conducted that use Kinect systems to extract features (Tong et al., 2012; Weiss et al., 2011). However, no research has been conducted to investigate the effect of scanning pose on the reliability of body dimensions extracted using the Kinect systems. In this study, the body dimensions were extracted by two different poses, the natural pose and PSI pose to understand the scanning pose effect. The results showed that different poses affect the candidate extraction. The possible

reason is that the natural pose can help Kinect systems detect the skeleton joints reliably but as the arms were close to the body, this affected the detection of the body boundaries. By contrast, PSI pose decreased the reliability of joint detection but increased the reliability of the body boundary detection. Therefore, the features of body dimensions will be extracted from both of the different poses in this research to increase the reliability of 3D human model generation. The results of the study showed that extracting candidates from multiple images with two different poses can increase the reliability. This reduces the noise problems of a Kinect system reported in previous studies (Khoshelham, 2011; Nguyen et al., 2012; Tong et al., 2012).

However, the reliability of upper arm breadth, lower arm breadth and ankle breadth was still higher than 5%. The possible reason might be that Kinect systems cannot measure small objects correctly from the long capturing distance (around 3m). Gonzalez-Jorge et al. (2013) found that the precision of Kinect systems was around 1 centimetre at the 3 metre capturing distance. The 1 cm error affects the small body dimensions more than the large body dimensions such as torso breadth (TB1, TB2, TB3 and TB4). The linear error might accumulate and lead to poor reliability while acquiring body volume data. Thus, these three candidates cannot be used for model generation in this research. The candidates of the remaining 15 body dimensions (neck height, upper arm length, lower arm length, neck to waist length, waist to hip length, shoulder distance, upper leg height, lower leg height, neck breadth, TB1, TB2, TB3, TB4, thigh breadth and calf breadth) were selected as the features extracted from multiple images for 3D model generation in this research.

All features associated with limbs used the right side and symmetry was assumed i.e. the left side features, segmental volumes and shape were assumed to be equal to those on the right side. This assumption was widely used in other methods including manual anthropometry and E-Zone (Deffeyes & Sanders, 2005). Leboucher et al. (2008) showed that the volume differences between dominant and non-dominant limbs are significant but small. The difference was much less than 10% error. Because the criterion of the segmental volume accuracy in this study is within 10%, it is reasonable to make the symmetric assumption.

This study identified reliable body dimensions as the representative features and determined their extraction methods for human modelling and body volume calculation for this research. Therefore, 19 reliable features were selected for 3D human model generation. Stature and mass were to be measured in accordance with the ISAK protocol while age and gender were to be obtained from manual input. Neck height, upper arm length, lower arm length, neck breadth and calf breadth were to be extracted from multiple images with the natural pose. Neck to waist length, waist to hip length, shoulder distance, upper leg height, lower leg height, TB1, TB2, TB3, TB4, thigh breadth will be extracted from multiple images with the PSI pose. These features provided the basis for altering the parameters of MakeHuman to generate 3D individual human models in this research. These features and their extraction methods are helpful to obtain reliable body volume data for monitoring purposes.

Chapter 4 Study 2. Parameter Setting for Building Individual 3D Human Models

4.1 Introduction

Template model matching generates individual 3D human models by altering a set of parameters to morph the shape of a parametric template model to match the extracted features of 3D point clouds (Weiss et al., 2011), silhouettes (Peng et al., 2009) or body dimensions (Buys et al., 2011; Chen et al., 2011; Lin & Wang, 2012). The principle of template model matching is that a realistic human model can be generated by altering a set of parameters while the difference between the real features and the corresponding measurements (features extracted from the model) are minimized (please see the illustration in Section 2.2.2.2). In theory, the individual models built by template model matching are known to be able to fulfil some of the purposes of this research, i.e. to develop a fast automatic, portable, inexpensive system to build 3D human models for acquiring personal body volume data. Template model matching can accept incomplete feature information obtained from multiple depth images and build individual 3D human models (Weiss et al., 2011). Hence, the body dimension features extracted with simple and portable equipment in Study 1 can be used for generating individual 3D models and obtaining body volume data. Further, the individual 3D human models are generated by deforming the template model and the vertices of the generated 3D meshes are all registered (please see the illustration in Section 2.2.2.2 and Section2.2.3). It means that the vertex order of the anatomical landmark on the generated models are identical. For instance, the vertex index of the right wrist is always the same (vertex order '9641') in every MH model. Thus, the anatomical landmarks on the generated 3D models can be identified easily without any

manual digitizing. This can make the post-processing of segmental volume acquisition time-efficient and automatic. The automatic post-process can also avoid some human error (e.g. mistakes in manual digitizing) and increase the reliability. Therefore, template model matching is an appropriate choice for the purpose of this research.

MH provides a parametric human model and has been used to complete the process of the template model matching and generate individual human models (Pirker et al., 2009; Van Deun et al., 2011). Because MH is open source software (Bastioni et al., 2012), it can be applied without paying any extra cost for a software licence and is therefore helpful to achieve the purpose of this research for developing an inexpensive system. Furthermore, the development of a customised parametric template human model is not required. Although previous research has used other parametric template human models such as SCAPE (Anguelov et al., 2005) and TenBo (Yinpeng et al., 2013) models, only the MH model has been used previously for acquiring body volume data (Pirker et al., 2009). Nevertheless, Pirker et al. (2009) used a multiple synchronized camera system for feature extraction. The hardware is complex and non-portable since it includes a control system with two computers for image capturing and 16 fixed cameras. To date, no study has demonstrated the ability to use MH models to match the features extracted from depth images (including the body dimension features in Study 1) in order to generate individual 3D human models and calculate body volume data accurately. It is unknown how to alter the MH parameter to deform the template MH model effectively in order to match the features extracted by a Kinect system with the method in Study 1 and generate a realistic 3D human model for body volume calculation.

Altering the MH parameters and morphing the template model to match the body dimension features extracted from manual input (age, gender, stature, mass) and depth images in Study 1, provides an opportunity to deliver a reliable, automatic, portable, and inexpensive process for generating individual human models and calculating body volume data, as in the original research purpose of this thesis. However the answers to some questions are still unknown and have not been discussed completely in previous studies; 1) which MH parameters should be used to morph the template MH model for matching the body dimension features and the features extracted from the model to provide accurate body volume data? and 2) how can the parameters be set to reduce the difference between the deformed MH model and the real body shapes efficiently?

There are over 200 MH parameters for morphing the MH template model (MH base mesh). Each part of the mesh can be deformed by different MH parameters. As shown in Figure 46, the body shape of the MH model can be changed by altering the 'waist girth' parameter. The mesh near the waist also changes while setting different 'weight' parameters as shown in Figure 47. In other words, each part of the mesh of the MH model is multi-dimensional, which can morph to various shapes by setting multiple parameters. It is possible to alter all parameters to make the measurement match the features extracted from participants and generate a realistic 3D human model to obtain accurate body volume data. However, increasing the number of parameters makes the matching process a high-dimensional and complex problem which is time-consuming. Previous authors (Pirker et al., 2009; Van Deun et al., 2011) have usually selected a small number of representative parameters to simplify the parameter setting work.

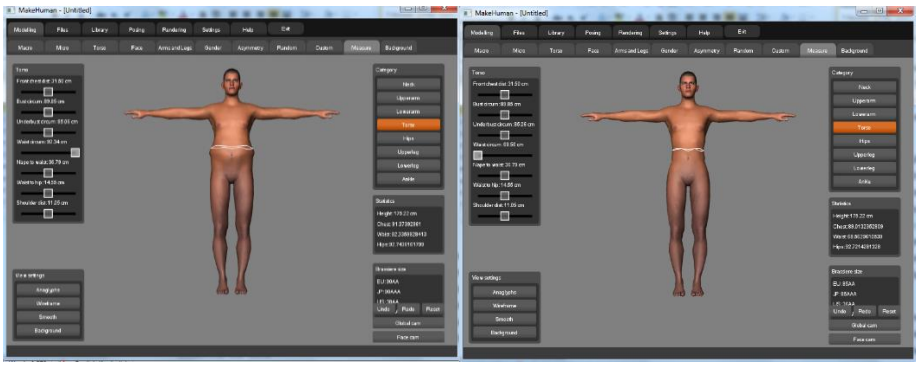

Figure 46 The body shape of the MH model can be changed by altering the 'waist girth' parameter.

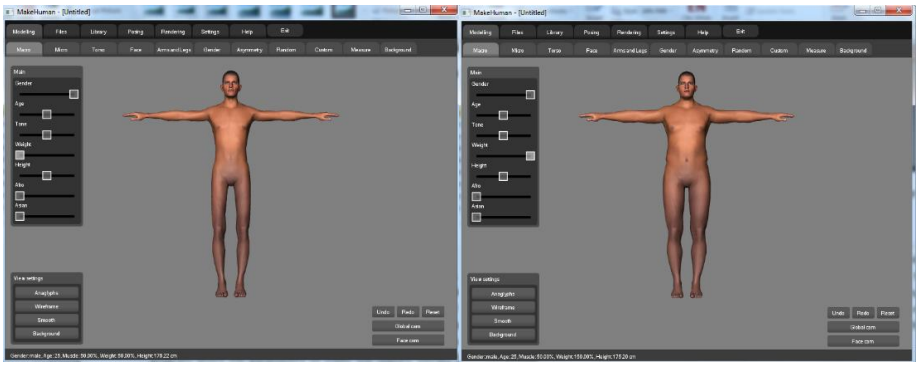

Figure 47 The mesh near the waist also changes while setting a different 'weight' parameter.

Pirker et al. (2009) used 10 parameters (stature, gender, age, body mass, torso thickness, torso length, thigh thickness, thigh length, shank thickness, shank length) to morph the MH template model for matching the features of the 3D point cloud. However, the error for arm volume estimation (up to 24.3%) seems too poor against that the accuracy criteria of the research purpose i.e. the inter relative TEM for segmental volume estimation should be under 10% (see Section 1.2.1). Van Deun et al. (2011) used six parameters, stature, gender, age, body mass, shoulder circumference and pelvis width, to generate individual 3D human models but the error

for matching the body dimension features was usually higher than 5% which would cause inaccurate volume estimation.

Selecting appropriate parameters is helpful to increase the accuracy and speed of acquiring the body volume data from generated individual 3D human models. To date, there is no study that has found a suitable group of MH parameters to morph the template model for matching the body dimension features extracted from depth images in Study 1 accurately. Thus, the first aim of this study was to determine the representative parameters from 200 MH parameters which can minimize the difference between the features extracted from the model and the features extracted from depth images in Study 1 effectively.

In addition to the parameter selection problems, setting the parameters to generate realistic 3D human models in the original interface is not feasible. In the original interface of MH, users needed to drag the toolbar to alter the MH parameters as shown in Figure 48. Setting multiple parameters in the original interface is time-consuming because users needed to control each toolbar repeatedly and manually and export the generated human models to third-party software to examine the difference between the features and the measurements.

Figure 49 shows the process of each MH parameter setting in the original interface. The import-export processes are not time efficient since generating one deformed MH model from the original MH interface and loading it into third-party software such as Blender (http://www.blender.org/), computer animation software, takes more than 15 seconds. Therefore, a custom command line program was developed to simplify the process of MH parameter setting (Buys et al., 2011). However, the body dimension

features extracted from depth images in Study 1 are specific to this data capture method so the corresponding measurements are different from the imported data used in other studies. Thus there is currently no custom program that can alter the specific parameters and examine the error between the measurements and the body dimension features used in this research.

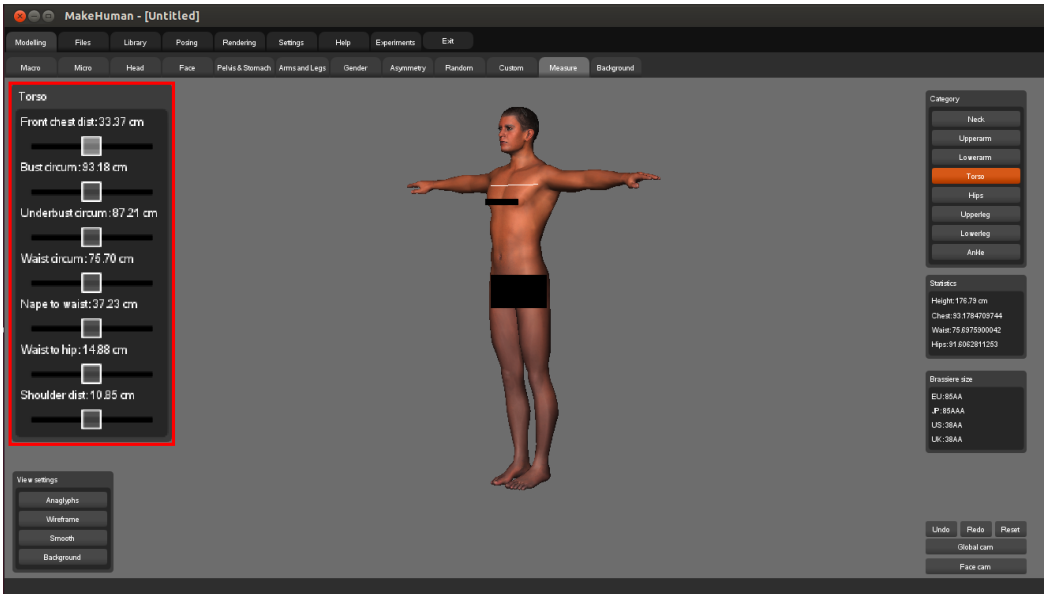

Figure 48 Users need to drag the toolbars (red box) to alter parameters in the original interface of MakeHuman.

Developing a custom command line program will enable an improvement in the processing speed for parameter setting. Thus, the second aim of this study was to develop a custom program for increasing the efficiency of parameter setting.

4.2 Method

4.2.1 Parameter Groups

In this study, two groups of MH parameters were used to morph the template model. The first group (PG1) was adjusted from the group proposed by Pirker et al. (2009).

Some parameters used in the previous study (Pirker et al., 2009) were selected for matching the 3D point cloud features and therefore were not appropriate for the body dimension features extracted from depth images. For instance, there were no depth features (e.g. torso depth, thigh depth and shank depth) extracted from depth images in Study 1 so the depth parameter cannot be set to deform the template model to match the realistic body shapes. The adjusted MH parameter groups used the segmental girth parameter to replace the depth parameters so the breadth measurement can be compared with the Kinect breadth features to set the depth of segments and morph realistic human models.

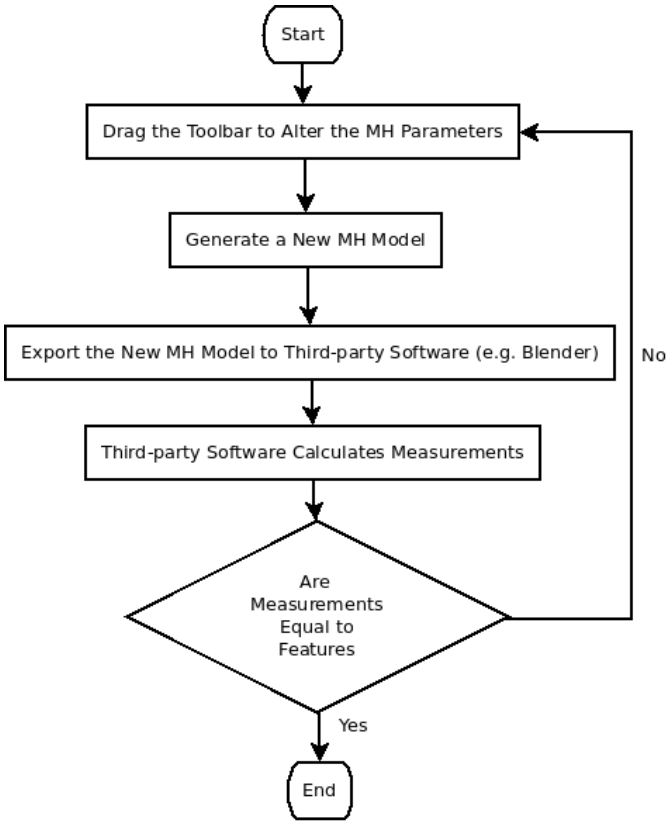

Figure 49 The process of each MH parameter setting in the original interface.

Another problem for the parameter groups used by Pirker et al. (2009) is that no parameters were used to deform the shape of neck segments and change the segmental length (e.g. torso height, arm length and leg height) of the template model . To solve this problem, the parameters for neck breadth, neck length, and segmental length were also selected. Table 5 shows the first MH parameter group including macro parameters (MP) and local parameters (LP).

Table 5 Parameters in PG1 including four macro parameters (MP) and 18 local parameters (LP).

MP_1	gender	MP_2	age
MP_3	mass	MP_4	stature
LP_1	neck height	LP_2	upper arm length
LP_3	lower arm length	LP_4	upper leg length
LP_5	lower leg length	LP_6	nape to waist length
LP_7	torso height	LP_8	waist to hip length
LP_9	hip height	LP_{10}	neck girth
LP_{11}	shoulder distance	LP_{12}	torso width
LP_{13}	bust girth	LP_{14}	under bust girth
LP_{15}	waist girth	LP_{16}	hips girth
LP_{17}	thigh girth	LP_{18}	calf girth

The second group of parameters (PG2) used to adjust the MH were those presented by Van Deun et al. (2011). Their parameter, ‘acromion circumference’, is a custom parameter and is not one of 200 standard MH parameters. Thus in this study, the standard parameter, ‘shoulder distance’, was used to replace the acromion circumference. Table 6 shows the second MH parameter group.

Table 6 Parameters in PG2 including four macro parameters (MP) and two local parameters (LP).

MP_1	gender	MP_2	age
MP_3	mass	MP_4	height
LP_{11}	shoulder distance	LP_{16}	hips girth

4.2.2 Criteria for Parameter Setting

The 19 real body dimension features ($f = (f_1, \cdots, f_{19})$) were extracted from a single person's manual inputs, anthropometric measures and depth images as shown in Table 7. Additionally, 19 corresponding features extracted from the model (from here on referred to as 'measurements') ($m = (m_1, \ldots, m_{19})$) were obtained from the MH model as shown in Table 7. Measurements of age, gender, stature and mass were calculated with MH programs (MH formulas). The other body dimension measurements were determined from the coordinates of the associated vertices on the MH model as shown in Figure 50. The definitions of the 19 measurements and 19 features were similar so the measurements should be equal to the features while generating realistic models.

In this study, the difference between the 19 features (f) and corresponding 19 measurements (m) was defined as the distance function $\|f - m\|$ as in Equation (19)

$$\|f - m\| = \|f - M[d(p)]\| = \sum_{i=1}^{19} \frac{|M_i[d(p)] - f_i|}{f_i} \qquad (19)$$

where p are the parameters in PG1 or PG2, M is the function for extracting measurements from the MH model, d is the MH human model deformation function.

Table 7 The features and the corresponding measurements used for parameter setting[14]

f_1	age	m_1
f_2	gender	m_2
f_3	stature	m_3
f_4	mass	m_4
f_5	neck height	m_5
f_6	upper arm length	m_6
f_7	lower arm length	m_7
f_8	upper leg height	m_8
f_9	lower leg height	m_9
f_{10}	neck to waist length	m_{10}
f_{11}	waist to hip length	m_{11}
f_{12}	neck breadth	m_{12}
f_{13}	shoulder distance	m_{13}
f_{14}	TB1	m_{14}
f_{15}	TB2	m_{15}
f_{16}	TB3	m_{16}
f_{17}	TB4	m_{17}
f_{18}	thigh breadth	m_{18}
f_{19}	calf breadth	m_{19}

4.2.3 Parameter Setting Process

The MH parameters ($p = (p_1, \dots, p_n)$) in the specific groups (PG1, PG2) were altered to deform the shape of the MH template mesh and generate individual human models. Based on the principle of template model matching, the differences of the measurements extracted from the deformed MH models and the body dimension features should be minimized while generating a realistic individual 3D human model. Therefore, the values of measurements were changed by altering the MH parameters to deform the shape of the human model to match the fixed features as in Equation (20).

[14] TB1, TB2, TB3, and TB4 are the torso breadths in four different levels.

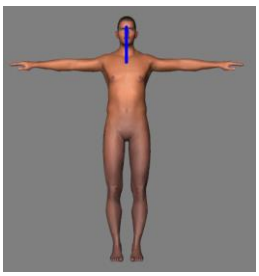

Neck height

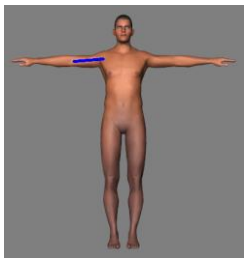

Upper arm length

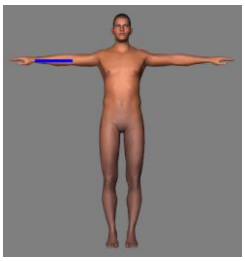

Lower arm length

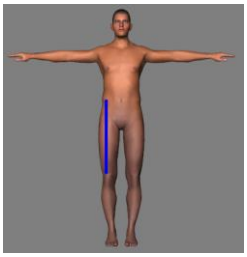

Upper leg length

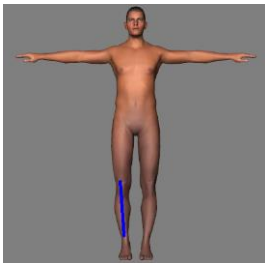

Lower leg length

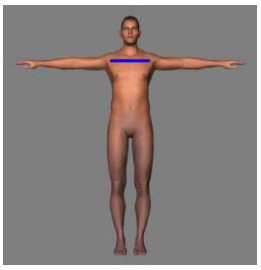

Shoulder distance

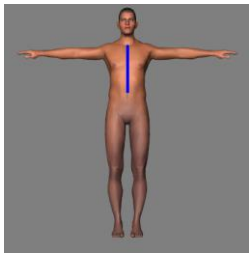

Neck to waist length

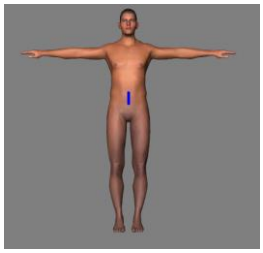

Waist to hip length

TB1

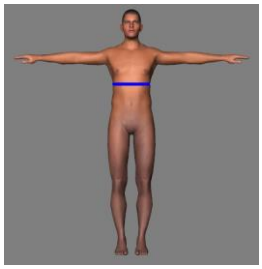

TB2

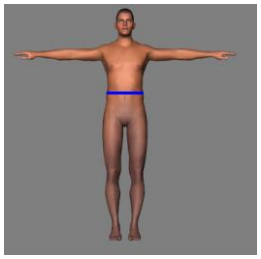

TB3

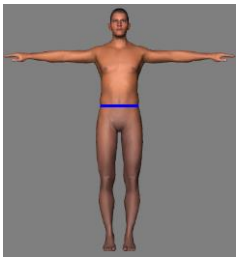

TB4

Thigh breadth

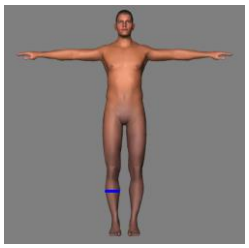

Calf breadth

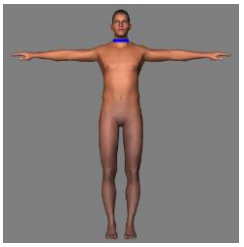

Neck breadth

Figure 50 The definition of the 15 body dimension measurements.

$$(\widehat{p_1}, \dots, \widehat{p_n}) = \hat{p} = \underset{p}{\operatorname{argmin}}(\|f - m\|) \\ = \underset{p}{\operatorname{argmin}}\{\|f - M[d(p)]\|\} \tag{20}$$

where $\hat{p} = (\widehat{p_1}, \dots, \widehat{p_n})$ is the best match to the MH parameters to minimise the error between the measurements and the features, M is the function for extracting measurements from the MH model and d is the MH human model deformation function.

To minimize the function $\|f - m\|$ effectively, the parameters were altered by the following steps according to previous studies (Pirker et al., 2009; Van Deun et al., 2011) and as shown in Figure 51. First, four 'macro' MH parameters (gender, age, stature and mass) were set to the same value of the body dimension features acquired manually from each participant. Three macro parameters (gender, age, mass) could be set easily by using the MH functions to minimize the distance between the features and the measurements of gender, age, mass. By contrast, there is no MH function for setting the stature parameter. To solve this problem, the bisection method (Burden & Faires, 1985) was applied to find the value of the stature parameter for making the stature of the deformed 3D model (the measurement) match the real stature (the feature) as shown in Algorithm 1.

Figure 51 The process for altering MH parameters.

```
INPUT: f - body dimension feature,
       m - MH measurement function (enables to return the
       corresponding measurement of input body dimension
       feature),
       (pmin, pmax) – parameter boundary,
       TOL - tolerance,
       MAX_iter - maximum iterations
OUTPUT: p - parameter value such that |m(p)-f| < TOL

# Set initial P
P ← (pmin + pmax)/2
If |f-m(p)| < TOL then # solution found
  Output(p)
Else
{
  (pl, pu) ← (pmin, pmax) # Set initial boundary
}
Do for step = 1 to Max_iter
{
  If f < m(p) then # overestimate
  {
    (pl, pu) ← (pl, p) # update upper bound
  }
  Else # underestimate
  {
    (pl, pu) ← (p, pu) # update lower bound
  }
  If pl = pu then # solution found
  {
    Output(p)
  }
  Else # keep finding
  {
    p ← (pl + pu)/2
  }
  If |f-m(p)| < TOL then # solution found
  {
   Output(p)
  }
}
Endfor
Output(p) # output last p if it cannot find within Max_iter
```

Algorithm 1 The algorithm for setting the stature or local parameters

After setting the parameters for manual features (gender, age, stature and mass), the local parameters (as shown in Table 8 and Table 9) were altered such that the difference between the corresponding measurements and each participant's body dimension features was smallest (minimizing the function $\|f - m\|$). The local parameters just deformed the template model locally so it can assume that setting one parameter only affected the value of one measurement. For example, setting the MH parameter of lower arm length only affected the value of the lower arm length measurements. Because of this assumption, the parameters for minimization of the function $\|f - m\|$ can be determined by solving simple equations. For obtaining the values of all local parameters in PG1, Equation (21) to Equation (35) needed to be solved. For obtaining the values of two local parameters in PG2, only Equation (33) and Equation (36) needed to be solved.

$$\widehat{LP_1} = \underset{LP_1}{\operatorname{argmin}}(\|f_5 - m_5\|) \tag{21}$$

$$\widehat{LP_2} = \underset{LP_2}{\operatorname{argmin}}(\|f_6 - m_6\|) \tag{22}$$

$$\widehat{LP_3} = \underset{LP_3}{\operatorname{argmin}}(\|f_7 - m_7\|) \tag{23}$$

$$\widehat{LP_4} = \underset{LP_4}{\operatorname{argmin}}(\|f_8 - m_8\|) \tag{24}$$

$$\widehat{LP_5} = \underset{LP_5}{\operatorname{argmin}}(\|f_9 - m_9\|) \tag{25}$$

$$(\widehat{LP_6}, \widehat{LP_7}) = \underset{LP_6, LP_7}{\operatorname{argmin}}(\|f_{10} - m_{10}\|) \tag{26}$$

$$(\widehat{LP_8}, \widehat{LP_9}) = \underset{LP_8, LP_9}{\operatorname{argmin}}(\|f_{11} - m_{11}\|) \tag{27}$$

$$\widehat{LP_{10}} = \underset{LP_{10}}{\operatorname{argmin}}(\|f_{12} - m_{12}\|) \tag{28}$$

$$(\widehat{LP_{11}}, \widehat{LP_{12}}) = \underset{LP_{11}, LP_{12}}{\operatorname{argmin}}(\|f_{13} - m_{13}\|) \tag{29}$$

$$\widehat{LP_{13}} = \underset{LP_{13}}{\operatorname{argmin}}(\|f_{14} - m_{14}\|) \tag{30}$$

$$\widehat{LP_{14}} = \underset{LP_{14}}{\operatorname{argmin}}(\|f_{15} - m_{15}\|) \tag{31}$$

$$\widehat{LP_{15}} = \underset{LP_{15}}{\operatorname{argmin}}(\|f_{16} - m_{16}\|) \tag{32}$$

$$\widehat{LP_{16}} = \underset{LP_{16}}{\operatorname{argmin}}(\|f_{17} - m_{17}\|) \tag{33}$$

$$\widehat{LP_{17}} = \underset{LP_{17}}{\operatorname{argmin}}(\|f_{18} - m_{18}\|) \tag{34}$$

$$\widehat{LP_{18}} = \underset{LP_{18}}{\operatorname{argmin}}(\|f_{19} - m_{19}\|) \tag{35}$$

$$\widehat{LP_{11}} = \underset{LP_{11}}{\operatorname{argmin}}(\|f_{13} - m_{13}\|) \tag{36}$$

Table 8 Local parameters in PG1

LP_1	neck height	LP_2	upper arm length
LP_3	lower arm length	LP_4	upper leg length
LP_5	lower leg length	LP_6	nape to waist length
LP_7	torso height	LP_8	waist to hip length
LP_9	hip height	LP_{10}	neck girth
LP_{11}	shoulder distance	LP_{12}	torso width
LP_{13}	bust girth	LP_{14}	under bust girth
LP_{15}	waist girth	LP_{16}	hips girth
LP_{17}	thigh girth	LP_{18}	calf girth

Table 9 Local parameters in PG2

LP_{11}	shoulder distance	LP_{16}	hips girth

Some measurements can be changed by more than one parameter due to altering of some parameters changing similar local meshes. For instance, the nape of the neck to waist length (LP_6) and the torso height (LP_7) can change the value of neck to waist length (m_{10}). To solve the equation (26), equation (27) and equation (29), the following assumptions (Equation (37), Equation (38), and Equation (39)) were applied to simplify the optimization works so the processes could be more time-efficient.

$$LP_6 = LP_7 \tag{37}$$

$$LP_8 = LP_9 \quad (38)$$

$$LP_{11} = LP_{12} \quad (39)$$

By these assumptions (Equation (37), Equation (38), and Equation (39)), each equation was reduced to one-dimensional optimization questions. These questions can be solved with the bisection method which is similar to the stature matching as shown in Algorithm 1.

A custom command line program in Python (cross-platform) for automatic parameter setting was developed. The program examined the errors between body dimension features and the corresponding measurements and increased or decreased the value of the parameters automatically by using the algorithm presented in this section. Thus, the developed program completed the MH parameter settings without manual intervention including dragging the toolbars in the original MH interface or examining the measurements in third-party software.

4.2.4 Data Collection

Figure 52 shows the flow chart for the data collection and the approach for measuring the processing time. The parameters in PG1 and PG2 were used for parameter setting for the custom command line program. Each participant's features (total 17 participants; please to refer Study 1 for the detail of participants) were extracted from manual input and depth images and there were two sets of body dimension features (f1 and f2) for each participant. Each sets contained 19 features as shown in Table 7 obtained from the test in Study 1. The two sets of features (f1 and f2) were the inputs for two parameter settings. After the parameter setting processes, the values of the parameters were determined and the measurements of the deformed 3D human models

were obtained. Four sets of measurements (m11, m21, m12, m22) were acquired from four combinations of features and parameter groups (f1-PG1, f2-PG1, f1-PG2, f2-PG2) accordingly. The processing time was measured from the moment the features were imported to the command line program and ended with exporting the measurement of the deformed 3D human models with a general laptop (i5-3210M and 8G RAM).

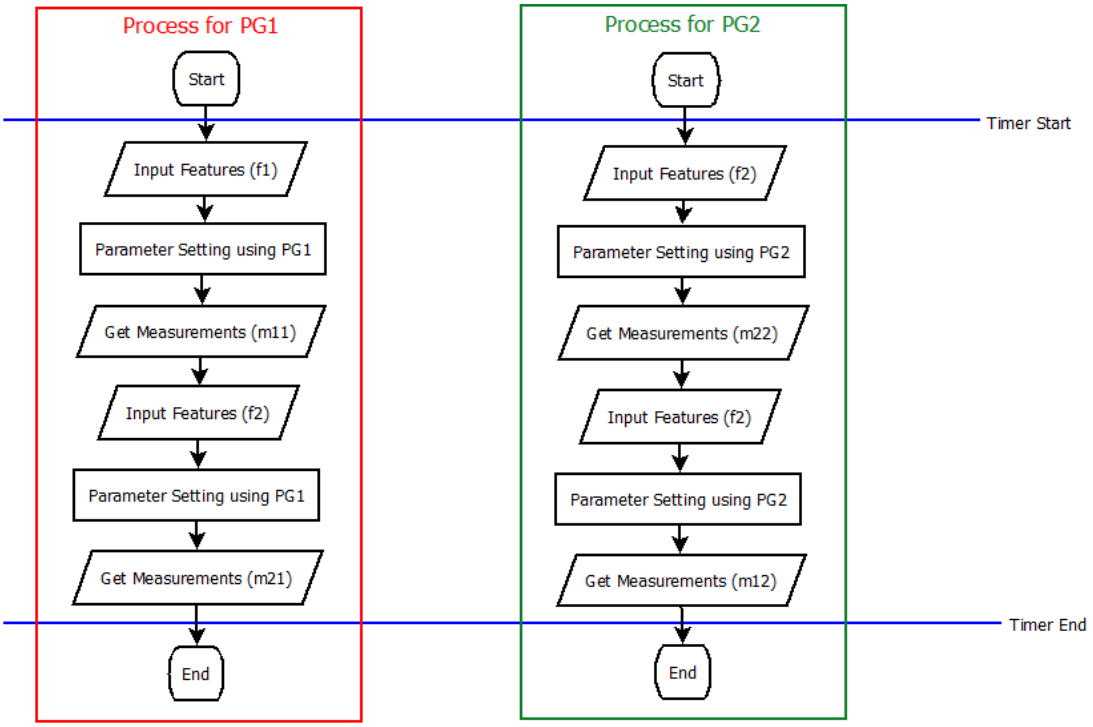

Figure 52 The flow chart for the data collecting and the approach for measuring the processing time in this study.

4.2.5 Statistical Analysis

Algorithm 2 shows the method for comparing the features and the measurements in this study. The mean of the body dimension features was compared with the mean of the measurements for two parameter groups (PG1 and PG2). The reason for using the mean was that it can help us determine the parameter setting difference for single

participants. The difference between the features and the measurements of each body dimension was quantified by the inter-method relative technical error of measurement (inter relative TEM). Inter relative TEM calculated the ratio of inter-method absolute technical error of measurements (inter absolute TEM) and the variable average value, is defined as Equation (40) and (41) (Perini et al., 2005).

$$\text{Inter absolute TEM} = \sqrt{\frac{\sum_{i=1}^{N}(\bar{F}_i - \bar{M}_i)^2}{2 * N}} \tag{40}$$

$$\text{Inter relative TEM} = \frac{\text{Inter Absolute TEM}}{\frac{\sum_{i=1}^{N}(\bar{F}_i + \bar{M}_i)}{2 * N}} * 100\% \tag{41}$$

where N is representative of the number of participants, $\bar{F}_i$ denotes the mean of features in two feature sets (f1 and f2) for the i^{th} participant's body dimension, and $\bar{M}_i$ stands for the mean of the corresponding measurements in m11 and m21 or m12 and m22 for the i^{th} participant's body dimensions. The relative TEM for intra-reliability were calculated with Microsoft Excel (Microsoft®).

```
INPUT: bd1 - body dimension feature in the feature sets f1
       acquired from Study 1,
       bd2- body dimension feature in the feature sets f2
       acquired from Study 1,
       m1 - MH measurement function for first parameter group
       (PG1) which can return the corresponding measurement
       of input body dimension feature,
       m2 - MH measurement function for second parameter group
       (PG2) which can return the corresponding measurement
       of input body dimension feature,
OUTPUT: Inter relative TEM for the parameter setting
        difference D1, D2,

#Average body dimension feature
F ← (bd1 + bd2)/2
#Average measurement for PG1
M1 ← (m1(bd1) + m1(bd2))/2
#Average measurement for PG2
M2 ← (m2(bd1) + m2(bd2))/2

# Calculate result
# The Inter relative TEM is defined as Equation (40) and (41)
D1 ← Inter relative TEM between F and M1
D2 ← Inter relative TEM between F and M2


# Output result
Output(D1, D2)
```

Algorithm 2 The algorithm for comparing the features and measurements in this study

4.3 Results

Table 10 shows the difference between the features and the measurements of 19 body dimensions. Because both parameter groups (PG1 and PG2) used the MH functions to set age, gender and mass, there was no difference (0% TEM) between the measurements and the features of these three body dimensions. Similarly, both PG1

and PG2 set the parameter of hips girth to match the measurement and the feature of TB4 (Equation (33)) so the error is identical (0.9% TEM).

Table 10 The difference (%TEM) between the features and the measurements of different body dimensions.

Body dimension	PG1	PG2
age	0	0
gender	0	0
stature	0.78	0.03
mass	0	0
neck height	2.47	6.69
upper arm length	3.22	6.55
lower arm length	1.63	4.24
upper leg height	0.64	4.18
lower leg height	0.95	3.70
neck to waist length	1.82	6.17
waist to hip length	1.48	23.13
neck breadth	2.59	7.23
shoulder distance	0.55	3.73
TB1	1.39	9.35
TB2	1.10	6.78
TB3	1.18	5.48
TB4	0.89	0.89
thigh breadth	0.74	2.05
calf breadth	2.36	7.20
Mean±SD	1.25±0.92	5.12±5.25

The difference of stature for PG1 was larger than the one for PG2, but the errors for both parameter groups were less than 1% TEM. For most body dimensions including neck height, upper arm length, lower arm length, upper leg height, lower leg height, neck to waist length, waist to hip length, neck breadth, shoulder distance, TB1, TB2, TB3, thigh breadth and calf breadth, the errors for PG1 were smaller than the errors for PG2. The errors for PG1 were usually less than 3% TEM while the errors for PG2 were usually larger than 3%.

Table 11 shows the total processing time for setting parameters to match 34 sets (two sets per one participant) of body dimension features and the mean processing time for setting parameters to match one set of body dimension features. The processing time for setting 22 parameters in PG1 was slightly longer than setting six parameters in PG2. The difference of the mean processing time between two parameter groups was within 1 second.

Table 11 The total processing time (s, seconds) for setting parameters to match 34 sets of body dimension features and the mean processing time for setting parameters to match 1 set of body dimension features.

	PG1	PG2
Total processing time	335.84s	318.12s
Mean processing time	9.88±0.000003s	9.36±0.000004s

4.4 Discussion

This study aimed 1) to determine the representative parameters from 200 MH parameters which can minimize the difference between the features extracted from the

model and the features extracted from depth images in Study 1 effectively and 2) to develop a custom program for increasing the efficiency of parameter setting. To achieve this, two parameter groups (PG1 and PG2) were compared to enable subsequent selection of appropriate parameters to generate realistic 3D human models. Furthermore, a command line program for parameter setting was developed, and was tested to examine whether the proposed procedure in this study is time-efficient for parameter setting.

The results showed that increasing the number of MH parameters to morph the template model can reduce the difference between the measurements and the features. The possible reason is that the participants provided a wide variety of combinations for body dimension features. Using more local parameters can deform the segmental meshes of the template model in various shapes and match different combinations of body dimensions. By contrast, it is difficult to use four macro parameters (gender, age, stature and mass) with two local parameters to match the wide range of the combinations of body dimension features. The errors between the features and the measurements while using PG2 for parameter setting were near to or larger than 5% which was similar to the results presented in the original study from which PG2 was selected (Van Deun et al., 2011). On the other hand, the errors for PG1 were under 3.5%. Referring to the principle of template model matching; by using more MH parameters (22 in PG1) more realistic human models are generated and more accurate body volume data can be obtained than with using fewer MH parameters (6 in PG2).

Buys et al. (2011) used only six parameters to generate individual 3D human models and body mass was able to be estimated within 5% from the generated 3D models.

However, since body mass was one of the parameters for the setting process, it may have increased the accuracy for the single specific body dimension. In other words, the error for body mass estimation might be reduced artificially by altering the mass parameters. Similarly, in this study, the hip breadth was more accurate than other body dimensions (e.g. upper arm length, waist to hip length) while using the parameter set PG2. The accuracy of hip breadth might be affected by the parameter setting of hip girth. The possible reason might be that altering the specific parameters can reduce the error between the corresponding features and measurements but it might not be helpful to reduce the error between all features and measurements. Therefore, it suggested that all the parameters which corresponded to the extracted features should be altered to minimize the error between all features and measurements.

A large error of the body dimensions without altering the corresponding parameters might cause a miscalculation in segmental volume estimation. For instance, Pirker et al. (2009) set the leg parameters but did not set the arm parameters for generating 3D human models. This caused the error for arm volume estimation to be much larger than leg volume estimation. Therefore, altering more local parameters can morph the template 3D models to match individual features and obtain accurate segmental volume data.

This study showed that using 22 parameters in PG1 can deform the MH template model to match the body dimension features within small errors (mean error = 1.25 ± 0.9%). Nevertheless, the difference between measurements and features of neck height, upper arm length, neck breadth, calf breadth (more than 2%) was slightly higher than other body dimensions. More parameters therefore might be required to increase the

range of deformation to that of the participants' body dimension. For instance, using the upper arm length parameter cannot extend the arm segmental mesh of the template MH model to match the real body shape with very long upper arms. However, adding more parameters increases the complexity of morphing the template model to match the extracted features which might increase the processing time. The differences between the measurements and the features were all less than 5% while using these 22 parameters. The small errors are likely to lead to the accurate estimation of segmental volume data (relative TEM < 10%, see Section 1.2.1).

The result of the processing speed test confirmed that more parameters results in more time to complete the parameter setting process. It illustrates why most studies select a few representative parameters instead of all 200 MH parameters to generate 3D human models (Buys et al., 2011; Chen et al., 2011; Pirker et al., 2009; Van Deun et al., 2011). Although previous studies (Buys et al., 2011; Pirker et al., 2009) also developed a custom command line program for MH parameter setting, there were no data presented by either of these authors that showed the processing time. By contrast, the current test results demonstrated that the parameter setting process and the developed command line program in this study provided a time-efficient procedure for setting the representative parameter group (PG1 and PG2). The difference of the processing time for PG1 and PG2 was very small. Even though the processing speed for PG1 was slightly slower than the speed in PG2, the difference was within 1 second. In other words, using PG1 for parameter setting can still generate individual 3D human models within 10 seconds. Compared to the long processing time (65 minutes) in the literature (Weiss et al., 2011), setting parameters by the proposed method (less than 10 second)

can be regarded as very efficient. The short processing time is helpful to provide a time-efficient system for obtaining body volume data.

Overall, this study showed that using the developed custom command line program can set the 22 parameters in PG1 effectively and deform the MH template model to match the features extracted from manual input and depth images accurately. Therefore, the methods in this study yield a valuable procedure to obtain realistic human models.

Chapter 5 Study 3. Development of an Automatic Program for Calculating Personal Body Volume Data from Individual 3D MakeHuman Models

5.1 Introduction

Study 2 used the MakeHuman (MH) parametric model to complete the process of template model matching and generating individual 3D human models for calculating personal body volume data. During this process, the generated 3D human models are completed without any holes or abnormal faces as shown in Figure 53. In contrast, models generated by traditional laser scanners have many holes and noise such as abnormal faces (Ma et al., 2011). Thus, an advantage of the MH model is that the reconstruction process such as hole-filling and noise reduction can be avoided while calculating whole-body volume. Reconstruction from laser scanner data, including the hole-filling and noise reduction, is time-consuming and relies on manual operation (Ma et al., 2011). Therefore, MH models provide an opportunity to obtain whole-body volume quickly and automatically.

Furthermore, the vertices of the generated 3D human models are all 'registered' which means the quantity and order of vertices of generated MH models are all identical. Thus, the anatomical landmarks or the boundaries between segments can be identified easily from the generated MH models by indicating the vertex numbers. For example, the vertex numbers of wrist joints for all generated MH models are all equal to '9641' as shown in Figure 54. The registered model allows for the acquisition of segmental mesh and the determination of segmental volume quickly without manual operation. The process for acquiring the segmental mesh and calculating body volume data from

registered 3D human models has previously been carried out automatically without manual digitizing for other models. For instance, Sheets et al. (2009) used the SCAPE model (Anguelov et al., 2005) to match the 3D point cloud features and obtain individual 3D models. The segmental meshes could then be obtained easily from the deformed SCAPE models.

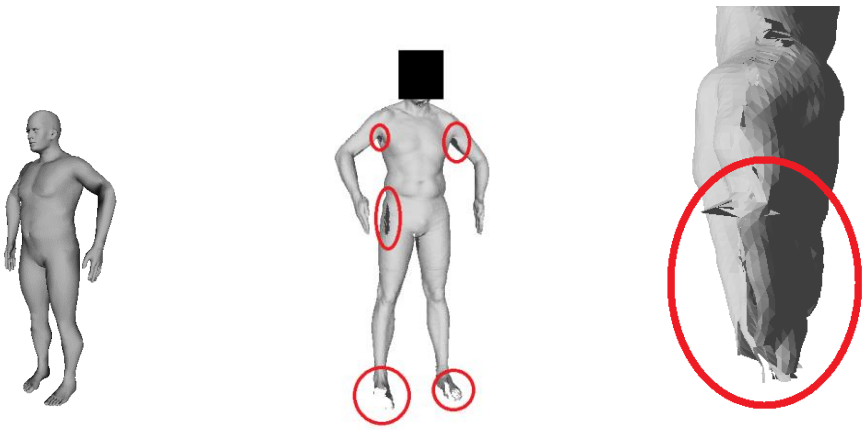

A B C

Figure 53 (A)The MH model without any holes and abnormal faces (B) The model obtained from the 3DPS scanner with holes (C) The hand model obtained from the 3DPS scanner with abnormal faces

However, no corresponding program has been developed for calculating body volume data automatically from MH models. Without this kind of program, expert users need to use specific software to complete the 'traditional manual process' including the mesh segmentation and volume calculation (Ma et al., 2011). While conducting the traditional manual process, users need to identify anatomical landmarks (the boundaries between segments) manually and manually set the locations and directions of segmental planes into the user interface as shown in Figure 55. These repeated

manual operations are time-consuming. Wicke and Lopers (2003) mentioned that manual digitizing for the body boundaries for E-Zone took approximately 10 minutes for each participant. Ma et al. (2011) and Sanders et al. (2015) showed that the between-assessor errors for manual digitizing segmental boundaries need to be considered and some small segment were particular prone to error (e.g. the between-assessor error of neck mass was up to 14.9%), so test results are likely to be affected by different operators.

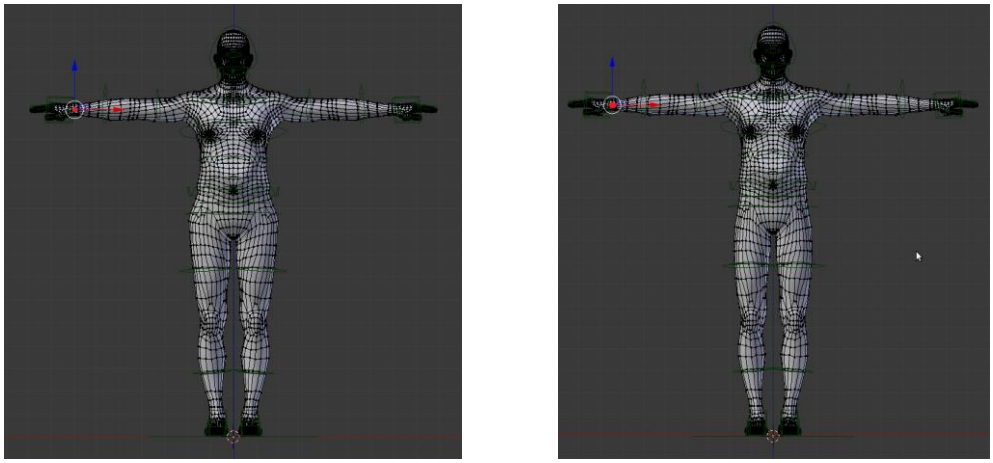

Figure 54 The vertex numbers of wrist joints for all generated MH models are all equal to '9641' (red points).

Furthermore, expert knowledge is needed to operate specific software for boundary setting in the process of mesh editing (Ma et al., 2011). Thus, using the traditional manual operation to obtain body volume data cannot deliver the fast and automatic process needed to achieve all of the criteria stated in the purpose of this research (to develop an accurate, reliable, fast, automatic, portable and inexpensive system to build 3D human models for acquiring personal body volume data (see section 1.2)).

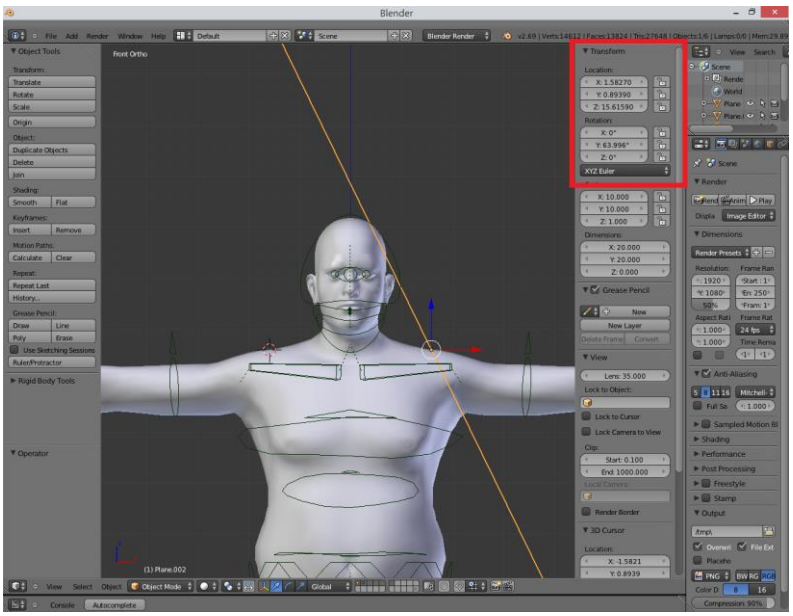

Figure 55 Adjusting the location and the angle of a segmental plane has needed an operator to enter the numbers in the Blender graphic user interface manually (in the red block panel).

Therefore, the aim of this study was to develop a customized program for acquiring body volume data from generated HM models automatically. The corresponding tests were conducted to examine whether the developed automatic body volume acquisition program could calculate body volume data more time-efficiently than using the traditional manual operation.

5.2 Method

5.2.1 Whole-body Volume Acquisition

The individual 3D human models were generated in MakeHuman eXchange file format (MHX) by the approaches presented in Study 2. The whole-body meshes were obtained after the MHX files were imported to Blender. Then, the whole-body MH meshes were triangulated by Blender functions as shown in Figure 56. After mesh

triangulation, the whole-body volume was obtained from the triangular meshes by applying tetrahedron volume techniques (Zhang & Chen, 2001). The tetrahedron volume techniques (Zhang & Chen, 2001) separated the triangular meshes into a set of tetrahedrons and calculated the volume by computing and accumulating the volume of each tetrahedron.

Original MH mesh Triangular mesh

Figure 56 The whole-body MH meshes can be triangulated by Blender functions.

5.2.2 Segmental Body Volume Acquisition

To acquire segmental body volume, the whole-body meshes needed to be divided into segmental triangular meshes in several steps. First, the positions of segmental planes were decided by the coordinates of specific vertices. For example, the boundary planes of the upper torso were determined by the location of highlighted points as shown in Figure 57. Second, the segment meshes were obtained by using the Boolean function in Blender as shown in Figure 58. The segmentation method (the location and orientation of boundary planes) was that used in the E-Zone (Deffeyes & Sanders, 2005) since the aim of the accuracy of the proposed method is to be similar to that

achieved with E-Zone (please refer to Study 4). The assumption of bilateral symmetry, which assumes segmental volumes of right limbs are equal to corresponding left limbs, was also applied in this research so 10 body segment meshes (right side) were obtained after the segmentation processing by Blender as shown in Table 12. Then, the segmented meshes were triangulated and used to calculate their volume by applying tetrahedron volume techniques (Zhang & Chen, 2001) as shown in Figure 59.

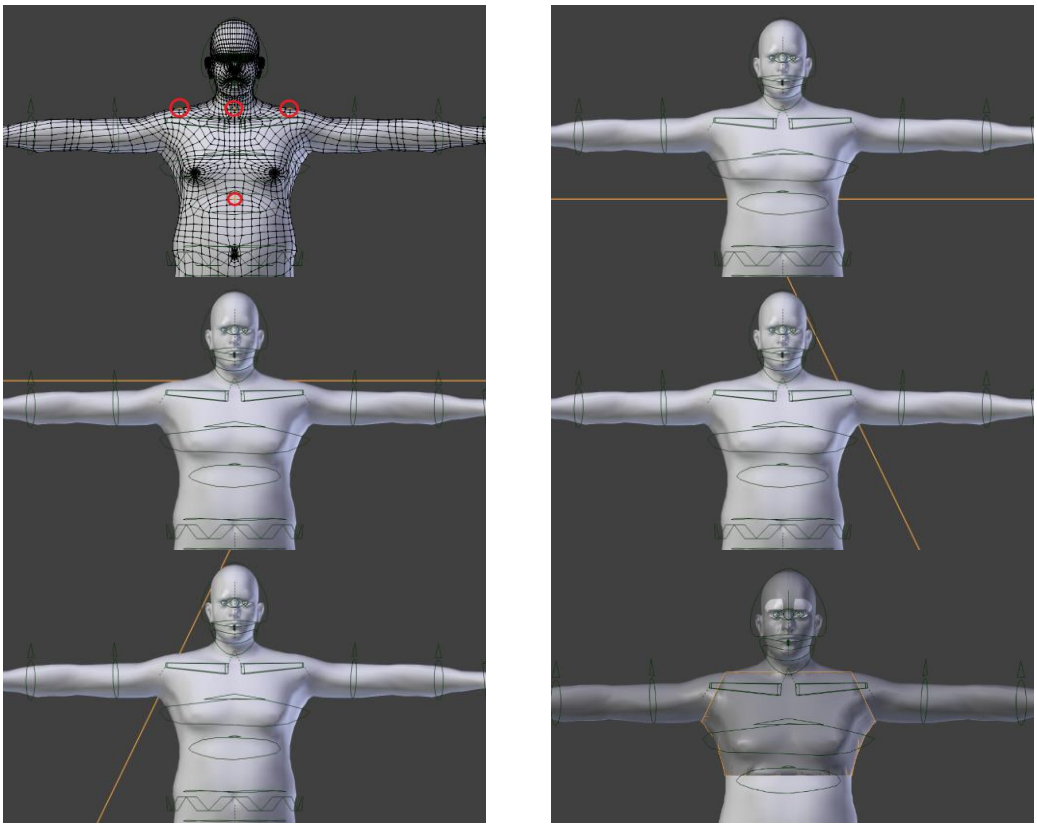

Figure 57 The boundaries of the upper torso were determined by the location of highlight points.[15]

[15] The green lines on the MH model are the MHX objects which are showed while using Blender.

5.2.3 Developing an Automatic Program for Calculating Personal Body Volume Data

The Blender scripts and shell scripts were developed to build an automatic program for body volume acquisition. Using the Blender scripts, the computer identified the specific vertices automatically by referring to the pre-defined vertex numbers and then providing their coordinate information for setting the segmental planes to complete the mesh segmentation without manual operation. The computer also completed mesh triangulation automatically. The Blender scripts for obtaining triangular meshes of whole bodies and segments are listed in Appendix A. The Blender script was connected to the mesh volume calculation program by shell scripts so the whole process for obtaining personal body volume could be completed without any manual operation.

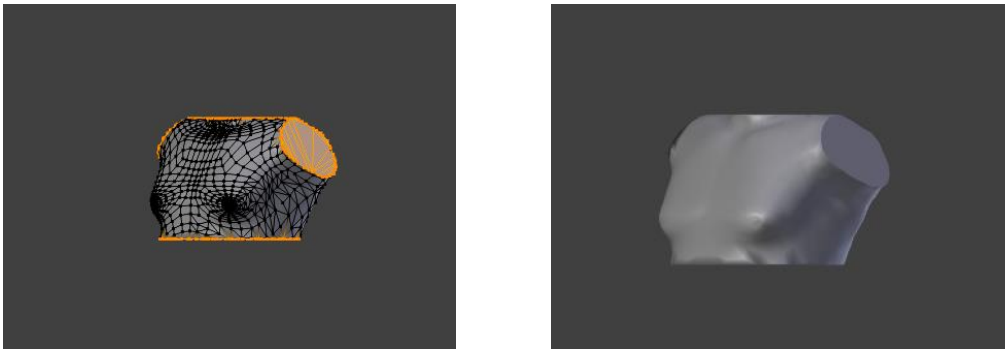

Figure 58 The segmented mesh was obtained by using the Boolean function in Blender.

Table 12 Ten body segment meshes were obtained after the segmentation processing by Blender

Body segment mesh				
Head	Neck	Upper torso	Lower torso	Right upper arm
Right lower arm	Right hand	Right thigh	Right shank	Right foot

5.2.4 Data Collection

The 3D models for 17 participants (please refer Study 1 for the detail of participants) in MHX format were generated by the approach presented in Study 2. Two individual 3D models were built for each participant so in total 34 MHX files were used for this study for comparing the processing time between the automatic program (to calculate whole-body volume and 10 segmental volumes) and traditional manual process (to calculate one segmental volume). Both the automatic program and the traditional manual process were conducted with a general laptop (i5-3210M and 8G RAM).

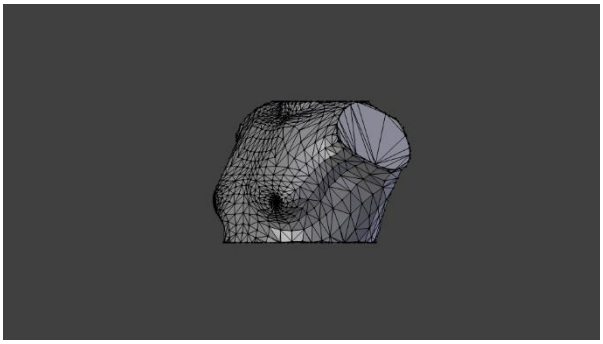

Figure 59 The segmented mesh was triangulated, and the triangulated mesh was used for calculating segmental volume.

The 34 MHX files were used as the input for the developed automatic program for calculating complete body volume data including whole-body volume and 10 segmental volumes. The automatic program completed all the processes including MHX importation, mesh segmentation (for segmental volume calculation), mesh triangulation, and volume calculation. The processing time was measured from the moment the first MHX file was imported and ended with displaying the volume results (whole-body and 10 segmental volumes) on the computer monitor.

The 34 MHX files were also used as the input for the traditional manual process to calculate one segmental volume (for right lower arm). A trained operator imported the MHX files into the graphic user interface of Blender and completed the segmentation and triangulation process with a similar approach of the automatic program. Then, the triangular meshes were exported and the program for mesh volume calculation was used to calculate the right lower arm volume. The processing time of the traditional manual process was measured in the same way as the automatic program.

5.2.5 Statistical Analysis

After data collection, 34 processing time values for the automatic program and 34 processing time values for the traditional manual process were obtained. An paired *t*-test was used to compare the processing speed for calculating complete body volume data by the automatic program with the one for acquiring one segmental body volume data by the traditional manual process. The paired *t*-test was conducted by commercial statistical software (IBM SPSS Statistics version 21.0).

5.3 Result

The mean and standard deviation of the processing speed for the automatic program were 52.33±0.26 seconds (whole-body volume and 10 segmental volume). The mean and standard deviation of the processing speed for the traditional manual process were 138.71±49.00 seconds (only one segmental volume). The result of the paired *t*-test shows that there was a significant difference in the processing speeds between the automatic program and the traditional manual process ($p<0.001$). Therefore, applying the developed automatic program to acquire complete body volume data (whole-body

volume with 10 segmental volumes) took significantly less time than using the traditional manual process to obtain one segmental volume.

5.4 Discussion

This study aimed to develop a customized program for acquiring body volume data from HM models automatically and examine whether the developed program could provide a time-efficient process. To achieve this, the Blender scripts and shell scripts were used in the program development. The corresponding tests were conducted to compare the processing time between the traditional manual process and the developed program.

No manual intervention was needed during the process of the automatic program, from identifying the import MHX file to displaying the complete body volume calculation results on the computer monitor. Therefore, non-expert users could avoid using the graphic user interface to segment and triangulate meshes for obtaining body volume data (i.e. the manual operation which was necessary in previous studies (Ma et al., 2011)). Moreover, the results obtained from the automatic program were not affected by the operator so between-assessor operation error (Ma et al., 2011; Sanders et al., 2015) can be avoided. Thus, the developed program completed the body volume calculation automatically which was a valuable development to reduce the requirement of expert knowledge and increase the inter-operator reliability.

The result shows that the mean processing time for that using the traditional manual process to obtain one segmental volume is more than two minutes. Although the traditional manual process was only used for one segment for comparative purposes, the procedure for acquiring volume for all body segments is similar. It means that

obtaining complete body volume data is simply repeating the process used to obtain one segmental volume and the processing time for completing the calculation of whole-body volume can be estimated by a simple linear multiplier. Thus, obtaining complete body volume data (one whole-body volume and 10 segmental volumes) by this technique might require more than 20 minutes. From this experience, obtaining one individual body volume data (one whole-body volume and 10 segmental volumes) by manual processing from a MH model would take 40 minutes since the operator's efficiency reduces while the processing tasks increase.

Other template models such as SCAPE (Anguelov et al., 2005) and TenBo (Yinpeng et al., 2013) can also be used to generate individual models and calculate body volume automatically. However, previous studies did not measure the processing time for calculating body volume from the individual 3D human model generated with SCAPE (Anguelov et al., 2005) and TenBo (Yinpeng et al., 2013). The result shows that the automatic program can complete the complex procedures with a time-efficient process (less than 1 minute) which is faster than the processing time for acquiring single segmental volume by the traditional manual process. Hence, the processing speed for acquiring complete body volume data by the automatic program is much faster than the processing speed for obtaining one whole-body and 10 segmental volumes by the traditional manual process. The main reason is that the automatic program avoided the time-consuming process which required human intervention. In other words, the developed script simplified the visual load to the command line tasks. The low processing time demonstrated that the developed program is therefore a valuable way to combine with the developed method for feature extraction (Study 1) and model generation (Study 2) to achieve aspects of the research purpose (delivering body

volume data in 10 minutes - refer to Section 1.2.3). Furthermore, the Blender scripts could be implemented in a parallel computing such as MPICH2 so that the processing time for obtaining body volume data could be further reduced.

The method developed in this study introduced a direct way to obtain body volume data from MH models. By this method, there was no need to use other parametric models such as SCAPE model (Anguelov et al., 2005) or TenBo model (Yinpeng et al., 2013) to register the generated MH models and determine the segmental boundaries. Because the automatic program can calculate body volume data from the MH models without the registration process, it can complete the calculation more rapidly than using other parametric models. Therefore, the automatic program will be beneficial for further research which needs to obtain body volume data from MH models.

Overall, this study shows that the developed program can obtain body volume data from MH models quickly and automatically. Therefore, the developed program is useful for developing a fast and automatic system to build 3D human models for acquiring personal body volume data.

The accuracy and test-retest reliability of the acquired body volume data was investigated in Study 4 to establish whether the proposed methods can provide accurate and reliable personal body volume data.

Chapter 6 Study 4. The Accuracy and Reliability of the Body Volume Acquisition

6.1 Introduction

In the past three studies (Study 1, Study 2 and Study3), a new technique (DScan) for obtaining personal body volume data from depth images has been developed. However, there were some assumptions in these studies. In Study 1, previous studies were referred to, in order to make the assumption that the extracted features were accurate for generating realistic human models (Samejima et al., 2012; Velardo et al., 2012). In Study 2 and Study 3, the assumption that the generated 3D models were realistic, so they can be used for obtaining accurate and reliable body volume data, was based on the principle of template model matching. These assumptions may in fact affect the accuracy and reliability of whole-body and segmental volume estimates using DScan, so it is important to compare the new technique with other body volume acquisition methods to determine its performance in terms of accuracy and reliability.

Several methods have been developed for body volume acquisition (see Section 2.1). DScan aims to deliver an analysis of body volume data (whole-body volume and segmental volume) and body shape variation from a few rapid scans similar to the 3D photonic scanning techniques (3DPS). The 3DPS can obtain body volume data directly instead of through indirect calculations which have some assumptions (e.g. tissue density assumption for DXA method, see Section 2.1.5). Moreover, the fast scanning process is efficient and, unlike anthropometric measurement and water displacement, avoids using a range of equipment to measure segmental volumes which make the procedure of the tests for accuracy examination quick and simple. The 3DPS is a

radiation-free method and can be applied to participants of diverse somatotype (Stewart et al., 2012). Given these advantages, both traditional and simplified 3DPS were used to compare to the DScan in this study.

The traditional 3DPS has been compared with water displacement methods establishing its good accuracy and reliability (Collins, 2006; Wang et al., 2006). A few simplified 3DPSs have been used for body volume acquisition, such as E-Zone (Deffeyes & Sanders, 2005) and the method presented by Pirker et al. (2009). However, all of them rely on manual digitizing so the operator's skill might affect the accuracy of body volume estimation. Among these simplified 3DPS, only the inter-assessor reliability of E-Zone has been investigated. Sanders et al. (2015) found that the inter-assessor reliability of E-Zone was good (within 5% error for main body segments). Therefore, E-Zone was also used as comparison for the developed procedure since its error between assessors has been quantified.

There were two aims of this study. The first aim was to examine the accuracy of the DScan, and compare this to the accuracy of E-Zone. The second aim was to compare the reliability of DScan to the reliability of E-Zone and the traditional 3DPS.

6.2 Method

6.2.1 Experimental Design

The accuracy of E-Zone and DScan and the repeat reliability of the traditional 3DPS, E-Zone and DScan were established and compared in this study. The experimental design to assess the reliability and accuracy of body volume data is shown in Figure 60. The 17 participants (please refer to Study 1 for the detail of participants) received

a same-day repeated 3D laser scan and depth and colour image capture. To avoid the effect of breathing, participants were requested to expel the air in their lungs to end tidal level and hold their breath for the period of image capture or body scanning (approximately 10 seconds).

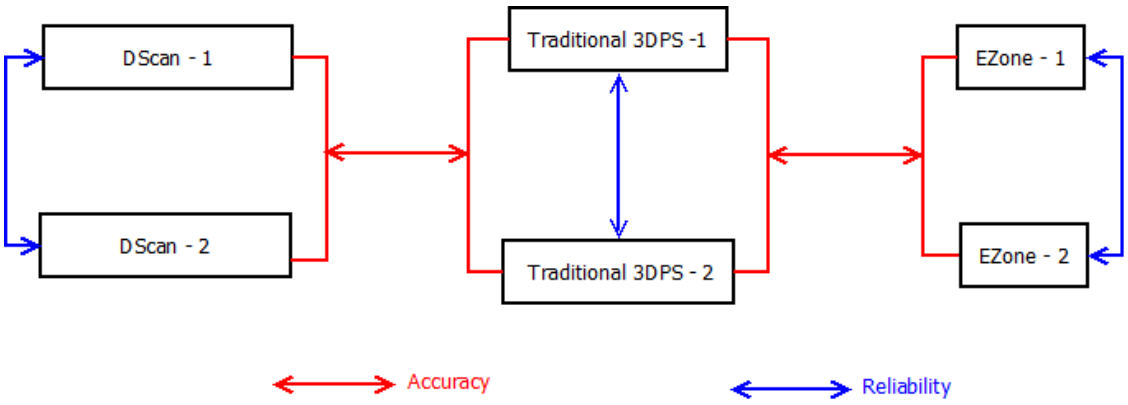

Figure 60 Experimental design for body volume tests in this study.

After data collection of 3D scanning results, depth and colour images, the same operators (OP1 and OP2), who were familiar with the use of the specific software, completed post-processing of laser scanning results, depth and colour images to obtain body volume data. OP1 completed the reconstruction tasks including noise cleaning, hole filling and mesh smoothing for the results from the traditional 3DPS. OP2 obtained the body volume data from the mesh processed by OP1 as well as depth images and colour images. OP2 obtained body volume data from the depth images by the developed procedure of DScan and acquired the result from colour images by E-Zone Software.

The mean body volume obtained from two 3D laser scans (traditional 3DPS) was used as the reference. The mean body volume data from DScan and E-Zone (two trials)

were compared against the traditional 3DPS to determine the accuracy. Intra-assessor reliability of body volume data obtained from the traditional 3DPS, DScan and E-Zone was determined with the repeated tests (two trials).

6.2.2 Acquiring Body Volume from the traditional 3DPS

Before scanning, specific markers were placed on each participant's body to indicate the segmental boundaries defined in the E-Zone (Deffeyes & Sanders, 2005) as shown in the following table (Table 13).

Table 13 Locations of marks for traditional 3DPS (adapted from Deffeyes and Sanders (2005)).

Marker	Marker Location
C2	Mandible Angle
C7	Adam's Apple
AC Joint	Acromiale
Elbow	Radiale
Wrist	Stylion
Xiphoid	Base of Sternum
Hip	Trochanterion
Knee	Tibiale laterale
Ankle	Lateral Malleolus of the Fibula

Figure 61 shows the marking examples for the segment endpoints. To ensure all the markers could be seen from the body scanning results, triangular marks were placed on the acromiale. This avoided the issue that the flat marks on the horizontal shoulder may not be detected. All markers were placed by an accredited anthropometrist.

A B C

Figure 61 Specific markers were placed on each participant's body to indicate the segmental boundaries. (A. acromiale; B. tibiale laterale; C. radiale)

A commercial full body scanner (Vitus Smart XXL scanner, Vitronic, Germany) was used to capture 3D human models as shown in Figure 62. The associated computer software, CySlice (headus 3D), was used to clean the noise, fill the 'holes' and smooth the mesh as shown in Figure 63.

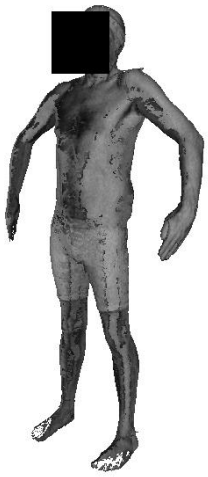

Figure 62 A 3D human model was captured by the 3D commercial scanner.

Figure 63 The 3D human model was processed with the associated computer software, CySlice, to clean the noise, fill the holes and smooth the mesh.

Computer software, Blender, was used to obtain a mesh of each segment after obtaining the smooth 3D human model as shown in Figure 64. The body volume data were calculated from whole-body mesh and segmental meshes by applying tetrahedron volume techniques (Zhang & Chen, 2001).

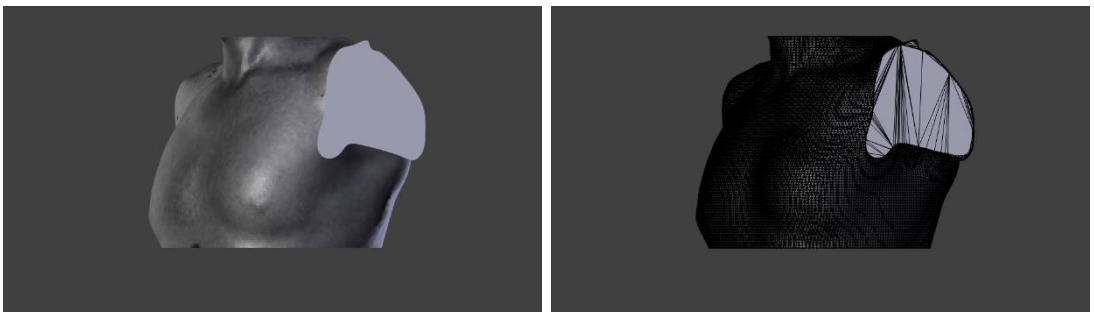

Figure 64 The segmented mesh, upper torso, can be obtained from the 3D human model by using the Boolean function in Blender.

6.2.3 E-Zone

The E-Zone method (Deffeyes & Sanders, 2005) was also used to collect body volume data to compare with those of the developed technique (DScan). Colour markers were placed to indicate each participant's body landmarks or segmental boundaries as shown in Table 14.

Table 14 Locations of marks for E-Zone (adapted from Deffeyes and Sanders (2005)).

Marker	Side View Marker Location	Frontal View of Marker Location
C2	Mandible Angle	Centre of chin
C7	At level of Adam's Apple, in centre of neck segment	Adam's Apple
Humerus Head	Greater tubercle of the Ulna (head of humerus)	Point between Acromiale and armpit on the level of humerus head
Elbow	Radiale	Level of Radiale
Wrist	Stylion	Level with the side marker
Xiphoid	Level with front marker, on the midline of the trunk.	Base of Sternum
Hip	Trochanterion	Level of Trochanterion
Knee	Tibiale laterale	Level of Tibiale laterale
Ankle	Lateral Malleolus of the Fibula	Level with the side marker, on the midline of the ankle.

Participants' images were captured from the front view and side view by calibrated cameras (Casio EX-FH100, resolution 2736×3648) as shown in Figure 65. The capturing distance was around 12 meters for both front and side view cameras as shown in Figure 66. Then, the corresponding Matlab program was used to build a 3D

elliptical model by applying the associated theory (Jensen, 1978) and calculate the body volume as shown in Figure 67.

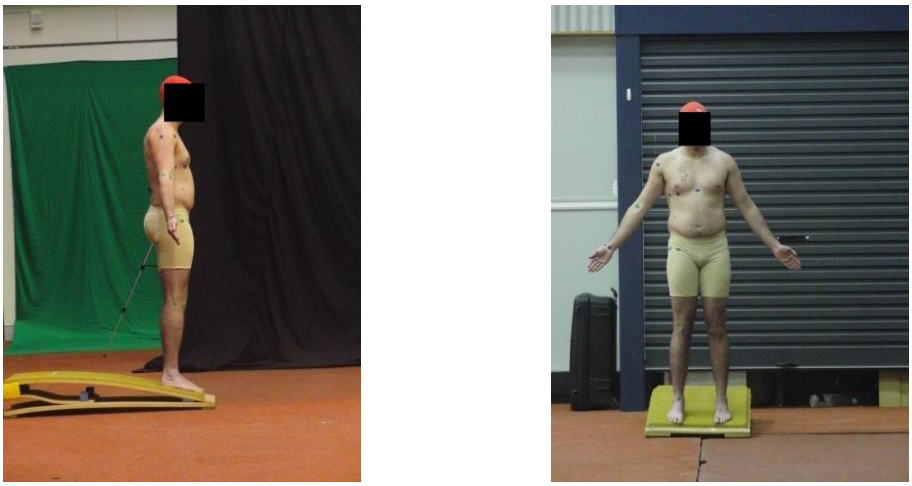

Figure 65 The colour markers were placed on each participant's body landmarks and participants' image will be captured from front and side views.

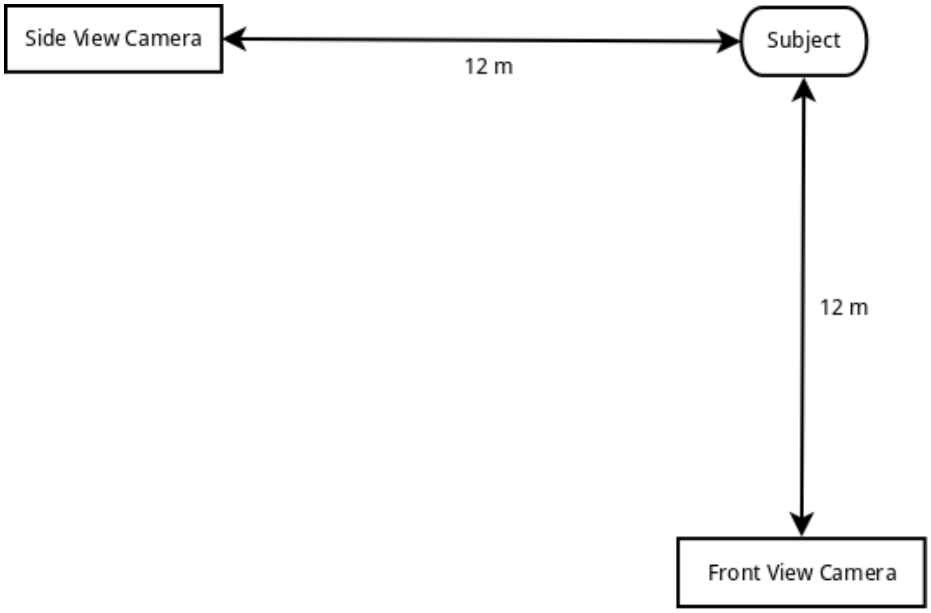

Figure 66 The camera setup for E-Zone tests

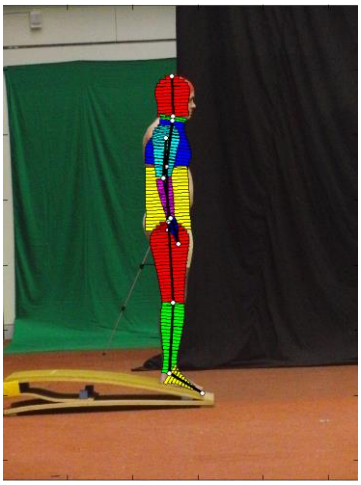
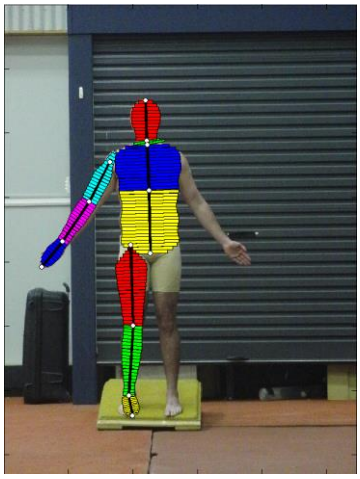

Figure 67 The corresponding E-Zone Matlab program was applied to build a 3D elliptical model and calculate whole-body and segmental volumes

6.2.4 Statistical Analysis

The inter-method absolute technical error of measurements (inter absolute TEM) and inter-method relative technical error of measurements (inter relative TEM) was used to quantify the accuracy and determine the difference between various methods as in the following equations (Equation (42) and Equation (43)) (Perini et al., 2005).

$$\text{Inter absolute TEM} = \sqrt{\frac{\sum_{i=1}^{N}(\bar{M}_{i1} - \bar{M}_{i2})^2}{2 * N}} \tag{42}$$

$$\text{Inter relative TEM} = \frac{\text{Inter Absolute TEM}}{\frac{\sum_{i=1}^{N}(\bar{M}_{i1} + \bar{M}_{i2})}{2 * N}} * 100\% \tag{43}$$

where N is representative of the number of participants, $\bar{M}_{i1}$ and $\bar{M}_{i2}$ denote the mean of repeated measurements separately obtained by a testing method (DScan or E-Zone)

and the reference method (the traditional 3DPS) for the i^{th} participant. The inter relative TEM for accuracy were calculated with Microsoft Excel (Microsoft®).

The analysis of Bland and Altman plots (Martin Bland & Altman, 1986) were also conducted to determine the bias of the body volumes acquired by DScan and E-Zone. Free statistic software, R (http://www.r-project.org/), was applied to generate the Bland and Altman plots.

Intra-method absolute TEM (intra absolute TEM) and intra-method relative TEM (intra relative TEM) was used to determine the reliability of repeated measurements for each body volume acquisition method as Equation (44) and Equation (45) (Perini et al., 2005).

$$\text{Intra absolute TEM} = \sqrt{\frac{\sum_{i=1}^{N}(M_{i1} - M_{i2})^2}{2 * N}} \tag{44}$$

$$\text{Intra relative TEM} = \frac{\text{Intra Absolute TEM}}{\frac{\sum_{i=1}^{N}(M_{i1} + M_{i2})}{2 * N}} * 100\% \tag{45}$$

where N is representative of the number of participants, M_{i1} and M_{i2} denote the first and second measurements separately obtained for the i^{th} participant. The intra relative TEM for intra-method reliability were calculated with Microsoft Excel (Microsoft®).

Furthermore, the intraclass correlation coefficient (ICC) was also used to determine the reliability of different methods. Free statistic software, R, was applied to calculate the test-retest reliabilities. The calculation method referred to the illustration in previous literature (Hopkins, 2000; Weir, 2005). The ICC(3,1) model of Shrout and

Fleiss (Shrout & Fleiss, 1979) was applied to calculate the reliability as it ignores the systematic error for the repeated measurement.

6.3 Results

6.3.1 Accuracy

The mean and standard deviation of the body volume data for all 17 participants measured by the traditional 3DPS, E-Zone and DScan is shown in Table 15. The accuracy of DScan and E-Zone is represented with the inter absolute TEM and the inter relative TEM as shown in Table 16. The relative TEMs of segmental volume acquisition for both methods were similar. Both methods can estimate the segmental volumes of upper torso, lower torso, thigh, shank, upper arm and lower arm accurately (relative TEM<10%) but the accuracy of small segments including neck and foot were poor.

Table 15 The body volume data for all 17 participants (Mean ± Standard Deviation in litre) measured by the traditional 3DPS, E-Zone and DScan

Segmental volume	Traditional 3DPS	E-Zone	DScan
Whole-body volume	82.33±8.97	79.57±8.09	81.79±8.14
Head volume	5.08±0.57	4.75±0.39	4.94±0.38
Neck volume	0.56±0.28	0.65±0.19	0.59±0.09
Upper torso volume	18.81±2.13	17.96±1.97	20.25±1.99
Lower torso volume	24.04±3.25	22.20±2.70	23.71±2.81
Thigh volume	8.82±1.34	8.48±1.31	8.62±1.17
Shank volume	3.44±0.48	3.49±0.47	3.45±0.30
Foot volume	0.80±0.14	0.98±0.19	0.75±0.06
Upper arm volume	2.25±0.33	2.14±0.30	2.26±0.21
Lower arm volume	1.24±0.16	1.33±0.18	1.22±0.16
Hand volume	0.43±0.05	0.55±0.11	0.41±0.03

The relative TEMs of whole-body volume estimations were around 3% for both E-Zone and DScan. E-Zone can estimate the leg volume including thigh and shank under 5% relative TEM and the trunk and arm volume with a little higher error (under 10%). Likewise, DScan can acquire the most segmental volumes (upper torso, lower torso, thigh, shank, upper arm, lower arm and hand) under 10%. The relative TEMs of the volume estimation for lower torso and shank were around 5%.

Table 16 The accuracy (absolute TEMs, Litre; relative TEMs, %TEM) of E-Zone and DScan. (A lower TEM value indicates better accuracy)

Segmental volume	E-Zone Absolute TEM	E-Zone Relative TEM	DScan Absolute TEM	DScan Relative TEM
Whole-body volume	2.27	2.8	2.51	3.1
Head volume	0.34	7.0	0.46	9.1
Neck volume	0.18	29.6	0.21	35.8
Upper torso volume	1.08	5.9	1.52	7.8
Lower torso volume	1.82	7.9	1.25	5.2
Thigh volume	0.42	4.9	0.71	8.2
Shank volume	0.10	2.9	0.23	6.6
Foot volume	0.16	18.2	0.08	10.9
Upper arm volume	0.14	6.5	0.18	7.8
Lower arm volume	0.09	6.6	0.10	8.4
Hand volume	0.10	21.0	0.03	6.9

The Bland-Altman plot of body volume data (one whole-body volume and 10 segmental volumes) from traditional 3DPS and DScan and traditional 3DPS and E-Zone as shown in Figure 68 to Figure 78. The bias of DScan for all body volumes (apart from upper torso volume) is smaller than the bias of E-Zone. The whole-body volume, foot volume, lower arm volume and hand volume acquired from E-Zone was likely (95% confidence) underestimated when the traditional 3DPS was the reference.

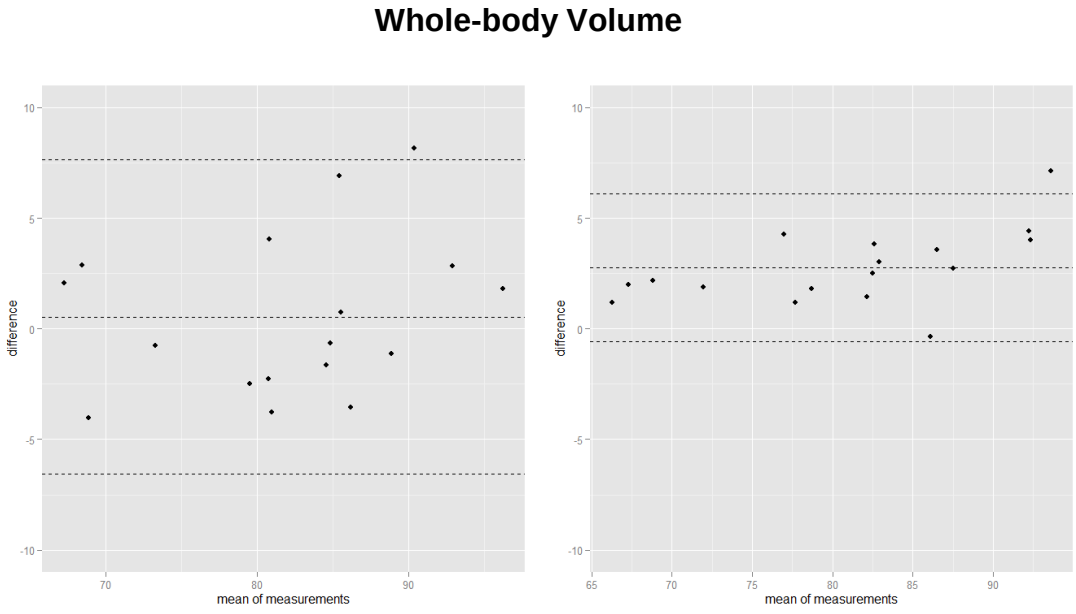

Traditional 3DPS – DScan: 0.54±3.62 Traditional 3DPS – E-Zone: 2.76±1.70

Figure 68 The Bland-Altman plot of whole-body volume (litre) measured from traditional 3DPS and DScan, traditional 3DPS and E-Zone.

Head Volume

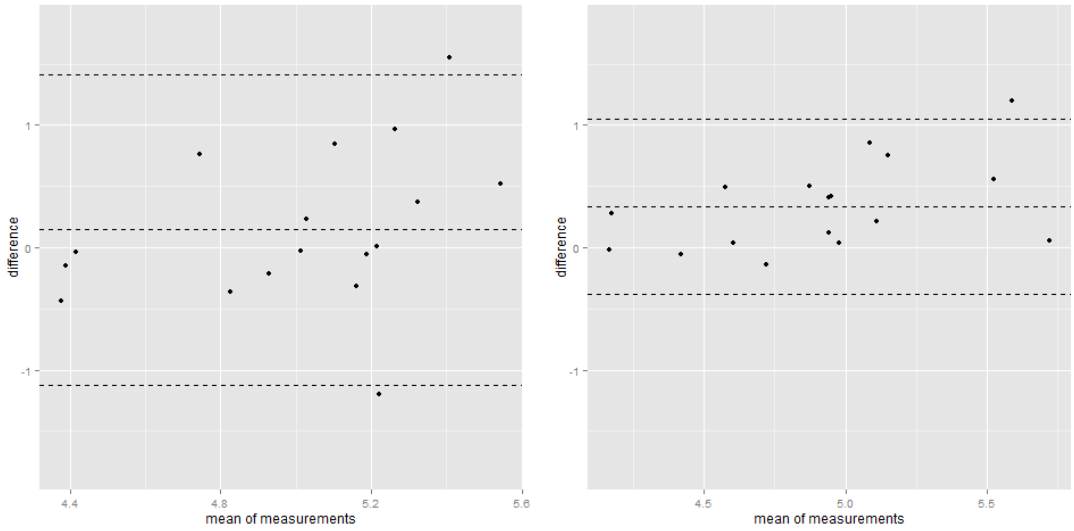

Traditional 3DPS – DScan: 0.14±0.65 Traditional 3DPS - E-Zone: 0.34±0.36

Figure 69 The Bland-Altman plot of head volume (litre) measured from traditional 3DPS and DScan, traditional 3DPS and E-Zone.

Neck Volume

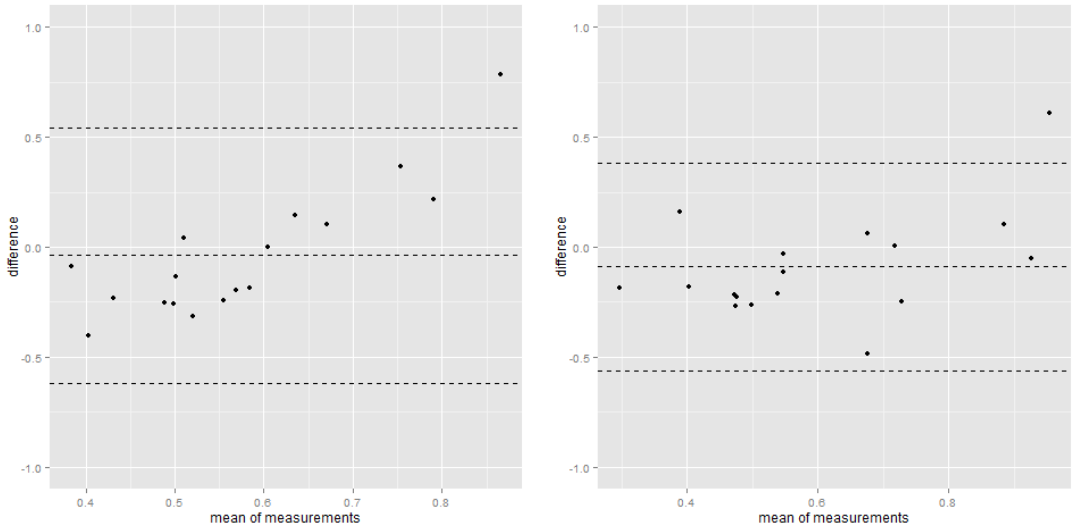

Traditional 3DPS – DScan: -0.04±0.30 Traditional 3DPS - E-Zone: -0.09±0.24

Figure 70 The Bland-Altman plot of neck volume (litre) measured from traditional 3DPS and DScan, traditional 3DPS and E-Zone.

Upper Torso Volume

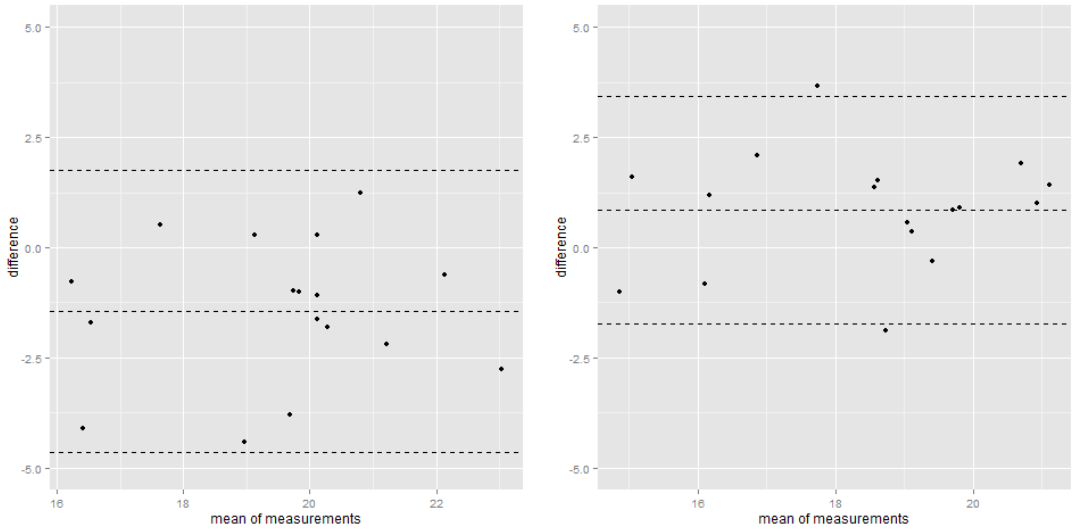

Traditional 3DPS – DScan: : -1.45±1.63 Traditional 3DPS – E-Zone: 0.84±1.32

Figure 71 The Bland-Altman plot of upper torso volume (litre) measured from traditional 3DPS and DScan, traditional 3DPS and E-Zone.

Lower Torso Volume

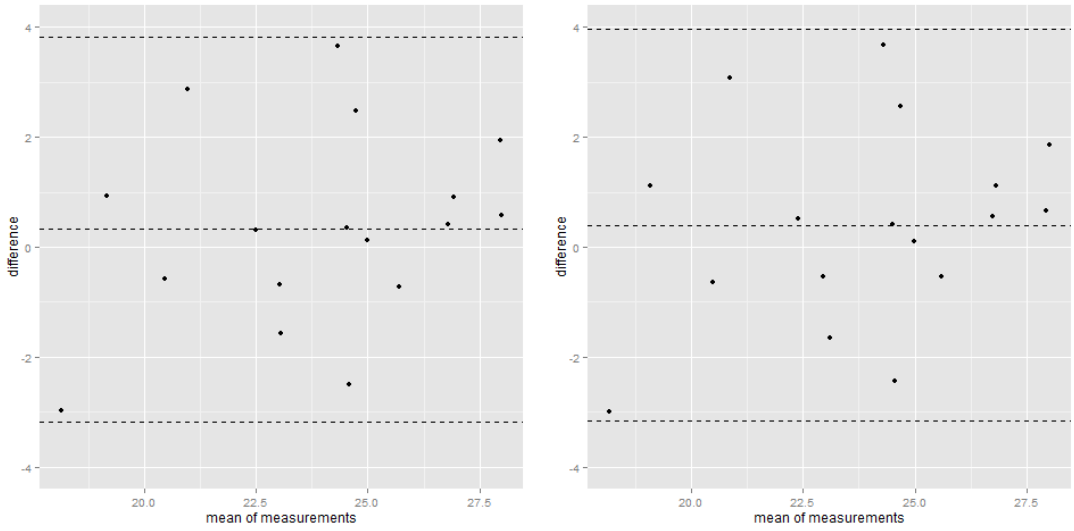

Traditional 3DPS – DScan: 0.32±1.78 Traditional 3DPS - E-Zone: 0.40±1.81

Figure 72 The Bland-Altman plot of lower torso volume (litre) measured from traditional 3DPS and DScan, traditional 3DPS and E-Zone.

Thigh Volume

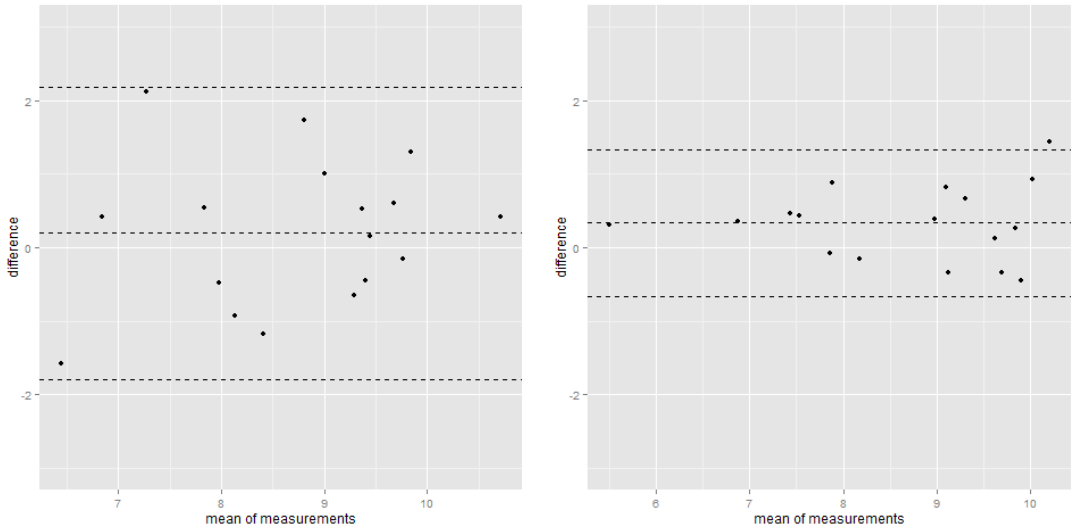

Traditional 3DPS – DScan: 0.20±1.02 Traditional 3DPS – E-Zone: 0.32±0.51

Figure 73 The Bland-Altman plot of thigh volume (litre) measured from traditional 3DPS and DScan, traditonal 3DPS and E-Zone.

Shank Volume

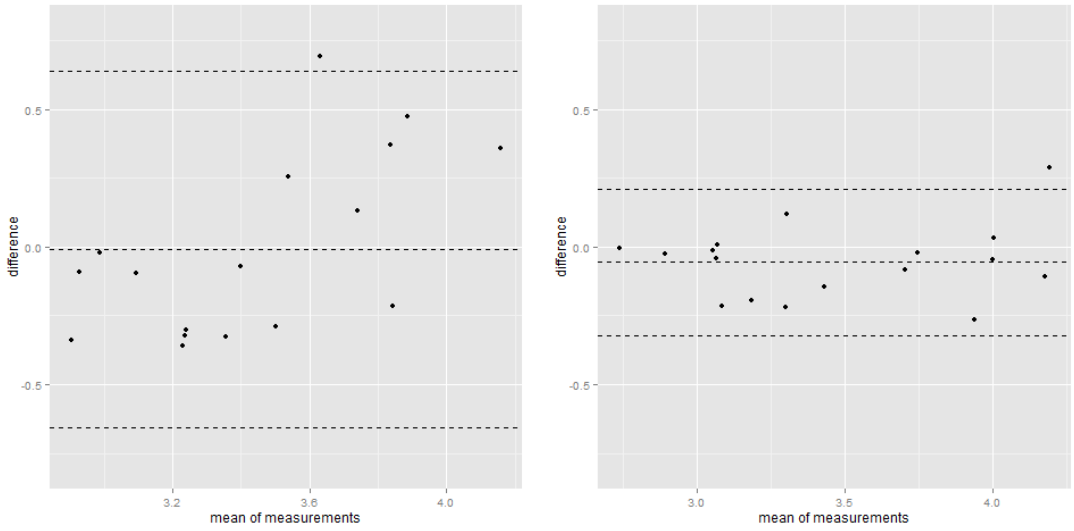

Traditional 3DPS – DScan: -0.01±0.33 Traditional 3DPS - E-Zone: -0.05±0.14

Figure 74 The Bland-Altman plot of shank volume (litre) measured from traditional 3DPS and DScan, traditional 3DPS and E-Zone.

Foot Volume

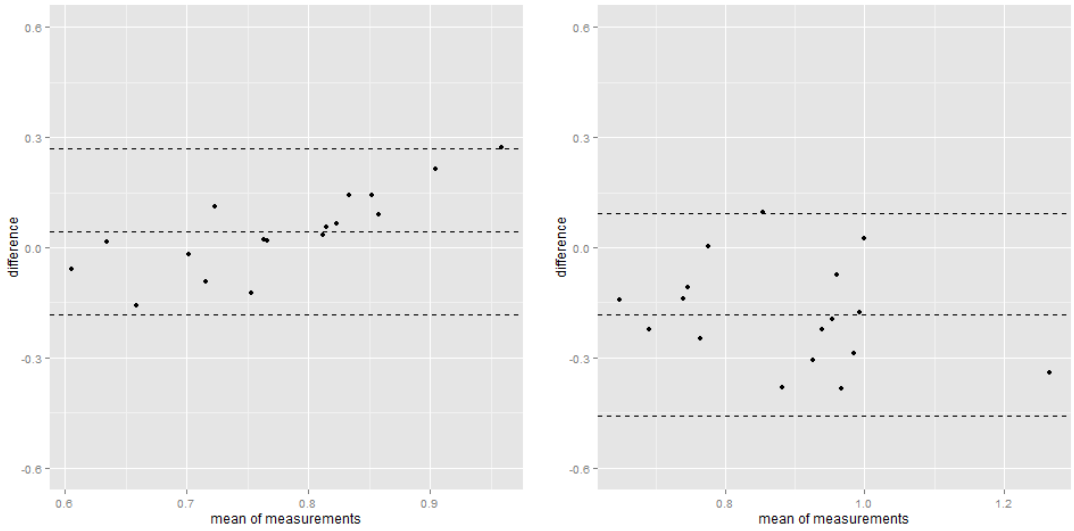

Traditional 3DPS – DScan: 0.04±0.12 Traditional 3DPS - E-Zone: -0.18±0.14

Figure 75 The Bland-Altman plot of foot volume (litre) measured from traditional 3DPS and DScan, traditional 3DPS and E-Zone.

Upper Arm Volume

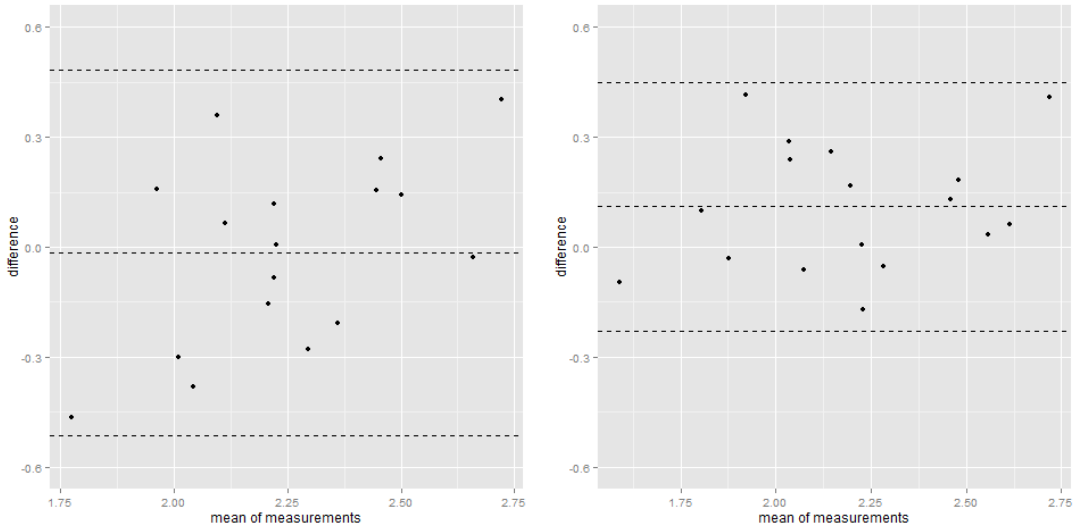

Traditional 3DPS – DScan: -0.01±0.25 Traditional 3DPS - E-Zone: 0.11±0.17

Figure 76 The Bland-Altman plot of upper arm volume (litre) measured from traditional 3DPS and DScan, traditional 3DPS and E-Zone.

Lower Arm Volume

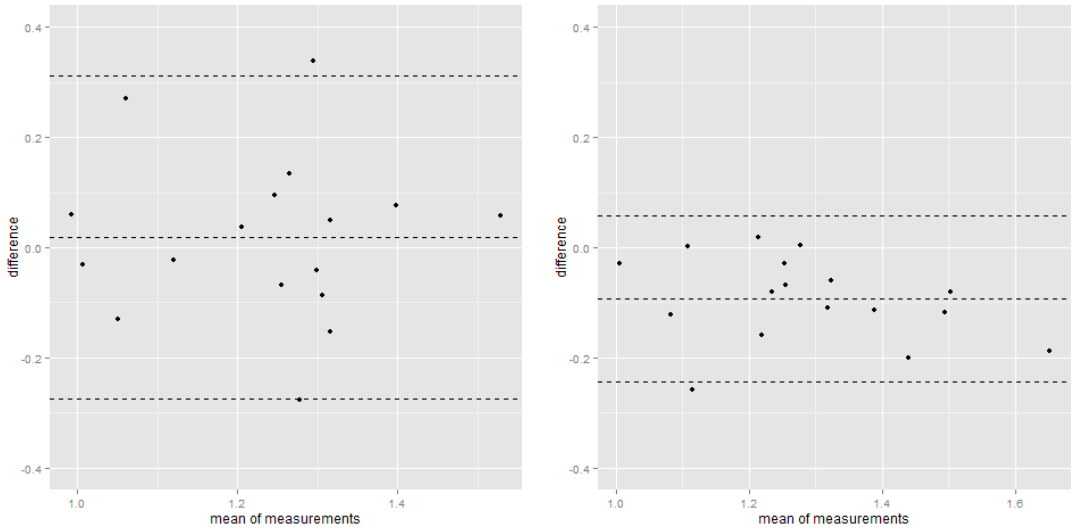

Traditional 3DPS – DScan: 0.02±0.15 Traditional 3DPS - E-Zone: -0.09±0.08

Figure 77 The Bland-Altman plot of lower arm volume (litre) measured from traditional 3DPS and DScan, traditional 3DPS and E-Zone.

Hand Volume

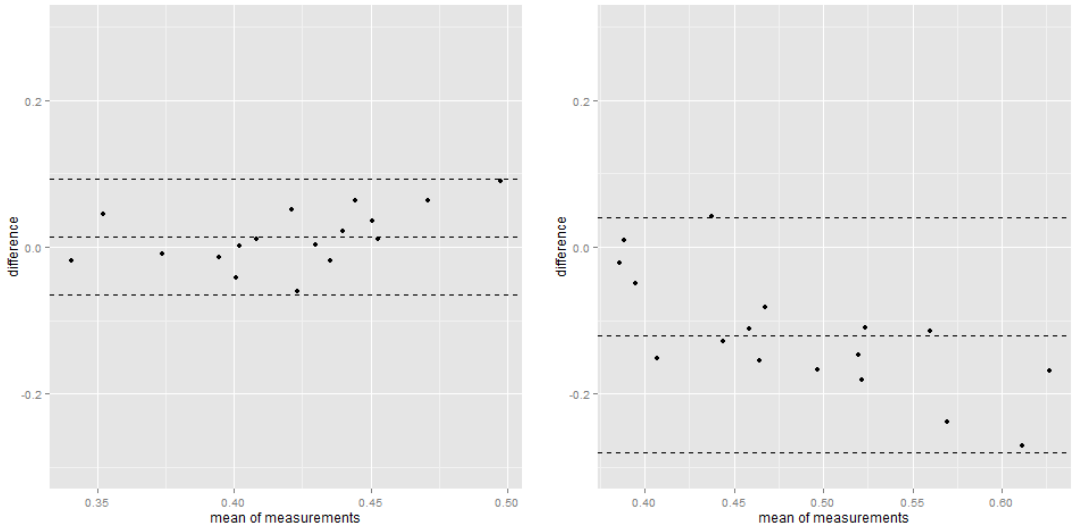

Traditional 3DPS – DScan: 0.01±0.04 Traditional 3DPS - E-Zone: -0.12±0.08

Figure 78 The Bland-Altman plot of hand volume (litre) measured from traditional 3DPS and DScan, traditional 3DPS and E-Zone.

6.3.2 Reliability

The repeated reliability is represented with the relative TEM and intraclass correlation coefficient (ICC). Table 17, Table 18 and Table 19 show the reliability of traditional 3DPS, E-Zone and DScan accordingly. The relative TEMs of the traditional 3DPS, E-Zone and DScan were all less than 5% in whole-body volume and most segmental volumes. The ICC values of these three methods were all above 0.8 in whole-body volume and most segmental volumes.

Table 17 The reliability (absolute TEMs, Litre; relative TEMs, %TEM) of the traditional 3DPS (A lower TEM value indicates better reliability)

Traditional 3DPS	Absolute TEM	Relative TEM	ICC
Whole-body volume	0.42	0.51	1.00
Head volume	0.22	4.35	0.85
Neck volume	0.13	22.77	0.80
Upper torso volume	0.29	1.53	0.98
Lower torso volume	0.55	2.31	0.97
Thigh volume	0.23	2.61	0.97
Shank volume	0.04	1.16	0.99
Foot volume	0.02	3.09	0.97
Upper arm volume	0.05	2.16	0.98
Lower arm volume	0.02	1.98	0.98
Hand volume	0.01	3.12	0.94

The traditional 3DPS can estimate whole-body volume estimation with good reliability. The relative TEM was less than 1% and the ICC was larger than 0.99. The ICC values of most segmental volume acquisitions were above 0.9 and the relative TEMs were less than 3.5%. By contrast, the reliability of head and neck volume estimation were lower than other segments.

Table 18 The reliability (absolute TEMs, Litre; relative TEMs, %TEM) of E-Zone (A lower relative TEM value indicates better reliability)

E-Zone	Absolute TEMs	Relative TEM	ICC
Whole-body volume	0.87	1.1	0.99
Head volume	0.10	2.0	0.95
Neck volume	0.14	21.0	0.51
Upper torso volume	0.29	1.6	0.98
Lower torso volume	0.45	2.0	0.97
Thigh volume	0.20	2.4	0.98
Shank volume	0.14	4.0	0.91
Foot volume	0.07	7.6	0.87
Upper arm volume	0.09	4.1	0.92
Lower arm volume	0.05	3.6	0.93
Hand volume	0.05	9.8	0.80

The reliability of the whole-body volume calculated by E-Zone was also good (relative TEM<1.5% and ICC=0.99). The relative TEM and ICC values of most large segments were lower than 5% and higher than 0.9 correspondingly. However, the estimates of

volumes of neck, foot and hand were higher in relative TEM and lower in ICCs than those of other segments.

Table 19 The reliability of (absolute TEMs, Litre; relative TEMs, %TEM) DScan (A lower relative TEM value indicates better reliability)

DScan	Absolute TEMs	Relative TEM	ICC
Whole-body volume	0.92	1.1	0.99
Head volume	0.01	0.3	1
Neck volume	0.06	10.1	0.51
Upper torso volume	0.26	1.3	0.98
Lower torso volume	0.73	3.1	0.93
Thigh volume	0.24	2.8	0.96
Shank volume	0.11	3.3	0.86
Foot volume	0.01	0.8	0.99
Upper arm volume	0.05	2.2	0.94
Lower arm volume	0.03	2.9	0.95
Hand volume	<0.01	<0.01	1

Relative TEM and ICC value of whole-body volume calculated by DScan were similar to the traditional 3DPS and E-Zone (relative TEM<1.5% and ICC=0.99). DScan can estimate the volumes of all segments (head, neck, upper torso, lower torso, thigh, shank, foot, upper arm, lower arm and hand) with acceptable reliability (relative TEM < 5% and ICC>0.8).

6.4 Discussion

The two aims of this study were 1) to compare the accuracy of E-Zone and DScan to 3DPS and 2) to compare the reliability of the traditional 3DPS, E-Zone, DScan. To complete these, three methods, the traditional 3D photonic scanning method, E-Zone and DScan were used to obtain body volume data repeatedly. The body volume data obtained from the traditional 3DPS method was regarded as the reference and used to compare the accuracy of E-Zone and DScan. The reliability of the three methods was established by comparing the body volume data obtained from repeated tests (two trials).

When the traditional 3D photonic scanning is the reference, the error of whole-body volume for both methods was less than 5% and most segmental volume errors were under 10%. Only the small segments, neck and foot cannot be estimated within 15% error. The accuracy of whole-body acquisition from E-Zone in this study (2.8%) is a little smaller than the test results (4.8%) presented in Wicke and Lopers (2003). The difference (2.8% vs 4.8%) might be generated by different assessors' manual digitizing results. This confirmed the test results that the whole-body volume acquired from E-Zone by different assessors might vary considerably (Sanders et al., 2015). DScan is automatic so it can provide stable body volume estimation with good accuracy and avoid the error generated by different assessors. Compared with the result shown by Pirker et al. (2009) which also used the MH model to match the extracted features (24.3% for arm volume estimation), the accuracy of arm volume (7.8% for lower arm; 8.4% for upper arm) estimation by DScan is good. The possible reason is that DScan used the arm parameters for altering the body shape of template models. This confirmed the argument in Study 2 that the parameters of arms are necessary for

acquiring the accurate segmental volume data. The accuracy of the small segments (neck, hand, foot) was poorer than the accuracy of other segments. The possible reason is that there were some errors generated in the optimization and volume acquisition processes and the small volumes were sensitive to the error which caused the high relative TEMs. For instance, the inter absolute TEMs of neck, hand and foot were smaller (<0.25 Litre) than most the other segments such as torso segments (>1 Litre) but the intra relative TEMs of small segments were larger than others.

Furthermore, the body volumes obtained from DScan demonstrated less bias than those acquired from E-Zone. The possible reason might be that the DScan can generate the realistic shapes of segments for volume calculation and E-Zone used simple geometries (elliptical cylinders) to approximate the segmental shapes. Some systematic error might be generated while using simple geometries to approximate the segmental shapes. This confirms the statements in a previous study (Wicke & Dumas, 2007) that using elliptical cylinders by E-Zone to approximate body shapes generated the error since there are some differences between realistic shapes and approximation shapes.

Although the accuracy of DScan can achieve the research purpose in terms of accuracy (less than 5%TEM in whole-body volume and 10%TEM in segmental volume, refer to Section 1.2.1), E-Zone is slightly more accurate than DScan. The possible reason is that E-Zone extracted the segmental breadth and width features every 2 centimetres, and the numerous (more than 100) features might be helpful to illustrate the detail of body shapes for calculating accurate body volume data. By contrast, DScan only

extracted 23 features. In future research it might be helpful to extract more body dimension features to improve the accuracy of body volume acquisition.

Another possible reason for DScan being less accurate than E-Zone is that, in Study 1, it was assumed that the extracted features were 'accurate' which might generate some error in human modelling and lead to miscalculations in body volume acquisition. Recently, a more accurate depth camera (Kinect Version 2) has been released (Microsoft, 2015a). The resolution is reported to be twice the resolution of the camera used in the current research and the depth detection to be more accurate. Furthermore, the positions of joint centres detected by the new camera system have been defined so the accuracy of body dimension features can be determined. Therefore, future research should use the Kinect Version 2, and the extracted body dimension features should be corrected before generating 3D human models to improve the accuracy for body volume acquisition.

The repeated reliability of most segments acquired from DScan achieved the research purpose in terms of reliability (<5%TEM). The repeated reliability of traditional 3DPS and E-Zone for the main segments (apart from neck, hand and foot) were also good and similar to the reliability of DScan. The reliability of body volume estimation from traditional 3DPS was similar to the results presented by Collins (2006). However, the reliability of small segmental volumes (neck, hand and foot) obtained from DScan was better than the ones acquired from traditional 3DPS and E-Zone. This might be because the automation of DScan standardizes the process for body volume acquisition and it avoided some human error in manual digitizing (segmentation for traditional 3DPS and boundary detection for E-Zone). The small segmental volumes were most sensitive

to human error, and it generated high relative TEMs in the small segmental volume acquisition from traditional 3DPS and E-Zone.

The reliability of neck segments is much poorer than the reliability of other segments while using DScan. The possible reason is that the reliability of the neck feature was the poorest (4.1% for neck breadth, refer to the result in Study 1) among the selected features. This result confirmed the argument in Study 1 that the reliability of the extracted feature affects the reliability of segmental volume acquisition. Therefore, the reliable feature extraction method should be investigated in further research to improve the reliability of body volume acquisition.

In summary, the developed DScan can achieve the research purposes in terms of accuracy and reliability. The accuracy of DScan is slightly poorer than the accuracy of E-Zone, but it can avoid the instability generated by human error. The reliability of the traditional 3DPS, E-Zone and DScan was similar. Further research including extracting numerous accurate and reliable features need to be conducted to improve the current accuracy and reliability.

Chapter 7 Technical Description. Body Shape Monitoring System

7.1 Introduction

In the first four studies of this thesis (Study 1, Study 2, Study 3 and Study 4), a new technique (DScan) for generating individual models and estimating body volume data from depth images has been developed. The accuracy and reliability of DScan for body volume data acquisition were also established. This technical description introduces a Body Shape Monitoring System (BSMS) which can help non-expert users complete all the procedures of the DScan automatically and visualize body shape changes. Boelaert et al. (2008) indicated that the visualization of body shapes can motivate people to reduce weight. Furthermore, this technical description shows a usage example of the BSMS and reveals the information of the BSMS including cost, processing time and portability in order to examine whether this system could achieve the research purposes in terms of speed, cost and portability (see Section 1.2).

7.2 Description of the Body Shape Monitoring System (BSMS)

The user-friendly body shape monitoring system (BSMS), included three components; input option, database and graphical display, and was developed for tracking the variation of body volumes and body shape. Figure 79 displays an overview of the developed BSMS. Users can choose ‘conduct a new scan’ or ‘search scanning history’ from the input options. The database stores users’ personal information, data of body volume data and body shapes. The graphic displays can show the scanning or searching

results to help users observe their changes in body volumes and body shapes. In the following three sections (7.2.1, 7.2.2 and 7.2.3), three components are described.

7.2.1 Input Option

The input option consisted of GUI programmed by C# and .NET Framework. The graphic user interfaces were created by multiple Windows Forms Applications including ‘Login App’, ‘Main Menu App’ and ‘Manual Measurement Input App’. The relationship of these Apps is shown in Figure 80.

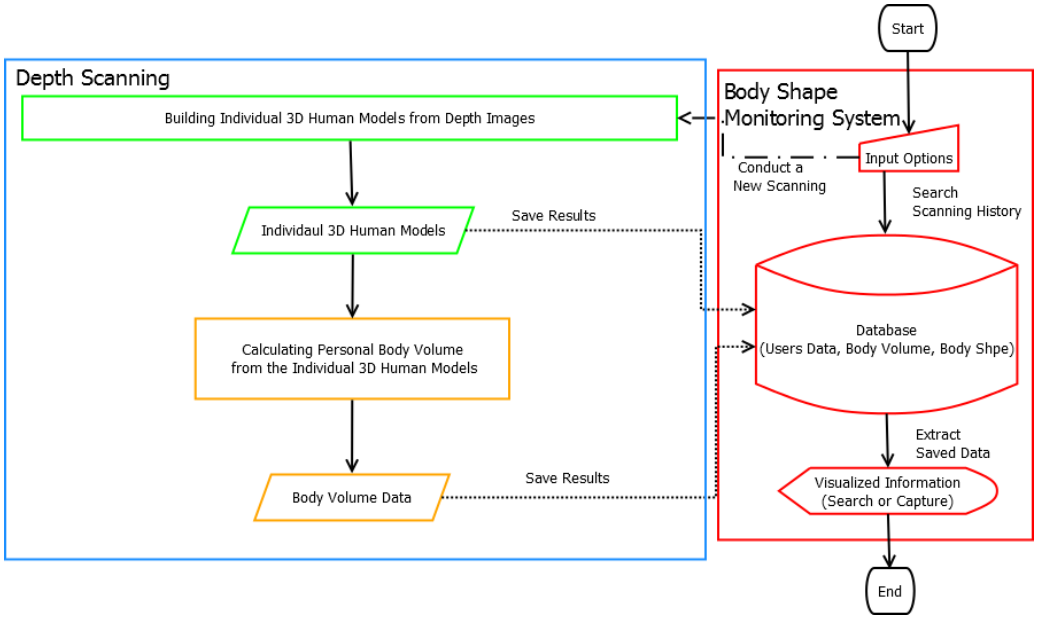

Figure 79 Overview for the body shape monitoring system.

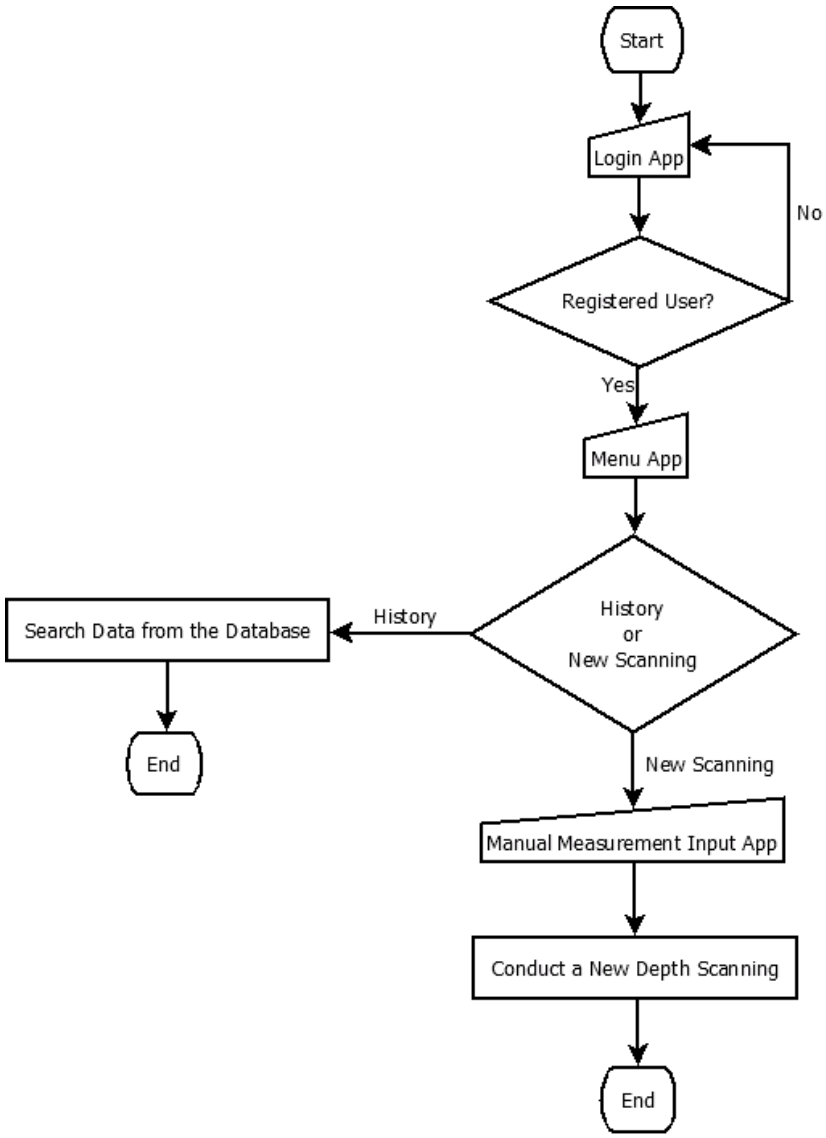

Figure 80 The relationship between 'Login App', 'Main Menu App' and 'Manual Measurement Input App'.

The Login App can help users enter their username and password and then the system can examine whether the input data are matched correctly as shown in Figure 81. If the input data are not correct, a warning message will show on the Login App as shown in Figure 82. Otherwise, the Main Menu App can connect to the Menu App as shown in Figure 83.

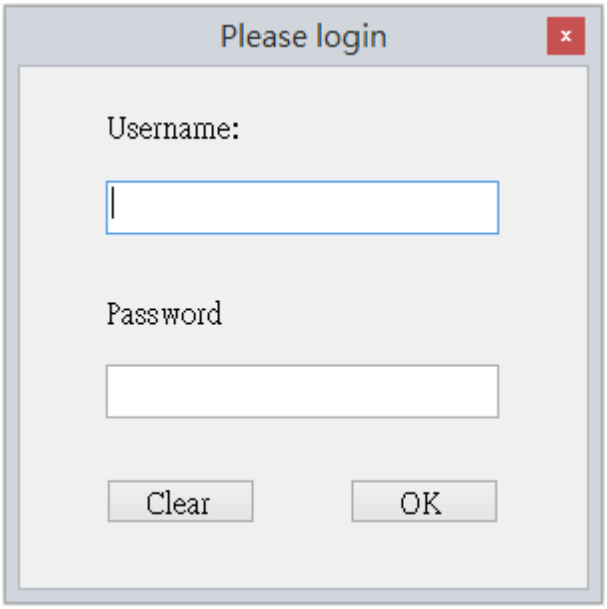

Figure 81 The GUI for login App

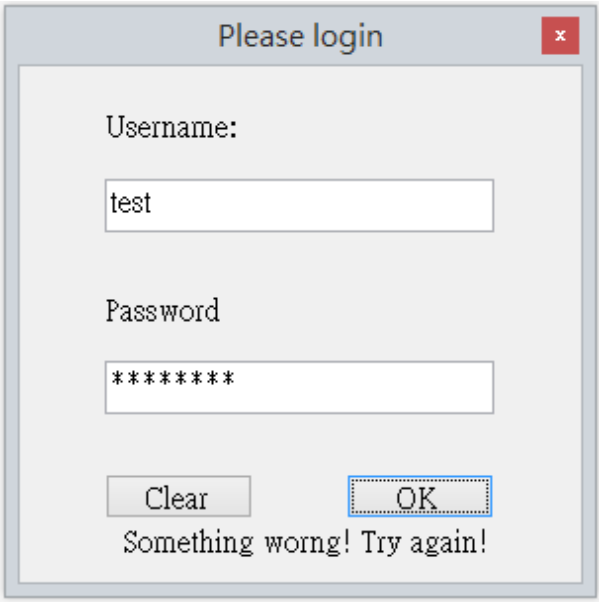

Figure 82 The warning message will show on the Login App when the entering information is not correct.

The Main Menu App contains two choice buttons, ‘History’ and ‘New scan’ as shown in Figure 83. While users choose ‘History’, the program can find the corresponding data automatically from the database and display graphically. Once users click the ‘New scan’ button, the App can connect to the Manual Measurement Input App as shown in Figure 84.

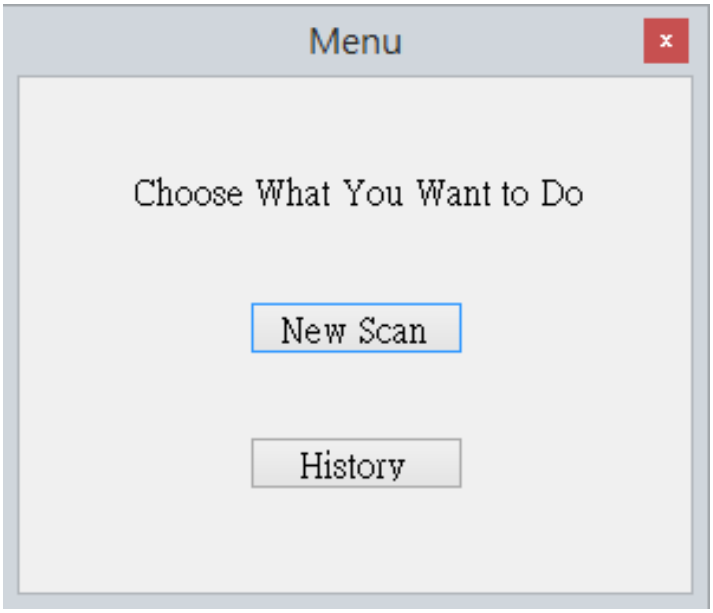

Figure 83 The GUI of Menu App

Users can enter the information which is required for the DScan such as gender, height (stature) and weight (mass) in the Manual Measurement Input App as shown in Figure 84. After input, the DScan can start without any need of expert knowledge. The scan results can be stored in the database automatically.

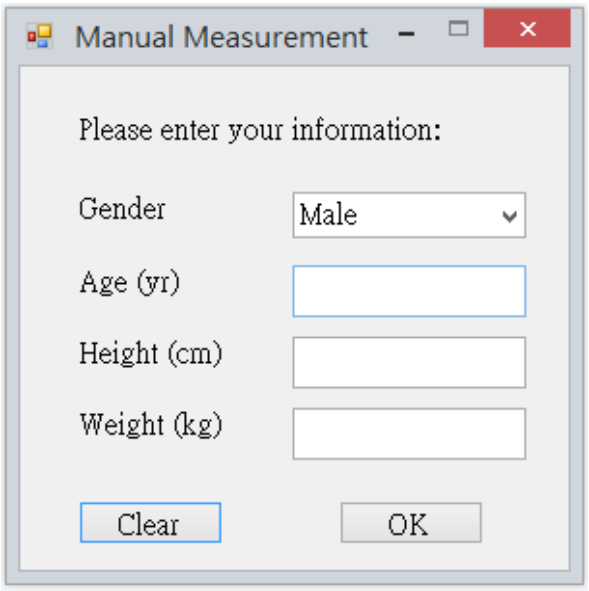

Figure 84 The GUI of Manual Measurement Input App

7.2.2 Database

The database in the monitoring body shape system was built with MySQL. It stores personal information, the parameters of the 3D individual human model and body volume data. In addition, the database can add the time stamp while updating so people can understand their body shape changes over time.

7.2.3 Graphical Displays

The graphical displays were developed with C# and .NET Framework. The graphical displays can show results obtained from the DScan. It reflects the current body shape in numbers, images and graphs as shown in Figure 85. Moreover, the graphic display can show the data stored in the database and visualize the body shape variation by overlapping two images as shown in Figure 86.

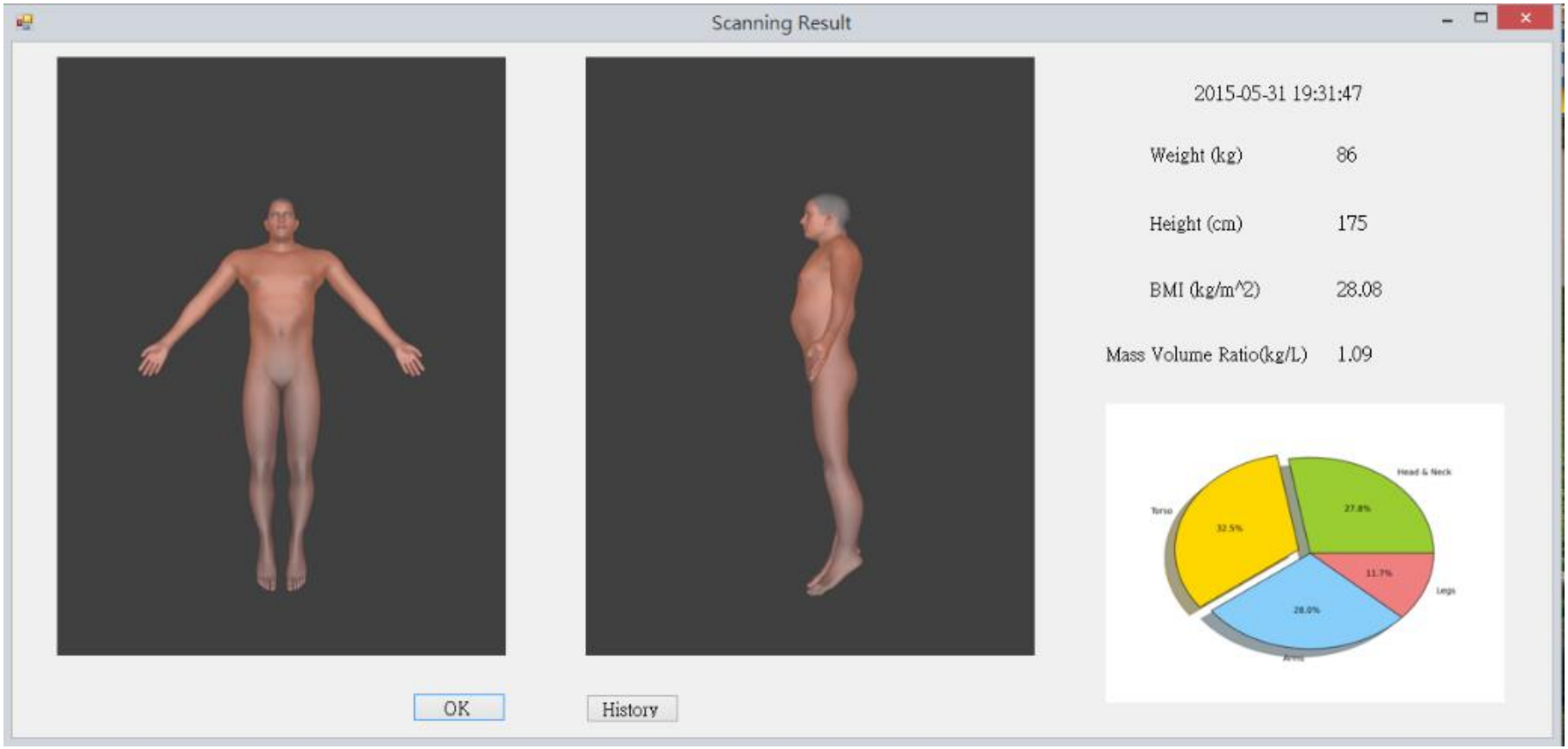

Figure 85 Graphic user interface shows the scanning result obtained from the purpose method.

7.3 An Usage Example for the Body Shape Monitoring System (BSMS) and Its Specification

One male participant (Height: 175 cm; Mass: 86 kg; Age: 30 years old) was invited to attend the tests for the usage example of the BSMS. To alter the participant's body shape and body volume for demonstrating the capability of visualizing changes, the participant received two repeated DScan trials by the BSMS with different requests regarding lung volume. For the first DScan trials, the participant was requested to inhale the air into his lungs as much as possible and hold his breath for the period of depth image capturing. For the second DScan trials, the participant was requested to expel the air from his lungs as much as possible and hold his breath for the period of depth image capturing.

Figure 86 shows graphic displays of the BSMS that can visualize body shape changes and provide some charts to indicate the variation of body measurements (Figure 87 and Figure 88). Figure 89 shows the images that displayed the body shape changes between the first and the second DScan trial by the developed BSMS. The red part presented where the body shape gained, the blue part presented where the body shape reduced and the black part showed the identical places. It can be seen that the shape around the trunk area was reduced from the first trial to the second trial. The limb hape was also altered in the same period.

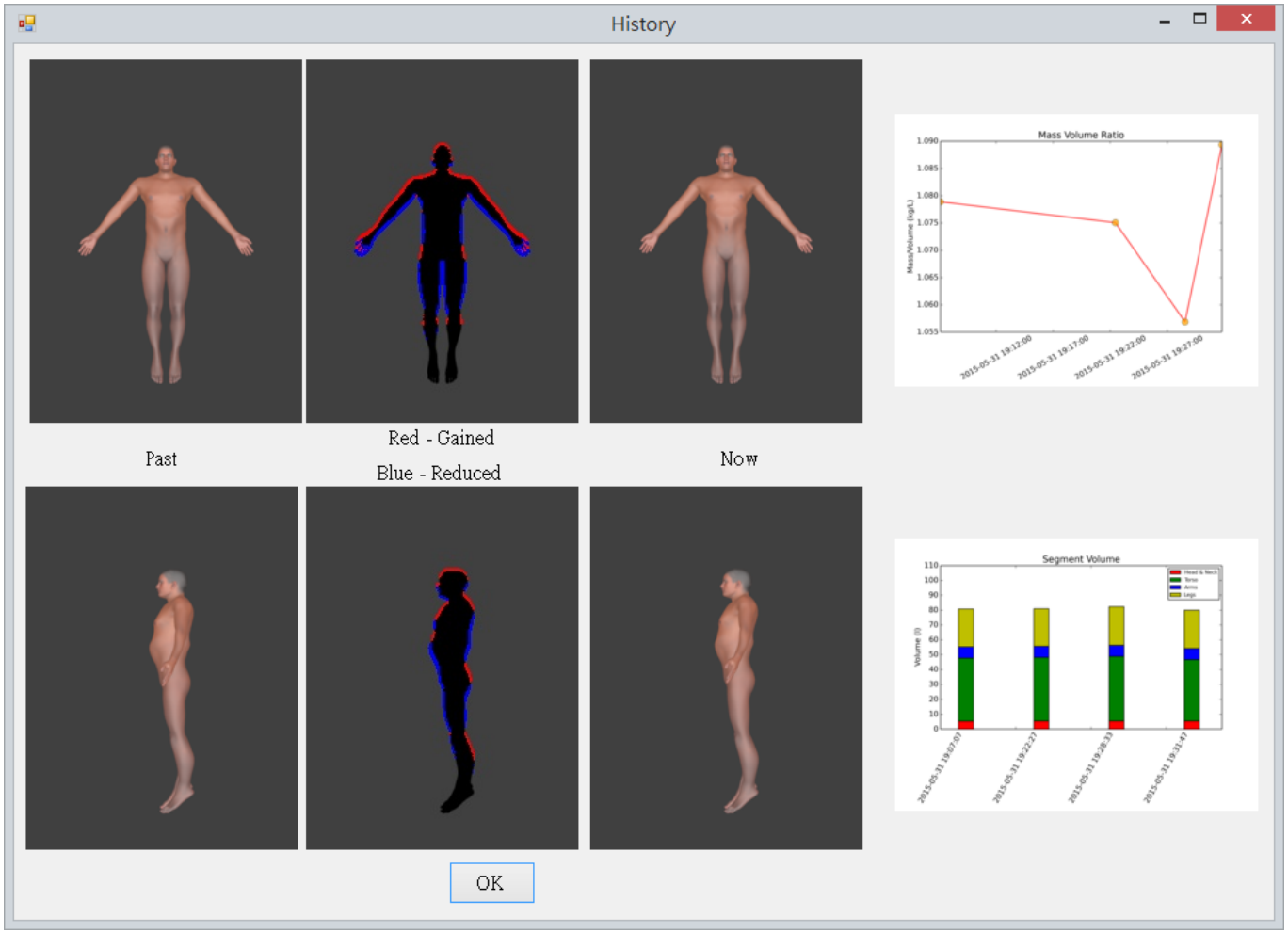

Figure 86 The graphic user interface can show the data stored in the database and visualize the body shape variation.

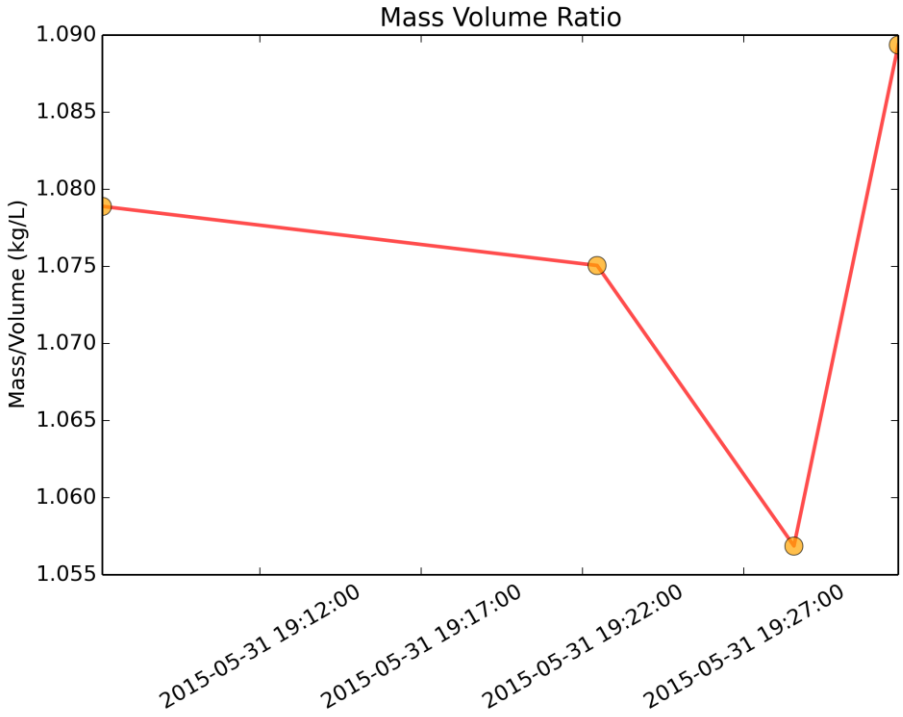

Figure 87 The chart for indicating the variation of mass volume ratio

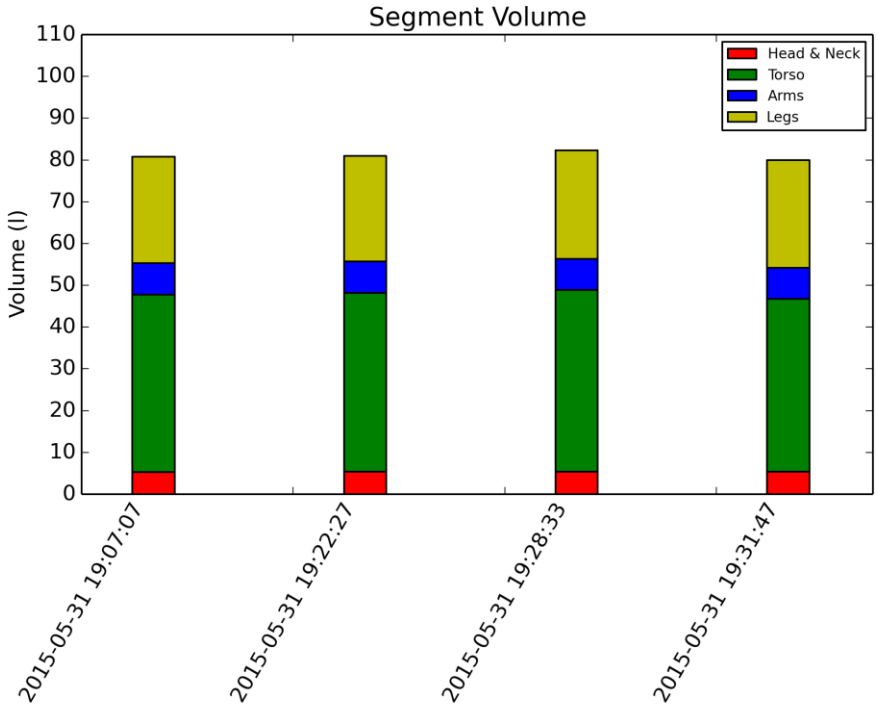

Figure 88 The chart for indicating the variation of segment volume

Table 20 shows the change of body volume data obtained by the BSMS between the first trial and the second trial. The whole-body volume decreased 2.42 litres from the first trial to the second trial which was mainly caused by the variation of the torso volume. However, the limb volume also changed slightly between the first and second trials.

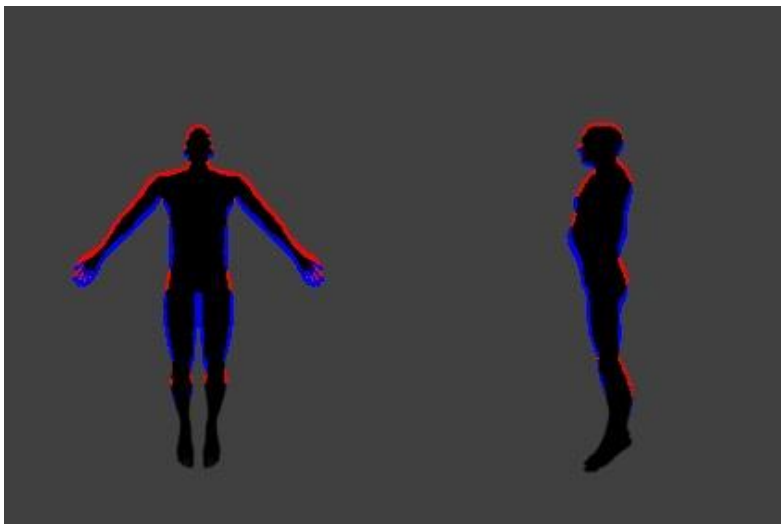

Figure 89 The images shows the body shape changes between the third and the fourth DScan trial by BSMS (Red: Gained; Blue: Reduced; Black: Identity)

The processing time for the two repeated DScan processed by the BSMS was measured. The processing time started from the point after pressing the OK button in the Manual Measurement Input App and finished with the graphic display (Figure 85) on the monitor of the controlled laptop. The processing time for the first trial and the second trial were 165.66 and 163.29 seconds respectively. The mean and standard deviation of the processing time were 165.48±1.68 seconds.

Table 20 The changes of body volume data (Litre) between the first and second trials of the BSMS.

	1st trial (inhale)	2nd trial (expel)	Change
Whole-body Volume	81.37	78.95	-2.42
Head Volume	4.54	4.56	0.02
Neck Volume	0.81	0.88	0.07
Upper Torso Volume	20.09	19.58	-0.51
Lower Torso Volume	23.42	21.69	-1.73
Thigh volume	2.22	2.20	-0.02
Shank volume	1.16	1.13	-0.03
Foot volume	0.38	0.39	0.01
Upper arm volume	8.91	8.80	-0.11
Lower arm volume	3.36	3.40	0.04
Hand volume	0.72	0.72	0

The hardware of the BSMS includes a controlled laptop (ASUS K45VS) and a Kinect camera. The purchase price for the Kinect system was AU$270 which was less than £130 (currency rate: 29.July.2015) and the price for the controlled laptop was NT$25900 which was less than £530 (currency rate: 29.July.2015). The total price for the hardware of the developed BSMS was less than £700.

The size and the weight of the hardware of the BSMS were measured by a tape ruler and a weighing scale (Salter Disc Electronic Scale with Stainless Steel Platform 1036). The Kinect camera (with the packing box) weight was 1.11 kg and its dimension (width × depth × height) was 38cm × 12cm × 15cm (Figure 90). The laptop (with a mouse, an adapter in a protection handbag) weight was 3.33 kg and its dimension

(width × depth × height) was 38cm × 35cm × 12cm (Figure 91). The total weight for the hardware of the developed BSMS was 4.44 kg and the dimension (width × depth × height) was 38cm × 47cm × 15cm (Figure 92).

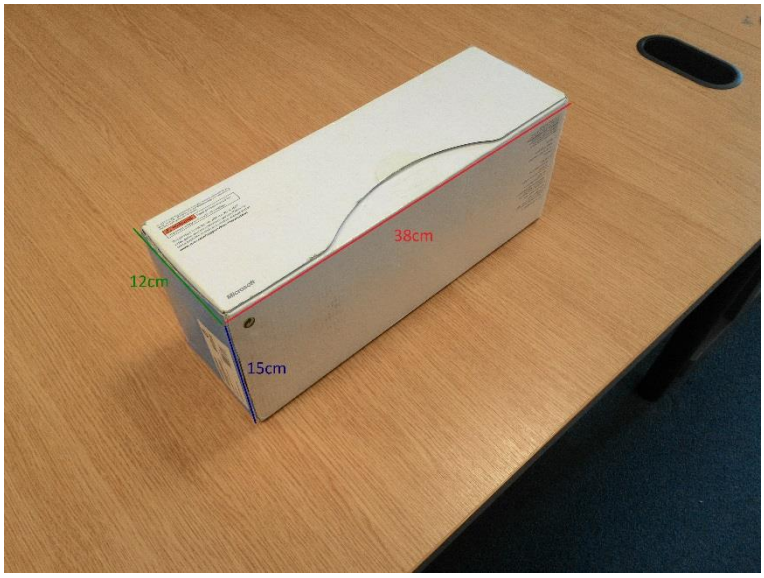

Figure 90 A Kinect camera in its packing box

Figure 91 The controlled laptop in the protection handbag

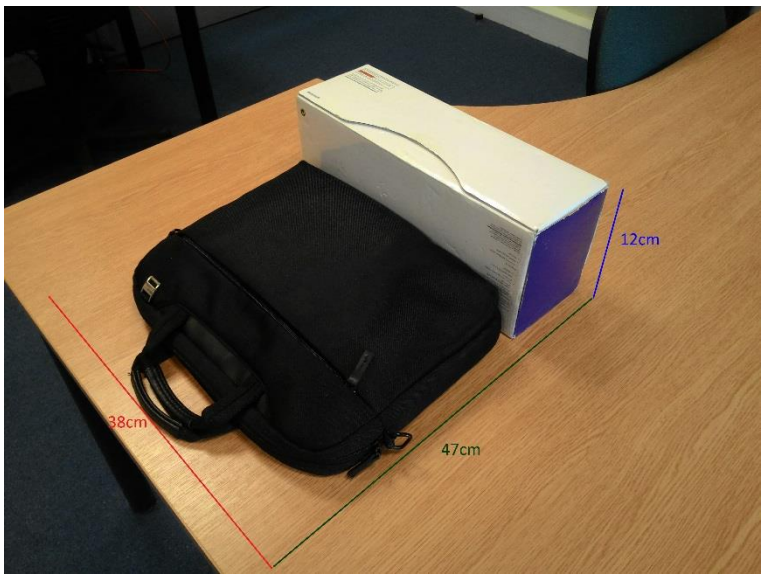

Figure 92 The hardware of the developed BSMS

7.4 Discussions and Summary

This technical description introduced a Body Shape Monitoring System (BSMS) which can help non-expert users complete all the procedures of the DScan automatically and visualize body shape changes. Furthermore, this technical description showed a usage example of the BSMS and revealed the specifictions of the BSMS including cost, processing time and portability.

The BSMS is a customized system which was developed with MySQL, C# and .NET Framework. A usage example was revealed to demonstrate the capacity for visualizing body shape variation and to describe the processing speed, portability and cost of the developed BSMS.

The repeated trials with the different requests regarding lung volume showed that the developed BSMS enables visualization of body shape changes. Thus, the BSMS

developed in this study provides a solution for non-expert users to conduct DScan for measuring body volume and to visualize body shape changes. The system provides functions similar to the relative software for a commercial scanner such as SIZEUK (Treleaven & Wells, 2007) and BVI (Boelaert et al., 2008) which is not compatible with the developed DScan.

The system identified limb position change as seen in the demonstration in Figure 89. The shoulders and arms for the first trial were slightly lower than the ones for the second trial. The possible reason is that with different lung volume conditions, the participant may have changed his body shape (e.g. extending his trunk) and this resulted in shape variation. Similarly, the participant might tense his leg muscles which led to the variation of leg shape between the two trials. Thus, while using the developed BSMS system to visualize body shape changes, the users should maintain the same breathing protocol for the purpose of attaining a stable lung volume condition and muscle relaxation.

The repeated trials with different requests to attain standardised lung volume conditions also showed that the developed BSMS can correctly indicate the variation of body volume, especially the trunk volume. However, the limb volumes might have some small, abnormal changes. The main possible reason is that some error for the repeated measurement of segmental volumes by the DScan (Study 4) might also lead to limb volumes varying from the first and second trials. Hence, further research to identify ways of avoiding the changes of the limb volumes is required.

The processing speed (165.48±1.68) confirmed that the developed BSMS system can complete the DScan process effectively, and its processing time (< 3 minutes) was less

than E-Zone (10 minutes; Wicke and Lopers (2003). Referring to the processing speed of parameter setting (around 9 seconds, Study 2) and body volume calculation (around 52 seconds, Study 3), the feature extraction including depth image capturing is less than 2 minutes. Therefore, the Kinect system with its relative software can capture the depth images effectively while extracting body dimension features for 3D human modelling, overcoming the limitations of previous studies (Tong et al., 2012; Wang et al., 2012; Weiss et al., 2011; Xu et al., 2013).

The mass (4.44kg) and the dimension (38cm × 47cm × 15cm) for the hardware of the developed BSMS is less than the maximum free cabin luggage dimensions for standard passengers for most airlines (BBC, 2015). For instance, the hand baggage allowances for British Airways and Flybe is 56cm x 45cm x 25cm with maximum weight 23kg and 55 x 40 x 23cm with maximum weight 10kg respectively. Thus the developed BSMS can achieve the research purpose in terms of portability, and users can bring this equipment easily to conduct the tests to serve clients in different places.

The purchase price for the hardware (£700) of the developed BSMS is less than other commercial body scanners which usually cost from US$10,000 ($TC^2$ KX-16, Cary, NC, USA; around £6,600; currency rate: 24.Nov.2015) to US$240,000 (Cyberware, Monterey CA, USA; around £158,600; currency rate: 24.Nov.2015) (Daanen & Ter Haar, 2013). The cost of the hardware can also meet the criteria of this research (£1,000; see Section 1.2.6). Furthermore, the controlled laptop was purchased in early 2013 so users should be able to buy a cheaper laptop with faster processing speeds. In other words, the current cost of the developed BSMS should now be less than the purchased prices quoted in this thesis.

In summary, this technical description shows that the BSMS can complete all the procedures of the DScan automatically whilst also enabling visualization of body shape changes. It was also demonstrated that the BSMS can achieve the present research purposes in terms of speed, cost, and portability.

Chapter 8 Discussion

The purpose of this research was to develop a fast, portable, inexpensive and automatic system to build individual 3D human models for acquiring multiple body measurements and visualizing body shape changes. To ensure that the system can be used for measurements and monitoring, the accuracy and reliability of the estimated body volumes needed to be established. Table 21 shows the criteria in term of the accuracy, reliability, speed, portability, cost and automation that was set for the system development.

Table 21 The performance criteria of the BSMS.

Criterion	Detail
Accuracy	The estimation of whole-body volume should be within 5% TEM and the approximation of large segmental volumes (apart from head, neck, hand, foot segments) should be within 10% TEM.
Reliability	The intra-method reliability should be under 5% TEM.
Processing Speed	The whole process of model building should take less than 10 minutes.
Portability	The equipment for the developed system including an operation laptop and a camera device should be less than 7 kilograms and meet the allowance of carry-on baggage for most of airlines. The developed system should be used in most indoor environments.
Cost	The cost of hardware for the developed method, including an operation computer and a camera system, should be under £1,000
Automation	The whole process should not require complex manual measurement and precise palpation for anatomical landmarks as well as specific machinery and software operation. The user without programming experience can input the basic information in graphic user interfaces and the system can complete the processes for generating individual 3D human models and calculating body volume automatically.

In this chapter, the specifications of the developed body shape monitoring system (BSMS) are described and it is discussed whether the developed system achieved the purpose of this body of work (Section 8.1). The limitations of the developed BSMS are described (Section 8.2). The applications of the developed BSMS in other fields are also elaborated (Section 8.3).

8.1 The Specifications of the BSMS

Section 2.1 reviewed the current methods of measuring body composition and body volume calculation and visualizing body shape variation. It was found that no fast, portable, inexpensive and automatic technique can measure body composition and body volume as well as visualise body shape variation. To develop a technique or a system with high performance in terms of processing speed, portability, cost and automation, four studies and one technical description were conducted for this research. In Study 1, a new method was developed for obtaining reliable body dimension features from a Kinect system. In Study 2, a new method was presented to increase the efficiency of parameter setting. In Study 3, an automatic method was developed for calculating body volume data from generated MH models. The methods developed in the first three studies were then connected together to form a new technique (DScan) for obtaining personal body volume data from depth images captured by a Kinect system. Study 4 established the accuracy and reliability of DScan and compared these with the traditional 3DPS and E-Zone method. The technical description introduced a customized system (BSMS) with graphic user interfaces for completing the DScan process and visualizing body shape variation automatically. The processing speed,

portability and cost of the developed BSMS were also examined in this technical description.

The developed BSMS can be seen as a simplified 3D photonic scanning method (3DPS), which measures body volume, visualises body shape variation and could be used to estimate body composition in a few rapid scans. Apart from the fast scanning process and complete data for body volume and body shape, the developed BSMS retained the advantages of traditional 3DPS and E-Zone including that it is a direct, and risk-free measurement (see Study 4, Section 6.1). For instance, it avoided the repeated and time-consuming procedures associated with water displacement or anthropometric measurements. The developed BSMS was also radiation-free which meant that participants can be tested regularly and frequently without any health risks.

Moreover, the developed BSMS system reduces the inconvenience of traditional 3DPS (Collins, 2006) and the other simplified method, E-Zone (Deffeyes & Sanders, 2005) with regard to reliability, processing speed, portability, cost and automation as shown in Table 22. The following sections discuss the specifications of the BSMS developed in this research in terms of accuracy, reliability, processing speed, portability, cost, and automation.

Table 22 Comparison of traditional 3DPS, E-Zone, and the developed BSMS.[16]

	Traditional 3DPS	E-Zone	The developed BSMS
Accuracy	Very good	Good	Good
Reliability	Good	Good	Good
Processing speed	10 seconds for scanning, 60 minutes for post-processing	Few second for image capturing 10 minutes for post-processing	Capturing and post-processing finished in 3 minutes
Portability	Fixed machinery need precise calibration	2 cameras with tripods need calibration	One sensor with laptop does not need calibration
Cost	Expensive, £6,600 to £158,600 (Daanen & Ter Haar, 2013)	Camera: around £120	Kinect: £130
Automation	Required manual post-processing with technical expertise	Required manual post-processing with technical expertise	Not required manual post-processing with technical expertise

8.1.1 Accuracy

When the traditional 3D photonic scanning is the reference, the BSMS (DScan) was slightly less accurate than the existing E-Zone method. The error of whole-body volume for both methods was less than 5%TEM (2.8%TEM for E-Zone and 3.1% for BSMS). Although both methods met the requirement of this research in terms of accuracy, the error in whole-body volume generates a large error while estimating the

[16] The definition of good in accuracy, reliability means the technique can achieve the corresponding purpose of this research. For example, the good accuracy means that the error of body composition or whole-body volume estimation less than 5%. By contrast, the definition of poor in accuracy, reliability means the technique cannot achieve the corresponding purpose of this research.

body composition using the formula by Siri (1961). With body composition estimated according to Siri (1961) and using an estimated lung volume (Ganong, 2003), percentage body fat calculated from the body volume for E-Zone and the developed BSMS demonstrated 12.0% and 13.8% error compared with the traditional 3DPS respectively. The possible reason for the high error might be that the formula for calculating body composition from whole-body volume is too sensitive to any error in whole-body volume which leads to the large error in body composition (Wang et al., 2006). The large error makes the body composition estimated from the BSMS (and E-Zone) unsuitable for previous studies, such as those conducting obesity diagnosis (Okorodudu et al., 2010; World Health Organization, 1995), disease detection (Rebuffé-Scrive et al., 1988; Wajchenberg et al., 1995) and sport performance determination (Ackland et al., 2012; Duthie et al., 2003; Milsom et al., 2015). However, the BSMS does provide an approach which can collect data easily from large cohorts. Further research might be conducted to create a new measurement or classification of body composition (e.g. the ratio of body mass and body volume) for assessing obesity level, health risk, fitness, condition, and sport performance, and for this the developed system may be useful.

The error of most segmental volumes estimated by both the BSMS and E-Zone was less than 10%TEM. Only the small segments, neck and foot could not be estimated within 15% error. Therefore, both methods can meet the requirement of this research in terms of accuracy and provide general ideas for body volume distribution. Therefore, the BSMS can calculate the advanced parameters such as Body volume Index

(Muralidhara, 2015) and segmental volume ratio (Lee et al., 2015; Wilson, Kanaya, et al., 2013) for health and sport training applications. The results in Study 4 demonstrated that the accuracy of segmental volumes estimated by the BSMS was slightly poorer than that calculated by E-Zone, especially for the leg volumes. However, considering the human error for post-processing of E-Zone (Sanders et al., 2015), it is suggested that using the BSMS instead of E-Zone to estimate segmental volumes will lead to better and more consistent accuracy.

The accuracy (<5% error in whole-body volume and <10% error in segmental volumes) for the BSMS might be adequate for general users rather than research and clinical examinations. Nevertheless, Study 4 indicated that there is a potential to improve the accuracy of body volume data by upgrading the depth camera (extracting more accurate features) and/or increasing the numbers of extracting features. Once the accuracy of the BSMS is improved, it will become a useful tool for research and clinical examinations.

8.1.2 Reliability

The repeated reliability of the whole-body volume acquired from the traditional 3DPS, E-Zone and the BSMS were all under 1.5%TEM (see the results in Study 4). Thus, the BSMS can achieve the requirement of this research in terms of the intra-method reliability. If using the whole-body volume to estimate the body composition by applying formula presented by Siri (1961), the repeated reliability of body composition for the traditional 3DPS, E-Zone and the developed BSMS was 2.3%TEM, 4.4%TEM and 5.2%TEM respectively. The error of the body composition estimated from the developed BSMS is a little higher in absolute terms than the traditional 3DPS and E-

Zone and other body composition methods such as underwater weighing, air displacement, near infrared interactance and bioelectrical impedance (Jensky-Squires et al., 2008; Rolland, 2012; Schreiner et al., 1995). Keating et al. (2014) indicated that the changes of body composition before and after a 12 week exercise training program might be less than 2% but Evans et al. (2012) mentioned that a four month dieting programme might reduce body fat by more than 6%. Therefore, the BSMS is similar to the traditional 3DPS and E-Zone in that it could only be used for detecting the effectiveness of similar long-term diet programmes. Therefore the reliability of the BSMS might need to be further developed for future applications. Nevertheless, the BSMS provided a fast, portable, inexpensive and automatic method for monitoring composition without any health risks. It shows the potential that the BSMS could be a useful monitoring tool for health, training and diet with improvements in its reliability.

The test results in Study 4 indicated that the repeated reliability of the segmental volume (apart from neck volume) acquired from the developed BSMS is good. Therefore, it can be a good tool for detecting segmental volume changes and understanding body shape changes (Wells, 2012). Furthermore, Study 2 and Study 3 developed the automatic processes for parameter setting and body volume calculation. The process of the BSMS does not contain any subjective interpretation and is therefore operator-independent. By contrast, traditional 3DPS and E-Zone require manual post-processing such as mesh editing (Ma et al., 2011) or digitizing the body boundaries (Deffeyes & Sanders, 2005) and similar issues arise with medical image methods and DXA (Burkhart et al., 2009). The procedures for these other methods include subjective interpretations and the analyses are affected by assessors' reliability. In other words, the inter-rater reliability should be considered if using these techniques

(the traditional 3DPS, E-Zone, DXA and the medical image methods) to monitor body composition or segmental volumes.

8.1.3 Processing Speed

The time required to acquire body volume data using the BSMS was less than 3 minutes (see the test results in the technical description) which satisfied the goal of developing a time-efficient system. The processing speed of the BSMS is much less than the manual mesh editing in traditional 3DPS (see the test results in Study 3) and manual digitizing for E-Zone (Wicke & Lopers, 2003). This also reduces labour costs when assessing large numbers of participants in studies related to sport, health and epidemiology.

Compared with other techniques such as manual anthropometry or underwater weighing, the traditional 3DPS, E-Zone and the BSMS can reduce the measurement processing time effectively. Both the traditional 3DPS and the BSMS can also transfer the image files to central control computers without manual processes. On the contrary, the images captured for E-Zone require transferring from the digital cameras to the processing computer manually. This might be time-consuming and annoying if conducting tests frequently or with a large number of participants.

Although traditional 3DPS does not require transferring captured files manually, manual post-processing is necessary for both traditional 3DPS and E-Zone. It usually takes approximately 60 and 10 minutes for traditional 3DPS and E-Zone respectively. The techniques for MRI, CT and DXA also need manual post-processing which reduces the processing speed. For the BSMS, Study 2 simplified the method and increased its processing speed for parameter setting, Study 3 developed an automatic

method and decreased the time requirement for mesh editing and finally the technical description showed that the developed BSMS can complete the depth image capturing rapidly.

The developed BSMS eliminates manual post-processing so that parallel computing techniques can be applied to enable large numbers of participants to be processed expediently. For instance, one operator can use multiple computers and the BSMS to acquire participants' body volume data simultaneously and the post-processing speed can be decreased.

8.1.4 Portability

The hardware of the developed BSMS comprises one Microsoft Kinect camera and a single laptop. The technical description showed that the developed BSMS satisfied the goal of ensuring that the system is portable. Compared with the water displacement, underwater weighing, air displacement plethysmography, medical imaging methods and traditional 3DPS, the BSMS is more portable and suitable for measurers to assess changes across time since the other methods all need fixed machinery (see review in Section 2.1).

The total weight and volume of E-Zone equipment (two digital cameras, two tripods and a controlled laptop) might be lighter than the developed BSMS. However, the testing environment for E-Zone is considerably larger than that required for the developed BSMS. E-Zone requires a 12m × 12m indoor space but Study 1 shows that BSMS requires only a 3m × 3m space (3m depth for capturing and 3m width for arm pose).

In addition, the Microsoft Kinect camera with its SDK can deliver the 3D coordinates without calibration so users can travel with the BSMS to collect data easily. By contrast, both 3D scanner systems and E-Zone need calibration to determine the scale of 3D models or images. The extra calibration equipment and processes decreases their portability.

8.1.5 Cost

Study 1 referred to previous studies (Tong et al., 2012; Wang et al., 2012; Weiss et al., 2011; Xu et al., 2013) and used the inexpensive depth camera (£130) in the development of BSMS. The technical description showed that the new BSMS system developed with open source or freeware software, and the new system can just be controlled by a general laptop (£530). By contrast, some techniques for calculating body volume and body composition such as air displacement plethysmography, isotope dilution methods, MRI, CT, DXA, traditional 3DPS, manual anthropometry and ultrasound need expensive machinery (see review in Section 2.1). E-Zone uses cost-effective general digital cameras (around £120) but the post-processing software built in Matlab requires purchasing of the license for Matlab. Hence, the new system provides an inexpensive solution which can avoid high costs in hardware and software and satisfy the goal of minimising cost.

8.1.6 Automation

The developed BSMS retains the advantage of 3DPS of a radiation-free scanning process so no certificated specialist is needed, in contrast to medical scanning systems such as MRI, CT and DXA. Moreover, no markers need to be placed for the BSMS so

the user can complete the tests without other people's help. By contrast, identifying segmental endpoints and placing markers is necessary for obtaining segmental volumes using the E-Zone and traditional 3DPS. Using palpation to determine the correct measurement locations is also necessary for manual anthropometry, near infrared interactance and ultrasound (see review in Section 2.1). Technical expertise is required to identify the correct position with good reliability. An extra operator with anatomical knowledge is needed since users cannot place the markers accurately by themselves.

The data obtained from traditional 3D body scanners requires specific CAD software for post-processing (Ma et al., 2011). Using the CAD software to complete 'holes', fill 'gaps', smooth 3D model outlines and establish segment borders efficiently requires training to familiarise the operator in the use of the user interface (Ma et al., 2011). The post-processing of E-Zone is much simpler than the traditional photonic scanning. Users do not need to use CAD software to complete post-processing. However, users need to type some commands in the Matlab command line window while applying E-Zone (Deffeyes & Sanders, 2005). Users without any programming experience might find this operation confusing. In other words, E-Zone might need further development of some graphic user interfaces to increase 'friendliness' and ease of use for users without any 'command line' knowledge.

In Study 3 an automatic method for mesh editing was developed, and the graphic user interface developed as part of the BSMS which introduced in the technical description can help users complete the DScan process without typing commands, altering parameters, and digitizing points. Furthermore, the database of the BSMS enables

visualization of body shape changes for monitoring purposes. Thus the BSMS reduced the requirement of expert knowledge and met the criteria of this research in terms of automation.

8.1.7 Summary

The BSMS achieved all the research purposes in terms of accuracy, reliability, processing speed, portability, cost, and automation. Further development for improving body composition estimation is needed to improve the accuracy and reliability of body composition measurement for clinical purposes. Nevertheless, the research shows the potential of the BSMS to be a useful tool for research and clinical application after these improvements are completed.

8.2 Limitations of the Body Shape Monitoring System

The new BSMS developed in this research contains some limitations which are described in the following sections.

8.2.1 Privacy issue

In this research, participants needed to wear close-fitting suits while capturing depth images. If participants dress in other clothes, the accuracy of the modelling is reduced. This means that the technique needs to be applied in areas where establishing privacy is possible. However, this limitation is common to all systems including commercial 3DPS scanning (Hasler et al., 2009) and E-Zone.

Recently, some researchers have developed techniques to extract anthropometric data (Xu et al., 2013) and estimate body shapes (Hasler et al., 2009) while participants are

wearing loose fitting clothes. Xu et al. (2013) captured depth images with different poses. Since different poses made the clothes attach to different parts of body surfaces closely and reduced the dressing effect, partially accurate body models could be estimated. The complete 3D human model could be generated by composing the partial models of different segments. Then, the body measurements including segmental volumes and body composition data could be estimated from the individual 3D human models. Hasler et al. (2009) also used a database of 3D human models to generate a template model. The template human model was driven to complete matching tasks and estimate the body shape under a normal dress. In the future, the system developed in this thesis might be able to be combined with these methods and present a new BSMS that can be used on participants wearing their normal dress. For instance, dressed participants' depth images in different movements could be captured and 3D point clouds could be extracted as features. These features could be matched by a deformable 3D model and realistic 3D human models could be generated.

8.2.2 Limitation of Depth Cameras

Because of the limitation of depth cameras, the depth image capturing might be affected by sunlight or other strong lights which illuminate participants directly. For this reason, the capturing process needs to be conducted in an indoor environment with homogeneous light. This limitation also affects commercial scanning. However, E-Zone can endure some direct strong lights because the segments are traced manually. To avoid strong directional light, users might need to cover sources of unwanted lighting. However, the second recently-released version of Kinect for Windows can

reduce this problem since the IR sensor is lighting-independent and can accept some strong directional light (Microsoft, 2015a).

8.2.3 Limitations of Matching with the MH Model

By using the MH model-matching the extracted features can be used to obtain complete individual models without 'holes' in the same posture. However, it is possible to lose some personal detail. For example, the BSMS cannot show the facial expression and hairstyle. Extracting more features and altering more MH parameters might enable more realistic human models, but this kind of model template matching is time-consuming because it is a high dimension optimization problem. However, the detail may not affect the body volume greatly and thus it would not lead to wrong analysis results of segmental volumes and body composition. Some applications such as 'virtual-try on' and computer animation (described in Section 8.3) might need the detail of individual 3D human models. The BSMS might be able to combine facial scanning techniques with a Kinect system (Zollhöfer et al., 2011). Facial scanning results could replace the face of the MH models generated by the BSMS and then personal detail could be shown. For instance, users could receive facial scanning first and then use the BSMS to estimate the body shape. After the scanning, the facial scanning result could replace the MH model faces to generate individual 3D human models with realistic faces.

Furthermore, using few features and assumptions of symmetry in the developed BSMS might cause some error when participants are not symmetrical, for example, amputees and athletes with asymmetrical limb volumes due to the differences in strength requirements bilaterally. A participant without his left leg would be modelled as a

person with two healthy legs while using the developed BSMS since the method only extracts the features from right sides. Therefore, his left leg volume would be overestimated. An athlete with weaker left limbs might also lead the BSMS to generate a human model with less muscle on the right side. By contrast, a participant without his right limb might cause the volume to be underestimated. An athlete with stronger right limbs might also lead the BSMS to generate a human model with more muscle mass elsewhere on the body. Nevertheless, Leboucher et al. (2008) showed that the volume differences between dominant and non-dominant limbs of healthy able bodied people are significant but small. The BSMS system is therefore suitable for use by the general population but needs further improvement before applying to people with major bilateral asymmetries.

8.3 Other Applications

The BSMS developed in this research provides a fast, portable, low cost and automatic method not only for obtaining body volume data and body composition but also for completing a DScan process to acquire individual 3D human models. Individual 3D human models are useful and essential for many fields including the fashion industry, ergonomics and sports science.

8.3.1 Fashion Industry

Nowadays, online shopping is becoming popular (Hauswiesner et al., 2011). Most clients need to see images of how they would look when dressed in their chosen clothes. A client's imagination is usually different from the real situation due to insufficient

information. Client dissatisfaction causes a high garment return rate which is around 30% (Kennedy, 2012).

'Virtual try on' is possibly an effective solution to increase client satisfaction. This technique can help people check the fit sizes and imagine the real situations while wearing their selections. In a previous survey (Hauswiesner et al., 2011), most users thought it was important to have a free-viewpoint 'virtual try on' which can help the user check how they look like in any direction. This technique is more realistic than a 'virtual mirror' which just 'attaches' clothes on human images.

The essential step in generating a free-viewpoint 'virtual try on' is to creating individual 3D human models (Hauswiesner et al., 2011; Matusik et al., 2000). However, the previous techniques for generating 3D human models are not convenient for home users due to the expensive machinery or complex setup. The BSMS could be adapted to help the user to complete the 'virtual try on' at home. This might benefit users who are busy and do not have time to travel to the real shops or specific places to complete 3D scanning. Table 23 shows the comparison of individual 3D human model generation for three methods including the previous techniques (Hauswiesner et al., 2011), a commercial solution (Body metric Ltd., London, the UK), and the BSMS.

8.3.2 Ergonomics

The BSMS can be used to conduct the DScan process for obtaining individual 3D human models for ergonomic applications such as product design. It is usually

important for people to use products with least effort since it can increase productivity and reduce the possibility of injury. Body segment parameter (BSP) data are needed to design products with suitable sizes and functionality.

Table 23 The comparison of individual 3D human model generation for the previous method (Hauswiesner et al., 2011), a commercial solution and the BSMS.

	Previous Method (Hauswiesner et al., 2011)	Commercial Solution	BSMS
Equipment	Multiple cameras	Multiple Kinects	Single Kinect
Portable	No, a precisely calibrated multi-camera system	No, a fixed booth for placing multiple Kinects	Yes
Cost	Higher	Higher	Lower

The BSMS can build individual 3D human models and obtain body segment meshes without any manual interpretation. The BSP data can be calculated from the obtained body segment mesh easily via the method developed by Mirtich (1996) with the density function presented by Wicke and Dumas (2010). The calculated BSP data can be used for application to, and research in, ergonomics.

The BSP data acquisition could be fast and fully automatic by using the BSMS. Hence, it is suitable to use for collecting real human data and building an ergonomic database. A company could use the BSMS to know the employees' BSP data and order suitable equipment for them and increase comfort and productivity.

8.3.3 Sports Science

The individual models obtained by the developed BSMS also can be used for sports science including coaching, motion tracking and performance analysis.

8.3.3.1 Sport Coaching

Because the MH model built by the DScan can be animated by motion capture files, visualization of athlete movement with realistic human characteristics becomes easy. For instance, the motion capture data in Biovision Hierarchy format (BVH) can be obtained from commercial motion capture systems such as Qualisys (Göteborg, Sweden) or Vicon (Oxford, UK). Then the athlete's MH model obtained from the BSMS could be imported into the computer animation software, Blender. Lastly, the BVH character animation file can be loaded and make the MH model simulate different poses. Figure 93 shows a MH human model obtained from the BSMS used for visualizing a runner's motion. This would benefit coaching since it can simulate the video from different angles. The realistic character can be easier than stick figures for coaches to observe any abnormal movements.

8.3.3.2 Motion tracking

Markerless motion tracking is a popular topic for sports science since sportsmen can perform as usual without being affected by sensors or placed markers. This is particularly useful in underwater sports such as swimming and water polo. The water environment is not friendly for sensors and the water splash usually increases the difficulties of automatic digitizing. Thus, time-consuming manual digitizing is usually

required. For instance, Psycharakis et al. (2010) and McCabe and Sanders (2012) used manual digitizing to track swimmers' motion and complete the sports analysis.

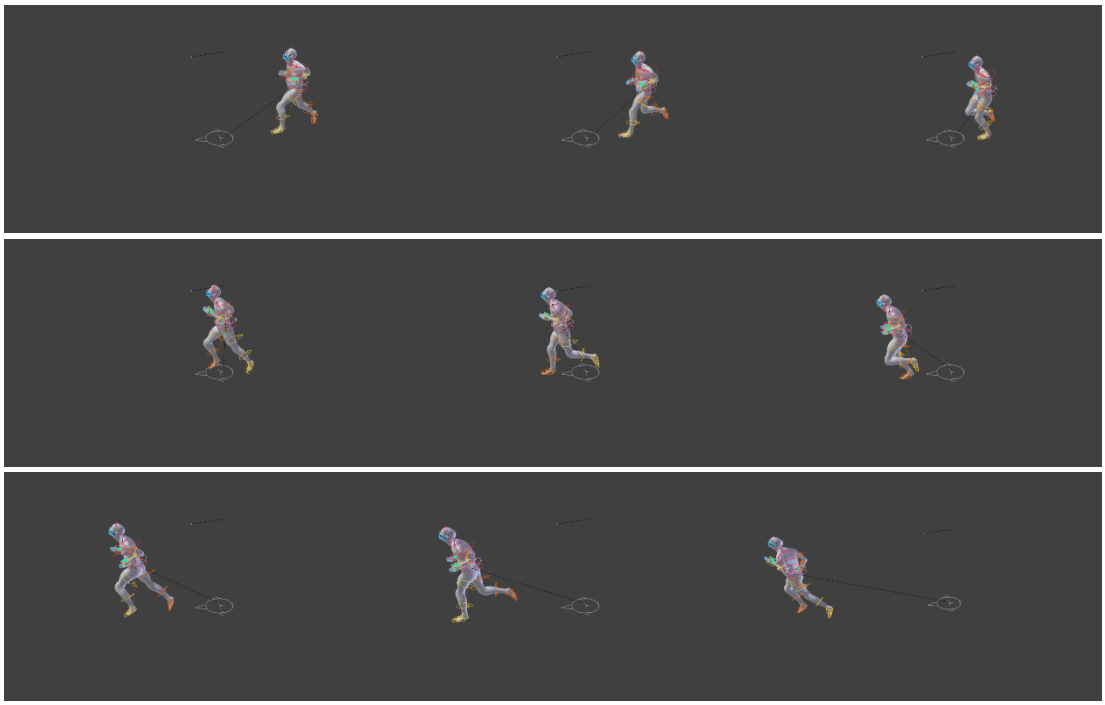

Figure 93 A MH human model obtained from the developed BSMS is used for visualizing a runner's motion

Corazza et al. (2009) developed markerless motion tracking methods and Ceseracciu et al. (2011) adapted it to conduct markerless tracking in an underwater environment. Figure 94 shows the process of the markerless motion capture. Both methods generated template individual 3D human models first. Then, the human motion images were captured by multiple cameras. The image processing and the 3D reconstruction techniques were employed to build visual hulls. The template models were used to match the visual hull results and determine the joint positions to complete the markerless tracking. Although the method presented by Ceseracciu et al. (2011) still

suffers from splash, this technique still showed its potential for motion tracking for swimming, gliding, and the water polo eggbeater kick.

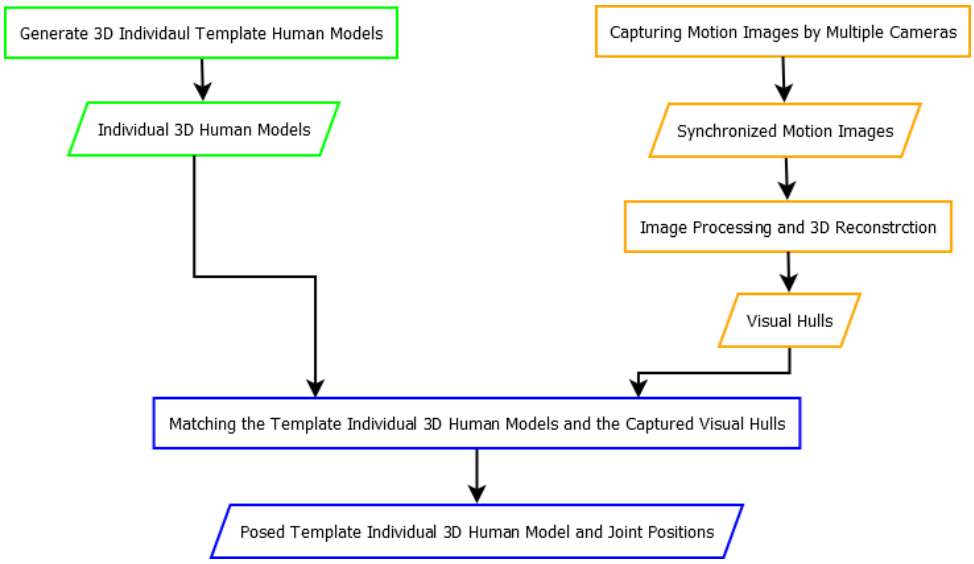

Figure 94 The process of markerless motion capture

It seems that this markerless tracking (Ceseracciu et al., 2011; Corazza et al., 2009) technique has the potential to simplify motion tracking. However, a template individual 3D human model is required and previous techniques (Ceseracciu et al., 2011; Corazza et al., 2009) contain some limitations. The BSMS can conduct the DScan process in order to provide a simple method for generating template human models with many advantages. Table 24 shows the comparison of the template individual 3D human model generation in previous methods (Ceseracciu et al., 2011; Corazza et al., 2009) and the BSMS.

8.3.3.3 Sport Performance Analysis

Three-dimensional human models are also important for performance analysis. Von Loebbecke et al. (2009) applied a commercial 3D whole-body scanner to establish a swimmer model and manage some computational fluid dynamics analyses. The analyses estimated the drag while swimming and claimed to be able to help people improve performance (University of Western Australia, 2007). However, static swimmer models generated by commercial scanners need to inject animation rigging manually before simulating the swimming movement. Animation rigging is manually placing the skeletons which determine how the static models move and is arbitrary, time-consuming, and contains some human errors.

Table 24 Comparison of the template individual 3D human model generation in previous methods (Ceseracciu et al., 2011; Corazza et al., 2009) or by the BSMS.

	Previous methods (Ceseracciu et al., 2011; Corazza et al., 2009)	BSMS
Template individual 3D human model generation	Using laser scanning or multiple cameras extracted features and deforming the template statistical model to build individual 3D human models	The MH model generated by the developed BSMS can be used for the template model in markerless motion tracking
Cost	Expensive equipment (3D scanner or at least three cameras)	One inexpensive Microsoft Kinect
Portable	No, a fixed 3D scanner or a precisely calibrated multi-camera system	Yes

The individual MH models generated from the BSMS include the 3D mesh and the animation rigging. As shown in Figure 95, the default rig has been injected into the MH model automatically following generation by the BSMS. Therefore, the generated MH models enable simulation of different movements by altering the parameters of animation rigging. Figure 96 shows a series of simulated images of swimming which apply the MH models generated from the developed BSMS. When applying the BSMS to generate 3D human models, no manual post-processing is needed. In other words, using the developed BSMS can save post-processing time and inject the animation rigging systematically and reliably.

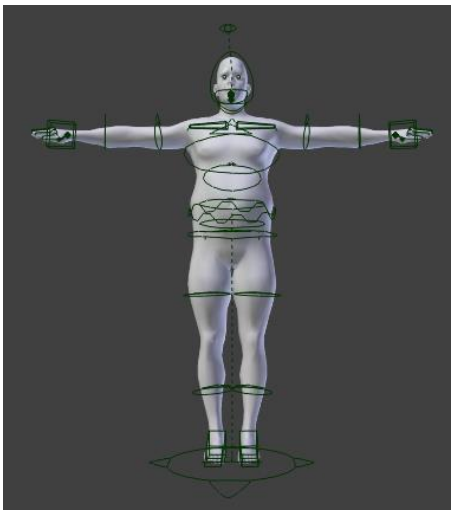

The MH model with the animation rigging.

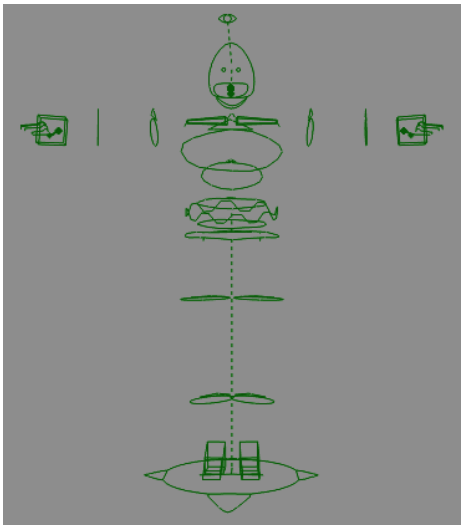

Only the default rigging.

Figure 95 The default rig of the MH model generated from the BSMS.

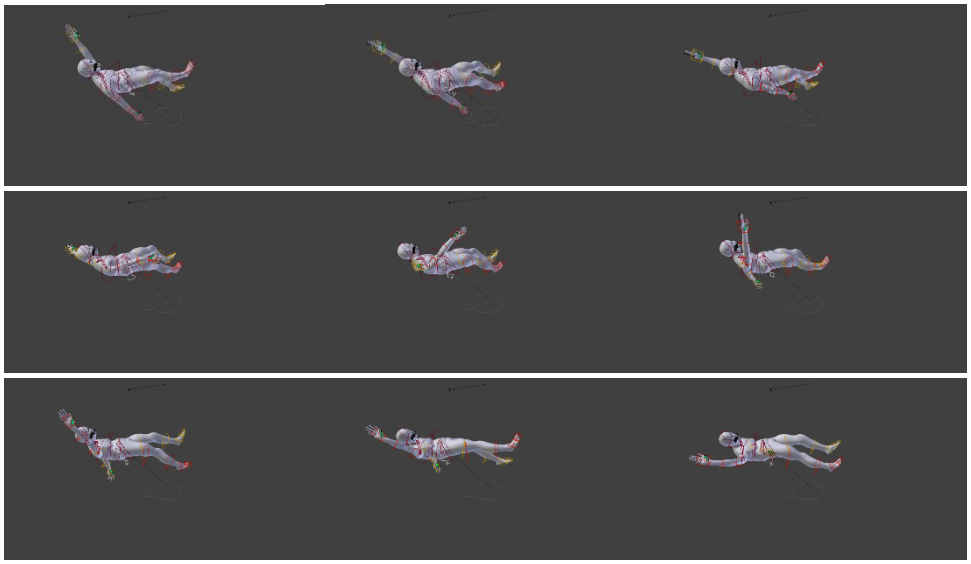

Figure 96 A series of simulated images of swimming which applying the MH models generated from the BSMS.

Chapter 9 Conclusion and Future Work

In this chapter, the conclusion of this research is described (9.1) and the future work is elaborated (9.2).

9.1 Conclusion

A fast, inexpensive, portable and automatic 3D scanning system for quantifying multiple body measurements (including whole-body volume and segmental volumes) and body shape was developed in this research. In Study 1, Study 2 and Study 3 a new technique, DScan, was developed for building individual 3D human models and obtaining body volume data. Study 1 developed a method for extracting reliable body dimension features (including stature, mass, age, gender, segment breadth and length) extracted from a few manual measurements and participants' front view depth images captured by a single Microsoft Kinect. In Study 2 a method of human modelling adapted from MakeHuman was developed to generate realistic individual 3D human models effectively and automatically. In Study 3 a fast and automatic solution for calculating body volume data from generated individual 3D models was presented. Study 4 established the accuracy and reliability of the body volume data acquired from DScan. In the technical description, a new system comprising graphic user interfaces and a database was introduced to help non-expert users apply the DScan and monitor their scanning results including the variations of body volumes and body shapes.

The test results showed that the accuracy of the BSMS achieved the purpose of this thesis and had performance similar to E-Zone when the traditional 3DPS was the

reference. However, some improvement might be needed before using the BSMS for calculating body composition. Likewise, the reliability of the BSMS met the criteria in this research and the BSMS has better performance than other 3DPS methods, especially for the small segments. Nevertheless, further research is required when applying it for body composition studies.

Compared with other techniques for estimating body composition and body volume, the BSMS reduced the requirement of hardware, software and the processing time as well as expert knowledge (namely increased automation). The hardware for the BSMS is an inexpensive depth camera (Microsoft Kinect) and a general laptop. The software used for developing the new BSMS in this research is all open source or freeware licenses. Hence, the system increased the portability and avoided expensive hardware and software to complete the body measurements (body composition, segmental volumes) and body shape visualization. People without specific training in computer programing or anthropometry can apply the BSMS to complete each analysis in less than 3 minutes without any manual interpretation (including manual digitizing and colour marker placing). In other words, the BSMS delivers a fast and automatic scanning service. Furthermore, the individual 3D model built from the BSMS can be applied to other fields including the fashion industry, ergonomics and sports science.

9.2 Future Work

Further development of the new BSMS and applications to obesity-related research are planned to be the main future work. The following sections illustrate the detail of each plan.

9.2.1 Further Development

Even though the developed BSMS reduced some limitations of current 3D scanning techniques, it could be further developed to increase the accuracy and reliability for clinical examination and monitoring. Using a newly-released depth camera, Microsoft Kinect for Windows version 2, and involving data mining techniques are among the possible solutions.

9.2.1.1 Upgrading the Depth Camera

Microsoft Kinect for Windows Version 2 improved the accuracy of depth detection and the resolution of capturing depth images (Microsoft, 2015a). Referring to the report (Microsoft, 2015a), the precision of the 3D point cloud of humans can increase four times approximately. The high resolution of the new depth camera is helpful for extracting additional features. Furthermore, the accuracy and reliability of joint detection also improved. It is highly possible to upgrade the current depth camera and extract additional body dimension features (segmental length, breadth and girth) with increased reliability and accuracy. This research showed that numerous accurate and reliable features can help to obtain realistic individual 3D human models with consistency. Thus, using the upgraded depth camera was expected to improve the accuracy and reliability at least three times compared with current BSMS system. This will be verified through further testing in future work.

9.2.1.2 Involving Data Mining Techniques

Involving data mining techniques to correct the body measurement from the BSMS might be another way of improving reliability and accuracy. With access to a commercial 3D scanner in the future, additional body volume data obtained from the developed BSMS and 3D photonic scanning methods could be collected. Then, the data mining techniques could be applied to build a mathematical model to illustrate the relationship between the body measurements acquired from the BSMS and 3D photonic scanning methods. The accuracy and reliability of the developed BSMS could be improved by correcting the obtained values using the mathematic models.

9.2.2 Application Research

The BSMS provides a fast, inexpensive, portable and automatic method for users to track their body measurements including segmental volumes and body composition easily. Once the accuracy and reliability are improved, it can be a research tool for obesity-related research. A large database could be built to store the data for diet, exercise, body measurements and body shapes. This might help researchers find the most effective diet and exercise regime for people with different body shapes and body measurements. Data mining techniques could be applied to build an expert system which can provide specific suggestions in diet and exercise to individuals with different body measurements and body shapes. The expert system and the BSMS could be combined so that users could receive specific suggestions on diet and exercise referring to the results obtained from the BSMS. This would motivate people to reduce weight or maintain fitness.

In summary, the body shape monitoring system (BSMS) was developed through the research presented in this thesis. The test results indicated the high performance of this system in terms of processing speed, portability, cost, and automation. The ability of the BSMS to enable users to determine and monitor personal body volume data and to visualize 3D personalised body shape was established. The BSMS developed in this research has the potential to be applied in the domains of health and medicine, the fashion industry, ergonomics, and sports science.

9.2.3 Further Research for the Body Shape Monitoring System

This research developed and introduced a concept system for providing useful information for health applications. However, further research should be conducted for improving the current BSMS system so it can come close to completion and consequently suitable for home use. Further research should consider validation studies with participants of different gender (female), age groups (children, elder people), ethnicities, and occupations, etc. so the system can be used for general people with large variation. The BSMS can be improved by conducting some surveys for gathering data required to complete the user centred design system. The information provided by the future BSMS needs more consideration since general people cannot fully understand the meaning of the measurement which supply by the current BSMS. The information provided by the BSMS system might generate various impacts for different users. Thus, some consultations and tests with users should be conducted to understand the impact of different displaying information should be conducted to design the best system which can provide the scanning feedback to the users appropriately.

References

Abe, T., Kondo, M., Kawakami, Y., & Fukunaga, T. (1994). Prediction equations for body composition of Japanese adults by B-mode ultrasound. *American Journal of Human Biology, 6*(2), 161-170. doi: 10.1002/ajhb.1310060204

Abe, T., Yokozawa, T., Takamatsu, J., Enomoto, Y., & Okada, H. (2010). *Determination of Body Segment Inertia Parameters Using 3D Human Body Scanner and 3D CAD Software*. Paper presented at the International Symposium on Biomechanics in Sports: Conference Proceedings Archive, 1-2.

Ackland, T., Lohman, T., Sundgot-Borgen, J., Maughan, R., Meyer, N., Stewart, A., & Müller, W. (2012). Current Status of Body Composition Assessment in Sport. *Sports Medicine, 42*(3), 227-249. doi: 10.2165/11597140-000000000-00000

Ackland, T. R. (2006). *Built for success: Homogeneity in elite athlete morphology.* Paper presented at the Kinanthropometry IX: Proceedings of the 9th International Conference of the International Society for the Advancement of Kinanthropometry, Thessaloniki, Greece, 26-34.

Anguelov, D., Srinivasan, P., Koller, D., Thrun, S., Rodgers, J., & Davis, J. (2005). SCAPE: shape completion and animation of people. *ACM Trans. Graph., 24*(3), 408-416. doi: 10.1145/1073204.1073207

Bailey, B. W., Tucker, L. A., Peterson, T. R., & LeCheminant, J. D. (2001). Test-retest reliability of body fat percentage results using dual energy x-ray absorptiometry and the Bod Pod. *Medicine and Science in Sports and Exercise, 33*(5), S174.

Bao, P., Zhang, D., & Xiaolin, W. (2005). Canny edge detection enhancement by scale multiplication. *IEEE Transactions on Pattern Analysis and Machine Intelligence, 27*(9), 1485-1490. doi: 10.1109/TPAMI.2005.173

Barmpoutis, A. (2012). Create avatars using kinect in real-time.

Barron, C., & Kakadiaris, I. A. (2000). Estimating anthropometry and pose from a single image.

Bastioni, M., Flerackers, M., & Capco, J. (2012). Makehuman. *Makehuman Team.* Retrieved 21.Nov, 2015, from http://www.makehuman.org/

Bastioni, M., Re, S., & Misra, S. (2008). *Ideas and methods for modeling 3D human figures: the principal algorithms used by MakeHuman and their implementation in a new approach to parametric modeling*. Paper presented at the Proceedings of the 1st Bangalore Annual Compute Conference, Bangalore, India. http://delivery.acm.org/10.1145/1350000/1341782/a10-bastioni.pdf?ip=194.81.242.166&acc=ACTIVE%20SERVICE&CFID=196215602&

CFTOKEN=39861550&__acm__=1352390691_cc251640351678de527a26cb2374790d

BBC. (2015). Who, What, Why: Is this the perfect size of carry-on air luggage? *BBC News Magazine*. Retrieved 21,Nov, 2015, from http://www.bbc.co.uk/news/magazine-33076492

Boelaert, K., Palin, S., Field, A., Rahim, A., & Barnes, R. (2008). *The impact of 3D body images on motivating weight loss in overweight individuals.* Paper presented at the Endocrine Abstracts, P125.

Bolles, R. C., & Fischler, M. A. (1981). *A RANSAC-based approach to model fitting and its application to finding cylinders in range data.* Paper presented at the Proceedings Seventh International Joint Conference on Artificial Intelligence, Vancouver, BC, Canada, 637-643.

Braune, W., & Fischer, O. (1889). The center of gravity of the human body as related to the equipment of the German infantryman. *Treat. of the Math.-Phys. Class of the Royal Acad. of Sc. of Saxony*.

Brožek, J., Grande, F., Anderson, J. T., & Keys, A. (1963). Densitometric analysis of body composition: Revision of some quantitative assumptions. *Annals of the New York Academy of Sciences, 110*(1), 113-140. doi: 10.1111/j.1749-6632.1963.tb17079.x

Burden, R. L., & Faires, J. D. (1985). *Numerical analysis* (3 ed.): Prindle, Weber & Schmidt.

Burkhart, T. A., Arthurs, K. L., & Andrews, D. M. (2009). Manual segmentation of DXA scan images results in reliable upper and lower extremity soft and rigid tissue mass estimates. *Journal of Biomechanics, 42*(8), 1138-1142. doi: http://dx.doi.org/10.1016/j.jbiomech.2009.02.017

Buys, K., Van Deun, D., De Laet, T., & Bruyninckx, H. (2011). On-line generation of customized human models based on camera measurements.

Camic, C. L., Housh, T. J., Zuniga, J. M., Traylor, D. A., Bergstrom, H. C., Schmidt, R. J., . . . Housh, D. J. (2014). The effects of polyethylene glycosylated creatine supplementation on anaerobic performance measures and body composition. *The Journal of Strength & Conditioning Research, 28*(3), 825-833. doi: 10.1519/JSC.0b013e3182a361a5

Carter, J. L., & Heath, B. H. (1990). *Somatotyping: development and applications* (Vol. 5): Cambridge University Press.

Ceseracciu, E., Sawacha, Z., Fantozzi, S., Cortesi, M., Gatta, G., Corazza, S., & Cobelli, C. (2011). Markerless analysis of front crawl swimming. *Journal of Biomechanics, 44*(12), 2236-2242. doi: 10.1016/j.jbiomech.2011.06.003

Chen, Y., & Cipolla, R. (2011). Single and sparse view 3D reconstruction by learning shape priors. *Computer Vision and Image Understanding, 115*(5), 586-602. doi: http://dx.doi.org/10.1016/j.cviu.2010.10.015

Chen, Y., Robertson, D., & Cipolla, R. (2011). *A practical system for modelling body shapes from single view measurements.* Paper presented at the Procedings of the British Machine Vision Conference 2011, Dundee, UK, 82.81-82.11.

Clauser, C. E., McConville, J. T., & Young, J. W. (1969). *Weight, volume, and center of mass of segments of the human body* (National Technical Information Service Ed.): DTIC Document.

Collins, J. (2006). *Volumetric analysis of human bodies.* University of South Australia School of Health Sciences. Available from http://worldcat.org /z-wcorg/ database.

Consultation, W. E. (2008). *Waist circumference and waist-hip ratio. Report of a WHO Expert Consultation*. Geneva.

Conway, J. M., Norris, K. H., & Bodwell, C. E. (1984). A new approach for the estimation of body composition: infrared interactance. *American Journal of Clinical Nutrition, 40*(6), 1123-1130.

Corazza, S., Mündermann, L., Gambaretto, E., Ferrigno, G., & Andriacchi, T. P. (2009). Markerless motion capture through visual hull, articulated ICP and subject specific model generation. *International Journal of Computer Vision, 87*, 156-169. doi: 10.1007/s11263-009-0284-3

Cui, Y., Chang, W., Nöll, T., & Stricker, D. (2013). KinectAvatar: fully automatic body capture using a single kinect. In J.-I. Park & J. Kim (Eds.), *Computer Vision - ACCV 2012 Workshops* (Vol. 7729, pp. 133-147): Springer Berlin Heidelberg.

D'Apuzzo, N. (2009). *Recent advances in 3D full body scanning with applications to fashion and apparel*. Paper presented at the Optical 3-D Measurement Techniques IX, Vienna, Austria.

Daanen, H. A. M., & Ter Haar, F. B. (2013). 3D whole body scanners revisited. *Displays, 34*(4), 270-275. doi: http://dx.doi.org/10.1016/j.displa.2013.08.011

Daanen, H. M., & van de Water, G. J. (1998). Whole body scanners. *19*, 111-120. doi: http://dx.doi.org/10.1016/S0141-9382(98)00034-1

Daniell, N., Olds, T., & Tomkinson, G. (2014). Volumetric differences in body shape among adults with differing body mass index values: An analysis using three-dimensional body scans. *American Journal of Human Biology, 26*(2), 156-163. doi: 10.1002/ajhb.22490

Danielsen, K. K., Svendsen, M., Mæhlum, S., & Sundgot-Borgen, J. (2013). Changes in body composition, cardiovascular disease risk factors, and eating behavior after an intensive lifestyle intervention with high volume of physical activity in severely obese

subjects: a prospective clinical controlled trial. *Journal of Obesity, 2013*, 1-12. doi: 10.1155/2013/325464

Deffeyes, J., & Sanders, R. H. (2005). *Elliptical zone body segment modelling software: digitising, modelling and body segment parameter calculation.* Paper presented at the ISBS Conference Proceedings, Beijing, China, 749-752.

Dempster, W. T. (1955). Space requirements of the seated operator: geometrical, kinematic, and mechanical aspects of the body, with special reference to the limbs: Carpenter Litho and Printing Co,.

Drillis, R., Contini, R., & Bluestein, M. (1964). Body segment parameters. *Artificial Limbs, 8*(1), 44-66.

Durnin, J., & Womersley, J. (1974). Body fat assessed from total body density and its estimation from skinfold thickness: measurements on 481 men and women aged from 16 to 72 years. *British Journal of Nutrition, 32*(01), 77-97.

Duthie, G., Pyne, D., & Hooper, S. (2003). Applied physiology and game analysis of rugby union. *Sports Medicine, 33*(13), 973-991. doi: 10.2165/00007256-200333130-00003

Elferink-Gemser, M. T., Huijgen, B. C. H., Coelho-E-Silva, M., Lemmink, K. A. P. M., & Visscher, C. (2012). The changing characteristics of talented soccer players – a decade of work in Groningen. *Journal of Sports Sciences, 30*(15), 1581-1591. doi: 10.1080/02640414.2012.725854

Ellis, K. J. (2000). Human body composition: in vivo methods. *Physiological Reviews, 80*(2), 649-680.

Evans, E., Mojtahedi, M., Thorpe, M., Valentine, R., Kris-Etherton, P., & Layman, D. (2012). Effects of protein intake and gender on body composition changes: a randomized clinical weight loss trial. *Nutrition & Metabolism, 9*(1), 55-63.

Fanelli, M. T., & Kuczmarski, R. J. (1984). Ultrasound as an approach to assessing body composition. *American Journal of Clinical Nutrition, 39*(5), 703-709.

Fields, D., Hunter, G., & Goran, M. (2000). Validation of the BOD POD with hydrostatic weighing: influence of body clothing. *International Journal of Obesity and Related Metabolic Disorders, 24*(2), 200-205.

Fomon, S. J., Haschke, F., Ziegler, E. E., & Nelson, S. E. (1982). Body composition of reference children from birth to age 10 years. *American Journal of Clinical Nutrition, 35*(5), 1169-1175.

Ford, P. A., Perkins, G., & Swaine, I. (2012). Effects of a 15-week accumulated brisk walking programme on the body composition of primary school children. *Journal of Sports Sciences, 31*(2), 114-122. doi: 10.1080/02640414.2012.723816

Ganong, W. (2003). *Review of Medical Physiology* (21 ed.): McGraw-Hill Professional , Lange Medical Books

Garcia, J., & Zalevsky, Z. (2008). Range mapping using speckle decorrelation. US7433024B2.

Garthe, I., Raastad, T., Refsnes, P. E., & Sundgot-Borgen, J. (2012). Effect of nutritional intervention on body composition and performance in elite athletes. *European Journal of Sport Science, 13*(3), 295-303. doi: 10.1080/17461391.2011.643923

Gonzalez-Jorge, H., Riveiro, B., Vazquez-Fernandez, E., Martínez-Sánchez, J., & Arias, P. (2013). Metrological evaluation of Microsoft Kinect and Asus Xtion sensors. *Measurement, 46*(6), 1800-1806. doi: http://dx.doi.org/10.1016/j.measurement.2013.01.011

Guerrero-Romero, F., & Rodríguez-Morán, M. (2003). Abdominal volume index. an anthropometry-based index for estimation of obesity is strongly related to impaired glucose tolerance and type 2 diabetes mellitus. *Archives of Medical Research, 34*(5), 428-432. doi: http://dx.doi.org/10.1016/S0188-4409(03)00073-0

Hanavan Jr, E. P. (1964). *A mathematical model of the human body* (Air Force Aerospace Medical Research Lab Wright-Patterson AFB OH Ed.): DTIC Document.

Hasler, N., Stoll, C., Rosenhahn, B., Thormählen, T., & Seidel, H.-P. (2009). Estimating body shape of dressed humans. *Computers & Graphics, 33*(3), 211-216. doi: http://dx.doi.org/10.1016/j.cag.2009.03.026

Hauswiesner, S., Straka, M., & Reitmayr, G. (2011). *Free viewpoint virtual try-on with commodity depth cameras.* Paper presented at the 10th International Conference on Virtual Reality Continuum and Its Applications in Industry, New York, USA, 23-30.

Hopkins, W. (2000). Measures of reliability in sports medicine and science. *Sports Medicine, 30*(1), 1-15. doi: 10.2165/00007256-200030010-00001

Jensen, R. K. (1978). Estimation of the biomechanical properties of three body types using a photogrammetric method. *Journal of Biomechanics, 11*(8), 349-358. doi: 10.1016/0021-9290(78)90069-6

Jensky-Squires, N. E., Dieli-Conwright, C. M., Rossuello, A., Erceg, D. N., McCauley, S., & Schroeder, E. T. (2008). Validity and reliability of body composition analysers in children and adults. *British Journal of Nutrition, 100*(04), 859-865.

Kass, M., Witkin, A., & Terzopoulos, D. (1988). Snakes: Active contour models. *International Journal of Computer Vision, 1*(4), 321-331. doi: 10.1007/BF00133570

Katch, V., Weltman, A., & Gold, E. (1974). Validity of anthropometric measurements and the segment-zone method for estimating segmental and total body volume. *Medicine and Science in Sports, 6*(4), 271-276.

Katch, V. L., & Katch, F. I. (1974). A simple anthropometric method for calculating segmental leg limb volume. *Research Quarterly. American Alliance for Health, Physical Education and Recreation, 45*(2), 211-214. doi: 10.1080/10671188.1974.10615262

Keating, S. E., Machan, E. A., O'Connor, H. T., Gerofi, J. A., Sainsbury, A., Caterson, I. D., & Johnson, N. A. (2014). Continuous exercise but not high intensity interval training improves fat distribution in overweight adults. *Journal of Obesity, 2014*, 1-12. doi: 10.1155/2014/834865

Kennedy, J. (2012). Virtual mirror shows how Kinect could transform online shopping. Retrieved 22.Nov, 2015, from http://www.siliconrepublic.com/new-media/item/25413-virtual-mirror-shows-how-ki

Ketel, I. J. G., Volman, M. N. M., Seidell, J. C., Stehouwer, C. D. A., Twisk, J. W., & Lambalk, C. B. (2007). Superiority of skinfold measurements and waist over waist-to-hip ratio for determination of body fat distribution in a population-based cohort of Caucasian Dutch adults. *European Journal of Endocrinology, 156*(6), 655-661. doi: 10.1530/eje-06-0730

Khoshelham, K. (2011). *Accuracy analysis of kinect depth data.* Paper presented at the ISPRS workshop laser scanning (29-31 Aug. 2011), Calgary, Canada, 133-138.

Kim, J., Wang, Z., Heymsfield, S. B., Baumgartner, R. N., & Gallagher, D. (2002). Total-body skeletal muscle mass: estimation by a new dual-energy X-ray absorptiometry method. *American Journal of Clinical Nutrition, 76*(2), 378-383.

Konarski, J., Krzykała, M., Podgórski, T., Pawlak, M., Strzelczyk, R., & Malina, R. M. (2012). Variations in functional and morphological characteristics of elite Polish field hockey players in a complete macrocycle. *International Journal of Sports Science and Coaching, 7*(3), 527-542.

Kotler, D. P., Thea, D. M., Heo, M., Allison, D. B., Engelson, E. S., Wang, J., . . . Keusch, G. T. (1999). Relative influences of sex, race, environment, and HIV infection on body composition in adults. *American Journal of Clinical Nutrition, 69*(3), 432-439.

Kulwich, R., Feinstein, L., & Anderson, E. C. (1958). Correlation of Potassium-40 concentration and fat-free lean content of hams. *Science, 127*(3294), 338-339. doi: 10.1126/science.127.3294.338-a

Kyle, U. G., Bosaeus, I., De Lorenzo, A. D., Deurenberg, P., Elia, M., Gómez, J. M., . . . Pichard, C. (2004). Bioelectrical impedance analysis—part I: review of principles and methods. *Clinical Nutrition, 23*(5), 1226-1243. doi: http://dx.doi.org/10.1016/j.clnu.2004.06.004

Ladikos, A., Benhimane, S., & Navab, N. (2008). *Efficient visual hull computation for real-time 3D reconstruction using CUDA.* Paper presented at the Proceedings of the

2008 Conference on Computer Vision and Pattern Recognition Workshops, Los Alamitos, CA, USA, 1-8.

Leboucher, J., Dumas, G. A., Pinti, A., & Lepoutre, F. X. (2008). Assessment of limb segment volume asymmetry. *Computer Methods in Biomechanics and Biomedical Engineering, 11*(sup001), 139-140. doi: 10.1080/10255840802296707

Lee, J. J., Freeland-Graves, J. H., Pepper, M. R., Yu, W., & Xu, B. (2015). Efficacy of thigh volume ratios assessed via stereovision body imaging as a predictor of visceral adipose tissue measured by magnetic resonance imaging. *American Journal of Human Biology*, 445-457. doi: 10.1002/ajhb.22663

Lin, Y.-L., & Wang, M.-J. J. (2012). Constructing 3D human model from front and side images. *Expert Systems with Applications, 39*(5), 5012-5018. doi: 10.1016/j.eswa.2011.10.011

Lohman, T. G., Harris, M., Teixeira, P. J., & Weiss, L. (2000). Assessing body composition and changes in body composition: another look at dual-energy X-ray absorptiometry. *Annals of the New York Academy of Sciences, 904*(1), 45-54.

Ma, Y., Kwon, J., Mao, Z., Lee, K., Li, L., & Chung, H. (2011). Segment inertial parameters of Korean adults estimated from three-dimensional body laser scan data. *International Journal of Industrial Ergonomics, 41*(1), 19-29. doi: 10.1016/j.ergon.2010.11.004

Martin Bland, J., & Altman, D. (1986). Statistical methods for assessing agreement between two methods of clinical measurement. *The Lancet, 327*(8476), 307-310. doi: http://dx.doi.org/10.1016/S0140-6736(86)90837-8

Matusik, W., Buehler, C., Raskar, R., Gortler, S. J., & McMillan, L. (2000). *Image-based visual hulls*. Paper presented at the Proceedings of the 27th annual conference on Computer graphics and interactive techniques, New Orleans, LA USA.

McCabe, C. B., Psycharakis, S., & Sanders, R. (2011). Kinematic differences between front crawl sprint and distance swimmers at sprint pace. *Journal of Sports Sciences, 29*, 115-123. doi: 10.1080/02640414.2010.523090

McCabe, C. B., & Sanders, R. H. (2012). Kinematic differences between front crawl sprint and distance swimmers at a distance pace. *Journal of Sports Sciences, 30*(6), 601-608.

Meunier, P., & Yin, S. (2000). Performance of a 2D image-based anthropometric measurement and clothing sizing system. *Applied Ergonomics, 31*(5), 445-451. doi: http://dx.doi.org/10.1016/S0003-6870(00)00023-5

Microsoft. (2015a). Kinect for Windows features. Retrieved 28.Nov, 2015, from http://www.microsoft.com/en-us/kinectforwindows/meetkinect/features.aspx

Microsoft. (2015b). Kinect for Windows SDK v1.8. Retrieved 22.Nov, 2015, from https://www.microsoft.com/en-us/download/details.aspx?id=40278

Microsoft. (2015c). Room lighting conditions for Kinect. Retrieved 22.Nov, 2015, from https://support.xbox.com/en-AU/xbox-360/kinect/lighting

Milsom, J., Naughton, R., O'Boyle, A., Iqbal, Z., Morgans, R., Drust, B., & Morton, J. P. (2015). Body composition assessment of English Premier League soccer players: a comparative DXA analysis of first team, U21 and U18 squads. *Journal of Sports Sciences, 33*(17), 1799-1806. doi: 10.1080/02640414.2015.1012101

Mirtich, B. (1996). Fast and accurate computation of polyhedral mass properties. *Journal of Graphics Tools, 1*(2), 31-50. doi: 10.1080/10867651.1996.10487458

Mulholland, Y., & Rolland, C. (2012). Portable methods of body composition analysis. In A. D. Stewart & L. Sutton (Eds.), *Body Composition in Sport, Exercise, and Health* (pp. 42-63): Abingdon, UK: Routledge.

Muralidhara, D. (2015). Come 2020!; Welcome body volume index!!; Bye bye body mass index!!! *Integrative Obesity and Diabetes, 1*(1), 26-27.

Nguyen, C. V., Izadi, S., & Lovell, D. (2012). *Modeling kinect sensor noise for improved 3D reconstruction and tracking.* Paper presented at the 2012 Second International Conference on 3D Imaging, Modeling, Processing, Visualization and Transmission (3DIMPVT), Zurich, Switzerland, 524-530.

Norton, K., & Olds, T. (1996). *Anthropometrica: a textbook of body measurement for sports and health courses*: Sydney: UNSW Press.

Okorodudu, D., Jumean, M., Montori, V., Romero-Corral, A., Somers, V., Erwin, P., & Lopez-Jimenez, F. (2010). Diagnostic performance of body mass index to identify obesity as defined by body adiposity: a systematic review and meta-analysis. *International Journal of Obesity, 34*(5), 791-799.

Olds, T., Daniell, N., Petkov, J., & Stewart, A. D. (2013). Somatotyping using 3D anthropometry: a cluster analysis. *Journal of Sports Sciences, 31*(9), 936-944. doi: 10.1080/02640414.2012.759660

Oliveira, N., Chiu, C.-Y., & Sanders, R. H. (2015). Kinematic patterns associated with the vertical force produced during the eggbeater kick. *Journal of Sports Sciences, 33*(16), 1675-1681. doi: 10.1080/02640414.2014.1003590

OpenNI. (2012). OpenNI. Retrieved 25.Dec, 2012, from http://www.openni.org/

Pearsall, D., Reid, J., & Ross, R. (1994). Inertial properties of the human trunk of males determined from magnetic resonance imaging. *Annals of Biomedical Engineering, 22*(6), 692-706. doi: 10.1007/bf02368294

Peng, G., Weiss, A., Balan, A. O., & Black, M. J. (2009). *Estimating human shape and pose from a single image.* Paper presented at the 2009 IEEE 12th International Conference on Computer Vision, Kyoto, Japan, 1381-1388.

Perini, T. A., Oliveira, G. L. d., Ornellas, J. d. S., & Oliveira, F. P. d. (2005). Technical error of measurement in anthropometry. *Revista Brasileira de Medicina do Esporte, 11*(1), 81-85.

Pirker, K., Rüther, M., Bischof, H., Skrabal, F., & Pichler, G. (2009). Human body volume estimation in a clinical environment. *AAPRIOAGM: Challenges in the Biosciences: Image Analysis and Pattern Recognition Aspects, Stainz Austria. Austrian Computer Society*.

Price, G. M., Uauy, R., Breeze, E., Bulpitt, C. J., & Fletcher, A. E. (2006). Weight, shape, and mortality risk in older persons: elevated waist-hip ratio, not high body mass index, is associated with a greater risk of death. *The American Journal of Clinical Nutrition, 84*(2), 449-460.

PrimeSensor. (2012). Prime Sensor™ NITE 1.3 algorithms notes. Retrieved 25.Dec, 2012, from http://www.primesense.com

Psycharakis, S. G., Naemi, R., Connaboy, C., McCabe, C., & Sanders, R. H. (2010). Three-dimensional analysis of intracycle velocity fluctuations in frontcrawl swimming. *Scandinavian Journal of Medicine and Science in Sports, 20*(1), 128-135.

Rebuffé-Scrive, M., Krotkiewski, M., Elfverson, J., & Björntorp, P. (1988). Muscle and Adipose Tissue Morphology and Metabolism in Cushing's Syndrome. *Journal of Clinical Endocrinology and Metabolism, 67*(6), 1122-1128. doi: doi:10.1210/jcem-67-6-1122

Rolland, C. (2012). Laboratory methods of body composition analysis. In A. D. Stewart & L. Sutton (Eds.), *Body Composition in Sport, Exercise, and Health* (pp. 20-41): Abingdon, UK: Routledge.

Rother, C., Kolmogorov, V., & Blake, A. (2004). *"GrabCut": interactive foreground extraction using iterated graph cuts*. Paper presented at the ACM SIGGRAPH 2004 Papers, Los Angeles, California.

Rusu, R. B., & Cousins, S. (2011). *3d is here: Point Cloud Library (PCL).* Paper presented at the 2011 IEEE International Conference on Robotics and Automation (ICRA), Shanghai, China, 1-4.

Samejima, I., Maki, K., Kagami, S., Kouchi, M., & Mizoguchi, H. (2012). *A body dimensions estimation method of subject from a few measurement items using KINECT.* Paper presented at the 2012 IEEE International Conference on Systems, Man, and Cybernetics (SMC), Seoul, Korea, 3384-3389.

Sanders, R. H., Chiu, C.-Y., Gonjo, T., Thow, J., Oliveira, N., Psycharakis, S. G., . . . McCabe, C. B. (2015). Reliability of the elliptical zone method of estimating body segment parameters of swimmers. *Journal of Sports Science and Medicine 14*, 215-224.

Schranz, N., Tomkinson, G., Olds, T., & Daniell, N. (2010). Three-dimensional anthropometric analysis: Differences between elite Australian rowers and the general

population. *Journal of Sports Sciences, 28*(5), 459-469. doi: 10.1080/02640411003663284

Schranz, N., Tomkinson, G., Olds, T., Petkov, J., & Hahn, A. G. (2012). Is three-dimensional anthropometric analysis as good as traditional anthropometric analysis in predicting junior rowing performance? *Journal of Sports Sciences, 30*(12), 1241-1248. doi: 10.1080/02640414.2012.696204

Schreiner, P. J., Pitäniemi, J., Pekkanen, J., & Salomaa, V. V. (1995). Reliability of near-infrared interactance body fat assessment relative to standard anthropometric techniques. *Journal of Clinical Epidemiology, 48*(11), 1361-1367. doi: http://dx.doi.org/10.1016/0895-4356(95)00052-6

Sheets, A. L., Andriacchi, T. P., & Corazza, S. (2009). An automated image-based method of 3D subject-specific body segment parameter estimation for Kinetic analyses of rapid movements. *Journal of Biomechanical Engineering, 132*(1), 011004-011004. doi: 10.1115/1.4000155

Shrout, P. E., & Fleiss, J. L. (1979). Intraclass correlations: uses in assessing rater reliability. *Psychological Bulletin, 86*(2), 420.

Sinha, S. N., & Pollefeys, M. (2004). *Visual-hull reconstruction from uncalibrated and unsynchronized video streams.* Paper presented at the 2nd International Symposium on 3D Data Processing, Visualization and Transmission, 2004. 3DPVT 2004. Proceedings, Thessaloniki, Greece, 349-356.

Siri, W. (1961). *Body composition from fluid spaces and density: analysis of methods*. Paper presented at the Techniques for Measuring Body Composition, Natick, Massachusetts, USA.

Siri, W. E. (1956). *Body composition from fluid spaces and density: analysis of methods* (B. R. L. California. Univ. Ed.). United States: California. Univ., Berkeley. Radiation Lab.

Stancic, I., Supuk, T., Cecic, M., Mastorakis, N., Croitoru, A., Balas, V., . . . Mladenov, V. (2009). *Human anthropometric parameters estimation using video based techniques.* Paper presented at the 10th WSEAS International Conference on Automation & Information, Prague, Czech, 169-174.

Stewart, A., Marfell-Jones, M., Olds, T., & Ridder, H. d. (2011). *International standards for anthropometric assessment*. Lower Hutt, New Zealand: International Society for the Advancement of Kinanthropometry.

Stewart, A. D. (2010). Kinanthropometry and body composition: A natural home for three-dimensional photonic scanning. *Journal of Sports Sciences, 28*(5), 455-457. doi: 10.1080/02640411003661304

Stewart, A. D., Klein, S., Young, J., Simpson, S., Lee, A. J., Harrild, K., . . . Benson, P. J. (2012). Body image, shape, and volumetric assessments using 3D whole body laser scanning and 2D digital photography in females with a diagnosed eating disorder:

Preliminary novel findings. *British Journal of Psychology, 103*(2), 183-202. doi: 10.1111/j.2044-8295.2011.02063.x

Stouffer, J. (1968). *Ultrasonic determination of body composition* (D. Wright-Patterson Air Force Base, OH Ed.): DTIC Document.

Sundgot-Borgen, J., & Garthe, I. (2011). Elite athletes in aesthetic and Olympic weight-class sports and the challenge of body weight and body compositions. *Journal of Sports Sciences, 29*(sup1), S101-S114. doi: 10.1080/02640414.2011.565783

Sutton, L., Scott, M., Wallace, J., & Reilly, T. (2009). Body composition of English Premier League soccer players: Influence of playing position, international status, and ethnicity. *Journal of Sports Sciences, 27*(10), 1019-1026. doi: 10.1080/02640410903030305

Takai, Y., Ohta, M., Akagi, R., Kato, E., Wakahara, T., Kawakami, Y., . . . Kanehisa, H. (2013). Validity of ultrasound muscle thickness measurements for predicting leg skeletal muscle mass in healthy Japanese middle-aged and older individuals. *Journal of Physiological Anthropology, 32*(1), 1-12.

Tong, J., Zhou, J., Liu, L., Pan, Z., & Yan, H. (2012). Scanning 3D full human bodies using Kinects. *IEEE Transactions on Visualization and Computer Graphics, 18*(4), 643-650. doi: 10.1109/tvcg.2012.56

Treleaven, P., & Wells, J. (2007). 3D body scanning and healthcare applications. *Computer, 40*(7), 28-34.

Trutschnigg, B., Kilgour, R. D., Reinglas, J., Rosenthall, L., Hornby, L., Morais, J. A., & Vigano, A. (2008). Precision and reliability of strength (Jamar vs. Biodex handgrip) and body composition (dual-energy X-ray absorptiometry vs. bioimpedance analysis) measurements in advanced cancer patients. *Applied Physiology, Nutrition, and Metabolism, 33*(6), 1232-1239.

University of Western Australia. (2007). Research gives swimmers a kick-start. Retrieved 21.Nov, 2015, from http://www.news.uwa.edu.au/content/research-gives-swimmers-kick-start

Van Deun, D., Verhaert, V., Buys, K., Haex, B., & Vander Sloten, J. (2011). *Automatic generation of personalized human models based on body measurements*. Paper presented at the International Symposium on Digital Human Modeling, Lyon, France.

Velardo, C., & Dugelay, J. (2012). *What can computer vision tell you about your weight?* Paper presented at the 2012 Proceedings of the 20th European Signal Processing Conference (EUSIPCO), Bucharest, Romania, 1980-1984.

Velardo, C., Dugelay, J., Paleari, M., & Ariano, P. (2012). *Building the space scale or how to weigh a person with no gravity*. Paper presented at the 2012 IEEE International Conference on Emerging Signal Processing Applications (ESPA), Las Vegas, Nevada, USA, 67-70.

Von Loebbecke, A., Mittal, R., Mark, R., & Hahn, J. (2009). A computational method for analysis of underwater dolphin kick hydrodynamics in human swimming. *Sports Biomechanics, 8*(1), 60-77.

Wajchenberg, B. L., Bosco, A., Marone, M. M., Levin, S., Rocha, M., Lerário, A. C., . . . Liberman, B. (1995). Estimation of body fat and lean tissue distribution by dual energy X-ray absorptiometry and abdominal body fat evaluation by computed tomography in Cushing's disease. *The Journal of Clinical Endocrinology & Metabolism, 80*(9), 2791-2794. doi: doi:10.1210/jcem.80.9.7673425

Wang, J., Gallagher, D., Thornton, J. C., Yu, W., Horlick, M., & Pi-Sunyer, F. X. (2006). Validation of a 3-dimensional photonic scanner for the measurement of body volumes, dimensions, and percentage body fat. *American Journal of Clinical Nutrition, 83*(4), 809-816.

Wang, R., Choi, J., & Medioni, G. (2012). *Accurate full body scanning from a single fixed 3D camera*. Paper presented at the 2012 Second International Conference on 3D Imaging, Modeling, Processing, Visualization and Transmission (3DIMPVT), Zurich, Switzerland.

Wang, Z. M., Visser, M., Ma, R., Baumgartner, R. N., Kotler, D., Gallagher, D., & Heymsfield, S. B. (1996). Skeletal muscle mass: evaluation of neutron activation and dual-energy X-ray absorptiometry methods. *Journal of Applied Physiology, 80*(3), 824-831.

Weir, J. P. (2005). Quantifying test-retest reliability using the intraclass correlation coefficient and the SEM. *Journal of Strength and Conditioning Research, 19*(1), 231-240.

Weiss, A., Hirshberg, D., & Black, M. J. (2011). *Home 3D body scans from noisy image and range data.* Paper presented at the 2011 IEEE International Conference on Computer Vision (ICCV), Barcelona, Spain, 1951-1958.

Wells, J. K. (2012). Three-dimensional (3-D) photonic scanning: a new approach to anthropometry. In V. R. Preedy (Ed.), *Handbook of Anthropometry* (pp. 205-217): New York: Springer.

Wicke, J., & Dumas, G. (2007). *A new trunk volume representation for geometric body segment models*. Paper presented at the American Society of Biomechanics, Stanford University, California, USA. http://www.asbweb.org/conferences/2007/52.pdf

Wicke, J., & Dumas, G. A. (2010). Influence of the volume and density functions within geometric models for estimating trunk inertial parameters. *Journal of Applied Biomechanics, 26*(1).

Wicke, J., & Dumas, G. A. (2014). A new geometric-based model to accurately estimate arm and leg inertial estimates. *Journal of Biomechanics, 47*(8), 1869-1875. doi: http://dx.doi.org/10.1016/j.jbiomech.2014.03.020

Wicke, J., Dumas, G. A., & Costigan, P. A. (2009). A comparison between a new model and current models for estimating trunk segment inertial parameters. *Journal of Biomechanics, 42*(1), 55-60. doi: 10.1016/j.jbiomech.2008.10.003

Wicke, J., & Lopers, B. (2003). Validation of the volume function within Jensen's (1978) elliptical cylinder model. *Journal of Applied Biomechanics, 19*(1), 3-12.

Wilson, J. P., Fan, B., & Shepherd, J. A. (2013). Total and regional body volumes eerived from dual-energy x-ray absorptiometry output. *Journal of Clinical Densitometry, 16*(3), 368-373. doi: http://dx.doi.org/10.1016/j.jocd.2012.11.001

Wilson, J. P., Kanaya, A. M., Fan, B., & Shepherd, J. A. (2013). Ratio of trunk to leg volume as a new body shape metric for diabetes and mortality. *PloS One, 8*(7), e68716. doi: 10.1371/journal.pone.0068716

World Health Organization. (1995). Physical status: the use and interpretation of anthropometry. Report of a WHO Expert Committee. *World Health Organisation Techical Report Series, 854*, 1-452.

Wuhrer, S., & Shu, C. (2013). Estimating 3D human shapes from measurements. *Machine Vision and Applications, 24*(6), 1133-1147. doi: 10.1007/s00138-012-0472-y

Xu, H., Yu, Y., Zhou, Y., Li, Y., & Du, S. (2013). Measuring accurate body parameters of dressed humans with large-scale motion using a Kinect sensor. *Sensors, 13*(9), 11362-11384.

Yeadon, M. R. (1990). The simulation of aerial movement—II. A mathematical inertia model of the human body. *Journal of Biomechanics, 23*(1), 67-74. doi: http://dx.doi.org/10.1016/0021-9290(90)90370-I

Yinpeng, C., Zicheng, L., & Zhengyou, Z. (2013). *Tensor-based human body modeling.* Paper presented at the 2013 IEEE Conference on Computer Vision and Pattern Recognition (CVPR), Portland, Oregon, USA, 105-112.

Yuhasz, M. S. (1974). *Physical Fitness Manual*: Canada: University of Western Ontario.

Zhang, C., & Chen, T. (2001). *Efficient feature extraction for 2D/3D objects in mesh representation.* Paper presented at the 2001 International Conference on Image Processing, Thessaloniki, Greece, 935-938.

Zollhöfer, M., Martinek, M., Greiner, G., Stamminger, M., & Süßmuth, J. (2011). Automatic reconstruction of personalized avatars from 3D face scans. *Computer Animation and Virtual Worlds, 22*(2-3), 195-202. doi: 10.1002/cav.405

Appendix A Volunteer Information Sheet

My name is Chuang-Yuan Chiu and I am a PhD student. I am seeking your involvement in my study. This study is to validate simple scanning techniques which can visualize the body shape variation and understand mass distribution. It can help people understand their body shape accurately and keep fit (reduce weight) more effectively.

Requirements of participant

You will need to be present at the laboratory on one occasion. All tests will be conducted in the Australian Institute of Sport.

In this test, you need to bring your own close-fitting suit (a two piece suit for females) such as swimming cloth or undergarment and sports bras for female. Your suit should be in light color. White is perfect. Your suit needs to avoid black, green and blue color including the small patterns or alphabets. If your suit does not follow this rule, we might ask you to change into ours to make sure the testing accuracy.

In the beginning of each test, we have explained the procedure again. Then, you will change into a close-fitting suit (a two piece suit for females) with a cap in the changing room. You will also be asked to remove any jewellery and watch. It is highly recommend that you bring your own jacket, robe, or bath towel to keep you warm between each assessment. Don't worry if you forget, we will have some available.

There will then be a series of assessments. Some will involve taking body measurements using a tape measure, and calipers. Others will involve you standing still while the images of your body are obtained. Details of these are below. The total process for each test will take less than 3 hours.

Details of the Experiment

Manual assessment

This will involve a standard ISAK procedure to identify anatomical landmarks that indicate the endpoints of body segments and marking those with a non-permanent marker. A tape measure will then be used to assess circumference of the body, and calipers will be used to assess skinfold (a light pinch of the skin and application of calipers).

Image capturing

Images of the body from the front and the side will be obtained using standard digital cameras. Some images will be captured with close-fitting clothing and some will be obtained while wearing a swimming suit.

Body scanning

In the body scanning test, you will be scanned by a commercial body scanner. We will use a non-invasive laser scanner in this study. You need to stand on the specific booth and attempt to keep still while scanning.

Benefits of Involvement

If you wish, you will receive the test results after conducting all assessments which will help you understand your body size.

Refusal or withdrawal of participation

You will be able to cease participation or withdraw consent at any time.

Additional Information

The image captured from the assessments will only be applied to generate your 3D human model and possibly used in my thesis and other publications to illustrate the testing process. We will use a virtual face to replace your face on your 3D human model(s) and a black box to hide your face in the relevant figures. We will not disclose your personal information or identity. Your 3D human model and the captured images will be used only for research purpose.

If you have any questions or concerns, please contact me without hesitation.

Sincerely,

Chuang-Yuan Chiu (Researcher)

Telephone: 0416105284

Email: thorsten.chiu@gmail.com

Prof Ross Sanders (Supervisor)

Email: ross.sanders@sydney.edu.au

Dr Samantha Fawkner (Supervisor)

Appendix B Informed Consent Form

Name:

Date of Birth:

Gender:

Email:

Telephone number:

Address:

I have read and understood the information about the study and consent voluntarily to participate. (YES/NO)

I agree that the image capturing in the study can be used for research, relevant scientific publications or presentations with the faces hidden or changed to avoid revealing your identity. (YES/NO)

I grant the permission that my test result in this study can be sent to me via internet. (YES/NO)

I understand that I can ask questions and stop my participating at any time. (YES/NO)

_____ _____

Signature participant *Date*

_____ _____

Signature researcher *Date*

Appendix C Blender Script for Calculating Body Volume Data

C.1 Blender Script “00bvstl” for obtaining the whole-body mesh (STL file) from the individual MH model (MHX file)

```
import bpy
# clear workspace
# bpy.ops.wm.read_homefile()
bpy.ops.object.select_all(action='SELECT')
bpy.ops.object.delete()

# import mhx file
bpy.ops.import_scene.makehuman_mhx(filepath='quick_export.mhx',scale=1)

# set pose
bpy.context.scene.objects.active = bpy.data.objects["Quick_export"]
bpy.context.active_object.select = True
bpy.ops.object.mode_set(mode='POSE')

bpy.data.objects["Quick_export"].pose.bones["UpLeg_L"].rotation_quaternion.w=0.991
bpy.data.objects["Quick_export"].pose.bones["UpLeg_L"].rotation_quaternion.x=0
bpy.data.objects["Quick_export"].pose.bones["UpLeg_L"].rotation_quaternion.y=0
bpy.data.objects["Quick_export"].pose.bones["UpLeg_L"].rotation_quaternion.z=-0.131

bpy.data.objects["Quick_export"].pose.bones["UpLeg_R"].rotation_quaternion.w=0.991
bpy.data.objects["Quick_export"].pose.bones["UpLeg_R"].rotation_quaternion.x=0
bpy.data.objects["Quick_export"].pose.bones["UpLeg_R"].rotation_quaternion.y=0
bpy.data.objects["Quick_export"].pose.bones["UpLeg_R"].rotation_quaternion.z=0.131

# select mesh
bpy.context.scene.objects.active = bpy.data.objects["Quick_exportMesh"]
bpy.context.active_object.select = True
'''''
# triangle mesh
##delete shape key
for i in range(29):
    bpy.ops.object.shape_key_remove()

# add modifier
bpy.ops.object.modifier_add(type='TRIANGULATE')

#apply modifier
bpy.ops.object.modifier_apply(apply_as="DATA", modifier="Triangulate")
'''
```

```
# export triangle obj file
bpy.ops.export_scene.obj(filepath="./exportwholebodytri.obj", check_existing=False, filter_glob="*.obj;*.mtl", use_selection=True, use_animation=False, use_edges=True, use_normals=False, use_uvs=False, use_materials=False, use_triangles=True, use_vertex_groups=False, use_nurbs=False, use_blen_objects=False, group_by_object=False, group_by_material=False, keep_vertex_order=True)

# clear workspace
# bpy.ops.wm.read_homefile()
bpy.ops.object.select_all(action='SELECT')
bpy.ops.object.delete()

# import triangle obj file
bpy.ops.import_scene.obj(filepath="./exportwholebodytri.obj", filter_glob="*.obj;*.mtl")

# select mesh
bpy.context.scene.objects.active = bpy.data.objects["exportwholebodytri"]
bpy.context.active_object.select = True

# export STL file
bpy.ops.export_mesh.stl(filepath="./tb.stl", check_existing=False, filter_glob="*.stl", ascii=False, use_mesh_modifiers=True, axis_forward='Y', axis_up='Z', global_scale=1.0)
```

C.2 Blender Script “01headstl” for obtaining the head mesh (STL file) from the individual MH model (MHX file)

```
import bpy
# clear workspace
# bpy.ops.wm.read_homefile()
bpy.ops.object.select_all(action='SELECT')
bpy.ops.object.delete()

# import mhx file
bpy.ops.import_scene.makehuman_mhx(filepath='quick_export.mhx',scale=1)

# set pose
bpy.context.scene.objects.active = bpy.data.objects["Quick_export"]
bpy.context.active_object.select = True
bpy.ops.object.mode_set(mode='POSE')

#bpy.data.objects["Quick_export"].pose.bones["LoArm_L"].rotation_euler.x=0
#bpy.data.objects["Quick_export"].pose.bones["LoArm_L"].rotation_euler.y=-1.570797

bpy.data.objects["Quick_export"].pose.bones["UpLeg_L"].rotation_quaternion.w=0.991
bpy.data.objects["Quick_export"].pose.bones["UpLeg_L"].rotation_quaternion.x=0

bpy.data.objects["Quick_export"].pose.bones["UpLeg_L"].rotation_quaternion.y=0

bpy.data.objects["Quick_export"].pose.bones["UpLeg_L"].rotation_quaternion.z=-0.131

bpy.data.objects["Quick_export"].pose.bones["UpLeg_R"].rotation_quaternion.w=0.991
```

```
bpy.data.objects["Quick_export"].pose.bones["UpLeg_R"].rotation_quaternion.x=0
bpy.data.objects["Quick_export"].pose.bones["UpLeg_R"].rotation_quaternion.y=0
bpy.data.objects["Quick_export"].pose.bones["UpLeg_R"].rotation_quaternion.z=0.131


# change to 'OBJECT' mode
bpy.ops.object.mode_set(mode='OBJECT')

# select mesh
bpy.context.scene.objects.active = bpy.data.objects["Quick_exportMesh"]
bpy.context.active_object.select = True

# Select fvertex point
fvertexVertices=[8147]
#Create a Vertex Group
fvertexGroup = bpy.context.object.vertex_groups.new('fvertexVertexGroup')
fvertexGroup.add(fvertexVertices, 1.0, 'ADD')

# change to 'EDIT' mode
bpy.ops.object.mode_set(mode='EDIT')

# delete others
bpy.ops.mesh.select_all(action='DESELECT')

# select vertex group
#Select the Vertex group
bpy.ops.object.vertex_group_set_active(group='fvertexVertexGroup')
bpy.ops.object.vertex_group_select()

# change to 'OBJECT' mode
bpy.ops.object.mode_set(mode='OBJECT')

# add plane
[bpy.context.scene.cursor_location] = [i.co for i in bpy.context.active_object.data.vertices if i.select]

bpy.ops.mesh.primitive_plane_add()

bpy.ops.transform.resize(value=(10,10,1))
#bpy.data.objects["Plane"].dimensions=Vector((5,10,0))
bpy.data.objects["Plane"].rotation_euler[1]=3.1415939331054688
#bpy.data.objects["Plane"].rotation_euler=Euler((0.0, 3.1415939331054688, 0.0), 'XYZ')

# boolean
bpy.ops.object.modifier_add(type='BOOLEAN')

bpy.data.objects["Plane"].modifiers["Boolean"].object=bpy.data.objects['Quick_exportMesh']

bpy.ops.object.modifier_apply(apply_as='DATA',modifier="Boolean")



# export triangle obj file
bpy.ops.export_scene.obj(filepath="./exportheadtri.obj", check_existing=False, filter_glob="*.obj;*.mtl", use_selection=True, use_animation=False, use_edges=True, use_normals=False, use_uvs=False, use_materials=False, use_triangles=True, use_vertex_groups=False, use_nurbs=False, use_blen_objects=False, group_by_object=False, group_by_material=False, keep_vertex_order=True)
```

```
77.
78. bpy.ops.object.select_all(action='SELECT')
79. bpy.ops.object.delete()
80.
81. # import triangle obj file
82. bpy.ops.import_scene.obj(filepath="./exportheadtri.obj", filter_glob="*.obj;*.m
    tl")
83.
84. # select mesh
85. bpy.context.scene.objects.active = bpy.data.objects["exportheadtri"]
86. bpy.context.active_object.select = True
87.
88. # select mesh
89. bpy.context.scene.objects.active = bpy.data.objects["exportheadtri"]
90. bpy.context.active_object.select = True
91.
92. # export STL file
93. bpy.ops.export_mesh.stl(filepath="./head.stl", check_existing=False, filter_glo
    b="*.stl", ascii=False, use_mesh_modifiers=True, axis_forward='Y', axis_up='Z',
     global_scale=1.0)
```

C.3 Blender Script “02neckstl” for obtaining the neck mesh (STL file) from the individual MH model (MHX file)

```
1.  import bpy
2.  # clear workspace
3.  # bpy.ops.wm.read_homefile()
4.  bpy.ops.object.select_all(action='SELECT')
5.  bpy.ops.object.delete()
6.
7.  # import mhx file
8.  bpy.ops.import_scene.makehuman_mhx(filepath='quick_export.mhx',scale=1)
9.
10. # set pose
11. bpy.context.scene.objects.active = bpy.data.objects["Quick_export"]
12. bpy.context.active_object.select = True
13. bpy.ops.object.mode_set(mode='POSE')
14.
15. #bpy.data.objects["Quick_export"].pose.bones["LoArm_L"].rotation_euler.x=0
16. #bpy.data.objects["Quick_export"].pose.bones["LoArm_L"].rotation_euler.y=-
    1.570797
17.
18. bpy.data.objects["Quick_export"].pose.bones["UpLeg_L"].rotation_quaternion.w=0.
    991
19. bpy.data.objects["Quick_export"].pose.bones["UpLeg_L"].rotation_quaternion.x=0

20. bpy.data.objects["Quick_export"].pose.bones["UpLeg_L"].rotation_quaternion.y=0

21. bpy.data.objects["Quick_export"].pose.bones["UpLeg_L"].rotation_quaternion.z=-
    0.131
22.
23. bpy.data.objects["Quick_export"].pose.bones["UpLeg_R"].rotation_quaternion.w=0.
    991
24. bpy.data.objects["Quick_export"].pose.bones["UpLeg_R"].rotation_quaternion.x=0

25. bpy.data.objects["Quick_export"].pose.bones["UpLeg_R"].rotation_quaternion.y=0
```

```
bpy.data.objects["Quick_export"].pose.bones["UpLeg_R"].rotation_quaternion.z=0.131


# change to 'OBJECT' mode
bpy.ops.object.mode_set(mode='OBJECT')

# select mesh
bpy.context.scene.objects.active = bpy.data.objects["Quick_exportMesh"]
bpy.context.active_object.select = True

# Select fvertex point
fvertexVertices=[8147]

f1vertexVertices=[8179]

#Create a Vertex Group
fvertexGroup = bpy.context.object.vertex_groups.new('fvertexVertexGroup')
fvertexGroup.add(fvertexVertices, 1.0, 'ADD')

f1vertexGroup = bpy.context.object.vertex_groups.new('f1vertexVertexGroup')
f1vertexGroup.add(f1vertexVertices, 1.0, 'ADD')

# change to 'EDIT' mode
bpy.ops.object.mode_set(mode='EDIT')

# deselete others
bpy.ops.mesh.select_all(action='DESELECT')

# select vertex group
#Select the Vertex group
bpy.ops.object.vertex_group_set_active(group='fvertexVertexGroup')
bpy.ops.object.vertex_group_select()

# change to 'OBJECT' mode
bpy.ops.object.mode_set(mode='OBJECT')

# add plane
[bpy.context.scene.cursor_location] = [i.co for i in bpy.context.active_object.data.vertices if i.select]

bpy.ops.mesh.primitive_plane_add()

bpy.ops.transform.resize(value=(10,10,1))
#bpy.data.objects["Plane"].dimensions=Vector((10,10,0))
#bpy.data.objects["Plane"].rotation_euler=Euler((0.0, 0, 0.0), 'XYZ')

# select mesh
bpy.context.scene.objects.active = bpy.data.objects["Quick_exportMesh"]
bpy.context.active_object.select = True

# change to 'EDIT' mode
bpy.ops.object.mode_set(mode='EDIT')

# deselete others
bpy.ops.mesh.select_all(action='DESELECT')

# select vertex group
#Select the Vertex group
bpy.ops.object.vertex_group_set_active(group='f1vertexVertexGroup')
bpy.ops.object.vertex_group_select()

# change to 'OBJECT' mode
```

```
bpy.ops.object.mode_set(mode='OBJECT')

# add plane
[bpy.context.scene.cursor_location] = [i.co for i in bpy.context.active_object.data.vertices if i.select]

bpy.ops.mesh.primitive_plane_add()

bpy.ops.transform.resize(value=(10,10,1))
#bpy.data.objects["Plane.001"].dimensions=Vector((10,10,0))
bpy.data.objects["Plane.001"].rotation_euler[1]=3.1415939331054688
#bpy.data.objects["Plane.001"].rotation_euler=Euler((0.0, 3.1415939331054688, 0.0), 'XYZ')


    # boolean
    bpy.context.scene.objects.active = bpy.data.objects["Plane"]
    bpy.ops.object.modifier_add(type='BOOLEAN')

    bpy.data.objects["Plane"].modifiers["Boolean"].object=bpy.data.objects['Quick_exportMesh']

    bpy.ops.object.modifier_apply(apply_as='DATA',modifier="Boolean")

    # boolean
    bpy.context.scene.objects.active = bpy.data.objects["Plane.001"]
    bpy.ops.object.modifier_add(type='BOOLEAN')

    bpy.data.objects["Plane.001"].modifiers["Boolean"].object=bpy.data.objects['Plane']

    bpy.ops.object.modifier_apply(apply_as='DATA',modifier="Boolean")

    # export triangle obj file
    bpy.ops.export_scene.obj(filepath="./exportnecktri.obj", check_existing=False, filter_glob="*.obj;*.mtl", use_selection=True, use_animation=False, use_edges=True, use_normals=False, use_uvs=False, use_materials=False, use_triangles=True, use_vertex_groups=False, use_nurbs=False, use_blen_objects=False, group_by_object=False, group_by_material=False, keep_vertex_order=True)

    bpy.ops.object.select_all(action='SELECT')
    bpy.ops.object.delete()

    # import triangle obj file
    bpy.ops.import_scene.obj(filepath="./exportnecktri.obj", filter_glob="*.obj;*.mtl")

    # select mesh
    bpy.context.scene.objects.active = bpy.data.objects["exportnecktri"]
    bpy.context.active_object.select = True

    # select mesh
    bpy.context.scene.objects.active = bpy.data.objects["exportnecktri"]
    bpy.context.active_object.select = True

    # export STL file
    bpy.ops.export_mesh.stl(filepath="./neck.stl", check_existing=False, filter_glob="*.stl", ascii=False, use_mesh_modifiers=True, axis_forward='Y', axis_up='Z', global_scale=1.0)
```

C.4 Blender Script “03utorsostl” for obtaining the upper torso mesh (STL file) from the individual MH model (MHX file)

```
import bpy
# clear workspace
# bpy.ops.wm.read_homefile()
bpy.ops.object.select_all(action='SELECT')
bpy.ops.object.delete()

# import mhx file
bpy.ops.import_scene.makehuman_mhx(filepath='quick_export.mhx',scale=1)

# set pose
bpy.context.scene.objects.active = bpy.data.objects["Quick_export"]
bpy.context.active_object.select = True
bpy.ops.object.mode_set(mode='POSE')

#bpy.data.objects["Quick_export"].pose.bones["LoArm_L"].rotation_euler.x=0
#bpy.data.objects["Quick_export"].pose.bones["LoArm_L"].rotation_euler.y=-1.570797

bpy.data.objects["Quick_export"].pose.bones["UpLeg_L"].rotation_quaternion.w=0.991
bpy.data.objects["Quick_export"].pose.bones["UpLeg_L"].rotation_quaternion.x=0
bpy.data.objects["Quick_export"].pose.bones["UpLeg_L"].rotation_quaternion.y=0
bpy.data.objects["Quick_export"].pose.bones["UpLeg_L"].rotation_quaternion.z=-0.131

bpy.data.objects["Quick_export"].pose.bones["UpLeg_R"].rotation_quaternion.w=0.991
bpy.data.objects["Quick_export"].pose.bones["UpLeg_R"].rotation_quaternion.x=0
bpy.data.objects["Quick_export"].pose.bones["UpLeg_R"].rotation_quaternion.y=0
bpy.data.objects["Quick_export"].pose.bones["UpLeg_R"].rotation_quaternion.z=0.131


# change to 'OBJECT' mode
bpy.ops.object.mode_set(mode='OBJECT')

# select mesh
bpy.context.scene.objects.active = bpy.data.objects["Quick_exportMesh"]
bpy.context.active_object.select = True

# Select fvertex point
fvertexVertices=[6913]

f1vertexVertices=[8179]

f2vertexVertices=[2839]

f3vertexVertices=[10811]

#Create a Vertex Group
fvertexGroup = bpy.context.object.vertex_groups.new('fvertexVertexGroup')
fvertexGroup.add(fvertexVertices, 1.0, 'ADD')
```

```
48.
49. f1vertexGroup = bpy.context.object.vertex_groups.new('f1vertexVertexGroup')
50. f1vertexGroup.add(f1vertexVertices, 1.0, 'ADD')
51.
52. f2vertexGroup = bpy.context.object.vertex_groups.new('f2vertexVertexGroup')
53. f2vertexGroup.add(f2vertexVertices, 1.0, 'ADD')
54.
55. f3vertexGroup = bpy.context.object.vertex_groups.new('f3vertexVertexGroup')
56. f3vertexGroup.add(f3vertexVertices, 1.0, 'ADD')
57.
58. # change to 'EDIT' mode
59. bpy.ops.object.mode_set(mode='EDIT')
60.
61. # deselete others
62. bpy.ops.mesh.select_all(action='DESELECT')
63.
64. # select vertex group
65. #Select the Vertex group
66. bpy.ops.object.vertex_group_set_active(group='fvertexVertexGroup')
67. bpy.ops.object.vertex_group_select()
68.
69. # change to 'OBJECT' mode
70. bpy.ops.object.mode_set(mode='OBJECT')
71.
72. # add plane
73. [bpy.context.scene.cursor_location] = [i.co for i in bpy.context.active_object.
    data.vertices if i.select]
74.
75. bpy.ops.mesh.primitive_plane_add()
76.
77. bpy.ops.transform.resize(value=(100,100,1))
78. bpy.data.objects["Plane"].rotation_euler[1]=3.1415939331054688
79. #bpy.data.objects["Plane"].dimensions=Vector((100,100,0))
80. #bpy.data.objects["Plane"].rotation_euler=Euler((0.0, 3.1415939331054688, 0.0),
     'XYZ')
81.
82. # select mesh
83. bpy.context.scene.objects.active = bpy.data.objects["Quick_exportMesh"]
84. bpy.context.active_object.select = True
85.
86. # change to 'EDIT' mode
87. bpy.ops.object.mode_set(mode='EDIT')
88.
89. # deselete others
90. bpy.ops.mesh.select_all(action='DESELECT')
91.
92. # select vertex group
93. #Select the Vertex group
94. bpy.ops.object.vertex_group_set_active(group='f1vertexVertexGroup')
95. bpy.ops.object.vertex_group_select()
96.
97. # change to 'OBJECT' mode
98. bpy.ops.object.mode_set(mode='OBJECT')
99.
100.    # add plane
101.    [bpy.context.scene.cursor_location] = [i.co for i in bpy.context.active_obj
    ect.data.vertices if i.select]
102.
103.    bpy.ops.mesh.primitive_plane_add()
104.
105.    bpy.ops.transform.resize(value=(10,10,1))
106.    #bpy.data.objects["Plane.001"].dimensions=Vector((10,10,0))
107.    #bpy.data.objects["Plane.001"].rotation_euler=Euler((0.0, 0, 0.0), 'XYZ')
```

```
108.
109.
110.    # select mesh
111.    bpy.context.scene.objects.active = bpy.data.objects["Quick_exportMesh"]
112.    bpy.context.active_object.select = True
113.
114.    # change to 'EDIT' mode
115.    bpy.ops.object.mode_set(mode='EDIT')
116.
117.    # deselete others
118.    bpy.ops.mesh.select_all(action='DESELECT')
119.
120.    # select vertex group
121.    #Select the Vertex group
122.    bpy.ops.object.vertex_group_set_active(group='f2vertexVertexGroup')
123.    bpy.ops.object.vertex_group_select()
124.
125.    # change to 'OBJECT' mode
126.    bpy.ops.object.mode_set(mode='OBJECT')
127.
128.    # add plane
129.    [bpy.context.scene.cursor_location] = [i.co for i in bpy.context.active_obj
    ect.data.vertices if i.select]
130.
131.    bpy.ops.mesh.primitive_plane_add()
132.
133.    bpy.ops.transform.resize(value=(10,10,1))
134.    bpy.data.objects["Plane.002"].rotation_euler[1]=1.1169413328170776
135.    #bpy.data.objects["Plane.002"].dimensions=Vector((10,10,0))
136.    #bpy.data.objects["Plane.002"].rotation_euler=Euler((0.0, 1.116941332817077
    6, 0.0), 'XYZ')
137.
138.    # select mesh
139.    bpy.context.scene.objects.active = bpy.data.objects["Quick_exportMesh"]
140.    bpy.context.active_object.select = True
141.
142.    # change to 'EDIT' mode
143.    bpy.ops.object.mode_set(mode='EDIT')
144.
145.    # deselete others
146.    bpy.ops.mesh.select_all(action='DESELECT')
147.
148.    # select vertex group
149.    #Select the Vertex group
150.    bpy.ops.object.vertex_group_set_active(group='f3vertexVertexGroup')
151.    bpy.ops.object.vertex_group_select()
152.
153.    # change to 'OBJECT' mode
154.    bpy.ops.object.mode_set(mode='OBJECT')
155.
156.    # add plane
157.    [bpy.context.scene.cursor_location] = [i.co for i in bpy.context.active_obj
    ect.data.vertices if i.select]
158.
159.    bpy.ops.mesh.primitive_plane_add()
160.
161.    bpy.ops.transform.resize(value=(10,10,1))
162.    bpy.data.objects["Plane.003"].rotation_euler[1]=5.16624641418457
163.    #bpy.data.objects["Plane.003"].dimensions=Vector((10,10,0))
164.    #bpy.data.objects["Plane.003"].rotation_euler=Euler((0.0, 5.16624641418457,
     0.0), 'XYZ')
165.
166.    # boolean
```

```
    bpy.context.scene.objects.active = bpy.data.objects["Plane"]
    bpy.ops.object.modifier_add(type='BOOLEAN')

    bpy.data.objects["Plane"].modifiers["Boolean"].object=bpy.data.objects['Quick_exportMesh']

    bpy.ops.object.modifier_apply(apply_as='DATA',modifier="Boolean")

    # boolean
    bpy.context.scene.objects.active = bpy.data.objects["Plane.001"]
    bpy.ops.object.modifier_add(type='BOOLEAN')

    bpy.data.objects["Plane.001"].modifiers["Boolean"].object=bpy.data.objects['Plane']

    bpy.ops.object.modifier_apply(apply_as='DATA',modifier="Boolean")

    # boolean
    bpy.context.scene.objects.active = bpy.data.objects["Plane.002"]
    bpy.ops.object.modifier_add(type='BOOLEAN')

    bpy.data.objects["Plane.002"].modifiers["Boolean"].object=bpy.data.objects['Plane.001']

    bpy.ops.object.modifier_apply(apply_as='DATA',modifier="Boolean")

    # boolean
    bpy.context.scene.objects.active = bpy.data.objects["Plane.003"]
    bpy.ops.object.modifier_add(type='BOOLEAN')

    bpy.data.objects["Plane.003"].modifiers["Boolean"].object=bpy.data.objects['Plane.002']

    bpy.ops.object.modifier_apply(apply_as='DATA',modifier="Boolean")

    # export triangle obj file
    bpy.ops.export_scene.obj(filepath="./exportutorsotri.obj", check_existing=False, filter_glob="*.obj;*.mtl", use_selection=True, use_animation=False, use_edges=True, use_normals=False, use_uvs=False, use_materials=False, use_triangles=True, use_vertex_groups=False, use_nurbs=False, use_blen_objects=False, group_by_object=False, group_by_material=False, keep_vertex_order=True)

    bpy.ops.object.select_all(action='SELECT')
    bpy.ops.object.delete()

    # import triangle obj file
    bpy.ops.import_scene.obj(filepath="./exportutorsotri.obj", filter_glob="*.obj;*.mtl")

    # select mesh
    bpy.context.scene.objects.active = bpy.data.objects["exportutorsotri"]
    bpy.context.active_object.select = True

    # select mesh
    bpy.context.scene.objects.active = bpy.data.objects["exportutorsotri"]
    bpy.context.active_object.select = True

    # export STL file
    bpy.ops.export_mesh.stl(filepath="./utorso.stl", check_existing=False, filter_glob="*.stl", ascii=False, use_mesh_modifiers=True, axis_forward='Y', axis_up='Z', global_scale=1.0)
```

C.5 Blender Script “04ltorsostl” for obtaining the lower torso mesh (STL file) from the individual MH model (MHX file)

```
import bpy
# clear workspace
# bpy.ops.wm.read_homefile()
bpy.ops.object.select_all(action='SELECT')
bpy.ops.object.delete()

# import mhx file
bpy.ops.import_scene.makehuman_mhx(filepath='quick_export.mhx',scale=1)

# set pose
bpy.context.scene.objects.active = bpy.data.objects["Quick_export"]
bpy.context.active_object.select = True
bpy.ops.object.mode_set(mode='POSE')

bpy.data.objects["Quick_export"].pose.bones["UpLeg_L"].rotation_quaternion.w=0.991
bpy.data.objects["Quick_export"].pose.bones["UpLeg_L"].rotation_quaternion.x=0
bpy.data.objects["Quick_export"].pose.bones["UpLeg_L"].rotation_quaternion.y=0
bpy.data.objects["Quick_export"].pose.bones["UpLeg_L"].rotation_quaternion.z=-0.131

bpy.data.objects["Quick_export"].pose.bones["UpLeg_R"].rotation_quaternion.w=0.991
bpy.data.objects["Quick_export"].pose.bones["UpLeg_R"].rotation_quaternion.x=0
bpy.data.objects["Quick_export"].pose.bones["UpLeg_R"].rotation_quaternion.y=0
bpy.data.objects["Quick_export"].pose.bones["UpLeg_R"].rotation_quaternion.z=0.131

# change to 'OBJECT' mode
bpy.ops.object.mode_set(mode='OBJECT')

# select mesh
bpy.context.scene.objects.active = bpy.data.objects["Quick_exportMesh"]
bpy.context.active_object.select = True
7361
# Select fvertex point
fvertexVertices=[6913]

f1vertexVertices=[7361]

f2vertexVertices=[7361]

#Create a Vertex Group
fvertexGroup = bpy.context.object.vertex_groups.new('fvertexVertexGroup')
fvertexGroup.add(fvertexVertices, 1.0, 'ADD')

f1vertexGroup = bpy.context.object.vertex_groups.new('f1vertexVertexGroup')
f1vertexGroup.add(f1vertexVertices, 1.0, 'ADD')

f2vertexGroup = bpy.context.object.vertex_groups.new('f2vertexVertexGroup')
f2vertexGroup.add(f2vertexVertices, 1.0, 'ADD')

```

```
# change to 'EDIT' mode
bpy.ops.object.mode_set(mode='EDIT')

# deselete others
bpy.ops.mesh.select_all(action='DESELECT')

# select vertex group
#Select the Vertex group
bpy.ops.object.vertex_group_set_active(group='fvertexVertexGroup')
bpy.ops.object.vertex_group_select()

# change to 'OBJECT' mode
bpy.ops.object.mode_set(mode='OBJECT')

# add plane
[bpy.context.scene.cursor_location] = [i.co for i in bpy.context.active_object.
data.vertices if i.select]

bpy.ops.mesh.primitive_plane_add()

bpy.ops.transform.resize(value=(100,100,1))
#bpy.data.objects["Plane"].dimensions=Vector((100,100,0))
#bpy.data.objects["Plane"].rotation_euler=Euler((0.0, 0, 0.0), 'XYZ')

# select mesh
bpy.context.scene.objects.active = bpy.data.objects["Quick_exportMesh"]
bpy.context.active_object.select = True

# change to 'EDIT' mode
bpy.ops.object.mode_set(mode='EDIT')

# deselete others
bpy.ops.mesh.select_all(action='DESELECT')

# select vertex group
#Select the Vertex group
bpy.ops.object.vertex_group_set_active(group='f1vertexVertexGroup')
bpy.ops.object.vertex_group_select()

# change to 'OBJECT' mode
bpy.ops.object.mode_set(mode='OBJECT')

# add plane
[bpy.context.scene.cursor_location] = [i.co for i in bpy.context.active_object.
data.vertices if i.select]

bpy.ops.mesh.primitive_plane_add()

bpy.ops.transform.resize(value=(10,10,1))
bpy.data.objects["Plane.001"].rotation_euler[1]=3.7873661518096924
#bpy.data.objects["Plane.001"].dimensions=Vector((10,10,0))
#bpy.data.objects["Plane.001"].rotation_euler=Euler((0.0, 3.7873661518096924, 0
.0), 'XYZ')

    # select mesh
    bpy.context.scene.objects.active = bpy.data.objects["Quick_exportMesh"]
    bpy.context.active_object.select = True

    # change to 'EDIT' mode
    bpy.ops.object.mode_set(mode='EDIT')

    # deselete others
    bpy.ops.mesh.select_all(action='DESELECT')
```

```
109.
110.    # select vertex group
111.    #Select the Vertex group
112.    bpy.ops.object.vertex_group_set_active(group='f2vertexVertexGroup')
113.    bpy.ops.object.vertex_group_select()
114.
115.    # change to 'OBJECT' mode
116.    bpy.ops.object.mode_set(mode='OBJECT')
117.
118.    # add plane
119.    [bpy.context.scene.cursor_location] = [i.co for i in bpy.context.active_obj
    ect.data.vertices if i.select]
120.
121.    bpy.ops.mesh.primitive_plane_add()
122.
123.    bpy.ops.transform.resize(value=(10,10,1))
124.    bpy.data.objects["Plane.002"].rotation_euler[1]=2.495821952819824
125.    #bpy.data.objects["Plane.002"].dimensions=Vector((10,10,0))
126.    #bpy.data.objects["Plane.002"].rotation_euler=Euler((0.0, 2.495821952819824
    , 0.0), 'XYZ')
127.
128.    # boolean
129.    bpy.context.scene.objects.active = bpy.data.objects["Plane"]
130.    bpy.ops.object.modifier_add(type='BOOLEAN')
131.
132.    bpy.data.objects["Plane"].modifiers["Boolean"].object=bpy.data.objects['Qui
    ck_exportMesh']
133.
134.    bpy.ops.object.modifier_apply(apply_as='DATA',modifier="Boolean")
135.
136.    # boolean
137.    bpy.context.scene.objects.active = bpy.data.objects["Plane.001"]
138.    bpy.ops.object.modifier_add(type='BOOLEAN')
139.
140.    bpy.data.objects["Plane.001"].modifiers["Boolean"].object=bpy.data.objects[
    'Plane']
141.
142.    bpy.ops.object.modifier_apply(apply_as='DATA',modifier="Boolean")
143.
144.    # boolean
145.    bpy.context.scene.objects.active = bpy.data.objects["Plane.002"]
146.    bpy.ops.object.modifier_add(type='BOOLEAN')
147.
148.    bpy.data.objects["Plane.002"].modifiers["Boolean"].object=bpy.data.objects[
    'Plane.001']
149.
150.    bpy.ops.object.modifier_apply(apply_as='DATA',modifier="Boolean")
151.
152.    # export triangle obj file
153.    bpy.ops.export_scene.obj(filepath="./exportltorsotri.obj", check_existing=F
    alse, filter_glob="*.obj;*.mtl", use_selection=True, use_animation=False, use_e
    dges=True, use_normals=False, use_uvs=False, use_materials=False, use_triangles
    =True, use_vertex_groups=False, use_nurbs=False, use_blen_objects=False, group_
    by_object=False, group_by_material=False, keep_vertex_order=True)
154.
155.    bpy.ops.object.select_all(action='SELECT')
156.    bpy.ops.object.delete()
157.
158.    # import triangle obj file
159.    bpy.ops.import_scene.obj(filepath="./exportltorsotri.obj", filter_glob="*.o
    bj;*.mtl")
160.
161.    # select mesh
```

```
    bpy.context.scene.objects.active = bpy.data.objects["exportltorsotri"]
    bpy.context.active_object.select = True

    # select mesh
    bpy.context.scene.objects.active = bpy.data.objects["exportltorsotri"]
    bpy.context.active_object.select = True

    # export STL file
    bpy.ops.export_mesh.stl(filepath="./ltorso.stl", check_existing=False, filter_glob="*.stl", ascii=False, use_mesh_modifiers=True, axis_forward='Y', axis_up='Z', global_scale=1.0)
```

C.6 Blender Script “05uarmstl” for obtaining the upper arm mesh (STL file) from the individual MH model (MHX file)

```
import bpy
# clear workspace
# bpy.ops.wm.read_homefile()
bpy.ops.object.select_all(action='SELECT')
bpy.ops.object.delete()

# import mhx file
bpy.ops.import_scene.makehuman_mhx(filepath='quick_export.mhx',scale=1)

# set pose
bpy.context.scene.objects.active = bpy.data.objects["Quick_export"]
bpy.context.active_object.select = True
bpy.ops.object.mode_set(mode='POSE')

bpy.data.objects["Quick_export"].pose.bones["UpLeg_L"].rotation_quaternion.w=0.991
bpy.data.objects["Quick_export"].pose.bones["UpLeg_L"].rotation_quaternion.x=0
bpy.data.objects["Quick_export"].pose.bones["UpLeg_L"].rotation_quaternion.y=0
bpy.data.objects["Quick_export"].pose.bones["UpLeg_L"].rotation_quaternion.z=-0.131

bpy.data.objects["Quick_export"].pose.bones["UpLeg_R"].rotation_quaternion.w=0.991
bpy.data.objects["Quick_export"].pose.bones["UpLeg_R"].rotation_quaternion.x=0
bpy.data.objects["Quick_export"].pose.bones["UpLeg_R"].rotation_quaternion.y=0
bpy.data.objects["Quick_export"].pose.bones["UpLeg_R"].rotation_quaternion.z=0.131

# change to 'OBJECT' mode
bpy.ops.object.mode_set(mode='OBJECT')

# select mesh
bpy.context.scene.objects.active = bpy.data.objects["Quick_exportMesh"]
bpy.context.active_object.select = True
7361
# Select fvertex point
fvertexVertices=[6913]

f1vertexVertices=[8179]
```

```
36.
37. f2vertexVertices=[10271]#[10702]
38.
39. f3vertexVertices=[10811]
40.
41. #Create a Vertex Group
42. fvertexGroup = bpy.context.object.vertex_groups.new('fvertexVertexGroup')
43. fvertexGroup.add(fvertexVertices, 1.0, 'ADD')
44.
45. f1vertexGroup = bpy.context.object.vertex_groups.new('f1vertexVertexGroup')
46. f1vertexGroup.add(f1vertexVertices, 1.0, 'ADD')
47.
48. f2vertexGroup = bpy.context.object.vertex_groups.new('f2vertexVertexGroup')
49. f2vertexGroup.add(f2vertexVertices, 1.0, 'ADD')
50.
51. f3vertexGroup = bpy.context.object.vertex_groups.new('f3vertexVertexGroup')
52. f3vertexGroup.add(f3vertexVertices, 1.0, 'ADD')
53.
54. # change to 'EDIT' mode
55. bpy.ops.object.mode_set(mode='EDIT')
56.
57. # deselete others
58. bpy.ops.mesh.select_all(action='DESELECT')
59.
60. # select vertex group
61. #Select the Vertex group
62. bpy.ops.object.vertex_group_set_active(group='fvertexVertexGroup')
63. bpy.ops.object.vertex_group_select()
64.
65. # change to 'OBJECT' mode
66. bpy.ops.object.mode_set(mode='OBJECT')
67.
68. # add plane
69. [bpy.context.scene.cursor_location] = [i.co for i in bpy.context.active_object.
    data.vertices if i.select]
70.
71. bpy.ops.mesh.primitive_plane_add()
72.
73. bpy.ops.transform.resize(value=(100,100,1))
74. bpy.data.objects["Plane"].rotation_euler[1]=3.1415939331054688
75. #bpy.data.objects["Plane"].dimensions=Vector((100,100,0))
76. #bpy.data.objects["Plane"].rotation_euler=Euler((0.0, 3.1415939331054688, 0.0),
     'XYZ')
77.
78. # select mesh
79. bpy.context.scene.objects.active = bpy.data.objects["Quick_exportMesh"]
80. bpy.context.active_object.select = True
81.
82. # change to 'EDIT' mode
83. bpy.ops.object.mode_set(mode='EDIT')
84.
85. # deselete others
86. bpy.ops.mesh.select_all(action='DESELECT')
87.
88. # select vertex group
89. #Select the Vertex group
90. bpy.ops.object.vertex_group_set_active(group='f1vertexVertexGroup')
91. bpy.ops.object.vertex_group_select()
92.
93. # change to 'OBJECT' mode
94. bpy.ops.object.mode_set(mode='OBJECT')
95.
96. # add plane
```

```
97. [bpy.context.scene.cursor_location] = [i.co for i in bpy.context.active_object.
    data.vertices if i.select]
98. 
99. bpy.ops.mesh.primitive_plane_add()
100. 
101.    bpy.ops.transform.resize(value=(10,10,1))
102.    #bpy.data.objects["Plane.001"].dimensions=Vector((10,10,0))
103.    #bpy.data.objects["Plane.001"].rotation_euler=Euler((0.0, 0, 0.0), 'XYZ')
104. 
105. 
106.    # select mesh
107.    bpy.context.scene.objects.active = bpy.data.objects["Quick_exportMesh"]
108.    bpy.context.active_object.select = True
109. 
110.    # change to 'EDIT' mode
111.    bpy.ops.object.mode_set(mode='EDIT')
112. 
113.    # deselete others
114.    bpy.ops.mesh.select_all(action='DESELECT')
115. 
116.    # select vertex group
117.    #Select the Vertex group
118.    bpy.ops.object.vertex_group_set_active(group='f2vertexVertexGroup')
119.    bpy.ops.object.vertex_group_select()
120. 
121.    # change to 'OBJECT' mode
122.    bpy.ops.object.mode_set(mode='OBJECT')
123. 
124.    # add plane
125.    [bpy.context.scene.cursor_location] = [i.co for i in bpy.context.active_obj
    ect.data.vertices if i.select]
126. 
127.    bpy.ops.mesh.primitive_plane_add()
128. 
129.    bpy.ops.transform.resize(value=(10,10,1))
130.    bpy.data.objects["Plane.002"].rotation_euler[1]=4.712390899658203
131.    #bpy.data.objects["Plane.002"].dimensions=Vector((10,10,0))
132.    #bpy.data.objects["Plane.002"].rotation_euler=Euler((0.0, 4.712390899658203
    , 0.0), 'XYZ')
133. 
134.    # select mesh
135.    bpy.context.scene.objects.active = bpy.data.objects["Quick_exportMesh"]
136.    bpy.context.active_object.select = True
137. 
138.    # change to 'EDIT' mode
139.    bpy.ops.object.mode_set(mode='EDIT')
140. 
141.    # deselete others
142.    bpy.ops.mesh.select_all(action='DESELECT')
143. 
144.    # select vertex group
145.    #Select the Vertex group
146.    bpy.ops.object.vertex_group_set_active(group='f3vertexVertexGroup')
147.    bpy.ops.object.vertex_group_select()
148. 
149.    # change to 'OBJECT' mode
150.    bpy.ops.object.mode_set(mode='OBJECT')
151. 
152.    # add plane
153.    [bpy.context.scene.cursor_location] = [i.co for i in bpy.context.active_obj
    ect.data.vertices if i.select]
154. 
155.    bpy.ops.mesh.primitive_plane_add()
```

```
156.
157.    bpy.ops.transform.resize(value=(10,10,1))
158.    bpy.data.objects["Plane.003"].rotation_euler[1]=2.024651288986206
159.    #bpy.data.objects["Plane.003"].dimensions=Vector((10,10,0))
160.    #bpy.data.objects["Plane.003"].rotation_euler=Euler((0.0, 2.024651288986206
    , 0.0), 'XYZ')
161.
162.    # boolean
163.    bpy.context.scene.objects.active = bpy.data.objects["Plane"]
164.    bpy.ops.object.modifier_add(type='BOOLEAN')
165.
166.    bpy.data.objects["Plane"].modifiers["Boolean"].object=bpy.data.objects['Qui
    ck_exportMesh']
167.
168.    bpy.ops.object.modifier_apply(apply_as='DATA',modifier="Boolean")
169.
170.    # boolean
171.    bpy.context.scene.objects.active = bpy.data.objects["Plane.001"]
172.    bpy.ops.object.modifier_add(type='BOOLEAN')
173.
174.    bpy.data.objects["Plane.001"].modifiers["Boolean"].object=bpy.data.objects[
    'Plane']
175.
176.    bpy.ops.object.modifier_apply(apply_as='DATA',modifier="Boolean")
177.
178.    # boolean
179.    bpy.context.scene.objects.active = bpy.data.objects["Plane.002"]
180.    bpy.ops.object.modifier_add(type='BOOLEAN')
181.
182.    bpy.data.objects["Plane.002"].modifiers["Boolean"].object=bpy.data.objects[
    'Plane.001']
183.
184.    bpy.ops.object.modifier_apply(apply_as='DATA',modifier="Boolean")
185.
186.    # boolean
187.    bpy.context.scene.objects.active = bpy.data.objects["Plane.003"]
188.    bpy.ops.object.modifier_add(type='BOOLEAN')
189.
190.    bpy.data.objects["Plane.003"].modifiers["Boolean"].object=bpy.data.objects[
    'Plane.002']
191.
192.    bpy.ops.object.modifier_apply(apply_as='DATA',modifier="Boolean")
193.
194.    # export triangle obj file
195.    bpy.ops.export_scene.obj(filepath="./exportuarmtri.obj", check_existing=Fal
    se, filter_glob="*.obj;*.mtl", use_selection=True, use_animation=False, use_edg
    es=True, use_normals=False, use_uvs=False, use_materials=False, use_triangles=T
    rue, use_vertex_groups=False, use_nurbs=False, use_blen_objects=False, group_by
    _object=False, group_by_material=False, keep_vertex_order=True)
196.
197.    bpy.ops.object.select_all(action='SELECT')
198.    bpy.ops.object.delete()
199.
200.    # import triangle obj file
201.    bpy.ops.import_scene.obj(filepath="./exportuarmtri.obj", filter_glob="*.obj
    ;*.mtl")
202.
203.    # select mesh
204.    bpy.context.scene.objects.active = bpy.data.objects["exportuarmtri"]
205.    bpy.context.active_object.select = True
206.
207.    # select mesh
208.    bpy.context.scene.objects.active = bpy.data.objects["exportuarmtri"]
```

```
    bpy.context.active_object.select = True

    # export STL file
    bpy.ops.export_mesh.stl(filepath="./uarm.stl", check_existing=False, filter_glob="*.stl", ascii=False, use_mesh_modifiers=True, axis_forward='Y', axis_up='Z', global_scale=1.0)
```

C.7 Blender Script “06larmstl” for obtaining the lower arm mesh (STL file) from the individual MH model (MHX file)

```
import bpy
# clear workspace
# bpy.ops.wm.read_homefile()
bpy.ops.object.select_all(action='SELECT')
bpy.ops.object.delete()

# import mhx file
bpy.ops.import_scene.makehuman_mhx(filepath='quick_export.mhx',scale=1)

# set pose
bpy.context.scene.objects.active = bpy.data.objects["Quick_export"]
bpy.context.active_object.select = True
bpy.ops.object.mode_set(mode='POSE')

bpy.data.objects["Quick_export"].pose.bones["UpLeg_L"].rotation_quaternion.w=0.991
bpy.data.objects["Quick_export"].pose.bones["UpLeg_L"].rotation_quaternion.x=0
bpy.data.objects["Quick_export"].pose.bones["UpLeg_L"].rotation_quaternion.y=0
bpy.data.objects["Quick_export"].pose.bones["UpLeg_L"].rotation_quaternion.z=-0.131

bpy.data.objects["Quick_export"].pose.bones["UpLeg_R"].rotation_quaternion.w=0.991
bpy.data.objects["Quick_export"].pose.bones["UpLeg_R"].rotation_quaternion.x=0
bpy.data.objects["Quick_export"].pose.bones["UpLeg_R"].rotation_quaternion.y=0
bpy.data.objects["Quick_export"].pose.bones["UpLeg_R"].rotation_quaternion.z=0.131

# change to 'OBJECT' mode
bpy.ops.object.mode_set(mode='OBJECT')

# select mesh
bpy.context.scene.objects.active = bpy.data.objects["Quick_exportMesh"]
bpy.context.active_object.select = True

# Select fvertex point
fvertexVertices=[10271]#[10702]

f1vertexVertices=[9641]#[9666]

#Create a Vertex Group
fvertexGroup = bpy.context.object.vertex_groups.new('fvertexVertexGroup')
fvertexGroup.add(fvertexVertices, 1.0, 'ADD')

```

```
f1vertexGroup = bpy.context.object.vertex_groups.new('f1vertexVertexGroup')
f1vertexGroup.add(f1vertexVertices, 1.0, 'ADD')

# change to 'EDIT' mode
bpy.ops.object.mode_set(mode='EDIT')

# deselete others
bpy.ops.mesh.select_all(action='DESELECT')

# select vertex group
#Select the Vertex group
bpy.ops.object.vertex_group_set_active(group='fvertexVertexGroup')
bpy.ops.object.vertex_group_select()

# change to 'OBJECT' mode
bpy.ops.object.mode_set(mode='OBJECT')

# add plane
[bpy.context.scene.cursor_location] = [i.co for i in bpy.context.active_object.
data.vertices if i.select]

bpy.ops.mesh.primitive_plane_add()

bpy.ops.transform.resize(value=(10,10,1))
bpy.data.objects["Plane"].rotation_euler[1]=1.5707969665527344
#bpy.data.objects["Plane"].dimensions=Vector((10,10,0))
#bpy.data.objects["Plane"].rotation_euler=Euler((0.0, 1.5707969665527344, 0.0),
 'XYZ')

# select mesh
bpy.context.scene.objects.active = bpy.data.objects["Quick_exportMesh"]
bpy.context.active_object.select = True

# change to 'EDIT' mode
bpy.ops.object.mode_set(mode='EDIT')

# deselete others
bpy.ops.mesh.select_all(action='DESELECT')

# select vertex group
#Select the Vertex group
bpy.ops.object.vertex_group_set_active(group='f1vertexVertexGroup')
bpy.ops.object.vertex_group_select()

# change to 'OBJECT' mode
bpy.ops.object.mode_set(mode='OBJECT')

# add plane
[bpy.context.scene.cursor_location] = [i.co for i in bpy.context.active_object.
data.vertices if i.select]

bpy.ops.mesh.primitive_plane_add()

bpy.ops.transform.resize(value=(10,10,1))
bpy.data.objects["Plane.001"].rotation_euler[1]=4.712390899658203
#bpy.data.objects["Plane.001"].dimensions=Vector((10,10,0))
#bpy.data.objects["Plane.001"].rotation_euler=Euler((0.0, 4.712390899658203, 0.
0), 'XYZ')


# boolean
bpy.context.scene.objects.active = bpy.data.objects["Plane"]
bpy.ops.object.modifier_add(type='BOOLEAN')
```

```
100.
101.    bpy.data.objects["Plane"].modifiers["Boolean"].object=bpy.data.objects['Qui
    ck_exportMesh']
102.
103.    bpy.ops.object.modifier_apply(apply_as='DATA',modifier="Boolean")
104.
105.    # boolean
106.    bpy.context.scene.objects.active = bpy.data.objects["Plane.001"]
107.    bpy.ops.object.modifier_add(type='BOOLEAN')
108.
109.    bpy.data.objects["Plane.001"].modifiers["Boolean"].object=bpy.data.objects[
    'Plane']
110.
111.    bpy.ops.object.modifier_apply(apply_as='DATA',modifier="Boolean")
112.
113.    # export triangle obj file
114.    bpy.ops.export_scene.obj(filepath="./exportlarmtri.obj", check_existing=Fal
    se, filter_glob="*.obj;*.mtl", use_selection=True, use_animation=False, use_edg
    es=True, use_normals=False, use_uvs=False, use_materials=False, use_triangles=T
    rue, use_vertex_groups=False, use_nurbs=False, use_blen_objects=False, group_by
    _object=False, group_by_material=False, keep_vertex_order=True)
115.
116.    bpy.ops.object.select_all(action='SELECT')
117.    bpy.ops.object.delete()
118.
119.    # import triangle obj file
120.    bpy.ops.import_scene.obj(filepath="./exportlarmtri.obj", filter_glob="*.obj
    ;*.mtl")
121.
122.    # select mesh
123.    bpy.context.scene.objects.active = bpy.data.objects["exportlarmtri"]
124.    bpy.context.active_object.select = True
125.
126.    # select mesh
127.    bpy.context.scene.objects.active = bpy.data.objects["exportlarmtri"]
128.    bpy.context.active_object.select = True
129.
130.    # export STL file
131.    bpy.ops.export_mesh.stl(filepath="./larm.stl", check_existing=False, filter
    _glob="*.stl", ascii=False, use_mesh_modifiers=True, axis_forward='Y', axis_up=
    'Z', global_scale=1.0)
```

C.8 Blender Script “07handstl” for obtaining the hand mesh (STL file) from the individual MH model (MHX file)

```
1.  import bpy
2.  # clear workspace
3.  # bpy.ops.wm.read_homefile()
4.  bpy.ops.object.select_all(action='SELECT')
5.  bpy.ops.object.delete()
6.
7.  # import mhx file
8.  bpy.ops.import_scene.makehuman_mhx(filepath='quick_export.mhx',scale=1)
9.
10. # set pose
11. bpy.context.scene.objects.active = bpy.data.objects["Quick_export"]
12. bpy.context.active_object.select = True
13. bpy.ops.object.mode_set(mode='POSE')
```

```
14.
15. bpy.data.objects["Quick_export"].pose.bones["UpLeg_L"].rotation_quaternion.w=0.
    991
16. bpy.data.objects["Quick_export"].pose.bones["UpLeg_L"].rotation_quaternion.x=0
17. bpy.data.objects["Quick_export"].pose.bones["UpLeg_L"].rotation_quaternion.y=0
18. bpy.data.objects["Quick_export"].pose.bones["UpLeg_L"].rotation_quaternion.z=-
    0.131
19.
20. bpy.data.objects["Quick_export"].pose.bones["UpLeg_R"].rotation_quaternion.w=0.
    991
21. bpy.data.objects["Quick_export"].pose.bones["UpLeg_R"].rotation_quaternion.x=0
22. bpy.data.objects["Quick_export"].pose.bones["UpLeg_R"].rotation_quaternion.y=0
23. bpy.data.objects["Quick_export"].pose.bones["UpLeg_R"].rotation_quaternion.z=0.
    131
24.
25. # change to 'OBJECT' mode
26. bpy.ops.object.mode_set(mode='OBJECT')
27.
28. # select mesh
29. bpy.context.scene.objects.active = bpy.data.objects["Quick_exportMesh"]
30. bpy.context.active_object.select = True
31.
32. # Select fvertex point
33. fvertexVertices=[9641]#[9666]
34. #Create a Vertex Group
35. fvertexGroup = bpy.context.object.vertex_groups.new('fvertexVertexGroup')
36. fvertexGroup.add(fvertexVertices, 1.0, 'ADD')
37.
38. # change to 'EDIT' mode
39. bpy.ops.object.mode_set(mode='EDIT')
40.
41. # delete others
42. bpy.ops.mesh.select_all(action='DESELECT')
43.
44. # select vertex group
45. #Select the Vertex group
46. bpy.ops.object.vertex_group_set_active(group='fvertexVertexGroup')
47. bpy.ops.object.vertex_group_select()
48.
49. # change to 'OBJECT' mode
50. bpy.ops.object.mode_set(mode='OBJECT')
51.
52. # add plane
53. [bpy.context.scene.cursor_location] = [i.co for i in bpy.context.active_object.
    data.vertices if i.select]
54.
55. bpy.ops.mesh.primitive_plane_add()
56.
57. bpy.ops.transform.resize(value=(10,10,1))
58. bpy.data.objects["Plane"].rotation_euler[1]=1.5707969665527344
59. #bpy.data.objects["Plane"].dimensions=Vector((10,10,0))
60. #bpy.data.objects["Plane"].rotation_euler=Euler((0.0, 1.5707969665527344, 0.0),
     'XYZ')
61.
62. # boolean
63. bpy.ops.object.modifier_add(type='BOOLEAN')
64.
65. bpy.data.objects["Plane"].modifiers["Boolean"].object=bpy.data.objects['Quick_e
    xportMesh']
```

```
66.
67. bpy.ops.object.modifier_apply(apply_as='DATA',modifier="Boolean")
68.
69.
70.
71. # export triangle obj file
72. bpy.ops.export_scene.obj(filepath="./exporthandtri.obj", check_existing=False,
    filter_glob="*.obj;*.mtl", use_selection=True, use_animation=False, use_edges=T
    rue, use_normals=False, use_uvs=False, use_materials=False, use_triangles=True,
     use_vertex_groups=False, use_nurbs=False, use_blen_objects=False, group_by_obj
    ect=False, group_by_material=False, keep_vertex_order=True)
73.
74. bpy.ops.object.select_all(action='SELECT')
75. bpy.ops.object.delete()
76.
77. # import triangle obj file
78. bpy.ops.import_scene.obj(filepath="./exporthandtri.obj", filter_glob="*.obj;*.m
    tl")
79.
80. # select mesh
81. bpy.context.scene.objects.active = bpy.data.objects["exporthandtri"]
82. bpy.context.active_object.select = True
83.
84. # select mesh
85. bpy.context.scene.objects.active = bpy.data.objects["exporthandtri"]
86. bpy.context.active_object.select = True
87.
88. # export STL file
89. bpy.ops.export_mesh.stl(filepath="./hand.stl", check_existing=False, filter_glo
    b="*.stl", ascii=False, use_mesh_modifiers=True, axis_forward='Y', axis_up='Z',
     global_scale=1.0)
```

C.9 Blender Script “08ulegstl” for obtaining the upper leg mesh (STL file) from the individual MH model (MHX file)

```
1.  import bpy
2.  # clear workspace
3.  # bpy.ops.wm.read_homefile()
4.  bpy.ops.object.select_all(action='SELECT')
5.  bpy.ops.object.delete()
6.
7.  # import mhx file
8.  bpy.ops.import_scene.makehuman_mhx(filepath='quick_export.mhx',scale=1)
9.
10. # set pose
11. bpy.context.scene.objects.active = bpy.data.objects["Quick_export"]
12. bpy.context.active_object.select = True
13. bpy.ops.object.mode_set(mode='POSE')
14.
15. bpy.data.objects["Quick_export"].pose.bones["UpLeg_L"].rotation_quaternion.w=0.
    991
16. bpy.data.objects["Quick_export"].pose.bones["UpLeg_L"].rotation_quaternion.x=0

17. bpy.data.objects["Quick_export"].pose.bones["UpLeg_L"].rotation_quaternion.y=0

18. bpy.data.objects["Quick_export"].pose.bones["UpLeg_L"].rotation_quaternion.z=-
    0.131
19.
```

```
bpy.data.objects["Quick_export"].pose.bones["UpLeg_R"].rotation_quaternion.w=0.991
bpy.data.objects["Quick_export"].pose.bones["UpLeg_R"].rotation_quaternion.x=0
bpy.data.objects["Quick_export"].pose.bones["UpLeg_R"].rotation_quaternion.y=0
bpy.data.objects["Quick_export"].pose.bones["UpLeg_R"].rotation_quaternion.z=0.131


# change to 'OBJECT' mode
bpy.ops.object.mode_set(mode='OBJECT')

# select mesh
bpy.context.scene.objects.active = bpy.data.objects["Quick_exportMesh"]
bpy.context.active_object.select = True

# Select fvertex point
fvertexVertices=[7361]

f1vertexVertices=[6913]

f2vertexVertices=[7361]

f3vertexVertices=[7046]#[7047]

#Create a Vertex Group
fvertexGroup = bpy.context.object.vertex_groups.new('fvertexVertexGroup')
fvertexGroup.add(fvertexVertices, 1.0, 'ADD')

f1vertexGroup = bpy.context.object.vertex_groups.new('f1vertexVertexGroup')
f1vertexGroup.add(f1vertexVertices, 1.0, 'ADD')

f2vertexGroup = bpy.context.object.vertex_groups.new('f2vertexVertexGroup')
f2vertexGroup.add(f2vertexVertices, 1.0, 'ADD')

f3vertexGroup = bpy.context.object.vertex_groups.new('f3vertexVertexGroup')
f3vertexGroup.add(f3vertexVertices, 1.0, 'ADD')

# change to 'EDIT' mode
bpy.ops.object.mode_set(mode='EDIT')

# deselete others
bpy.ops.mesh.select_all(action='DESELECT')

# select vertex group
#Select the Vertex group
bpy.ops.object.vertex_group_set_active(group='fvertexVertexGroup')
bpy.ops.object.vertex_group_select()

# change to 'OBJECT' mode
bpy.ops.object.mode_set(mode='OBJECT')

# add plane
[bpy.context.scene.cursor_location] = [i.co for i in bpy.context.active_object.data.vertices if i.select]

bpy.ops.mesh.primitive_plane_add()

bpy.ops.transform.resize(value=(100,100,1))
bpy.data.objects["Plane"].rotation_euler[1]=1.5707969665527344
#bpy.data.objects["Plane"].dimensions=Vector((100,100,0))
```

```
#bpy.data.objects["Plane"].rotation_euler=Euler((0.0, 1.5707969665527344, 0.0), 'XYZ')


# select mesh
bpy.context.scene.objects.active = bpy.data.objects["Quick_exportMesh"]
bpy.context.active_object.select = True

# change to 'EDIT' mode
bpy.ops.object.mode_set(mode='EDIT')

# deselete others
bpy.ops.mesh.select_all(action='DESELECT')

# select vertex group
#Select the Vertex group
bpy.ops.object.vertex_group_set_active(group='f1vertexVertexGroup')
bpy.ops.object.vertex_group_select()

# change to 'OBJECT' mode
bpy.ops.object.mode_set(mode='OBJECT')

# add plane
[bpy.context.scene.cursor_location] = [i.co for i in bpy.context.active_object.data.vertices if i.select]

    bpy.ops.mesh.primitive_plane_add()

    bpy.ops.transform.resize(value=(100,100,1))
    #bpy.data.objects["Plane.001"].dimensions=Vector((10,10,0))
    #bpy.data.objects["Plane.001"].rotation_euler=Euler((0.0, 0.6457720994949341, 0.0), 'XYZ')




    # select mesh
    bpy.context.scene.objects.active = bpy.data.objects["Quick_exportMesh"]
    bpy.context.active_object.select = True

    # change to 'EDIT' mode
    bpy.ops.object.mode_set(mode='EDIT')

    # deselete others
    bpy.ops.mesh.select_all(action='DESELECT')

    # select vertex group
    #Select the Vertex group
    bpy.ops.object.vertex_group_set_active(group='f2vertexVertexGroup')
    bpy.ops.object.vertex_group_select()

    # change to 'OBJECT' mode
    bpy.ops.object.mode_set(mode='OBJECT')

    # add plane
    [bpy.context.scene.cursor_location] = [i.co for i in bpy.context.active_object.data.vertices if i.select]

    bpy.ops.mesh.primitive_plane_add()

    bpy.ops.transform.resize(value=(10,10,1))
    bpy.data.objects["Plane.002"].rotation_euler[1]=0.6457720994949341
```

```
    #bpy.data.objects["Plane.002"].dimensions=Vector((10,10,0))
    #bpy.data.objects["Plane.002"].rotation_euler=Euler((0.0, 0.645772099494934
1, 0.0), 'XYZ')

    # select mesh
    bpy.context.scene.objects.active = bpy.data.objects["Quick_exportMesh"]
    bpy.context.active_object.select = True

    # change to 'EDIT' mode
    bpy.ops.object.mode_set(mode='EDIT')

    # deselete others
    bpy.ops.mesh.select_all(action='DESELECT')

    # select vertex group
    #Select the Vertex group
    bpy.ops.object.vertex_group_set_active(group='f3vertexVertexGroup')
    bpy.ops.object.vertex_group_select()

    # change to 'OBJECT' mode
    bpy.ops.object.mode_set(mode='OBJECT')

    # add plane
    [bpy.context.scene.cursor_location] = [i.co for i in bpy.context.active_obj
ect.data.vertices if i.select]

    bpy.ops.mesh.primitive_plane_add()

    bpy.ops.transform.resize(value=(10,10,1))
    bpy.data.objects["Plane.003"].rotation_euler[1]=3.1415939331054688
    #bpy.data.objects["Plane.003"].dimensions=Vector((10,10,0))
    #bpy.data.objects["Plane.003"].rotation_euler=Euler((0.0, 3.141593933105468
8, 0.0), 'XYZ')

    # boolean
    bpy.context.scene.objects.active = bpy.data.objects["Plane.001"]
    bpy.ops.object.modifier_add(type='BOOLEAN')

    bpy.data.objects["Plane.001"].modifiers["Boolean"].object=bpy.data.objects[
'Quick_exportMesh']

    bpy.ops.object.modifier_apply(apply_as='DATA',modifier="Boolean")

    # boolean
    bpy.context.scene.objects.active = bpy.data.objects["Plane"]
    bpy.ops.object.modifier_add(type='BOOLEAN')

    bpy.data.objects["Plane"].modifiers["Boolean"].object=bpy.data.objects['Pla
ne.001']

    bpy.ops.object.modifier_apply(apply_as='DATA',modifier="Boolean")

    # boolean
    bpy.context.scene.objects.active = bpy.data.objects["Plane.002"]
    bpy.ops.object.modifier_add(type='BOOLEAN')

    bpy.data.objects["Plane.002"].modifiers["Boolean"].object=bpy.data.objects[
'Plane']

    bpy.ops.object.modifier_apply(apply_as='DATA',modifier="Boolean")

    # boolean
    bpy.context.scene.objects.active = bpy.data.objects["Plane.003"]
```

```
    bpy.ops.object.modifier_add(type='BOOLEAN')

    bpy.data.objects["Plane.003"].modifiers["Boolean"].object=bpy.data.objects['Plane.002']

    bpy.ops.object.modifier_apply(apply_as='DATA',modifier="Boolean")

    # export triangle obj file
    bpy.ops.export_scene.obj(filepath="./exportulegtri.obj", check_existing=False, filter_glob="*.obj;*.mtl", use_selection=True, use_animation=False, use_edges=True, use_normals=False, use_uvs=False, use_materials=False, use_triangles=True, use_vertex_groups=False, use_nurbs=False, use_blen_objects=False, group_by_object=False, group_by_material=False, keep_vertex_order=True)

    bpy.ops.object.select_all(action='SELECT')
    bpy.ops.object.delete()

    # import triangle obj file
    bpy.ops.import_scene.obj(filepath="./exportulegtri.obj", filter_glob="*.obj;*.mtl")

    # select mesh
    bpy.context.scene.objects.active = bpy.data.objects["exportulegtri"]
    bpy.context.active_object.select = True

    # select mesh
    bpy.context.scene.objects.active = bpy.data.objects["exportulegtri"]
    bpy.context.active_object.select = True

    # export STL file
    bpy.ops.export_mesh.stl(filepath="./uleg.stl", check_existing=False, filter_glob="*.stl", ascii=False, use_mesh_modifiers=True, axis_forward='Y', axis_up='Z', global_scale=1.0)
```

C.10 Blender Script “09llegstl” for obtaining the lower leg mesh (STL file) from the individual MH model (MHX file)

```
import bpy
# clear workspace
# bpy.ops.wm.read_homefile()
bpy.ops.object.select_all(action='SELECT')
bpy.ops.object.delete()

# import mhx file
bpy.ops.import_scene.makehuman_mhx(filepath='quick_export.mhx',scale=1)

# set pose
bpy.context.scene.objects.active = bpy.data.objects["Quick_export"]
bpy.context.active_object.select = True
bpy.ops.object.mode_set(mode='POSE')

bpy.data.objects["Quick_export"].pose.bones["UpLeg_L"].rotation_quaternion.w=0.991
bpy.data.objects["Quick_export"].pose.bones["UpLeg_L"].rotation_quaternion.x=0

bpy.data.objects["Quick_export"].pose.bones["UpLeg_L"].rotation_quaternion.y=0
```

```
bpy.data.objects["Quick_export"].pose.bones["UpLeg_L"].rotation_quaternion.z=-0.131

bpy.data.objects["Quick_export"].pose.bones["UpLeg_R"].rotation_quaternion.w=0.991
bpy.data.objects["Quick_export"].pose.bones["UpLeg_R"].rotation_quaternion.x=0

bpy.data.objects["Quick_export"].pose.bones["UpLeg_R"].rotation_quaternion.y=0

bpy.data.objects["Quick_export"].pose.bones["UpLeg_R"].rotation_quaternion.z=0.131

# change to 'OBJECT' mode
bpy.ops.object.mode_set(mode='OBJECT')

# select mesh
bpy.context.scene.objects.active = bpy.data.objects["Quick_exportMesh"]
bpy.context.active_object.select = True

# Select fvertex point
fvertexVertices=[7361]

f1vertexVertices=[7046]#[7047]

f2vertexVertices=[13953]

#Create a Vertex Group
fvertexGroup = bpy.context.object.vertex_groups.new('fvertexVertexGroup')
fvertexGroup.add(fvertexVertices, 1.0, 'ADD')

f1vertexGroup = bpy.context.object.vertex_groups.new('f1vertexVertexGroup')
f1vertexGroup.add(f1vertexVertices, 1.0, 'ADD')

f2vertexGroup = bpy.context.object.vertex_groups.new('f2vertexVertexGroup')
f2vertexGroup.add(f2vertexVertices, 1.0, 'ADD')

# change to 'EDIT' mode
bpy.ops.object.mode_set(mode='EDIT')

# deselete others
bpy.ops.mesh.select_all(action='DESELECT')

# select vertex group
#Select the Vertex group
bpy.ops.object.vertex_group_set_active(group='fvertexVertexGroup')
bpy.ops.object.vertex_group_select()

# change to 'OBJECT' mode
bpy.ops.object.mode_set(mode='OBJECT')

# add plane
[bpy.context.scene.cursor_location] = [i.co for i in bpy.context.active_object.data.vertices if i.select]

bpy.ops.mesh.primitive_plane_add()

bpy.ops.transform.resize(value=(100,100,1))
bpy.data.objects["Plane"].rotation_euler[1]=1.5707969665527344

# select mesh
bpy.context.scene.objects.active = bpy.data.objects["Quick_exportMesh"]
bpy.context.active_object.select = True

```

```
# change to 'EDIT' mode
bpy.ops.object.mode_set(mode='EDIT')

# deselete others
bpy.ops.mesh.select_all(action='DESELECT')

# select vertex group
#Select the Vertex group
bpy.ops.object.vertex_group_set_active(group='f1vertexVertexGroup')
bpy.ops.object.vertex_group_select()

# change to 'OBJECT' mode
bpy.ops.object.mode_set(mode='OBJECT')

# add plane
[bpy.context.scene.cursor_location] = [i.co for i in bpy.context.active_object.data.vertices if i.select]

bpy.ops.mesh.primitive_plane_add()

bpy.ops.transform.resize(value=(10,10,1))
#bpy.data.objects["Plane.001"].dimensions=Vector((10,10,0))
#bpy.data.objects["Plane.001"].rotation_euler=Euler((0.0, 0, 0.0), 'XYZ')

# select mesh
bpy.context.scene.objects.active = bpy.data.objects["Quick_exportMesh"]
    bpy.context.active_object.select = True

    # change to 'EDIT' mode
    bpy.ops.object.mode_set(mode='EDIT')

    # deselete others
    bpy.ops.mesh.select_all(action='DESELECT')

    # select vertex group
    #Select the Vertex group
    bpy.ops.object.vertex_group_set_active(group='f2vertexVertexGroup')
    bpy.ops.object.vertex_group_select()

    # change to 'OBJECT' mode
    bpy.ops.object.mode_set(mode='OBJECT')

    # add plane
    [bpy.context.scene.cursor_location] = [i.co for i in bpy.context.active_object.data.vertices if i.select]

    bpy.ops.mesh.primitive_plane_add()

    bpy.ops.transform.resize(value=(10,10,1))
    bpy.data.objects["Plane.002"].rotation_euler[1]=3.1415939331054688
    #bpy.data.objects["Plane.002"].dimensions=Vector((10,10,0))
    #bpy.data.objects["Plane.002"].rotation_euler=Euler((0.0, 3.1415939331054688, 0.0), 'XYZ')

    # boolean
    bpy.context.scene.objects.active = bpy.data.objects["Plane"]
    bpy.ops.object.modifier_add(type='BOOLEAN')

    bpy.data.objects["Plane"].modifiers["Boolean"].object=bpy.data.objects['Quick_exportMesh']

    bpy.ops.object.modifier_apply(apply_as='DATA',modifier="Boolean")

```

```
    # boolean
    bpy.context.scene.objects.active = bpy.data.objects["Plane.001"]
    bpy.ops.object.modifier_add(type='BOOLEAN')

    bpy.data.objects["Plane.001"].modifiers["Boolean"].object=bpy.data.objects['Plane']

    bpy.ops.object.modifier_apply(apply_as='DATA',modifier="Boolean")

    # boolean
    bpy.context.scene.objects.active = bpy.data.objects["Plane.002"]
    bpy.ops.object.modifier_add(type='BOOLEAN')

    bpy.data.objects["Plane.002"].modifiers["Boolean"].object=bpy.data.objects['Plane.001']

    bpy.ops.object.modifier_apply(apply_as='DATA',modifier="Boolean")

    # export triangle obj file
    bpy.ops.export_scene.obj(filepath="./exportllegtri.obj", check_existing=False, filter_glob="*.obj;*.mtl", use_selection=True, use_animation=False, use_edges=True, use_normals=False, use_uvs=False, use_materials=False, use_triangles=True, use_vertex_groups=False, use_nurbs=False, use_blen_objects=False, group_by_object=False, group_by_material=False, keep_vertex_order=True)

    bpy.ops.object.select_all(action='SELECT')
    bpy.ops.object.delete()

    # import triangle obj file
    bpy.ops.import_scene.obj(filepath="./exportllegtri.obj", filter_glob="*.obj;*.mtl")

    # select mesh
    bpy.context.scene.objects.active = bpy.data.objects["exportllegtri"]
    bpy.context.active_object.select = True

    # select mesh
    bpy.context.scene.objects.active = bpy.data.objects["exportllegtri"]
    bpy.context.active_object.select = True

    # export STL file
    bpy.ops.export_mesh.stl(filepath="./lleg.stl", check_existing=False, filter_glob="*.stl", ascii=False, use_mesh_modifiers=True, axis_forward='Y', axis_up='Z', global_scale=1.0)
```

C.11 Blender Script “10footstl” for obtaining the foot mesh (STL file) from the individual MH model (MHX file)

```
import bpy
# clear workspace
# bpy.ops.wm.read_homefile()
bpy.ops.object.select_all(action='SELECT')
bpy.ops.object.delete()

# import mhx file
bpy.ops.import_scene.makehuman_mhx(filepath='quick_export.mhx',scale=1)

# set pose
```

```
bpy.context.scene.objects.active = bpy.data.objects["Quick_export"]
bpy.context.active_object.select = True
bpy.ops.object.mode_set(mode='POSE')

bpy.data.objects["Quick_export"].pose.bones["UpLeg_L"].rotation_quaternion.w=0.991
bpy.data.objects["Quick_export"].pose.bones["UpLeg_L"].rotation_quaternion.x=0
bpy.data.objects["Quick_export"].pose.bones["UpLeg_L"].rotation_quaternion.y=0
bpy.data.objects["Quick_export"].pose.bones["UpLeg_L"].rotation_quaternion.z=-0.131

bpy.data.objects["Quick_export"].pose.bones["UpLeg_R"].rotation_quaternion.w=0.991
bpy.data.objects["Quick_export"].pose.bones["UpLeg_R"].rotation_quaternion.x=0
bpy.data.objects["Quick_export"].pose.bones["UpLeg_R"].rotation_quaternion.y=0
bpy.data.objects["Quick_export"].pose.bones["UpLeg_R"].rotation_quaternion.z=0.131

# change to 'OBJECT' mode
bpy.ops.object.mode_set(mode='OBJECT')

# select mesh
bpy.context.scene.objects.active = bpy.data.objects["Quick_exportMesh"]
bpy.context.active_object.select = True

# Select fvertex point
fvertexVertices=[7361]

f1vertexVertices=[13953]

#Create a Vertex Group
fvertexGroup = bpy.context.object.vertex_groups.new('fvertexVertexGroup')
fvertexGroup.add(fvertexVertices, 1.0, 'ADD')

f1vertexGroup = bpy.context.object.vertex_groups.new('f1vertexVertexGroup')
f1vertexGroup.add(f1vertexVertices, 1.0, 'ADD')

# change to 'EDIT' mode
bpy.ops.object.mode_set(mode='EDIT')

# deselete others
bpy.ops.mesh.select_all(action='DESELECT')

# select vertex group
#Select the Vertex group
bpy.ops.object.vertex_group_set_active(group='fvertexVertexGroup')
bpy.ops.object.vertex_group_select()

# change to 'OBJECT' mode
bpy.ops.object.mode_set(mode='OBJECT')

# add plane
[bpy.context.scene.cursor_location] = [i.co for i in bpy.context.active_object.data.vertices if i.select]

bpy.ops.mesh.primitive_plane_add()

bpy.ops.transform.resize(value=(100,100,1))
bpy.data.objects["Plane"].rotation_euler[1]=1.5707969665527344
```

```
#bpy.data.objects["Plane"].dimensions=Vector((1000,1000,0))
#bpy.data.objects["Plane"].rotation_euler=Euler((0.0, 1.5707969665527344, 0.0), 'XYZ')

# select mesh
bpy.context.scene.objects.active = bpy.data.objects["Quick_exportMesh"]
bpy.context.active_object.select = True

# change to 'EDIT' mode
bpy.ops.object.mode_set(mode='EDIT')

# deselete others
bpy.ops.mesh.select_all(action='DESELECT')

# select vertex group
#Select the Vertex group
bpy.ops.object.vertex_group_set_active(group='f1vertexVertexGroup')
bpy.ops.object.vertex_group_select()

# change to 'OBJECT' mode
bpy.ops.object.mode_set(mode='OBJECT')

# add plane
[bpy.context.scene.cursor_location] = [i.co for i in bpy.context.active_object.data.vertices if i.select]

bpy.ops.mesh.primitive_plane_add()

bpy.ops.transform.resize(value=(10,10,1))
#bpy.data.objects["Plane.001"].dimensions=Vector((10,10,0))
#bpy.data.objects["Plane.001"].rotation_euler=Euler((0.0, 0, 0.0), 'XYZ')


# boolean
bpy.context.scene.objects.active = bpy.data.objects["Plane"]
bpy.ops.object.modifier_add(type='BOOLEAN')

    bpy.data.objects["Plane"].modifiers["Boolean"].object=bpy.data.objects['Quick_exportMesh']

    bpy.ops.object.modifier_apply(apply_as='DATA',modifier="Boolean")

    # boolean
    bpy.context.scene.objects.active = bpy.data.objects["Plane.001"]
    bpy.ops.object.modifier_add(type='BOOLEAN')

    bpy.data.objects["Plane.001"].modifiers["Boolean"].object=bpy.data.objects['Plane']

    bpy.ops.object.modifier_apply(apply_as='DATA',modifier="Boolean")

    # export triangle obj file
    bpy.ops.export_scene.obj(filepath="./exportfoottri.obj", check_existing=False, filter_glob="*.obj;*.mtl", use_selection=True, use_animation=False, use_edges=True, use_normals=False, use_uvs=False, use_materials=False, use_triangles=True, use_vertex_groups=False, use_nurbs=False, use_blen_objects=False, group_by_object=False, group_by_material=False, keep_vertex_order=True)

    bpy.ops.object.select_all(action='SELECT')
    bpy.ops.object.delete()

    # import triangle obj file
```

```
119.    bpy.ops.import_scene.obj(filepath="./exportfoottri.obj", filter_glob="*.obj
    ;*.mtl")
120.
121.    # select mesh
122.    bpy.context.scene.objects.active = bpy.data.objects["exportfoottri"]
123.    bpy.context.active_object.select = True
124.
125.    # select mesh
126.    bpy.context.scene.objects.active = bpy.data.objects["exportfoottri"]
127.    bpy.context.active_object.select = True
128.
129.    # export STL file
130.    bpy.ops.export_mesh.stl(filepath="./foot.stl", check_existing=False, filter
    _glob="*.stl", ascii=False, use_mesh_modifiers=True, axis_forward='Y', axis_up=
    'Z', global_scale=1.0)
```